2016

# Autotaxin in Central Nervous System Development and Disease

Natalie A. Wheeler

# Autotaxin in Central Nervous System Development and Disease

A dissertation submitted in partial fulfillment of the requirements for the degree of Doctor of Philosophy at Virginia Commonwealth University

By

Natalie Allen Wheeler
B.S. Biology and Psychology
Virginia Tech, 2010

Advisor: Babette Fuss, Ph.D.
Professor, Anatomy and Neurobiology

Virginia Commonwealth University
Richmond, Virginia
May 2016

# ACKNOWLEDGEMENTS

I would first like to thank my advisor, Dr. Babette Fuss. She has pushed me to think more critically, independently, and be more confident in my research. I have grown tremendously since I walked through her laboratory doors five years ago, and I owe this improvement to Babette. I have very much enjoyed talking through experiments and scientific ideas throughout my time in her laboratory and I wish her the very best as she continues to mentor future students.

For my training and studies in the zebrafish, I would like to thank Dr. James Lister. He provided me with the tools and knowledge to pursue experiments within the zebrafish, as well as aided in experimental designs. I thank Dr. Lister for also being a part of my committee and for his mentorship throughout my graduate program.

In addition to Drs. Fuss and Lister, I would like to acknowledge the faculty members of my committee who have taken part in my success as a graduate student. These members include, Dr. Jeff Dupree, Dr. Shirley Taylor, and Dr. Gregory Walsh. I thank you for your knowledge in planning experiments as well as your constant guidance over the years. I would also like to kindly thank Dr. Pamela Knapp for her support in pursuing a collaborative project with one of her previous students, Dr. Patrick Zou. I am thankful that Dr. Knapp trusted in our scientific ideas and encouraged them. Moreover, I would like to extend my sincere gratitude to the neuroscience program director, Dr. John Bigbee, for his support and mentorship through the years. Furthermore, I would like to thank members of the core facilities, namely, Dr. Scott Henderson and Frances White from the microscopy facility and Julie Farnsworth from the flow facility.

Throughout my time as a graduate student, members of the lab as well as other graduate students have granted me much knowledge and support and I owe them a special thank you. I am thankful for the friendships I have made and hope to continue. These people include, Dr. Christopher Waggener, Dr. Magdalena Morgan, Dr. Zila Martinez-Lozada, Dr. Sheila Espirito Santo Araujo, Dr. Patrick Zou, Joyce Balinang and Savannah Benusa.

Lastly, I would like to thank my family. To my Mom, Dad, and sister, Stephanie, I would not be here today if it had not been for your insurmountable support. You have all shown me the importance of continued education and working hard to reach your goals. I am also grateful for my husband, Jeff, who has stood by my side through the successes and failures of my graduate career. I thank you for your continual support and encouragement. We did it.

To the above- mentioned as well as friends and family not listed, I would not be here today if it wasn't for your guidance. For that, I am forever grateful.

TABLE OF CONTENTS

# LIST OF FIGURES

# LIST OF ABBREVIATIONS

| | |
|---|---|
| ATX | autotaxin |
| BBB | blood brain barrier |
| bp | base pair |
| bFGF | basic fibroblast growth factor |
| BSA | bovine serum albumin |
| cAMP | cyclic AMP |
| cldnk | claudink |
| CNS | central nervous system |
| CNP | 2',3'-cyclic nucleotide 3'-phosphodiesterase |
| CRISPR | clustered regularly-interspaced short palindromic repeats |
| CSF | cerebrospinal fluid |
| dpf | days post fertilization |
| DMEM | Dubecco's modified essential medium |
| E | embryonic day |
| ECM | extracellular matrix |
| Edg | endothelial differentiation gene |
| Egr1 | early growth response element 1 |
| ENPP | ecto-nucleotide pyrophosphatase / phosphodiesterase |
| ERK | extracellular signal-regulated kinases |
| Ezh2 | enhancer of zeste homologue 2 |
| FCS | fetal calf serum |

| | |
|---|---|
| FGF | fibroblast growth factor |
| FN | fibronectin |
| GalC | galactocerebroside |
| GPCR | G protein-coupled receptor |
| HAT | histone acetyltransferase |
| HDAC | histone deacetylase |
| HMTase | histone methyltransferases |
| hpf | hours post fertilization |
| kDa | kilodalton |
| KO | knock-out |
| LPA | lysophosphatidic acid |
| LPAR | lysophosphatidic acid receptor |
| LPC | lysophosphatidylcholine |
| lysoPLD | lysophospholipase D |
| MAPK | mitogen- activated protein kinases |
| MBP | myelin basic protein |
| MO | morpholino |
| MOG | myelin oligodendrocyte glycoprotein |
| MORFO | modulator of oligodendrocyte remodeling and focal adhesion organization |
| mRNA | messenger RNA |
| MS | Multiple Sclerosis |
| Nkx2.2a | NK2 homeobox 2a |
| NPC | neural progenitor cells |

| | |
|---|---|
| NPP | nucleotide pyrophosphatase/phosphodiesterase |
| Olig1 | oligodendrocyte transcription factor 1 |
| Olig2 | oligodendrocyte transcription factor 2 |
| OLG | oligodendrocyte |
| OPC | oligodendrocyte progenitor cell |
| P | postnatal |
| P1 | primer 1 |
| P2 | primer 2 |
| PBS | phosphate-buffered saline |
| PDGF | platelet-derived growth factor |
| PDGFαR | platelet-derived growth factor alpha receptor |
| PLP | proteolipid protein |
| pMN | motor neuron progenitor domain |
| PNS | peripheral nervous system |
| qRT-PCR | quantitative RT-PCR |
| RNA | ribose nucleic acid |
| S1P | sphingosine-1-phosphate |
| SEM | standard error of mean |
| Shh | sonic hedgehog |
| siRNA | short interfering RNA |
| SPC | sphingosylphosphorylcholine |
| Tat | HIV-1- trans-activating protein |
| TSA | Trichostatin A |

| | |
|---|---|
| Ugt8 | 2-hydroxyacylsphingosine 1-beta-galactosyltransferase |
| VPA | Valporaic acid |
| WM | white matter |
| YY1 | Yin Yang 1 |

# ABSTRACT

Autotaxin in Central Nervous System Development and Disease

By Natalie A. Wheeler

A dissertation submitted in partial fulfillment of the requirements for the degree of Doctor of Philosophy at Virginia Commonwealth University

Virginia Commonwealth University, 2016

Advisor: Babette Fuss, Ph.D., Professor, Department of Anatomy and Neurobiology

During development, oligodendrocytes (OLGs), the myelinating cells of the central nervous system (CNS), undergo a stepwise progression during which OLG progenitors, specified from neural stem/progenitor cells, differentiate into fully mature myelinating OLGs. This progression along the OLG lineage is characterized by well-synchronized changes in morphology and gene expression patterns. The studies presented in this dissertation identified the extracellular factor Autotaxin (ATX) as a novel upstream signal modulating HDAC1/2 activity and gene expression in cells of the OLG lineage. Using the zebrafish as an *in vivo* model system, as well as rodent primary OLG cultures, this functional property of ATX was found to be mediated by its lysoPLD activity, which has been well-characterized to generate the lipid signaling molecule lysophosphatidic acid (LPA). LPA binds to Gprotein-coupled LPA receptors (LPARs) on the surface of OLGs to initiate downstream signaling events. ATX's lysoPLD activity was found to modulate HDAC1/2 regulated gene expression during a time window coinciding with the transition from OLG progenitor to early differentiating OLG. When looking further downstream of the ATX-LPA axis, down-regulation of LPA receptor 6 ($LPA_6$) was found

to reduce the expression of OLG differentiation genes as well as the overall process network area of OLGs. Thus, $LPA_6$ plays a role in both the gene expression and morphology changes seen in OLG differentiation. These findings prove useful for future therapeutic targets needed for demyelinating diseases of the CNS such as Multiple Sclerosis (MS), in which OLGs fail to differentiate into mature OLGs, needed for remyelination.

Additionally, white matter injury has been frequently reported in $HIV^+$ patients. Previous studies showed that HIV-1 Tat (transactivator of transcription), a viral protein that is produced and secreted by HIV-infected cells, is a toxic factor to OLGs. We show here that Tat treatment reduces the expression of OLG differentiation genes and the overall process network area of OLGs. Additionally, Tat-treated OLGs have reduced ATX lysoPLD activity and there is a physical interaction between Tat and ATX. Together, these data strongly suggest functional implications of Tat blocking ATX's lysoPLD activities and thus the ATX-LPA signaling axis proves to play a significant role in the development of OLGs.

# CHAPTER 1

## Introduction to Myelin, Oligodendrocytes and Influential factors

### Myelin and its functional significance

Communication throughout the brain relies on electrical signals between neurons. Just as wires need insulation, neurons require the lipid rich multilamellar myelin membrane for proper conduction. The highly insulated myelin membrane provides support for brain conductivity and can be considered a defining characteristic of vertebrates, though myelin-like sheaths have been found in invertebrates. Oligodendrocytes (OLGs) and Schwann cells are the cells responsible for producing myelin in the central nervous system (CNS) and peripheral nervous system (PNS), respectively.

To ensure electrical signals are maintained and transmitted throughout the body, ions pass through axons at areas of myelin gaps or so called “nodes of Ranvier.” This passage of ions helps to retain electrical signals, as they appear to “jump” from one node to another, and is therefore termed, saltatory conduction (Baumann and Pham-Dinh, 2001). Evolutionarily, myelin was one of the later structures of the nervous system to evolve (Baumann and Pham-Dinh, 2001; Hartline and Colman, 2007). As animals developed more sophisticated behaviors, the ability to act fast to capture or escape prey was needed and rapid conductance of nerve impulses became a high priority for the nervous systems of animals (Hartline and Colman, 2007). To allow for increased speed of conductance, larger axons could be used to decrease the overall resistance of the electrical signal and allow for faster conduction. This proves to be an impractical solution for mammals, however, as the conduction speed needed would result in a large

distribution of nerve fibers that would be disproportionate to their body size. The myelin membrane proved to circumvent this problem by allowing insulation to the axons, thereby increasing the resistance of the electrical field (Hartline and Colman, 2007). The myelin membrane serves as an integral part of the nervous system. Additionally, not only does myelin act as an insulator of axons, it is now known that myelin also provides axonal support (Saab et al., 2013). This idea becomes important when considering the consequences of myelin loss on axons in pathology. The significance of myelin becomes increasingly evident in pathological conditions where the myelin membrane is disrupted, such as in the demyelinating disease Multiple Sclerosis (MS).

**Multiple Sclerosis (MS)**

Multiple Sclerosis (MS) is the most common demyelinating disease, for which there is no present cure, and is usually seen in patients ranging from 20 to 50 years old, although it has been reported in individuals as young as 2 and as old as 75. Currently, there are approximately 2.3 million people worldwide affected by MS (Multiple Sclerosis Society, 2016). MS proves to be the leading cause of non-traumatic disability with symptoms encompassing vision loss, pain, fatigue, cognitive dysfunction and impaired coordination (Fox et al., 2006). Both the diagnosis and treatment of MS is difficult as the symptoms, severity and duration of MS can vary from person to person.

It is not clear as to the cause of MS, however, both genetic and environmental factors have been argued to play a role in the development of the disease (Hauser and Oksenberg, 2006). One of the environmental factors that may contribute to the disease is a deficiency in vitamin D, which is produced when the body is exposed to natural sunlight. The idea of a vitamin D deficiency in relation to MS was initially theorized when

an epidemiological study showed that MS cases tend to occur less frequently in populations of people living closer to the equator. This goes along with the idea that by living closer to the equator, a person would have more sun exposure and thus would make more vitamin D than those living farther away from the equator (Freedman et al., 2000; Raghuwanshi et al., 2008).

The genetic prolife of MS remains unknown and has not been strictly linked to heredity. Those who have a first-degree relative (parent or sibling) with MS, however, are more at risk of developing MS than the general population. Researchers have also speculated that individuals can be born with a genetic predisposition that makes them more sensitive to environmental agents that can cause the disease (Multiple Sclerosis Society, 2016). Genome-wide association studies have identified over a hundred polymorphisms with modest individual effects in MS susceptibility and confirmed the main individual effect of the Major Histocompatibility Complex (Burrell et al., 2011; Hoppenbrouwers and Hintzen, 2011). Additional immunological relevant genes were found significantly overexpressed (Gutierrez-Arcelus et al., 2016). These studies, however, involve patients diagnosed with MS and as such use blood or cerebrospinal fluid (CSF), thus, the result obtained cannot be used to address any potential genetic associations with parenchymal gene expression. Nonetheless, it is generally accepted that the genetic contribution to MS susceptibility remains to be defined. Additionally, there are certain risk factors including age, sex, race, smoking, infections, etc., that have been linked to MS (Mayo Clinic, 2016). Though the exact cause of MS is unknown, it is plausible that responsibility lies on the combination of genetic and environmental risk factors.

There are four main clinically defined forms of MS that can be classified as: relapsing remitting, primary progressive, secondary progressive and progressive-relapsing. RRMS is the most common form as 85% of patients start with this disease course. Patients with RRMS have periods of MS “attacks,” called relapses, followed by partial or complete recovery periods, known as remission. During remission, patients display improved symptoms with no apparent progression of the disease. Interestingly, patients suffering from RRMS have more brain lesions (plaques or scars) containing inflammatory cells. As time progresses, patients with RRMS may transition to secondary progressive MS (SPMS) (Multiple Sclerosis Society, 2016). Another form of MS, primary progressive MS (PPMS) is seen in roughly 10-15% of patients. PPMS is characterized by a steady, but gradual, worsening of neurologic functioning, without any distinct relapses or periods of recovery. People with PPMS tend to have more spinal cord lesions than cortical lesions (Multiple Sclerosis Society, 2016). Lastly the rarest form of MS is progressive relapsing (PRMS), with only 5% occurrence in the population. PRMS is characterized by a steady worsening disease course from onset with additional attacks of more severe neurological symptoms. Some PRMS patients experience times of remission, although this is not true for all patients (Multiple Sclerosis Society, 2016). Due to the capricious symptoms, severity and progression of MS, it is sometimes difficult to classify as well as treat patients with MS.

As MS is classified as an autoimmune disease, current therapies target the inflammation side of the disease. These therapies, however, fail to treat the loss of myelin or any axonal damage caused by the disease. Though these treatments help patients short term, remyelination by OLGs and axonal repair is needed to correctly

cure the disease. In this therapeutic paradigm, remyelination of axons, by OLGs, will reinstate the proper neural circuitry needed for normal brain activity. Interestingly, OLG progenitor cells (OPCs) are found in MS lesions, however, they are limited in their ability to remyelinate or remyelinate sufficiently (Bradl and Lassmann, 2010; Chang et al., 2002a; Goldschmidt et al., 2009). Therefore, with the notion that regeneration of the myelin sheath follows the same mechanisms present during development, obtaining a better understanding of OLG development from a progenitor cell to a fully myelinating cell is integral to target specific mechanisms that are altered in demyelinated conditions.

**Oligodendrocyte specification in the Central Nervous System (CNS)**

OLGs were originally discovered by Rio Hortega in 1921 (Iglesias-Rozas and Garrosa, 2012). Though the cellular origins of this myelinating cell in the brain and spinal cord have been debated, research advances using transgenic mouse models have given us insight into OLG specification (Richardson et al., 2006). CNS cell initiation and proliferation develops within distinct layers and zones, of neuroectodermal origin, where each zone comprises distinct cell types and morphologies (Brazel et al., 2003; Marshall et al., 2003; Pringle et al., 1996; Richardson et al., 2006; Woodruff et al., 2001). The ventricular zone of the brain is the first to develop and houses the origin of neurons, as well as some astrocytes. This zone is made of pseudostratified epithelial-like tissue consisting of neuroectodermal tissue (Kettenmann and Ransom, 2013). As development progresses, a new proliferative area, the subventricular zone, begins to thicken and remains actively proliferative during early postnatal development (Brazel et al., 2003). Cortical progenitor cells follow a developmental sequence in which cell types develop in temporally distinct, yet overlapping patterns beginning with neuronal

development, followed by astrocyte development, and lastly OLG development (Sauvageot and Stiles, 2002; Spassky et al., 1998, 2000).

During development, OPCs are generated in sequential waves from specific germinal regions. OPCs arise from the ventricular zone of the spinal cord and the ventral forebrain of the developing brain (Baracskay et al., 2007; Brazel et al., 2003; Kettenmann and Ransom, 2013; Levison et al., 1993; Marshall et al., 2003; Privat and Leblond, 1972) (Kessaris et al., 2006). Research conducted in the rat elucidated that there are multiple areas along the ventral and dorsal axes of the spinal cord that produce OLGs and that OLGs originate in subventral regions and later move to more dorsal regions. Starting around E12.5, the pMN (motor neuron progenitor) domain of the spinal cord produces 85-90% of the OPCs (Miller, 1996; Pringle and Richardson, 1993; Pringle et al., 1996; Richardson et al., 1988, 2006; Woodruff et al., 2001). This is followed by a second wave of OPC genesis emanating from more dorsal progenitor domains starting at E15.5 (Cai et al., 2005a; Fogarty et al., 2005). Dorsally-derived progenitors only contribute 10-15% of adult OLGs.

In the developing forebrain, OPCs also migrate in a series of waves. At about E12.5 in mice (E5-6 in chicks), the initial wave of OPC production unfolds in the medial ganglionic eminence and the closely associated enteropeduncular area of the ventral telencephalon (Olivier et al., 2001; Spassky et al., 2001; Tekki-Kessaris et al., 2001). These ventrally-derived OPCs then migrate into the cortex (Kessaris et al., 2006; Richardson et al., 2006) and can be observed throughout the cortex around E18 (Kessaris et al., 2006; Richardson et al., 2006; Woodruff et al., 2001). The second and third wave of OPCs emanating from the lateral and caudal ganglionic eminences, at

E15.5 and from the cortex after birth, give rise to the majority of adult OLGs in mice (Brazel et al., 2003; Kessaris et al., 2006; Richardson et al., 2006; Woodruff et al., 2001). Additionally, OLGs origin in the brain surfaces in the medial and lateral ganglionic eminences, which are considered to be transient and only appear present during embryonic development (Brazel et al., 2003; de Castro and Bribián, 2005; Kessaris et al., 2006; Richardson et al., 2006; Woodruff et al., 2001). Though some differences are seen, the overall spatiotemporal specification of OLGs originate in the ventral regions of the brain and spinal cord, and as development continues, these cells migrate in a radial dorsolateral migration pattern (Cai et al., 2005b; Emery, 2010; Fogarty et al., 2005; Richardson et al., 2006; Vallstedt et al., 2005). Specification of OPCs is highly regulated and requires the expression of essential transcription factors. Sox9 and Olig2 are two early transcription factors that are necessary for specification into the OLG lineage (Ben-Hur et al., 2003; Stolt et al., 2003; Zhou and Anderson, 2002). Olig2 then induces the expression of Sox10, Nkx2.2, and platelet-derived growth factor (PDGFR)-alpha (Cai et al., 2005b; Liu et al., 2007; Vallstedt et al., 2005; Zhou et al., 2001).

OLG specification, development and myelination in the zebrafish share many similarities with the mammalian system (Buckley et al., 2008; Czopka, 2016; Preston and Macklin, 2015; Sidik and Talbot, 2015). The development of the transient, embryonic midline structure, the notochord, is essential for OLG specification in the spinal cord (Stemple, 2005). The notochord is required for the formation of the dorsal-ventral axis of the overlying neural tube, which includes the specification of the floor plate, the ventral-most portion of the spinal cord (Dodd et al., 1998; Placzek and

Briscoe, 2005; van Straaten and Hekking, 1991; van Straaten et al., 1989). OPCs are generated adjacent to the floor plate in the same location that gives rise to motor neurons, named the motor neuron progenitor domain (Noll and Miller, 1993; Pringle and Richardson, 1993; Warf et al., 1991; Yu et al., 1994) and specification of OPCs begins when motor neuron production has ended (Park et al., 2004; Zhou and Anderson, 2002).

**Oligodendrocyte development**

OLG differentiation is an essential part of overall OLG development, with the notion that many progenitor cells are present at lesion sites in MS, but fail to properly differentiate and develop further along the lineage (Kuhlmann et al., 2008a). This crucial step is highlighted throughout my dissertation, as it is the main focus of my studies regarding overall OLG development. OLG development can be characterized by four different stages identified by both the expression of specific cell markers (surface antigens, transcription factors, etc.) as well as changes in cellular morphology (Baumann and Pham-Dinh, 2001; Bradl and Lassmann, 2010; Pfeiffer et al., 1993). These markers display specific functions and are needed for proper development along the lineage (Fig.1.1)

Early stages of OLG development can be recognized by the presence of certain genes, cell surface gangliosides, as well as mitogens. Both Olig2 and Sox10 are expressed early in OLG development and remain expressed throughout the lineage in rodents (Liu et al., 2007). In addition to these early markers, in the rodent model system, the antibody A2B5 can be used to identify cell surface gangliosides found on OPCs. The lipids recognized by A2B5 are down-regulated as the cell differentiates into

a more mature OLG (Baracskay et al., 2007; Baumann and Pham-Dinh, 2001; Bradl and Lassmann, 2010; Pfeiffer et al., 1993; Raff et al., 1983, 1984). In the early stages of OLG development, mitogens, specifically platelet-derived growth factor (PDGF) and basic fibroblast growth factor (bFGF), are present in order to increase cell survival, aid in cell migration and proliferation, and prevent cell differentiation (Fok-Seang and Miller, 1994; Gard and Pfeiffer, 1993; Hart et al., 1989a, 1989b; Pringle and Richardson, 1993; Richardson et al., 1988). Platelet derived growth factor receptor alpha (PDGFRα) is specifically expressed in immature OPCs, but its expression is rapidly extinguished as OPCs undergo terminal differentiation (Gard and Pfeiffer, 1993; Pringle and Richardson, 1993; Richardson et al., 1988).

As OLG development progresses, there is a decline in mitogenic factors and OLGs are instead introduced to the differentiating factor thyroid hormone (TH). Both the removal of mitogens and TH are necessary for OPC differentiation (Barres et al., 1994; Franco et al., 2008). At this stage, OLGs start to display a multipolar morphology that can be identified by the mouse monoclonal antibody O4, which binds to an uncharacterized surface antigen (POA) and sulfatide (Bansal et al., 1989, 1992). *Cnp, Ugt8, Mbp* and *Plp* are induced immediately after mitogen withdrawal and TH exposure (Dugas et al., 2006). CNP (2',3'-cyclic nucleotide 3'-phosphodiesterase) activity appears to be one of the earliest events in OLG differentiation and thought to play a critical role in the events leading to myelination. It has also been seen in uncompact myelin in the paranodal loops (Nave and Trapp, 2008; Wells and Sprinkle, 1981). When CNP is overexpressed in mice, premature and abnormal myelination is observed and when overexpressed *in vitro,* it promotes process outgrowth (Lee et al., 2005; Nave and

Trapp, 2008). *Cnp1* null mutant mice, although fully myelinated, develop progressive axonopathy and die prematurely (Edgar et al., 2009; Lappe-Siefke et al., 2003), thereby suggesting its role in axonal support. UGT8 (UDP- galactose ceramide galactosyltransferase 8) is an endoplasmic reticulum-localized enzyme (Kapitonov and Yu, 1997; Schulte and Stoffel, 1993; Sprong et al., 1998) that is responsible for the synthesis of galactosylceramide, the major glycosphingolipid of myelin produced by OLGs (Marcus and Popko, 2002). A knock-out (KO) mouse model lacking UGT8 revealed that galactosylceramide, together with sulfatide, is involved in myelin function and stability, but not in myelin biogenesis (Bosio et al., 1996; Coetzee et al., 1996; Dupree et al., 1999).

Two extensively studied myelin genes that encode major myelin protein components in the CNS are *Mbp* (myelin basic protein) and *Plp (*proteolipid protein). Membrane associated MBP is abundant in myelin, representing 30% of the total myelin protein and is significantly involved in the compaction and binding of opposing cytoplasmic myelin membranes (Readhead et al., 1990)**.** In the *shiverer* mouse line, in which MBP is absent, hypomyelination and the formation of uncompact myelin is apparent in the CNS (Readhead and Hood, 1990; Readhead et al., 1990; Shine et al., 1990)**,** therefore solidifying its significance in the generation of myelin. PLP, a 4-pass transmembrane protein, is thought to mediate adhesion between the outer membranes of the myelin sheath (Baumann and Pham-Dinh, 2001; Popot et al., 1991)**.** Interestingly, PLP has a splice variant with the name DM20 (Campagnoni, 1988; Nave and Trapp, 2008; Timsit et al., 1995) that is expressed earlier in OLG development and is later followed by the expression of PLP (Timsit et al., 1995)**.** Mice harboring the *jimpy*

mutation, the first *Plp* mutation identified, express a reduction in OLGs and display thin myelin, ultimately leading to premature death (Duncan et al., 1989; Knapp et al., 1986). The phenotypic response seen in the *jimpy* mice is a result of protein misfolding in the mutant PLP (Griffiths et al., 1998a, 1998b). Conversely, and similar to what is seen in *Cnp1* null mutant mice, *Plp1*-null mice, in which the *Plp1* gene is inactivated, show no signs of OLG or myelin loss, however, older age mutant mice develop progressive axonopathy throughout the CNS, with transport defects, swellings and widespread axonal degeneration. Since the prominent axonal transport defects in *Plp1* null mutant mice (Edgar et al., 2004) resemble those observed in mitochondrial disorders (Ferreirinha et al., 2004; Tarrade et al., 2006), it is suggested that OLGs require PLP to support the axonal energy metabolism.

**OLG development in the zebrafish**

As seen in the mammalian system, gene regulation plays a large role in the timely development and differentiation of OLGs. To start, *olig1* and *olig2* are expressed in cells of the motor neuron domain, containing both OPCs and motor neurons (Zhou and Anderson, 2002; Zhou et al., 2001). It has been shown, in both mice and zebrafish, that *olig2* is necessary for the specification of both motor neurons and OLGs (Park et al., 2002; Takebayashi et al., 2002; Zhou and Anderson, 2002). Additionally, *olig1* expression in the zebrafish is important in OLG differentiation and can activate MBP transcription as seen in the mouse (Li et al., 2007; Xin et al., 2005). Near the end of embryogenesis and during postnatal stages, many OPCs stop dividing and differentiate to become mature myelinating cells, whereas others persist as nonmyelinating cells. The expression of *nkx2.2a* (NK2 transcription factor 2a) was found to be a prominent

factor in this fate determining step as OPCs that express *nkx2.2a* were found to differentiate as OLGs, whereas those that did not express the gene mostly remained nonmyelinating OPCs (Kucenas et al., 2008). Thus, *nkx2.2a* promotes the specification and differentiation of a myelinating subset of OLG lineage cells (Kucenas et al., 2008).

In order for differentiation of OLGs to occur in the zebrafish, the expression of genes such as *cldnk* (claudink) and *plp1b* (proteolipid protein) are needed. Genechip analysis studies revealed *cldnk* and *plp1b* to be among 119 genes predicted to be expressed at elevated levels in differentiating OLGs (Takada and Appel, 2010). Additionally, microarray screen analysis studies indicated that these genes are highly elevated in mature OLGs (Chung et al., 2011). Thus, both genes prove important in the crucial differentiation stage of OLG development, and remain expressed into mature stages. The relevance of *cldnk* in OLG maturation can be inferred as it encodes a protein that is a member of a family of tight junction components and is expressed specifically in OLGs and Schwann cells associated with the lateral line (Takada and Appel, 2010). Likewise, *plp1b* encodes proteolipid protein 1b, whose importance has been extensively studied in the mammalian system with regards to OLG development and myelination. In addition to these genes, *mbp* and *p0* appear later in OLG development showing initial expression at 48hpf in cells of the ventral medial hindbrain and at 72hpf in cells of the spinal cord (Brösamle and Halpern, 2002; Buckley et al., 2010). The overall functions of the above stated genes have not been thoroughly studied in the zebrafish, however, conservation of their predicted protein sequences with those of the mammalian sequences and their overall expression patterns make it

likely to predict they serve similar functions (Brösamle and Halpern, 2002; Buckley et al., 2008, 2010).

All together, in both mammalian and zebrafish systems there are many steps along the developmental pathway of OLGs. The timing of gene expression and extracellular factors alike contribute to the precise maturation of these cells. It is crucial that the mechanisms behind each stage of development be understood to the highest degree, so that progenitor cell maturation can be obtained. As previously discussed, OPCs are present and recruited to MS lesions initially, however, they become depleted over time and fail to develop into mature cells (Kuhlmann et al., 2008b). The limitations of remyelination seen in MS lesions suggests that though myelination is possible, OPCs need to be stimulated in order to become fully myelinating cells and this action must remain consistent. One molecule known to stimulate OLG differentiation is the extracellular protein, Autotaxin (ATX) (Dennis et al., 2005, 2008; Fox et al., 2003; Fuss et al., 1997; Nogaroli et al., 2009a; Yuelling and Fuss, 2008; Yuelling et al., 2012). Its importance in MS became increasing interesting when ATX expression was found reduced in MS lesions (Comabella and Martin, 2007). Thus, further investigation of this extracellular protein in OLG development could pave the way towards potential targets for MS treatment.

**Autotaxin**

Autotaxin (ATX), also known as ecto-nucleotide pyrophoshatase/phosphodiesterase (ENPP)2, was first introduced as a cell motility-stimulating factor in human melanoma cells (Stracke et al., 1992), and has since been extensively studied in different areas of research. Though initially ATX did not exhibit

any significant homologies to characterized motility and growth factors, ATX was found to contain a domain that displayed high homology with the enzymatically active domain of proteins known to possess nucleotide phosphodiesterase and pyrophosphatase activity (Buckley et al., 1990; Culp and Butler, 1985; van Driel and Goding, 1987; Murata et al., 1994). It was later discovered, through recombinant forms of ATX, that the catalytic domain of ATX is crucial for motility stimulation (Lee et al., 1996). This enzymatic activity led to the inclusion of ATX into the family of nucleotide pyrophosphatase/phosphodiesterase (NPP)-type ectophosphodiesterases and was additionally termed (E)NPP2 (Bollen et al., 2000; Goding et al., 2003; Stefan et al., 2005). The idea that ATX possessed enzymatic activity prompted the finding that all (E)NPPs hydrolyze both pyrophosphate and phosphodiester bonds present in nucleotides and their derivatives (Bollen et al., 2000). Although at the time the physiological substrates of (E)NPPs remained unidentified, it was later uncovered that, though structurally related, (E)NPPs differ in their enzymatic substrate specificities (Cimpean et al., 2004; Gijsbers et al., 2001; Stefan et al., 2005). A turning point in research related to ATX later revealed that ATX's enzymatic activity catalyzed the conversion of extracellular lysophosphatidylcholine (LPC) to the lipid mediator, lysophosphatidic acid (LPA), and displayed molecular identity to the extracellular lysoPLD (Ferry et al., 2003; Tokumura et al., 2002; Umezu-Goto et al., 2002; Xie and Meier, 2004). Moreover, the affinity for ATX towards LPC was significantly greater than its affinity towards nucleotides (Tokumura et al., 2002; Umezu-Goto et al., 2002). Currently, the phosphodiesterase activity of ATX is considered unlikely (Gijsbers et al.,

2003; van Meeteren et al., 2006). The lysoPLD properties of ATX remain the focus of my research with regard to the effects of ATX on OLG differentiation in the CNS.

ATX is synthesized as a pre-pro-enzyme and, after N-glycosylation and proteolytic maturation, is secreted as an active lysoPLD along the classical secretory route (Jansen et al., 2005; Koike et al., 2006). Additionally, ATX is seen present in the circulation where it accounts for maintaining plasma LPA levels. This circulating ATX has a short half-life as it is rapidly cleared by the liver (Jansen et al., 2009). The brain displays relatively high expression levels of ATX, especially in the choroid plexus, along with the spinal cord, ovary, lung, intestines, kidney and lymphoid organs, and CSF (Kanda et al., 2008; Koike et al., 2010; van Meeteren et al., 2006; Nakamura et al., 2009; Nakasaki et al., 2008; Tanaka et al., 2006). Currently, three splice variants/isoforms of ATX have been identified in both human and mouse, referred to as ATX α, β, and γ, that do not seem to display any major functional isoform differences, although show characteristic expression patterns (Fuss et al., 1997; Giganti et al., 2008; Lee et al., 1996).

It wasn't until the creation of ATX knockout (KO) mice (*Enpp2*$^{-/-}$mutants) that the physiological importance of ATX was revealed. *Enpp2*$^{-/-}$ mice displayed embryonic lethality (E9.5–E11.5) due to prominent vasculature and neural tube defects (van Meeteren et al., 2006; Tanaka et al., 2006). Intriguingly, mice expressing ATX with inactivated lysoPLD activity displayed the same embryonic lethality that was previously observed in *Enpp2*$^{-/-}$ mice (Ferry et al., 2007). Heterozygote *Enpp2*$^{-/+}$ mice survived until adulthood and, interestingly, revealed to have LPA plasma levels that were half that of wild-type mice; thus confirming the notion that ATX activity is the major source of LPA in

plasma. Accordingly, the ATX-LPA signaling axis is essential for the formation of the vasculature and neural tube and proper embryonic development, though these effects may be secondary to the vasculature effects.

**ATX: enzymatic activity via the catalytic lysoPLD active site**

The cell motility effect of ATX was originally thought to be due to ATX's reported function as a nucleotide phosphodiesterase (Bollen et al., 2000), however, it later became clear that the cell motility-stimulating activity of ATX is mediated, at least in part, via the production of LPA and its action on its respective LPA receptors (Hama et al., 2004; Lee et al., 1996; Okudaira et al., 2010). ATX's NPP activity was known to be dependent on a single threonine residue located within the enzymatic active site (Clair et al., 1997), which was ultimately found to be the same residue critical for ATX's lysoPLD activity (Gijsbers et al., 2003; Koh et al., 2003). In addition to the threonine residue, it was revealed that the lysoPLD activity was also stringent upon sequences within the N- and C-terminal domains of ATX, a finding unique to ATX (Cimpean et al., 2004; Gijsbers et al., 2003; Stefan et al., 2005). Since these initial findings, a number of studies have set forth to further characterize the functions of ATX's lysoPLD active site.

ATX's enzymatic lysoPLD activity has been shown to play a large role in biological processes related to development, as well as those in pathological conditions. The best-known cellular responses to LPA include the stimulation of cell migration, proliferation, and survival, although inhibitory responses have also been implicated (Jongsma et al., 2011; Oda et al., 2013). The ATX-LPA signaling axis has been implicated in a variety of physiological and pathological processes, including lymphocyte homing, pulmonary fibrosis, neuropathic pain, cardiovascular disease, cholestatic

pruritus, tumor progression, Alzheimer's disease, chronic Hepatitis C, obesity and rheumatoid arthritis, and as outlined in this dissertation, Multiple Sclerosis (Bai et al., 2013; Boucher et al., 2005; Ferry et al., 2003; Hammack et al., 2004; Inoue et al., 2011, 2004, 2008a, 2008b; Kanda et al., 2008; Kremer et al., 2010; Oikonomou et al., 2012; Santos et al., 1996; Smyth et al., 2014; Tager et al., 2008; Watanabe et al., 2007a, 2007b; Zhang et al., 2012; Zhao et al., 2008). Importantly, LPA has also been described to be a regulator of epigenetic modifications, specifically histone deacetylase (HDAC) regulation, at least in cancer cell lines (Ishdorj et al., 2008). In an attempt to link ATX's lysoPLD activity with the known epigenetic changes seen throughout OLG development, I investigated the gene regulatory mechanisms controlled by ATX's lysoPLD activity during OLG differentiation.

**Epigenetic Regulation in OLG Development**

Epigenetics refers to the study of changes in gene expression, that may or may not be heritable, without changing the sequence of DNA. Epigenetic modifications include DNA methylation, post-translational modification of histone tails, nucleosomal remodeling, and modifications by small non-coding RNAs (Berger, 2007; Goldberg et al., 2007). Post-translational modifications include acetylation/deacetylation, methylation (Shilatifard, 2006), phosphorylation of serine and threonine residues (Dyson et al., 2005), sumoylation (Iñiguez-Lluhí, 2006), ubiquitination of lysine residues(Shilatifard, 2006; Weake and Workman, 2008), and citrullination of arginine residues (Mastronardi et al., 2006), as well as ADP- ribosylation and isomerization of prolines (Kouzarides, 2007). These modifications make up the "histone code" that is cell-type specific. A dynamic balance of these modifications dictates the transcriptional state of chromatin,

as some histone changes confer a more open and transcriptionally competent state and others silence gene activation by chromatin compaction.

Epigenetic regulation of gene expression during OLG development has recently been recognized as a fundamental contributing player in (re)myelination. It is anticipated that insights into the epigenetic regulation of myelin formation and repair will provide novel targets for therapeutic intervention (Copray et al., 2009). OLGs need to go through several steps of development before ultimately producing myelin. A large network of transcriptional activators and repressors are known to control each stage (Miller, 2002; Wegner, 2008). With regard to differentiation, Olig1, Olig2, Sox10 and more recently myelin gene regulatory factor (Myrf) are needed in order to terminally differentiate and activate myelin protein expression (Ben-Hur et al., 2003; Emery et al., 2009; Liu et al., 2007; Stolt et al., 2002; Xin et al., 2005). In addition, inhibitors of OLG differentiation are needed in order to fine-tune this transcriptional network and prevent precocious differentiation. These inhibitors include Hes5 (Kondo and Raff, 2000a; Liu et al., 2006), Sox11 and Tcf4 (He et al., 2007a), and Id2 and Id4 (Kondo and Raff, 2000b; Marin-Husstege et al., 2002; Samanta and Kessler, 2004). Selective expression or silencing of genes at each stage of OLG development is ultimately controlled by epigenetic regulatory mechanisms, which determine the accessibility of the transcriptional machinery to the chromosomal territories containing the specific genes (Copray et al., 2009).

Though increasing evidence points to the substantial role for HDACs in OLG development, which will be further elucidated, methylation serves to play a fascinating role as well. Histone methyltransferases (HMTases) are histone-modifying enzymes that

catalyze the transfer of methyl groups to lysine and arginine residues. Distinct enzymes mediate methylation of specific residues. A prominent HMTase that catalyzes histone H3 lysine 27 trimethylation (H3K27me3) is enhancer of zeste homologue 2 (Ezh2). It has been shown that methylation at H3K27 by Ezh2 plays a role in the specification of the OLG lineage. Ezh2 is completely down-regulated during specification towards neurons and astrocytes allowing transcription of these programs (Sher et al., 2012). Ezh2 expression is present in the early proliferating OPCs up to the stage of premyelinating OLGs. Ezh2 expression is down-regulated, however, in mature OLGs at the onset of myelination

**Introduction to HATs and HDACs**

One of the best-characterized histone modifications that modulate OLG development is the equilibrium between histone acetylation and deacetylation (Copray et al., 2009). Histone acetyltransferases (HATs) and histone deacetylases (HDACs) finely tune cellular acetylation, targeting not only histones, but also numerous proteins with key roles in cell metabolism, signaling and death (Kazantsev and Thompson, 2008; Langley et al., 2005; Saha and Pahan, 2006). HATs provide for acetylation of the conserved N-terminal histone tails, resulting in relaxation of the nucleosomes by decreasing the interaction of the positively charged histone tails with the negatively charged phosphate backbone of DNA. HATs have been shown to play an important role in neural stem cell differentiation (Asklund et al., 2004; Hsieh et al., 2004; Song and Ghosh, 2004), however, the role of HATs in OLG differentiation is less pronounced. In fact, deacetylation by HDACs has been shown to play a more critical role in the progression of progenitor cells toward the OLG lineage.

In most cases, HDACs remove the acetyl groups from histone lysine residues favoring condensed chromatin that prevents access of transcriptional activators to their target sites and results in transcriptional repression. The mammalian members of the HDAC family are, based on their structures, subdivided into four main classes: Class I (HDAC1, 2, 3, and 8), Class II (HDAC4, 5, 6, 7, 9, and 10), Class III (SIRT1-7) and Class IV (HDAC11). The classical, class I, II and IV, HDACs are structurally related and need the presence of $Zn^{+2}$ to be active (de Ruijter et al., 2003), whereas class III HDACs, the sirtuins, are a group of enzymes dependent on $NAD^{+}$ and are structurally unrelated to the classical HDACs (Michan and Sinclair, 2007).

OLG specification is unique in that it is initiated by a global histone deacetylation program. During the early stages of OLG specification, HDACs mediate the suppression of alternative lineages and, later in development, regulate the repression of inhibitors of myelin specific genes. HDAC inhibition by trichostatin A (TSA) in neural stem cells favors the neuronal fate, while inhibiting specification into OPCs. The loss of HDACs also reprograms OPCs into neural stem-like cells capable of neurogenesis (Aixiao Liu, 2007; Kondo and Raff, 2004; Lyssiotis et al., 2007a). More specifically, HDACs block critical transcription factors of alternative lineages such as the stem cell marker Sox2 (Lyssiotis et al., 2007a; Shen and Casaccia-Bonnefil, 2008). Taken together, HDAC inhibition results in the reactivation of other genes that mark the stem cell state, along with the silencing of OLG lineage-specific genes (Lyssiotis et al., 2007b). The importance of histone deacetylation in determining the direction of neural stem cell specification is further supported by evidence in which HDAC inhibitors cause a

noticeable reduction in OPCs on the account of a larger population of astrocytes and neurons (Aixiao Liu, 2007; He et al., 2007a; Siebzehnrubl et al., 2007; Ye et al., 2009).

Once specification has taken place, HDACs continue to serve a crucial role in the differentiation stage of OLG development. The timely differentiation of progenitor cells is indispensable for development. With that in mind, investigators demonstrated deacetylation of histone H3 is a critical mechanism for myelination onset *in vivo* as it is required for the down-regulation of differentiation inhibitors and early progenitor markers. During the first 10 postnatal days in rats, administration of valproic acid (VPA, a Class I HDAC inhibitor) resulted in significant hypomyelination, while administration of VPA after onset of myelination had no effect on myelin gene expression. During the time after the onset of myelination, a more stable repression of the transcriptional inhibitors of the myelin genes is carried out by methylation at H3K9 (Shen and Casaccia-Bonnefil, 2008). This methylation is coupled with increased association of HP1, a protein that directs chromatin compaction by binding to adjacent H3K9 sites. These results thereby indicate that histone deacetylation is the molecular link of the transition between cell cycle exit and differentiation onset (Shen and Casaccia-Bonnefil, 2008). Additionally, pharmacological inhibitors of HDACs increase histone acetylation and prevent differentiation of OLG progenitors *in vitro (*Hsieh et al., 2004; Marin-Husstege et al., 2002) and *in vivo* (Aixiao Liu, 2007; Shen et al., 2005). Accordingly, in the rodent model, HDACs prove to be necessary for OLG development, not only for OPC specification, but also for differentiation.

As just described, HDAC inhibition is correlated with the induction of Sox2 and increased neurogenic capacity from treated OPCs (Kondo and Raff, 2004; Lyssiotis et

al., 2007a). Unlike rodent OPCs, however, acutely isolated human OPCs express both Sox2 protein and mRNA (Sim et al., 2011) and are neurogenic in the absence of reprogramming (Tripathi et al., 2010). These observations led to the idea that the role of HDACs on OLG development may differ between species. This was further tested by treatment with HDAC inhibitors, TSA and sodium butyrate, on human primary OPCs. HDAC inhibition (HDACi) resulted in significant dose-dependent inhibition of O4+ OLG cell differentiation, reduction of OLG morphological maturation and down-regulation of *Mbp* mRNA (Conway et al., 2012). Along with these results, HDACi treatment prevented down-regulation of Sox2, Id4 and Tcf4/Tcf7l2 mRNAs, but did not regulate Hes5 (Conway et al., 2012). Thus, suggesting that HDAC activity plays an essential role in the specification of OPCs (rodent), as well as the differentiation of progenitor cells into OLGs (rodent, human). Interestingly, studies describing the role of the ATX-LPA axis in epigenetic modulation of OLGs, presented in this dissertation, are limited to OPCs committed to the lineage and have no effect on specification. These data parallel what is seen in the human and further signifies the importance of ATX in OLG differentiation. Pharmacological inhibition of HDACs provided for a clear proof of concept that histone deacetylation is crucial for OLG development, however, the identification of individual members of the HDAC family was, and partly remains, the next step into understanding the role of HDACs in OLG differentiation.

**Regulation by HDAC1 and HDAC2**

HDAC1 and HDAC2 are of particular interest in OLG development as they have been reported to be recruited to the promoters of inhibitory molecules of myelin specific genes to initiate OLG differentiation (Dewald et al., 2011; He et al., 2007a; Shen and

Casaccia-Bonnefil, 2008; Ye et al., 2009). The RE1-silencing transcription factor (REST) recruits HDAC1 and HDAC2 to stimulate OPC differentiation by repressing several neuronal genes and thereby favoring glial cell specification (Dewald et al., 2011). In mice, conditional ablation of *Hdac1* and *Hdac2* results in the stabilization and nuclear translocation of β-catenin, which negatively regulates OLG specification by repressing *Olig2* expression (Ye et al., 2009). A severe impairment in the formation and differentiation of OPCs was observed in these double KO mice. Furthermore, mouse genetic approaches identified Yin Yang1 (YY1) as the essential transcription factor that facilitates the recruitment of HDAC1 to the promoters of the transcriptional inhibitors, Tcf4 and Id4, allowing for expression of myelin specific genes (He et al., 2007a). These data indicate that HDAC1 and HDAC2 are required for both specification and differentiation of OPCs.

Moreover, the role of HDAC1 activity in OLG development appears to be conserved across a wide range of species. In *hdac1* zebrafish mutants, specification of OPCs fails, but persistence of neural progenitors in the hindbrain ventricular zone is independent of *hdac1* activity (Cunliffe and Casaccia-Bonnefil, 2006). zHDAC-1 null neural stem cells continue to express Sox2 and fail to express Olig2 required for specification into the OLG lineage. In addition, sonic hedgehog (Shh) is normally expressed in the zHDAC-1 mutant hindbrain, however, it's signaling is inefficient in inducing Olig2 expression (Cunliffe and Casaccia-Bonnefil, 2006). Thus, the global deacetylation program initiated by HDACs, especially specific isoforms of Class I HDACs, enables expression of the OLG transcriptional profile.

In a different study, Nkx2.2 recruited the HDAC1/mSin3a complex to repress the

MBP promoter in immature OLGs (Wei et al., 2005). In addition, Nkx2.2 binds to and represses the promoter of the class III HDAC Sirt2 in CG4 cells, an oligodendroglial precursor cell line, and Sirt2 promoted the differentiation of CG4 cells (Ji et al., 2011). Similarly, HDAC1/2 heterodimers, in association with Sin3B, were detected in complex with Myt-1 on the proximal region of the PLP promoter (Romm et al., 2005). These results may appear contradictory to the described functions of HDAC1 in promoting OLG differentiation, however, it is also conceivable that tightly regulated repression of precocious differentiation may be a prerequisite to adequate OLG lineage progression (Jacob et al., 2011).

**The Role of Histone Deacetylation on Later Stages of Oligodendrocyte Development**

Not only do HDACS play a crucial role in the actual generation and differentiation of early OLGs, but they also act on immature OLGs (after established lineage choice) up to the onset of myelination. Histone deacetylase 11, HDAC11, plays a distinct role in OLG development. HDAC11 catalyzes deacetylation of lysine 9 and 14 on histone H3 (H3K9; H3K14) and it has been proposed to activate the expression of both, *MBP* and *PLP* genes, possibly by modulating specific regulatory regions (Liu et al., 2009). Indeed, disruption of HDAC11 expression increased acetylation at the promoter region of both *MBP* and *PLP* and led to a subsequent decrease in their transcript levels (Liu et al., 2009). In accordance to these studies, in the mouse brain, HDAC11 shows strong expression in OLGs that increases during postnatal development (Liu et al., 2008). These studies support an important function of HDAC11 in OLG terminal differentiation and myelination.

Histone modifications have been shown to display an important role in OLG development along the lineage and have such been studied in a more clinical standpoint by examining modifications in patients suffering from MS. Brain samples revealed that there is a shift toward histone acetylation in the white matter of the frontal lobes of aged subjects and in patients with chronic MS (Pedre et al., 2011). These changes were associated with high levels of transcriptional inhibitors of OLG differentiation, *TCF7l2*, *ID2* and *SOX2*, and higher HAT transcript levels, *CBP* and *P300*, in female MS patients compared with non-neurological control and correlated with disease duration (Pedre et al., 2011). These data suggest that histone deacetylation is a process that occurs at the early stages of the disease, and displays decreased efficiency with disease duration. The role of HDACs on OLG development is increasingly critical to understand, as it proves to be involved in essential stages and plays a role in disease pathology.

**Conclusions**

There are many mechanisms that regulate both the specification and development of OLGs. With regards to MS, it is imperative that we gain a better understanding of these mechanism in order to stimulate the specification of OPCs or, and more suitable for lesions in which adult OPCs are present, drive differentiation of progenitor cells into cells with the capacity to (re)myelinate. To achieve functional maturity of OLGs needed for (re)myelination, there must be a dynamic chemistry between extrinsic and intrinsic signals. Epigenetic modifications have been shown to play a large role in OLG development. The rate and type of these modifications in OLGs is controlled by many factors and depends on the developmental stage and health of

the cells (Copray et al., 2009).

The data presented in this dissertation reveal the discovery of the first extracellular signal, ATX, that regulates HDAC activity in the transition from progenitor cells to OLGs (differentiation), which is indispensable for proper OLG development. As OPCs are found in MS lesions, but are limited in their ability to differentiate, this step becomes a crucial area of investigation when searching for therapeutic advances. The novel finding that ATX, through its ability to form LPA via the lysoPLD active site, regulates the epigenetic modifications needed for proper OLG differentiation is a turning point in the field, and further shows its importance in OLG development. The role that the ATX-LPA- epigenetic regulatory pathway plays in relation to MS is so impacting, they may offer to be future therapeutic targets.

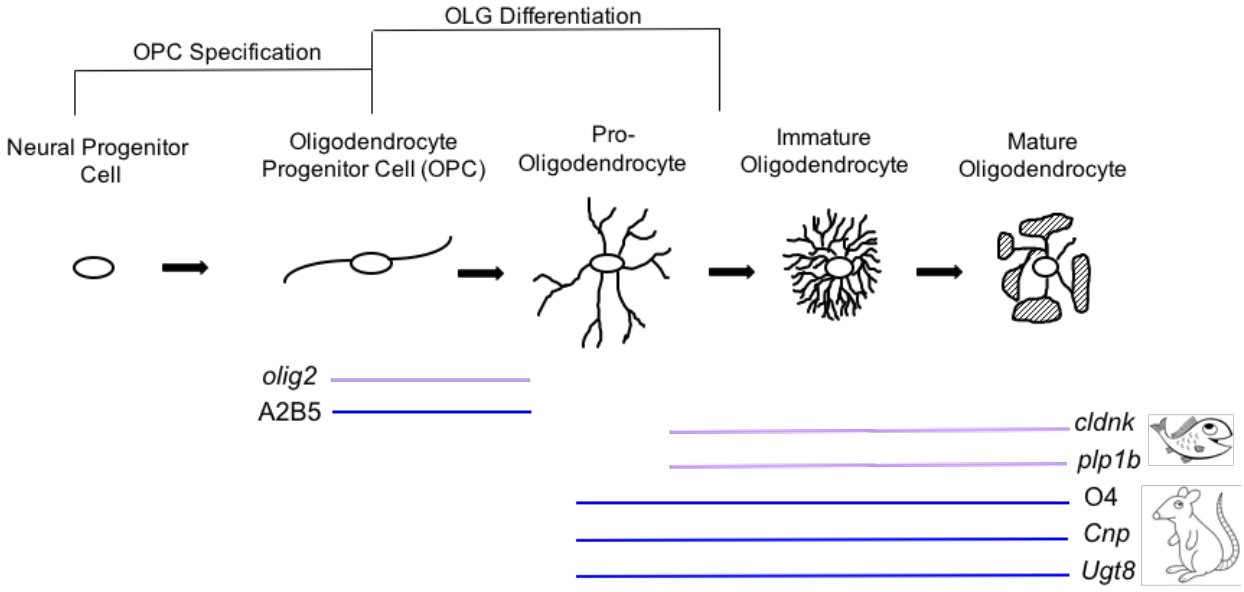
OLG Differentiation
OPC Specification
Neural Progenitor Cell
Oligodendrocyte Progenitor Cell (OPC)
Pro-Oligodendrocyte
Immature Oligodendrocyte
Mature Oligodendrocyte
olig2
A2B5
cldnk
plp1b
O4
Cnp
Ugt8

Figure 1.1. **The oligodendrocyte lineage.** This figure depicts both the changes in morphology and gene expression/cell surface markers that OLGs undergo as they develop. OPCs are specified (neural progenitor cell to OPC) in restricted regions of the central nervous system where they migrate from and proliferate extensively, populating the brain and spinal cord. Once they have reached their destination, they begin to develop a complex process network and eventually form membranous structures which wrap around axons *in vivo*. OLG differentiation, as denoted in this schematic, is the main focus of this dissertation. As changes are observed morphologically, OLGs also undergo changes in gene expression/cell surface markers as shown underneath the pictures. The genes/cell surface markers listed are used to identify different stages of the OLG lineage and are delineated for the developing zebrafish (purple) and rat (blue): oligodendrocyte transcription factor 2 (*olig2*), ganglioside (A2B5), proteolipid protein (*plp1b*), claudink (*cldnk*), pro-oligodendrocyte surface antigen or sulfatide (O4), 2,3-cyclic nucleotide 3-phosphodiesterase (*Cnp*) and UDP- galactose ceramide galactosyltransferase (*Ugt8*).

# Chapter 2

## The Autotaxin-LPA Axis Modulates Histone Acetylation and Gene Expression during Oligodendrocyte Differentiation

*(This chapter was accepted as a paper in the Journal of Neuroscience in August of 2015. The work reported for this manuscript is based primarily on my own efforts. Assistance was provided by Dr. James Lister (CRISPR-Cas9 genome editing Figure 2.1)*

### Introduction

The differentiation of the myelinating cells of the central nervous system (CNS), namely oligodendrocytes (OLGs), follows a step-wise program that is characterized by well-coordinated changes in gene expression and cellular morphology (Bauer et al., 2009; Mitew et al., 2014; Wegner, 2008). The developmental timing of this progression along the OLG lineage is finely tuned by extracellular signals and intracellular pathways. In particular, and at the transition from OLG progenitor to differentiating OLG, epigenetic mechanisms associated with a progressive compaction of chromatin have been found to play a central role (Bischof et al., 2015; Copray et al., 2009; Jacob et al., 2011; Liu and Casaccia, 2010; Liu et al., 2015; Mori and Leblond, 1970; Shen and Casaccia-Bonnefil, 2008; Yu et al., 2013). The current understanding of the above mechanisms affecting the chromatin landscape involves histone deacetylation via the action of the class I histone deacetylase (HDAC) members HDAC1 and HDAC2 (Shen et al., 2005, 2008; Wu et al., 2012; Ye et al., 2009). In general, HDAC1/2 containing complexes are considered to remove acetyl groups from histone tails, thereby favoring a condensed chromatin structure and limiting DNA access for transcription factors (Grunstein, 1997). In the case of the OLG lineage, it has been demonstrated that the target genes affected by HDAC1/2 deacetylation include clusters of co-regulated genes implicated in

transcriptional repression (Swiss et al., 2011). Thus, it is deacetylation-mediated repression of transcriptional inhibitors of OLG differentiation, such as *Egr1*, *Id2* and *Sox11*, that is thought to promote progression along the OLG lineage. While the intracellular aspects of this mechanism have been well-characterized, little is known about the extracellular signals that may be modulating it (Wu et al., 2012).

In our previous studies, we identified autotaxin (ATX), also known as ENPP2, phosphodiesterase-Iα/ATX or lysophospholipase D (lysoPLD), as an extracellular factor that promotes OLG differentiation at various steps along the progression of the lineage and via the action of two distinct functionally active domains (Dennis et al., 2005, 2008; Nogaroli et al., 2009b; Yuelling and Fuss, 2008; Yuelling et al., 2012). In this regard, ATX's so-called modulator of oligodendrocyte remodeling and focal adhesion organization (MORFO) domain was found to regulate primarily the morphological aspects of OLG differentiation (Dennis et al., 2008, 2012; Fox et al., 2003), while its lysoPLD-active site, which generates the lipid signaling molecule lysophosphatidic acid (LPA) (van Meeteren and Moolenaar, 2007; Nakanaga et al., 2010; Tokumura et al., 2002; Umezu-Goto et al., 2002), may be predominantly modulating gene expression (Nogaroli et al., 2009b). Intriguingly, studies assessing ATX's functions as a whole and *in vivo* in the developing zebrafish revealed a lineage promoting, and likely gene expression regulatory, role at the transition from OLG progenitor to differentiating OLG (Yuelling et al., 2012). Thus, we investigated here a possible role of, in particular, ATX's lysoPLD activity in modulating histone deacetylation and gene expression during the early stages of the OLG lineage.

**Materials and Methods**

*Animals.* Zebrafish embryos were obtained through natural matings, raised at 28.5°C and staged according to morphological criteria and hours post fertilization (hpf) (Kimmel et al., 1995). Wildtype fish were of the AB strain and *Tg*(*nkx2.2a:megfp)*$^{vu17}$ (Kirby et al., 2006; Kucenas et al., 2008), abbreviated *Tg(nkx2.2a:megfp), as well as Tg(olig2:dsred2)*$^{vu19}$ (Kucenas et al., 2008), abbreviated *Tg(olig2:dsred2),* fish were kindly provided by Sarah Kucenas and Bruce Appel. Sprague Dawley female rats with early postnatal litters were obtained from Harlan Laboratories (Indianapolis, IN). All animal studies were approved by the institutional animal care and use committee at Virginia Commonwealth University.

*Antibodies.* Supernatants from cultured hybridoma cells (clone A2B5; ATCC, Manassas, VA) were used for immunopanning. Anti-acetyl-Histone H3 (Lys 9) antibodies (Cell Signaling Technology, Inc., Danvers, MA) were used for Western blot analysis as well as immunocytochemistry. Anti-Histone H3 antibodies (Cell Signaling Technology, Inc., Danvers, MA) as well as IRDye 680RD- and 800CW-conjugated secondary antibodies (LI-COR Biosciences, Lincoln, NE) were used for Western blot analysis. Supernatants from cultured hybridoma cells (clone O4; gift from S.E. Pfeiffer), anti-Caspase 3, active (cleaved) form (EMD Millipore, Billerica, MA), anti-Ki67 (Leica Microsystems, Buffalo Grove, IL) and Alexa 488- and/or Alexa 568-conjugated secondary antibodies (Life Technologies, Grand Island, NY) were used for immunocytochemistry.

*Pharmacological compounds.* Zebrafish embryos and primary cultures of differentiating OLGs were treated with the following compounds: ATX-lysoPLD activity

inhibitors S32826 and HA130 (Tocris/Bio-Techne, Minneapolis, MN), HDAC1/2/3 inhibitor C1944 and HDAC6 inhibitor Tubastatin A (Selleckchem, Houston, TX) all of which were dissolved in dimethyl sulfoxide (DMSO) resulting in a final experimental concentration of 0.1% of DMSO, which is well tolerated in both the zebrafish as well as the cell culture system (Lyssiotis et al., 2007b; Maes et al., 2012). Lysophosphatidic acid (LPA; 18:1; Sigma, St. Louis, MO) was dissolved in DMEM containing 0.1% fatty acid-free bovine serum albumin. Control in all experiments where pharmacological compounds were used refers to vehicle treatment.

*Cell culture.* Primary OLG progenitors were isolated from postnatal day 2 (P2) rat brains by A2B5 immunopanning and cultured as previously described (Barres et al., 1992; Lafrenaye and Fuss, 2010; Martinez-Lozada et al., 2014). Briefly, immunopanned OLG progenitors were plated onto fibronectin (10 µg/ml)-coated tissue culture dishes, glass coverslips or 96-well plates. Plated OLG progenitors were cultured in serum-free proliferation medium (Dulbecco's modified Eagle's medium (DMEM) containing human PDGF and basic fibroblast growth factor (bFGF) (Gemini Bio-Products, Sacramento, CA) for 24 hrs, after which cells were allowed to differentiate in serum-free medium (DMEM containing 40 ng/mL tri-iodo-thyronine (T3; Sigma, St. Louis, MO) and N2 supplement (Life Technologies, Grand Island, NY); DMEM/T3/N2) over the time periods indicated. Differentiating OLGs were either directly analyzed or treated as indicated. Typically, at least three independent experiments were performed, whereby an independent experiment refers to an experiment in which cells were isolated from a separate P2 rat litter at an independent time point (day) and treated separately from all other independent experiments.

*CRISPR/Cas9 genome editing*. CRISPR target sequences for *atx* (*enpp2*), as depicted in Fig. 1, were identified using the online tools crispr.mit.edu and chopchop.rc.fas.harvard.edu (Montague et al., 2014). sgRNAs were generated using the cloning-free/short oligonucleotide approach described by Talbot and Amacher (2014). Briefly, short-guide oligonucleotides containing a T7 promoter and genomic target site were synthesized by Eurofins MWG Operon LLC (Huntsville, AL). Guide-constant oligonucleotides were obtained from Life Technologies (Grand Island, NY). Full length templates for sgRNA synthesis were generated by PCR using short-guide and guide-constant oligonucleotides, and PCR templates were purified using ISOLATE II PCR cleanup columns (Bioline, Taunton, MA). The plasmid pT7tyrgRNA (Addgene 46761; kindly provided by Wenbiao Chen) (Jao et al., 2013) was used as a template for the generation of the *tyrosinase* (*tyr*) control sgRNA. sgRNAs were transcribed from their templates using the MEGAshortscript T7 kit (Life Technologies, Grand Island, NY). Cas9 mRNA was synthesized from the plasmid pT3TS-nCas9n (Addgene 46757; kindly provided by Wenbiao Chen) (Jao et al., 2013) using the mMESSAGE mMACHINE T3 Transcription Kit (Life Technologies, Grand Island, NY). 1 nanoliter of a mixture of Cas9 mRNA (100 ng/µl) and sgRNA (80 ng/µl for *atx*-E2; 95 ng/µl for *atx*-E7; 100ng/µl for *tyr*) was injected per one-cell stage zebrafish embryo. Zebrafish were analyzed at 48 hpf. Brightfield images of whole embryos were taken using an Olympus SZX12 zoom stereo microscope (Olympus America Inc., Melville, NY) equipped with an Olympus DP70 digital camera system.

*Genomic DNA analysis*. Genomic DNA was isolated from control and Cas9 mRNA/sgRNA injected embryos using the DNeasy Blood and Tissue kit (Qiagen,

Valencia, CA). DNA fragments spanning genomic target sites were amplified by PCR using the following primer pairs:

*atx*-E2$^{(ZDB\text{-}GENE\text{-}040426\text{-}1156)}$: forward (5' AAATTGTTGAAACCATATGCGA 3'), reverse (5' GCATCCTACTTTTTGAGAGCGA)

*atx*-E7$^{(ZDB\text{-}GENE\text{-}040426\text{-}1156)}$: forward (5' TGTTTAGGTGTGTGCTTAGTGC 3'), reverse (5' AATCTGCAATTAATACATACCGTTG 3').

To assess for indels generated by CRISPR/Cas9 genome editing, PCR fragments were sequenced (VCU's Nucleic Acid Research Facilities) and the Surveyor Mutation Detection Kit (Integrated DNA Technologies, Inc., Coralville, IA) was used.

*ATX-lysoPLD activity assay.* ATX-lysoPLD activity was determined using the fluorogenic assay as described by Ferguson et al. (Ferguson et al., 2006). Whole zebrafish homogenates diluted in 140 mM NaCl, 5 mM KCl, 1 mM $CaCl^2$, 1 mM $MgCl^2$, 5 mM Tris/HCl (pH 8.0), 1 mg/ml fatty acid-free BSA (Sigma-Aldrich, St. Louis, MO) or concentrated (40x) conditioned medium from primary OLG cultures grown in phenol-red-free DMEM were incubated with 2.5 μM FS-3 substrate (Echelon Biosciences Inc., Salt Lake City, UT) for 4 hrs at 37°C. Increase in fluorescence with time was measured at an excitation wavelength of 485 nm and an emission wavelength of 520 nm using a PHERAstar multimode microplate reader (BMG LABTECH Inc. Cary, NC.).

*RNA isolation and real-time RT-qPCR Analysis.* For the isolation of RNA from whole zebrafish embryos or cultured rodent OLGs, samples were collected in Trizol (Invitrogen, Carlsbad, CA) and immediately homogenized. RNA was extracted as described by Chomczynski and Sacci (1987) (Chomczynski and Sacchi, 1987). For the isolation of RNA from FACS-isolated cells, cells were collected directly in Trizol and

then immediately processed using the RNeasy Micro Kit from Qiagen (Valencia, CA). All RNA samples were treated with DNase (DNA-Free Kit; Applied Biosystems/Ambion, Austin, TX). RNA concentrations were determined using a Nanodrop ND 1000 Spectrophotometer (Thermo Scientific/NanoDrop, Wilmington, DE) and purity was assessed by the ratio of absorbance at 260 and 280 nm ($OD_{260/280}$ ≥ 1.8). Oligo(dT)-primed cDNAs were synthesized from 50 ng to 1 µg of RNA using the Omniscript or Sensiscript RT Kit (Qiagen, Valencia, CA) according to the manufacturer's guidelines. RNA samples were normalized to the same approximate concentration and the same amount of RNA was used for all conditions of an individual independent experiment. As control, cDNA reactions without reverse transcriptase were performed for all samples. PCR reactions performed with such no-reverse-transcriptase cDNAs as template yielded quantitation cycle (Cq) numbers that were at least 5 cycles below the lowest Cq for any of the experimental samples (unknowns), whereby Cq values for unknowns were within the linear quantifiable range as determined by calibration curves. Gene-specific primers were designed and *in silico* tested for specificity using NCBI/Primer-BLAST (Ye et al., 2012). All primers were designed to amplify all known splice variants. For each primer pair listed below, amplicon length is noted in bp. In addition, PCR efficiencies are given in % and correlation coefficients ($r^2$ values) as single numbers, whereby the latter were determined from calibration curves using RNA samples derived from species and tissue/cell type equivalent sources.

The following unmodified zebrafish gene-specific primer pairs were used:

*atx/enpp2*$^{(ZDB\text{-}GENE\text{-}040426\text{-}1156)}$: forward (5'-CAATGTATGCAGCATTCAAACGAGTG-3', exon 22), reverse (5'CACCATTTTTCTCACTAGCGTAACG-3', exon 23), 79 bp, 107%,

0.996

*plp1b*(ZDB-GENE-030710-6)*:* forward (5'TGCCATGCCAGGGGTTGTTTGTGGA-3, exon 5), reverse (5'-GGCGACCATGTAAACGAACAGGGC-3, exon 6/7); 143 bp, 96%, 1,000

*cldnk*(ZDB-GENE-040801-201): forward (5'-TGGCATTTCGGCTCAAGCTCTGGA-3', exon 1), reverse: (5'GGTACAGACTGGGCAATGGACCTGA-3, exon 2); 135 bp, 93%, 0.999

*inab (gefiltin)*(ZDB-GENE-990415-83): forward: 5'-CTCTCCATCCCGGCTGAGCAGCT -3', exon 1), reverse: (5'AGCCTGGGATGTTGGGGCGGTT-3', exon 1); 74 bp, 105%, 0,997

*gfap*(ZDB-GENE-990914-3): forward (5'-TGAGACAAGCGAAGCAGGAGGCCA-3', exon 5), reverse (5'GGCGCTCCAGGGACTCATTAGACCC-3', exon5/6); 102 bp, 101%, 0.997

*prph* (*plasticin*)(ZDB-GENE-990415-207): forward (5'-ACTCCTACCGCACCTCTCACCACCG -3', exon 1), reverse (5'-TAGCGGCCCCCGATGCGACTG-3', exon 1); 70 bp, 93%, 0.997

*sox10*(ZDB-GENE-011207-1): forward (5'-TGGACACCACCCTCACGCTA-3', exon 3), reverse (5'-CTGCAGTTCCGTCTTGGGGG-3', exon 4); 76 bp, 94%, 0.966

*β-actin (actb2*(ZDB-GENE-000329-3)) (Buckley et al., 2010) was used as reference gene (60bp, 95%, 0.999); *eef1a1/1*(ZDB-GENE-990415-52) has been assessed as additional reference gene for the analysis of RNA derived from the developing zebrafish and no pronounced differences were noted (Yuelling et al., 2012).

The following unmodified rat gene-specific primer pairs were used:

*Cnp*(NM_012809.2): forward (5'-ATGCCCAACAGGATGTGGTG-3', exon 3/4), reverse (5'-AGGGCTTGTCCAGGTCACTT-3', exon 4); 150 bp, 103%, 0.990

*Ugt8*(NM_019276.3): forward (5'-AGGAGCTCTGGGGAGATTGC-3', exon 3), reverse (5'-TTTGAATGGCCAAGCAGGTCA-3', exon 4/5); 126 bp, 108%, 0.960

*Egr1*(NM_012551.2): forward (5'-CCTGACCACAGAGTCCTTTTCT-3', exon 1/2), reverse

(5’-AAAGTGTTGCCACTGTTGGG-3’, exon 2); 150 bp, 93%, 0.996

*Pgk1*(NM_053291.3) (as reference gene): forward (5’-ATGCAAAGACTGGCCAAGCTAC-3’, exon 8), reverse (5’-AGCCACAGCCTCAGCATATTTC-3’, exon 9), 103 bp, 103%, 0.997

*Pgk1* was used as reference gene due to its previously established expression stability in rat OLGs (Nelissen et al., 2010). In addition, *Ppia*(NM_017101.1) has been assessed as additional reference gene for the analysis of RNA derived from differentiating OLG cultures and no pronounced differences were noted.

RT-qPCR reactions with at least 2 technical replicates per sample were performed on a CFX96 real-time PCR detection system (BioRad, Hercules, CA) using the iQ SYBR Green Supermix (BioRad, Hercules, CA). PCR conditions were as follows: 95°C for 3 min followed by 40 cycles of 95°C for 15 s, 58°C for 30 s, and 95°C for 10 s. For all primer pairs, melting curves were used to ensure specificity. Relative expression levels were determined using the ΔΔCT method (Livak and Schmittgen, 2001).

*Whole mount in situ hybridization.* Zebrafish embryos were fixed in 4% paraformaldehyde in PBS overnight at 4°C and stored in methanol at 22°C for at least 1 day. Colorimetric *in situ* hybridizations using digoxigenin-labeled antisense cRNA probes were performed by standard methods and as previously described (Thisse and Thisse, 2014, 2008; Yuelling et al., 2012). *In situ* hybridized embryos were mounted in 90% glycerol/PBS and whole mount images were acquired using the extended focus module of the axiovision software package in combination with an Axio Observer Z.1 or SteREO Discovery.V20 microscope equipped with an AxioCam MRc digital camera (Carl Zeiss MicroImaging, Inc., Thornwood, NY). Once captured, images were imported into Adobe Photoshop and adjustments were limited to cropping and brightness/contrast

adjustments which were applied equally across the entire image and to controls. *In situ*-labeled cells were counted using the Cell Counter plugin to the ImageJ software package (Abramoff et al., 2004).

*Isolation of OLG progenitors from zebrafish embryos using fluorescent activated cell-sorting (FACS). Tg(nkx2.2a:megfp;olig2:dsred2)* zebrafish embryos (up to 300 per sample) were anesthetized with tricaine methanesulfonate (MS-222; Sigma Aldrich Corp., St. louis, MO) and subjected to enzymatic (trypsin and DNAse) and mechanical (20 and 26 gauge needle) dissociation. Cell suspensions were resuspended first in 1ml and then in 500 µl of ice cold 5% Goat Serum in PBS after centrifugation (at 956xg for 2 min at 4°C) and then subjected once again to mechanical dissociation (26-gauge needle). Cell suspensions were passed through a 40 micron filter and then through a fluorescence activated cell sorter (FACS Aria II, BD Biosciences, San Jose, CA) using an 85 µM nozzle. Cell sorting was performed at room temperature using a 488 nm laser (>20mW power, Coherent solid-state) for excitation and 530/30 nm and 585/42 nm bandpass filters for the collection of emission. Settings were carefully determined empirically and exactly reproduced in each experiment. Gates were demarcated to sort only mEGFP/DsRed2 double-positive cells. The speed of sorting (usually no more than 1–2 drops per event) was adjusted to obtain a purity of >95%. Cells were suspended in either PBS (HDAC activity assay) or Trizol (RNA isolation).

*HDAC activity assay.* FACS-isolated cells were plated into 96-well plates ($1x10^4$ cells/well) and directly assayed. Rodent OLG progenitor cells were cultured and treated in fibronectin coated 96-well plates ($1x10^5$ cells/well) and then assayed. HDAC activity was determined using the fluorometric HDAC Activity Assay Kit from BioVision

Inc. (Milpitas, CA). Briefly, the cell permeable HDAC Substrate Boc-Lys(AC)-AMC was added and cells were incubated for 3 hrs at 37 °C. Subsequent incubation with the Lysine Developer (30 min at 37 °C) was used to produce a fluorophore from substrate sensitized through deacetylation. Fluorescence, as a measure of HDAC activity, was determined using a Spectra Max M5 fluorescent plate reader (Molecular Devices, Sunnyvale, CA) with excitation/emission at 360/460 nm. In each experiment, triplicates were prepared for all conditions and treatments.

*Immunocytochemistry*. For immunocytochemistry using O4 hybridoma supernatants, cells were fixed in 4% paraformaldehyde/PBS, nonspecific binding sites were blocked in 10% FCS/DMEM, and cells were incubated with the supernatant (1:1 diluted in 10% FCS/DMEM) overnight. Cells were fixed and in case of dual staining permeabilized using 0.5% Triton X-100/0.4 M sucrose/PBS and then incubated for 30 min in blocking solution (10% FCS/DMEM). Subsequently, cells were incubated overnight with anti-acetyl-histone H3 (Lys 9), anti-Caspase 3 (active (cleaved) form) or anti-Ki67 antibodies overnight. Primary antibodies were detected using Alexa 488- or Alexa 568-conjugated secondary antibodies (Life Technologies, Grand Island, NY) and nuclei were counterstained using Hoechst 33342 (EMD Millipore, Billerica,MA). For the generation of representative images, confocal laser scanning microscopy was used (Zeiss LSM 700, Carl Zeiss Microscopy, LLC, Thornwood, NY). Images represent 2D maximum projections of stacks of 0.5 µm optical sections.

*Nuclear histone acetylation analysis.* Cells double-labeled for O4 and acetyl-histone H3 (Lys 9) were imaged using confocal laser scanning microscopy (LSM 700 Carl Zeiss Microscopy, LLC, Thornwood, NY). Single focal plane images were taken using a

40x/1.3 n.a. plan-apochromat objective lens. Images were taken from O4-positive cells and focused on the region of the nucleus as marked by staining with Hoechst. Laser intensity, detector gain and amplifier offset were optimized and kept constant throughout the imaging of all samples from one experiment. Fluorescence intensity, i.e. average pixel intensity, for the anti-acetyl histone H3 (Lys 9) signal, as a measure for the level of histone acetylation, was determined over the area of the nucleus using IP Lab imaging software (BD Biosciences Bioimaging, Rockville, MD). Unprocessed confocal images were used for analysis and threshold settings were kept constant once determined.

*Western blot analysis.* Cells were homogenized in lysis buffer (150 mM NaCl, 10 mM KCl, 20 mM HEPES (pH 7.0), 1 mM $MgCl^2$, 20% glycerol, and 1% Triton X-100) including the complete protease and phosphatase inhibitor cocktail (Thermo Scientific, Rockford, IL). 5 µg per sample were used for Western blot analysis to detect acetyl histone H3 (Lys 9) and total H3. Bound primary antibodies were detected using IRDye 680RD- and 800CW-conjugated secondary antibodies (LI-COR Biosciences, Lincoln, NE). Signal intensities were determined using a LI-COR Odyssey infrared imaging system (LI-COR Biosciences, Lincoln, NE).

*Cell survival and proliferation analysis.* Cells were subjected to immunostaining using O4 hybridoma cell supernatants and antibodies specifically recognizing the active (cleaved) form of caspase-3 or the Ki67 antigen. To determine the number of caspase-3 or Ki67 immunopositive cells, images of four fields per coverslip were taken with a 20x/0.8 n.a. plan-apochromat objective lens using a confocal laser scanning microscope (LSM 700 Carl Zeiss Microscopy, LLC, Thornwood, NY). Three coverslips per condition for each of three independent experiments were analyzed, and Hoechst 33342-positive

nuclei as well as caspase-3 or Ki67 immunopositive oligodendrocytes were counted using the Cell Counter plugin to the ImageJ software package (Abramoff et al., 2004).

*Statistical Analysis.* To determine significance, GraphPad Prism (GraphPad Software, La Jolla, CA) or SigmaPlot (Systat Software, Inc., San Jose, CA) software was used. Data composed of two groups were analyzed using the two-tailed Student's *t*-test or the Mann-Whitney *U*-test and presented in bar graphs depicting means ± SEM or box and whisker plots depicting medians and quartiles. Data compared to a set control value lacking variability were analyzed using the one-sample *t*-test (Dalgaard, 2008; Robert R. Sokal, 2013) and presented in bar graphs.

## Results

### In the developing zebrafish hindbrain, ATX promotes the timely appearance of differentiating OLGs via its lysoPLD activity

Our previous studies, using antisense morpholino oligonucleotide-mediated knock-down of *atx* expression, revealed that in the developing zebrafish hindbrain, ATX promotes the timely appearance of cells committed to the OLG lineage without affecting the number of *olig2*-positive progenitor cells, the overall morphology of the axonal network or the differentiation of somatic abducens motor neurons (Yuelling et al., 2012). As recent studies have questioned the correlation between morpholino oligonucleotide-induced and mutant phenotypes in the zebrafish (Kok et al., 2015), we used clustered regularly interspaced short palindromic repeats (CRISPR)/Cas9 genome editing to substantiate the above proposed *in vivo* role of ATX. For these studies, we used the codon-optimized Cas9 with nuclear localization signals system described by Jao et al. (2013). This optimized system has been described to lead to an increased frequency of

biallelic disruption so that injected ($F_0$) embryos phenocopy known mutant phenotypes (Jao et al., 2013). As shown in Fig. 2.1A-E, injection of guide RNAs against exon 2 or 7 of the *atx* (*enpp2*) gene and *in vitro* transcribed, capped, polyadenylated *nls-zCas9-nls* RNA into one-cell stage zebrafish embryos resulted in the generation of indel mutations over and upstream of the CRISPR targeting sequence. These mutations resulted in reduced levels of *atx* mRNA (Fig. 2.1F) (*atx*-E2, n=4, *t*-test, p=0.0038; *atx*-E7, n=6, *t*-test, P=0.0006), an effect that was not observed when using a guide RNA against *tyrosinase* (*tyr*) (*tyr*, n=3, *t*-test, p=0.3468). Most importantly, the CRISPR/Cas9-mediated reduction in *atx* expression was found associated with a decrease in the transcript levels for the later stage OLG differentiation marker genes *claudin K (cldnk)* and *proteolipid protein* (*plp1b)* (Fig, 2.1G) (*cldnk atx*-E2, n=4, *t*-test, p=0.0188; *cldnk atx*-E7, n=5, *t*-test, p=0.0006; *plp1b atx*-E2, n=6, *t*-test, p=0.0155*; plp1b atx*-E7, n=5, *t*-test, p=0.0203). As shown in Fig. 2.1H, injection of Cas9 mRNA with either of the guide RNAs was not found to be associated with changes in the gross morphology of the embryos. The above described data, therefore, corroborate our earlier morpholino oligonucleotide-mediated knock-down results and confirm a critical *in vivo* role of ATX in the regulation of OLG differentiation.

To assess the extent to which this functional role of ATX may be dependent on its lysoPLD activity, the inhibitors HA130 and S32826, which have been well-characterized to block ATX's lysoPLD activity (Albers et al., 2010; Ferry et al., 2008), were used. Of these inhibitors, HA130 has previously been demonstrated to effectively block ATX's lysoPLD activity in the developing zebrafish at concentrations similar to the ones found to block human ATX (Lai et al., 2012). Two experimental designs were used (see

Figs. 2.2A and 2.3A). First, to determine the effect of an inhibition of ATX's lysoPLD activity on OLG differentiation, inhibitors were added to zebrafish embryos at 44 hrs post fertilization (hpf), i.e. at a time point when OLG progenitors arise in the ventral hindbrain and start to differentiate (Zannino and Appel, 2009)(Fig. 2.2A). Zebrafish embryos were analyzed at 48 hpf, a time point at which transcripts for *cldnk* and *plp1b* start to become detectable (Brösamle and Halpern, 2002; Münzel et al., 2012; Takada and Appel, 2010). As shown in Fig. 2.2B, treatment with either of the inhibitors at both 1μM and 10μM concentrations significantly reduced ATX's lysoPLD activity (HA130 1μM, n=4, *t*-test, p=0.0166; HA130 10μM, n=4, *t*-test, p=0.0132; S32826 1μM, n=6, *t*-test, p=0.0008; S32826 10μM, n=5, *t*-test, p=0.0131). Importantly, both inhibitors significantly reduced the mRNA levels for *cldnk* and *plp1b* at both concentrations used (Fig. 2.2C,D) (*cldnk*: HA130 1μM, n=3, *t*-test, p=0.0144; HA130 10μM, n=3, *t*-test, p=0.0413; S32826 1μM, n=3, *t*-test, p=0.0006; S32826 10μM, n=3, *t*-test, p=0.0166; *plp1b:* HA130 1μM, n=5, *t*-test, p=0.0038; HA130 10μM, n=5, *t*-test, p=0.0325; S32826 1μM, n=5, *t*-test, p=0.0071; S32826 10μM, n=5, *t*-test, p=0.0031). In contrast, there was no change in the number of *olig2*-positive progenitors (Fig. 2.2E,F) (HA130 1μM, n=5, *t*-test, p=0.7184; HA130 10μM, n=5, *t*-test, p=0.5050; S32826 1μM, n=5, *t*-test, p=0.7679; S32826 10μM, n=5, *t*-test, p=0.7277), which at 48 hpf represent early stages of both motor neuron and OLG lineages (Park et al., 2002; Zannino and Appel, 2009). It is of note that neither S32826 nor HA130 were found to exert cytotoxic effects when treating zebrafish embryos or cells in culture at the concentrations used here (Albers et al., 2010; Ferry et al., 2008; Iyer et al., 2012; Lai et al., 2012, see also description to Fig. 2.7 below). Consistently, no gross morphological defects were noted upon the treatment

of zebrafish embryos with HA130 or S32826 (Fig. 2.2G) and no noticeable increase in 7-aminoactinomycin D (7-AAD) staining, as a measure for increased cell death (Philpott et al., 1996), was detected when analyzing single cell suspensions from control and inhibitor treated whole fish embryos by flow cytometry (data not shown). Hence, the data shown in Fig. 2 suggest that ATX's lysoPLD activity, as ATX as a whole (Yuelling et al., 2012), regulates the progression of *olig2*-positive progenitor cells into lineage committed and differentiating OLGs, but not the appearance of *olig2*-positive progenitors itself.

To further confirm the above conclusion, ATX-lysoPLD inhibitors were added at a time point at which *olig2*-positive progenitors begin to arise in the hindbrain, i.e. at 24 hpf (Zannino and Appel, 2009) (Fig. 2.3A). As shown in Fig. 2.3B-E, treatment with HA130 had a comparable effect in both experimental designs (ATX activity: HA130 1µM, n=5, *t*-test, p=0.0051; HA130 10µM, n=4, *t*-test, p=0.0130; *cldnk*: HA130 1µM, n=4, *t*-test, p=0.0037; HA130 10µM, n=5, *t*-test, p=0.0167; *plp1b*: HA130 1µM, n=4, *t*-test, p=0.0272; HA130 10µM, n=4, *t*-test, p=0.0111; *olig2*: HA130 1µM, n=5, *t*-test, p=0.1867; HA130 10µM, n=5, *t*-test, p=0.8770). Interestingly, treatment with S32826, when applied at 24 hpf, did not cause a significant effect on ATX's lysoPLD activity or *cldnk/plp1b* mRNA levels when used at 1µM and a much-reduced effect when used at 10µM (Fig. 2.3B-E) (ATX activity: S32826 1µM, n=3, *t*-test, p=0.0566; S32826 10µM, n=4, *t*-test, p=0.0322; *cldnk*: S32826 1µM, n=5, *t*-test, p=.3999; S32826 10µM, n=5, *t*-test, p=0.0145; *plp1b*: S32826 1µM, n=3, *t*-test, p=0.9437; S32826 10µM, n=3, *t*-test, p=0.0162; *olig2:* S32826 1µM, n=5, *t*-test, p=0.2823; S32826 10µM, n=5, *t*-test, p=0.8073). This lack of effective inhibition of ATX's lysoPLD activity is likely due to the

known poor *in vivo* stability and/or bioactivity of S32826 (Ferry et al., 2008; Gupte et al., 2011). As in the studies to the experimental design shown in Fig. 2.2, no gross morphological defects (Fig. 2.3G) or noticeable increase in cell death (not shown) were noted.

Taken together, the above data demonstrate that inhibition of ATX's lysoPLD activity mimics the effects on the OLG lineage as seen upon morpholino oligonucleotide-mediated knock-down of *atx* expression (Yuelling et al., 2012) or CRISPR/Cas9-mediated genome editing at the *atx* locus (Fig. 2.1). Thus, they establish that it is ATX's lysoPLD activity that is necessary for the timely appearance of differentiating OLGs in the developing zebrafish hindbrain.

**In the developing zebrafish, ATX-lysoPLD promoted progression along the early stages of the OLG lineage is associated with an increase in HDAC activity**

The progression along the early stages of the OLG lineage, as seen regulated by ATX's lysoPLD activity, has been well-established to be associated with epigenetic modifications and in particular with an increase in histone deacetylation (He et al., 2007a; Liu and Casaccia, 2010; Marin-Husstege et al., 2002; Shen et al., 2005, 2008; Swiss et al., 2011; Takada and Appel, 2010). In addition, in studies unrelated to ATX, it has been shown that LPA, for which enzymatic lysoPLD activity represents one of the known biosynthetic pathways (Aoki et al., 2008a), can increase histone deacetylation in a number of human cancer cell lines (Ishdorj et al., 2008). Thus, and in an effort to identify downstream targets of ATX's lysoPLD activity involved in the regulation of OLG differentiation, we focused on HDACs and their activity. For these studies, the experimental design as depicted in Fig. 2.4A was used. In addition, and to enable an

analysis of HDAC activity explicitly in cells of the OLG lineage, the double transgenic zebrafish line *Tg(nkx2.2a:megfp;olig2:dsred2)* was used in which a subset of OLG lineage cells can be identified by the concurrent expression of mEGFP and DsRed2 (Kucenas et al., 2008) and thus be isolated by fluorescence-activated cell sorting (FACS). In agreement with an OLG lineage commitment, such sorted and double-positive cells were characterized under control conditions by an enriched expression of the OLG marker gene *cldnk* (Fig. 2.4B) (n=5, *t*- test, p=0.0262, compared to whole fish embryo expression). In contrast, there were, if at all, only slight levels of expression detectable for the radial/ependymal/enteric glia marker *gfap* (Fig. 2.4B) (n=4, *t*-test, p= 0.0023, compared to whole fish embryo expression) (Bernardos and Raymond, 2006; Doodnath et al., 2010; Grupp et al., 2010; Hagström and Olsson, 2010; Lam et al., 2009) and the neuronal intermediate filament encoding genes *gefiltin (inab)* (Fig. 2.4B) (n=4, *t*-test, p=0.0014, compared to whole fish embryo expression) and *plasticin (prph)* (Fig. 2.4B) (n=4, *t*-test, p=0.0019, compared to whole fish embryo expression) (Leake et al., 1999). In addition, and similar to the rodent system (Savaskan et al., 2007), such early stages of the OLG lineage were found to express *atx* (Fig. 2.4B) (n=4, *t*-test, p=0.0464). It is of note that such early, and relatively low, expression during the OLG lineage remained undetected in our earlier studies (Yuelling et al., 2012) due to the use of less sensitive detection methods. Upon inhibition of ATX's lysoPLD activity, and consistent with the previously observed lack of an effect on the number of *olig2* expressing progenitor cells (Fig. 2.2E,F), no change in the number of double-positive cells was observed (Fig. 2.4C) (HA130, n=4, *t*-test, p=0.4722; S32826, n=4, *t*-test, p=0.3765). To further assess potential effects of ATX-lysoPLD inhibition on progenitor

marker expression levels, the fluorescence intensities for mEGFP and DsRed2 were monitored, as they are indicators for *nkx2.2a* and *olig2* promoter activities. A shown in Fig. 2.4D and E, no changes were observed (n=5, *t*-test, p=0.5855, mEGFP; n=5, *t*-test, p=0.6436, DsRed2). In contrast, and in agreement with our previous findings (Fig. 2.2C,D), the expression of *sox10*, which at the developmental stage analyzed marks *olig2/nkx2.2a* double-positive cells that are OLG lineage committed and differentiating (Kucenas et al., 2008), was found to be decreased (Fig. 2.4F) (HA130, n=4, *t*-test, p=0.0358). Importantly, such a reduction in the expression of a gene characteristic for recently specified and differentiating OLGs was associated with a reduction in overall HDAC activity (Fig. 2.4G) (HA130, n=4, *t*-test, p=0.0275; S32826, n=4, *t*-test, p=0.0106). This effect was found to not be associated with a noticeable decrease in cell viability as assessed by propidium iodide staining and flow cytometry (Sasaki et al., 1987) (data not shown).

Taken together, the above data demonstrate that in the developing zebrafish, ATX, via its lysoPLD activity, promotes the lineage progression from an *olig2/nkx2.2a* double-positive progenitor cell to a *sox10* expressing fully committed and early differentiating OLG by a mechanism that is associated with an increase in overall HDAC activity.

**In enriched primary cultures of rodent OLG lineage cells, ATX's lysoPLD activity promotes OLG differentiation**

To more precisely define the functional correlation between ATX's lysoPLD activity and changes in HDAC activity/histone acetylation and to assess evolutionary conservation of this mechanism, we turned to the well-established culture system of

enriched primary rodent OLG lineage cells. In this culture system, OLG differentiation follows the same sequence of events as observed *in vivo* but provides the advantage of studying intrinsic cellular mechanisms (Temple and Raff, 1985). In addition, the role of HDACs and histone acetylation has been well-characterized in this system (Marin-Husstege et al., 2002; Swiss et al., 2011). More specifically, an increase in histone deacetylation as early as 6 hrs post-mitogen withdrawal has been found crucial for the transition from a proliferating OLG progenitor to a differentiating OLG (Marin-Husstege et al., 2002). To establish the role of ATX's lysoPLD activity on OLG differentiation during this developmental time window, we, therefore, employed the experimental design as depicted in Fig. 2.5A. First, we established the expression profile of transcriptional targets previously shown to be regulated by histone deacetylation, namely 2',3'-Cyclic-nucleotide 3'-phosphodiesterase (*Cnp*), UDP glycosyltransferase 8 (*Ugt8*) and the transcriptional regulator *Egr1* (Swiss et al., 2011). In agreement with the findings described by Swiss et al., OLG differentiation was found in our system to be characterized by an increase in the expression of the OLG marker genes *Cnp* and *Ugt8* and a decrease in the expression of *Egr1* (Fig. 2.5B) (*Cnp*: n=5, *t*-test, p=0.0134; *Ugt8:* n=5, *t*-test, p=0.0429; *Egr1*: n=3, *t*-test, p=0.0362). In addition, there was a slight increase in the expression of *Atx* (Fig. 2.5B) (n=5, *t*-test, p=0.0118). As shown in Fig. 2.5C, treatment with either of the ATX-lysoPLD activity inhibitors, HA130 or S32826, significantly reduced ATX's lysoPLD activity after 4 and 24 hrs (Fig. 2.5C) (HA130 10μM 28 hrs, n=4, *t*-test, p=0.0004; HA130 10μM 48 hrs, n=5, *t*-test, p=0.0001; S32826 10μM 28 hrs, n=4, *t*-test, p=0.0078; S32826 10μM 48 hrs, n=5, *t*-test, p=0.0095). This inhibition of ATX-lysoPLD activity resulted in an attenuation of both the

upregulation of *Cnp* and *Ugt8* expression and the downregulation of *Egr1* expression (Fig. 2.5D) (*Cnp:* HA130 10μM, n=3, *t*-test, p=0.0224, S32826 10μM, n=3, *t*-test, p=0.0159; *Ugt8:* HA130 10μM, n=3, *t*-test, p=0.0321, S32826 10μM, n=3, *t*-test, p=0.0063; *Egr1*: HA130 10μM, n=4, *t*-test, p=0.0051, S32826 10μM, n=3, *t*-test, p=0.0345). The above findings demonstrate that ATX, via its lysoPLD activity and similar to what we have seen in the developing zebrafish (Figs. 2.1-4), promotes gene expression changes associated with OLG differentiation in primary cultures of rodent OLGs.

**In primary cultures of rodent OLGs, ATX-lysoPLD promoted progression along the early stages of the OLG lineage is associated with an increase in HDAC activity**

The gene expression changes observed upon inhibition of ATX's lysoPLD activity (Fig. 2.5D) mimicked those changes previously described to occur upon inhibition of HDAC activity (Swiss et al., 2011), thus suggesting that, as in the zebrafish, these changes may be associated with a decrease in overall HDAC activity. To assess this possibility, the experimental design as shown in Fig. 2.6A was used. Indeed, HDAC activity was found to be decreased as early as 4 hrs and up to 24 hrs post-application of ATX-lysoPLD inhibitors (Fig. 2.6B) (HA130 10μM 28 hrs, n=5, *t*-test, p=0.0280; HA130 10μM 48 hrs, n=7, *t*-test, p=0.0001; S32826 10μM 28 hrs, n=3, *t*-test, p=0.0004; S32826 10μM 48 hrs, n=5, *t*-test, p=0.0034). To provide further evidence for a direct link between ATX's lysoPLD activity and the regulation of HDAC activity, we performed rescue experiments in which LPA, the enzymatic product of ATX's lysoPLD activity, was added concurrent with ATX-lysoPLD inhibitors. As shown in Fig. 2.6C, addition of LPA

(10 μM) attenuated the effect of HA130 on HDAC activity (n=7, *t*-test, p=0.0003). Consistent with LPA's thereby suggested HDAC activity promoting role in differentiating OLGs, LPA treatment alone was found to lead to an increase in HDAC activity (Fig. 2.6D) (n=4, *t*-test, p=0.0052). Taken together, the above data confirm that, as in the developing zebrafish, progression along the early stages of the OLG lineage in rodents is promoted by ATX's lysoPLD activity via the generation of LPA and a downstream mechanism that involves an increase in HDAC activity.

**ATX-lysoPLD promoted increase in HDAC activity is associated with a decrease in nuclear histone acetylation**

It has been previously shown that HDAC activity in differentiating OLGs is primarily directed to lysine residues of histones H4 and H3 including the lysine residue on the tail of histone H3 at position 9 (H3K9) (Swiss et al., 2011). To assess changes in acetylation at this site, cells treated as depicted in Fig. 2.5A were analyzed at 48 hrs by immunocytochemistry combined with confocal microscopy. As shown in Fig. 2.7A, nuclear histone acetylation can be readily detected in O4-positive differentiating OLGs by this method. Most importantly, inhibition of ATX's lysoPLD activity led to a significant increase in the levels of H3K9 acetylation (Fig. 2.7C) (HA130: n=3, Mann-Whitney *U*-test, p=0.00005; S32826: n=3, Mann-Whitney *U*-test, p=0.0003). This effect was not found to be associated with changes in cell survival or proliferation as determined by immunostaining using antibodies specifically recognizing the active (cleaved) form of caspase-3 (n=3, *t*-test, p=0.1355) or the Ki67 antigen (n=3, *t*-test, p=0.1189). In addition, no prominent changes in cellular morphology or nuclear appearance were noted (Fig. 2.7B). The above described increase in H3K9 acetylation upon ATX-

lysoPLD inhibition could be further confirmed by Western blot analysis of cell homogenates (Fig. 7D) (n=3, *t*-test, p=0.0442). Taken together, our data so far demonstrate that attenuation of OLG differentiation via inhibition of ATX's lysoPLD activity (Figs. 2.2, 2.3 and 2.5) is associated with a decrease in HDAC activity (Figs. 2.4 and 2.6) and an increase in histone acetylation (Fig. 2.7).

**ATX-lysoPLD promoted progression along the early stages of the OLG lineage is dependent on the activity of HDAC1/2 but not HDAC6**

The general requirement of HDAC activity for OLG differentiation has been previously shown to involve particularly the class I HDAC members HDAC1 and HDAC2 (Shen et al., 2008; Wu et al., 2012; Ye et al., 2009). To investigate the extent to which ATX's lysoPLD activity may represent an upstream signal regulating especially the activity of the class I HDAC members HDAC1 and HDAC2, we used a pharmacological HDAC1/2/3 inhibitor, namely CI994 (Beckers et al., 2007; Kraker et al., 2003), in the experimental design as depicted in Fig. 2.8A. It is of note that HDAC3 was found to not be involved in the regulation of OLG differentiation at the stages analyzed here (Shen et al., 2008; Wu et al., 2012). In addition, at the concentration used (2.5 μM), CI994 is considered to effectively inhibit HDAC1 (Beckers et al., 2007). The effectiveness of HDAC1/2 inhibition in our system is corroborated by the observed reduction in *Ugt8* mRNA levels (Fig. 2.8B), as its expression has been previously shown to be regulated by direct targets of HDAC1/2-mediated histone deacetylation (Swiss et al., 2011). Furthermore, and as a control, inhibition of HDAC6, which represents a class II HDAC member, was performed by using the inhibitor Tubastatin A (Butler et al., 2010). At the concentration used (5 μM), Tubastatin A is considered to effectively inhibit HDAC6 with

additional but only moderate activity at HDAC8 (Beckers et al., 2007). Neither HDAC6 nor HDAC8 have been found involved in the regulation of gene expression changes associated with OLG differentiation (Noack et al., 2014; Shen et al., 2005, 2008; Wu et al., 2012), and HDAC6 has in OLGs functionally been primarily implicated in contributing to the clearing process of misfolded protein aggregates (Leyk et al., 2015; Noack et al., 2014). As indicated above and shown in Fig. 2.8, application of CI994, but not Tubastatin A, attenuated the expression of the OLG differentiation genes *Ugt8* and *Cnp* to a similar extent as the application of the ATX-lysoPLD activity inhibitor HA130 (*Ugt8*: HA130, n=3, *t*-test, p=0.0299; CI994, n=3, *t*-test, p=0.0176; Tubastatin A, n=3, *t*-test, ns; *Cnp*: HA130, n=3, *t*-test, p=0.0382; CI994, n=3, *t*-test, p=0.0270; Tubastatin A, n=3, *t*-test, ns). To assess the extent to which HDAC1/2 activity may be required for the observed ATX-lysoPLD-mediated changes in gene expression, the effect of HDAC1/2/3 or HDAC6 inhibition on LPA-stimulated rescue was determined. In agreement with a critical role of HDAC1/2, but not HDAC6, the addition of LPA was unable to rescue the effect of ATX-lysoPLD inhibition on *Ugt8* and *Cnp* mRNA levels in the presence of CI994, but not Tubastatin A (Fig. 2.8B,C) (*Ugt8:* HA130+CI994+LPA, n=3, *t*-test, p=0.0033; HA130+Tubastatin A+LPA, n=3, *t*-test, p=0.0373; *Cnp*, HA130+CI994+LPA, n=3, *t*-test, p=0.0036; HA130+Tubastatin A+LPA, n=3, *t*-test, p=0.0325). It is of note that ATX-lysoPLD inhibition could be observed as early as 2 hrs post-application of HA130 (not shown) and was thus fully effective at the time-point of HDAC inhibition. Furthermore, no additive or synergistic effects were observed upon additional inhibition of HDAC1/2/3 or HDAC6 (data not shown). Moreover, CI994 (Kraker et al., 2003), tubastatin A (Parab et al., 2015) and LPA (our own data, not

shown) have been shown to exert their effects within the first 2 hrs of treatment, thus largely excluding a timely separation of their actions. Thus, the above data provide strong support for a crucial role of the class I HDAC members HDAC1 and HDAC2 as downstream targets mediating the OLG differentiation promoting effect of ATX's lysoPLD activity.

**Discussion**

Our data presented here, suggest a modulatory role of ATX during the transition from an OLG progenitor to an early stage differentiating OLG as depicted in our proposed model shown in Fig. 2.9. In this model, LPA, generated via ATX's lysoPLD activity, activates one (or more) of its cognate G protein-coupled receptors, which are referred to as LPA receptors (Choi and Chun, 2013; Chun et al., 2010; Kihara et al., 2014) and have been found expressed by cells of the OLG lineage (Dawson et al., 2003; Nogaroli et al., 2009b; Stankoff et al., 2002; Weiner et al., 1998; Zhang et al., 2014). Activation of the above ATX-LPA axis initiates a downstream signaling cascade leading to the activation of HDAC1/2, which in turn mediates histone deacetylation and repression of transcriptional inhibitors of OLG differentiation, thereby promoting gene expression changes that are associated with the transition from an OLG progenitor to an early stage differentiating OLG. ATX has been found to be expressed and secreted by OLG progenitors and differentiating OLGs (Figs. 2.4, 2.5 and Fox et al., 2003; Fuss et al., 1997; Savaskan et al., 2007) thus suggesting an autocrine signaling mechanism. However, and during development, paracrine regulation may also occur via the secretion of ATX by cells of the floor plate (Yuelling et al., 2012). Importantly, the regulatory mechanism described here appears evolutionarily conserved, at least from

zebrafish to rodents.

In the context of histone deacetylation during the early stages of OLG differentiation, it is of note that HDAC1/2 activity has not only been implicated in modulating the transition from an OLG progenitor to an early stage differentiating OLG, but also the specification of an OLG progenitor from a multipotent neural progenitor cell (Copray et al., 2009; Jacob et al., 2011). However, and based on the data shown here, HDAC1/2-mediated regulation of OLG progenitor specification is unlikely to be modulated by ATX and its lysoPLD activity. First, inhibition of ATX-lysoPLD activity was not found to affect the expression of *nkx2.2.a* (Fig. 2.4), which has been described to be upregulated upon early developmental loss of HDAC1 activity (Cunliffe and Casaccia-Bonnefil, 2006). Second, ATX and its lysoPLD activity were not found to affect the expression of *olig2*, which during OLG progenitor specification has been proposed to be modulated via HDAC1/2 activity and upstream of sonic hedgehog signaling (Cunliffe and Casaccia-Bonnefil, 2006; Ye et al., 2009). Hence, it appears that ATX, via its lysoPLD activity, modulates HDAC1/2-regulated gene expression explicitly during a developmental time window that coincides with the transition from OLG progenitor to early stage differentiating OLG and that likely occurs post-sonic hedgehog-modulated HDAC1/2-regulated gene expression implicated in OLG progenitor specification. Future work will, however, be necessary to more precisely define the relationships between the ATX-LPA axis, sonic hedgehog signaling and their downstream effects on HDAC1/2-regulated gene expression.

In general, it is becoming more and more clear that histone acetylation and deacetylation events represent dynamic modifications (Peserico and Simone, 2011).

Consistent with this notion, histone deacetylation in cells of the OLG lineage has been found to be transient and reversible (Shen et al., 2005). In a search for more stable repressive histone modifications, marks of trimethylation of lysine residue K9 on histone 3 (H3K9) have recently been found to coincide with the transition from OLG progenitor to differentiating OLG (Liu et al., 2015). Thus, it will be interesting to explore in subsequent studies a potential role of the ATX-LPA axis in modulating H3K9 methyltransferases.

ATX has been demonstrated to possess two functionally distinct domains, the lysoPLD active site and the MORFO domain. Our data presented here, demonstrate that ATX's lysoPLD active site affects epigenetic and gene expression aspects of OLG differentiation. In contrast, and based on our previous data, the function of ATX's MORFO domain, as it relates to OLG differentiation, appears restricted to promoting cytoskeletal and thus morphological changes (Dennis et al., 2008, 2012; Fox et al., 2003). This concept that OLG morphogenesis is regulated, at least in part, by mechanisms distinct from the ones affecting gene expression is supported by previous findings (Buttery and ffrench-Constant, 1999; Ishii et al., 2012; Osterhout et al., 1999; Sloane and Vartanian, 2007; Younes-Rapozo et al., 2009). At the same time, however, it is also well-known that both of the above stated aspects of OLG differentiation occur well-synchronized during development (Bauer et al., 2009; Mitew et al., 2014; Wegner, 2008). Taken together, these observations raise the exciting possibility that ATX, via the concerted action of its two distinct functional activities, may be one of the critical players coordinating gene expression and morphological changes during OLG differentiation.

The functional effects of ATX's lysoPLD activity have been well-described to be mediated by signaling through a family of G protein-coupled receptors, the so-called LPA receptors. To date, there are six receptors that are recognized as *bona fide* LPA receptors, all of which appear to be expressed, at least to some degree, in cells of the OLG lineage (Zhang et al., 2014). Notably, $LPA_1$ has long been known to be present on OLGs (Dawson et al., 2003; Nogaroli et al., 2009b; Stankoff et al., 2002; Weiner et al., 1998), and a number of functional roles have been proposed based on tissue culture studies. Somewhat disappointingly, *Lpar1* knock-out mice have initially not been found to display CNS myelin-related pathologies (Contos et al., 2000, 2002). Myelin defects were, however, reported in more recent studies analyzing the so-called *Málaga* variant (*maLpar1* null mice), a stable variant of the original *Lpar1* knock-out mouse strain in which defects are more pronounced likely due to interactions of $LPA_1$ with currently unknown genetic modifiers (Estivill-Torrús et al., 2008; García-Díaz et al., 2015). In *maLpar1* null mice, impaired transport of one of the major myelin proteins, namely proteolipid protein, was found to be impaired leading to loss of OLGs most likely due to stress-induced apoptosis. No deficits in OLG differentiation were noted in these mice. Thus, and despite its prominent expression in OLGs, $LPA_1$ appears unlikely to play a major role in mediating the ATX-LPA-HDAC1/2 axis described here.

To our knowledge, null mice have been generated for all currently recognized LPA receptors with the exception of $LPA_6$ (Contos et al., 2000, 2002; Lin et al., 2012; Liu et al., 2010; Ye et al., 2005). In addition, knock-down studies have been performed in the zebrafish and in *Xenopus laevis* that cover all known *bona fide* LPA receptors (Geach et al., 2014; Yukiura et al., 2011). In neither of the studies have myelin defects been

reported. This does not exclude a prominent role of LPA receptor signaling in OLGs but rather highlights the complication of functional redundancy and compensation when eliminating a single LPA receptor. For example, it has been shown that combined knock-down of *lpar1* and *lpar4* in the zebrafish leads to vascular defects while single *lpar* knock-down has no effect (Yukiura et al., 2011). Similarly, male reproductive defects have been observed in triple *Lpar1/2/3* knockout mice but not any of the single *Lpar* knockout mice (Ye et al., 2008). In the context of our studies it is interesting that for the triple knockout mice no myelin defects have been reported, thus suggesting an involvement of at least one of the remaining LPA receptors, namely $LPA_4$, $LPA_5$ and/or $LPA_6$. Out of these, $LPA_4$ has been shown to activate PKA via coupling to the heterotrimeric G-protein $G_{\alpha s}$ and increase in cyclic AMP (cAMP) levels (Gardell et al., 2006). PKA, in turn, has been implicated in regulating HDAC activity via phosphorylation (Sengupta and Seto, 2004). While $LPA_5$ was found to not couple to $G_{\alpha s,}$ its stimulation was nevertheless found to be associated with an increase in cAMP levels possibly through involvement of G protein βγ subunits (Lee et al., 2006). $LPA_6$ may couple to $G_{\alpha s,}$ however with likely much lower potency than $LPA_4$ (Yanagida et al., 2009a). Clearly, more comprehensive analyses will be necessary to dissect the exact roles for each of the LPA receptors in the regulation of OLG differentiation and via the ATX-LPA axis. Our data presented here, reveal a novel functional role for ATX's lysoPLD activity, namely the promotion of OLG differentiation via an increase in HDAC1/2 activity and associated changes in gene expression. In the context of human diseases and in particular the major demyelinating disease in human, Multiple Sclerosis (MS), it is worth mentioning that *ATX* mRNA levels have been found reduced within the MS CNS

(Raddatz et al., 2014) and that a shift toward a decrease in histone deacetylation has been implicated in contributing to the limitations in myelin repair seen in MS (Pedre et al., 2011). These findings further support a critical role of ATX in the regulation of CNS myelination, and they suggest that misregulation of the ATX-LPA-HDAC1/2 axis may contribute to the pathology seen in MS.

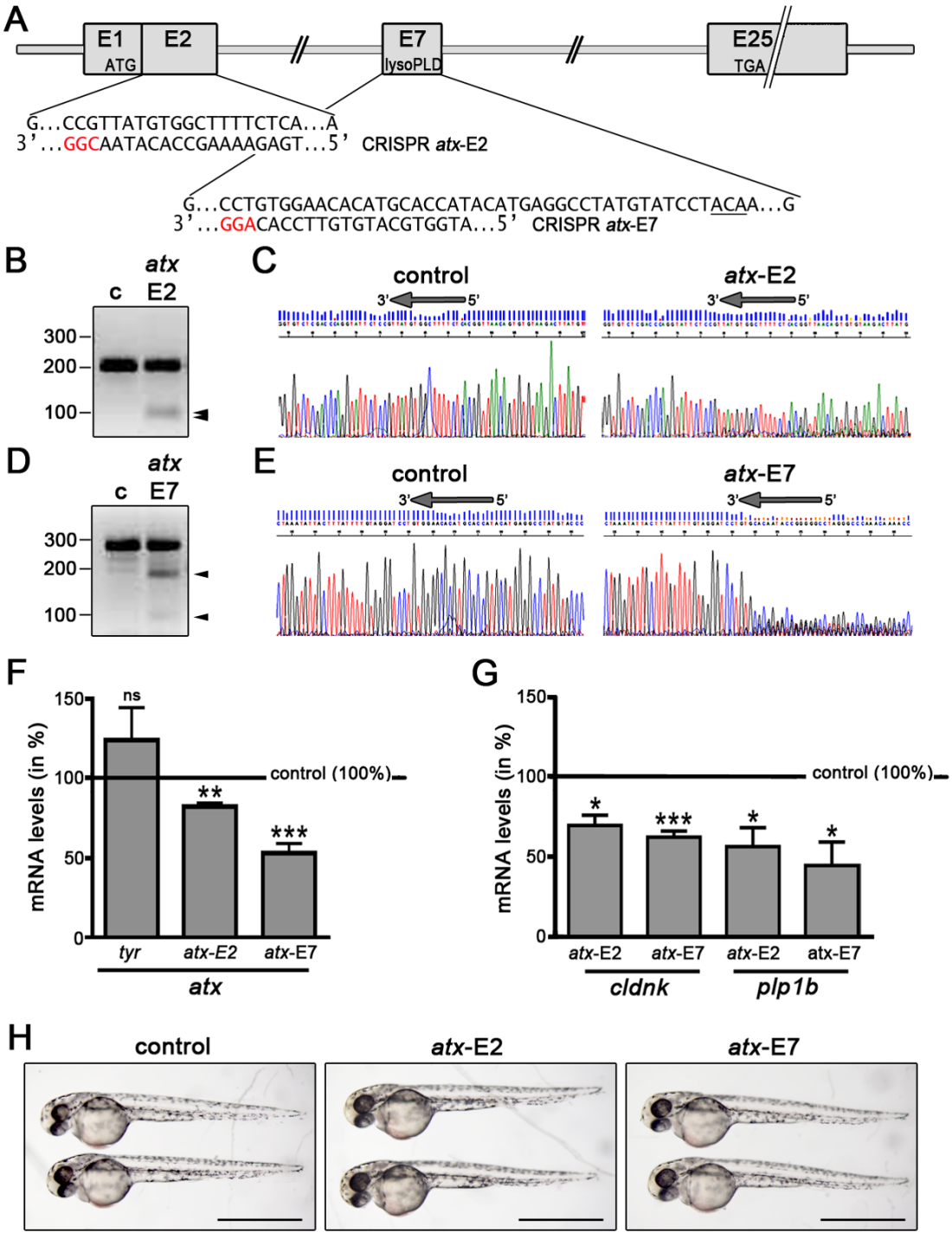
A
E1
ATG
E2
E7
lysoPLD
E25
TGA
G...CCGTTATGTGGCTTTTCTCA...A
3'...GGCAATACACCGAAAAGAGT...5' CRISPR atx-E2
G...CCTGTGGAACACATGCACCATACATGAGGCCTATGTATCCTACAA...G
3'...GGACACCTTGTGTACGTGGTA...5' CRISPR atx-E7
B
atx
c E2
300
200
100
C
control
atx-E2
3'
5'
D
atx
c E7
300
200
100
E
control
atx-E7
3'
5'
F
mRNA levels (in %)
150
100
50
0
ns
**
***
control (100%)
tyr
atx-E2
atx-E7
atx
G
mRNA levels (in %)
150
100
50
0
*
***
*
*
control (100%)
atx-E2
atx-E7
atx-E2
atx-E7
cldnk
plp1b
H
control
atx-E2
atx-E7

**Figure 2.1**. In the developing zebrafish, CRISPR-Cas9-mediated mutagenesis of *atx* leads to a reduction in the mRNA levels for OLG marker genes. ***A,*** *atx* (*enpp2*) genomic structure and CRISPR target sequences. ATG and TGA indicate the locations of the translation start and stop sites. Protospacer adjacent motif (PAM) sequences are highlighted in red. The sequence encoding T210, the threonine residue shown to be obligatory for ATX's enzymatic activity, is underlined. ***B,D,*** Representative images of agarose gels showing DNA fragments upon Surveyor nuclease treatment of control homoduplexes (c) and control/*atx*-E2 (***B***) or control/*atx*-E7 (***D***) homo/heteroduplexes. Numbers on the left indicate DNA sizes in bp. Arrowheads indicate cleaved PCR amplicon fragments at the expected sizes indicative of indel mutations generated by genome editing. ***C,E,*** Representative images of sequencing traces obtained from genomic DNA-derived PCR amplicons from control and Cas9 mRNA/sgRNA injected zebrafish embryos. Arrows at the top of each trace indicate the location of the target sequence, over and upstream of which a composite sequence trace indicates the presence of indel mutations generated by genome editing. ***F,G,*** Bar graphs illustrating mRNA levels for *atx* (***F***) or the OLG marker genes *cldnk* and *plp1b* (***G***) in whole embryos as determined by real-time reverse transcription (RT)-qPCR analysis. Control (uninjected embryos) values were set to 100% (see horizontal line) and experimental values were calculated accordingly. Data shown represent means ± SEM. $^{ns}$not significant, *p≤0.05, **p≤0.01, ***p≤0.001. ***H***, Representative brightfield images of control (uninjected) and Cas9 mRNA/sgRNA injected embryos at 48 hpf. Scale bar: 1 mm.

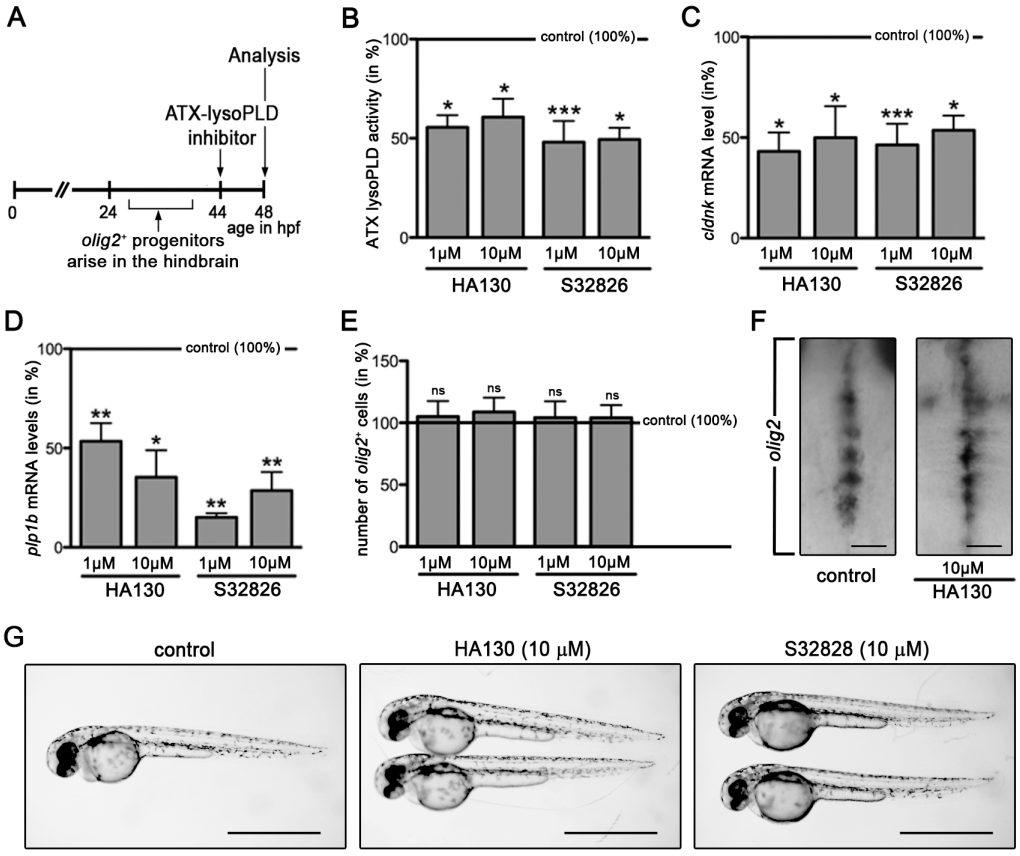
A
Analysis
ATX-lysoPLD
inhibitor
0
24
44
48
age in hpf
olig2+ progenitors
arise in the hindbrain
B
control (100%)
ATX lysoPLD activity (in %)
100
50
0
1µM
10µM
1µM
10µM
HA130
S32826
C
control (100%)
cldnk mRNA level (in%)
HA130
S32826
D
control (100%)
plp1b mRNA levels (in %)
HA130
S32826
E
number of olig2+ cells (in %)
ns
control (100%)
HA130
S32826
F
olig2
control
10µM
HA130
G
control
HA130 (10 µM)
S32828 (10 µM)

**Figure 2.2.** In the developing zebrafish, inhibition of ATX's lysoPLD activity during early stages of OLG differentiation leads to a reduction in the levels of OLG-enriched transcripts without apparent effects on the number of *olig2*-positive cells. ***A*****,** Experimental design. Embryos were treated with the ATX-lysoPLD inhibitors HA130 and S32826 at a time point when newly specified OLG progenitors start to differentiate. ***B,*** Bar graph depicting ATX-lysoPLD activity in whole embryos as assessed by using the fluorogenic substrate FS-3. ***C,D,*** Bar graphs illustrating mRNA levels for the OLG marker genes *cldnk* (***C***) and *plp1b* (***D***) in whole embryos as determined by real-time reverse transcription (RT)-qPCR analysis. ***E,*** Bar graph showing the number of *olig2*-positive progenitors in whole embryos as determined through whole mount *in-situ* hybridization. ***F,*** Representative extended focus images of whole mount embryos after *in situ* hybridization with a probe specific for *olig2*. Dorsal views over the hindbrain are shown with anterior to the top. Scale bar: 50 μm. ***G***, Representative brightfield images of control (vehicle-treated) and ATX-lysoPLD inhibitor treated embryos at 48 hpf. Scale bar: 1 mm. For all bar graphs, control (vehicle-treated) values were set to 100% (see horizontal line) and experimental values were calculated accordingly. Data shown represent means ± SEM. $^{ns}$not significant, *p≤0.05, **p≤0.01, ***p≤0.001.

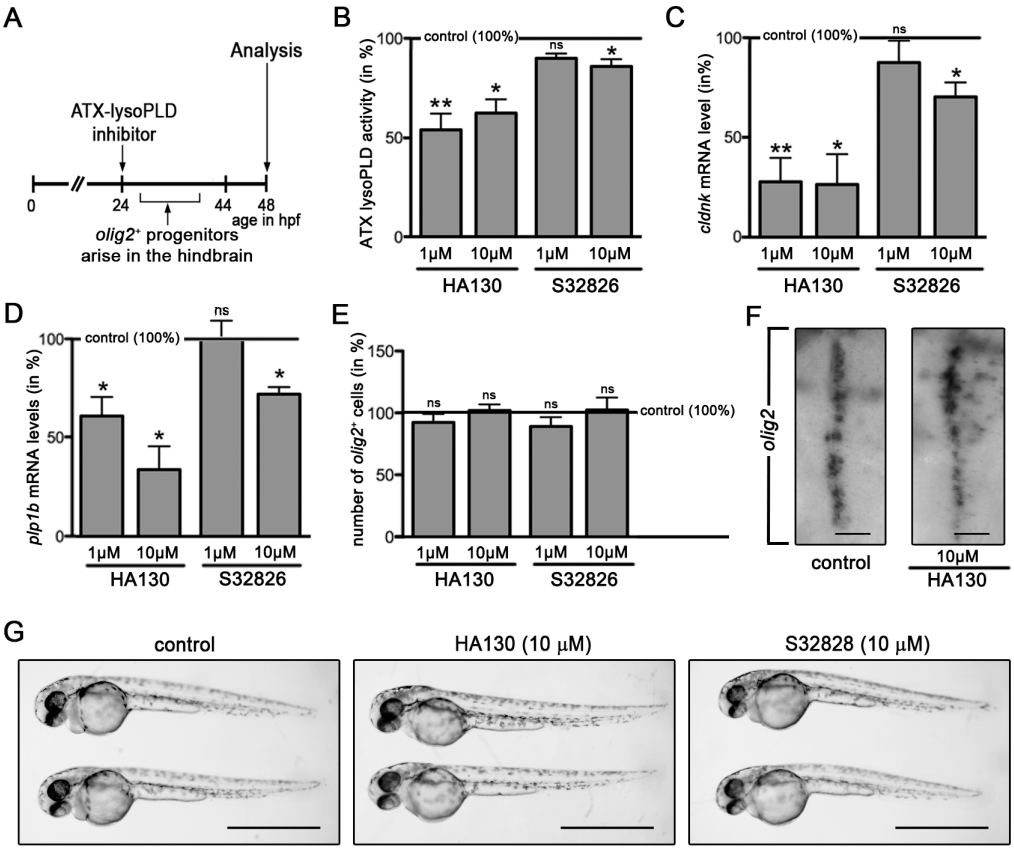
A
Analysis
ATX-lysoPLD
inhibitor
0
24
44
48
age in hpf
olig2+ progenitors
arise in the hindbrain
B
ATX lysoPLD activity (in %)
control (100%)
ns
**
*
*
1μM
10μM
1μM
10μM
HA130
S32826
C
cldnk mRNA level (in%)
control (100%)
ns
**
*
*
1μM
10μM
1μM
10μM
HA130
S32826
D
plp1b mRNA levels (in %)
control (100%)
ns
*
*
*
1μM
10μM
1μM
10μM
HA130
S32826
E
number of olig2+ cells (in %)
ns
ns
ns
ns
control (100%)
1μM
10μM
1μM
10μM
HA130
S32826
F
olig2
control
10μM
HA130
G
control
HA130 (10 μM)
S32828 (10 μM)

**Figure 2.3.** In the developing zebrafish, inhibition of ATX's lysoPLD activity during the time window when *olig2*-positive progenitors arise in the hindbrain leads to a reduction in the levels of OLG-enriched transcripts without apparent effects on the number of *olig2*-positive cells. ***A*****,** Experimental design. Embryos were treated with the ATX-lysoPLD inhibitors HA130 and S32826 during the time window when *olig2*-positive progenitors arise in the ventral hindbrain. ***B,*** Bar graph depicting ATX-lysoPLD activity in whole embryos as assessed by using the fluorogenic substrate FS-3. ***C,D,*** Bar graphs illustrating mRNA levels for the OLG marker genes *cldnk* (***C***) and *plp1b* (***D***) in whole embryos as determined by real-time reverse transcription (RT)-qPCR analysis. Note that loss of inhibitory activity as seen for S32826 results in an attenuated effect on *cldnk* and *plp1b* mRNA levels, thus suggesting that ATX, via its lysoPLD activity, regulates OLG differentiation during a critical developmental window. ***E,*** Bar graph showing the number of *olig2*-positive progenitors in whole embryos as determined through whole mount *in-situ* hybridization. ***F,*** Representative extended focus images of whole mount embryos after *in situ* hybridization with a probe specific for *olig2*. Dorsal views over the hindbrain are shown with anterior to the top. Scale bar: 50 μm. ***G***, Representative brightfield images of control (vehicle-treated) and ATX-lysoPLD inhibitor treated embryos at 48 hpf. Scale bar: 1 mm. For all bar graphs, control (vehicle-treated) values were set to 100% (see horizontal line) and experimental values were calculated accordingly. Data shown represent means ± SEM. $^{ns}$not significant, *p≤0.05, **p≤0.01, ***p≤0.001.

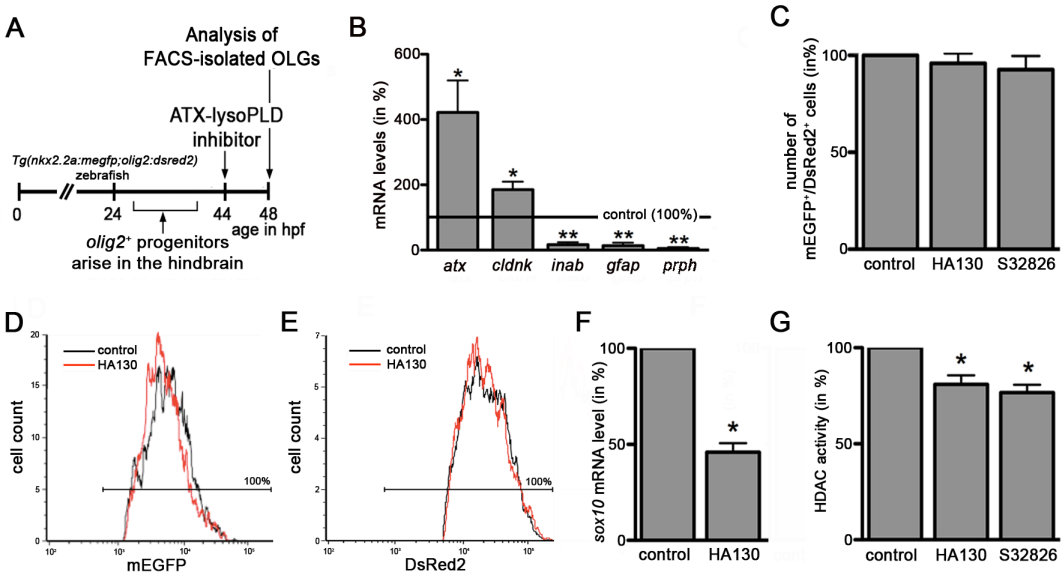
A
Analysis of
FACS-isolated OLGs
ATX-lysoPLD
inhibitor
Tg(nkx2.2a:megfp;olig2:dsred2)
zebrafish
0
24
44
48
age in hpf
olig2+ progenitors
arise in the hindbrain
B
mRNA levels (in %)
600
400
200
0
control (100%)
atx
cldnk
inab
gfap
prph
C
number of
mEGFP+/DsRed2+ cells (in%)
100
50
0
control
HA130
S32826
D
cell count
control
HA130
100%
mEGFP
E
cell count
control
HA130
100%
DsRed2
F
sox10 mRNA level (in %)
100
50
0
control
HA130
G
HDAC activity (in %)
100
50
0
control
HA130
S32826

**Figure 2.4.** In the developing zebrafish, inhibition of ATX's lysoPLD activity during early stages of OLG differentiation leads to a reduction in HDAC activity within cells of the OLG lineage. ***A*,** Experimental design using *Tg(nkx2.2a:megfp;olig2:dsred2)* zebrafish embryos, which were treated with the ATX-lysoPLD inhibitors HA130 (10 µM) or S32826 (10 µM) at a time point when newly specified OLG progenitors start to differentiate. ***B,*** Bar graph illustrating the mRNA expression profile under control conditions for FACS-isolated mEGFP/DsRed2 double-positive cells as determined by real-time reverse transcription (RT)-qPCR analysis. mRNA levels in whole fish were set to 100% for each gene individually (marked by the horizontal line) and the values for sorted cells were calculated accordingly. ***C,*** Bar graph showing the number of mEGFP/DsRed2 double-positive cells as determined by FACS analysis. Values for vehicle-treated embryos were set to 100% (see control bar) and experimental values were calculated accordingly. ***D,E,*** Representative single-parameter fluorescence histograms (*x* axis: fluorescence intensity, logarithmic scale; *y* axis: cell number) depicting mEGFP (***D***) or DsRed2 (***E***) intensities of mEGFP/DsRed2 double-positive cells under control conditions (black line) and upon treatment with HA130 (red line). Cells within the area marked by the horizontal line were considered mEGFP (***D***)- or DsRed2 (***E***)-positive. Note the high purity (100%) of the sorted cell population. ***F,*** Bar graph depicting *sox10* mRNA levels for FACS-isolated mEGFP/DsRed2 double-positive cells as determined by real-time reverse transcription (RT)-qPCR analysis. Values for vehicle-treated embryos were set to 100% (see control bar) and experimental values were calculated accordingly. ***G,*** Bar graph depicting HDAC activity as determined by using the fluorogenic substrate Boc-Lys(Ac)-AMC. Values for vehicle-treated embryos were set to 100% (see control bar) and experimental values were calculated accordingly. Data shown in all bar graphs represent means ± SEM. $^{ns}$not significant, *p≤0.05, **p≤0.01, ***p≤0.001.

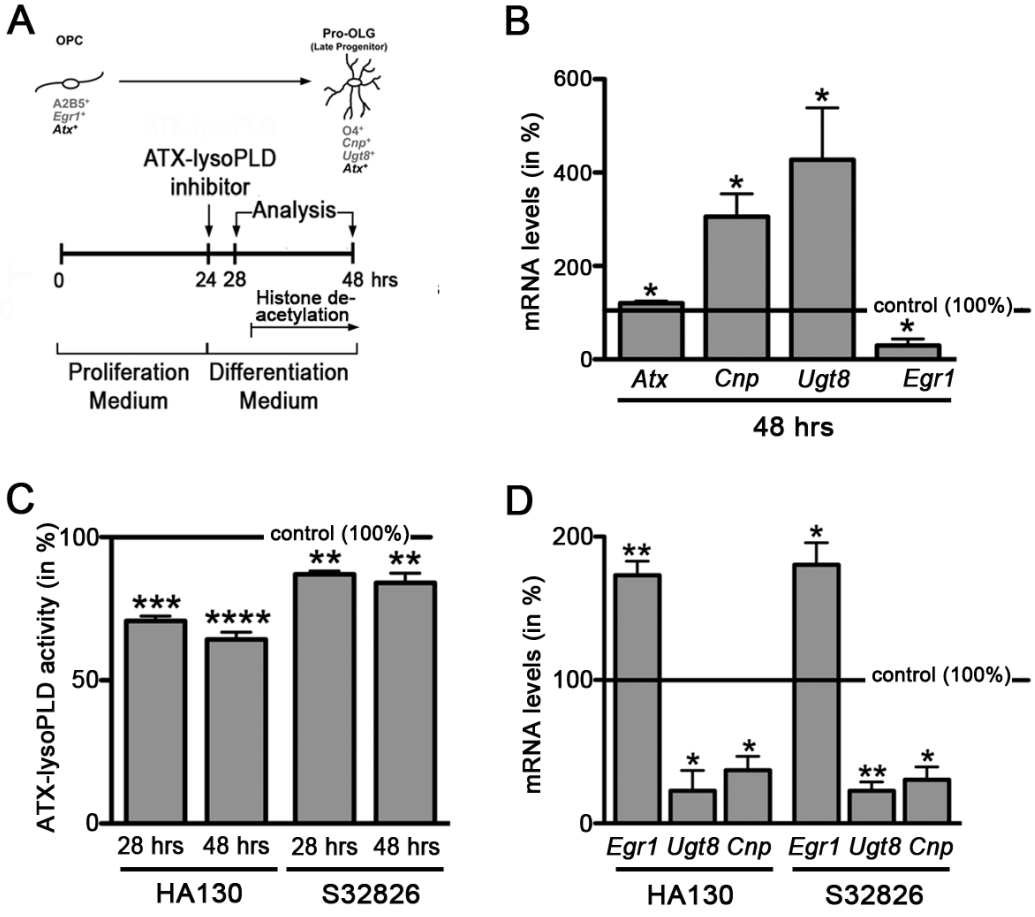
A
OPC
A2B5+
Egr1+
Atx+
Pro-OLG
(Late Progenitor)
O4+
Cnp+
Ugt8+
Atx+
ATX-lysoPLD
inhibitor
Analysis
0
24 28
48 hrs
Histone de-
acetylation
Proliferation
Medium
Differentiation
Medium
B
mRNA levels (in %)
600
400
200
0
control (100%)
Atx
Cnp
Ugt8
Egr1
48 hrs
C
ATX-lysoPLD activity (in %)
100
50
0
control (100%)
***
****
**
**
28 hrs
48 hrs
28 hrs
48 hrs
HA130
S32826
D
mRNA levels (in %)
200
100
0
control (100%)
Egr1 Ugt8 Cnp
Egr1 Ugt8 Cnp
HA130
S32826

**Figure 2.5.** In rodent OLG cultures, inhibition of ATX's lysoPLD activity leads to a reduction in the levels of mRNAs encoding OLG differentiation genes and to an increase in the level of mRNA encoding the transcriptional OLG differentiation inhibitor *Egr1*. ***A,*** Experimental design. Timing of histone deacetylation is marked as described by Marin-Husstege et al. (2002). OPC: OLG progenitor. ***B,*** Bar graph depicting mRNA levels for the OLG differentiation genes *Cnp* and *Ugt8* and the transcriptional inhibitor *Egr1* as well as *Atx* as determined by real-time reverse transcription (RT)-qPCR analysis. mRNA levels at 24 hrs were set to 100% for each gene and 48 hrs values were calculated accordingly. ***C,*** Bar graph illustrating ATX-lysoPLD activity as assessed by using the fluorogenic substrate FS-3. Control (vehicle-treated) values were set to 100% (see horizontal line) and experimental values were calculated accordingly. ***D,*** Bar graph depicting mRNA levels for the OLG differentiation genes *Cnp* and *Ugt8* and the transcriptional inhibitor *Egr1* as determined by real-time RT-qPCR analysis. Control (vehicle-treated) values were set to 100% (see horizontal line) and experimental values were calculated accordingly. Data shown in all bar graphs represent means ± SEM. $^{ns}$not significant, *p≤0.05, **p≤0.01, ***p≤0.001.

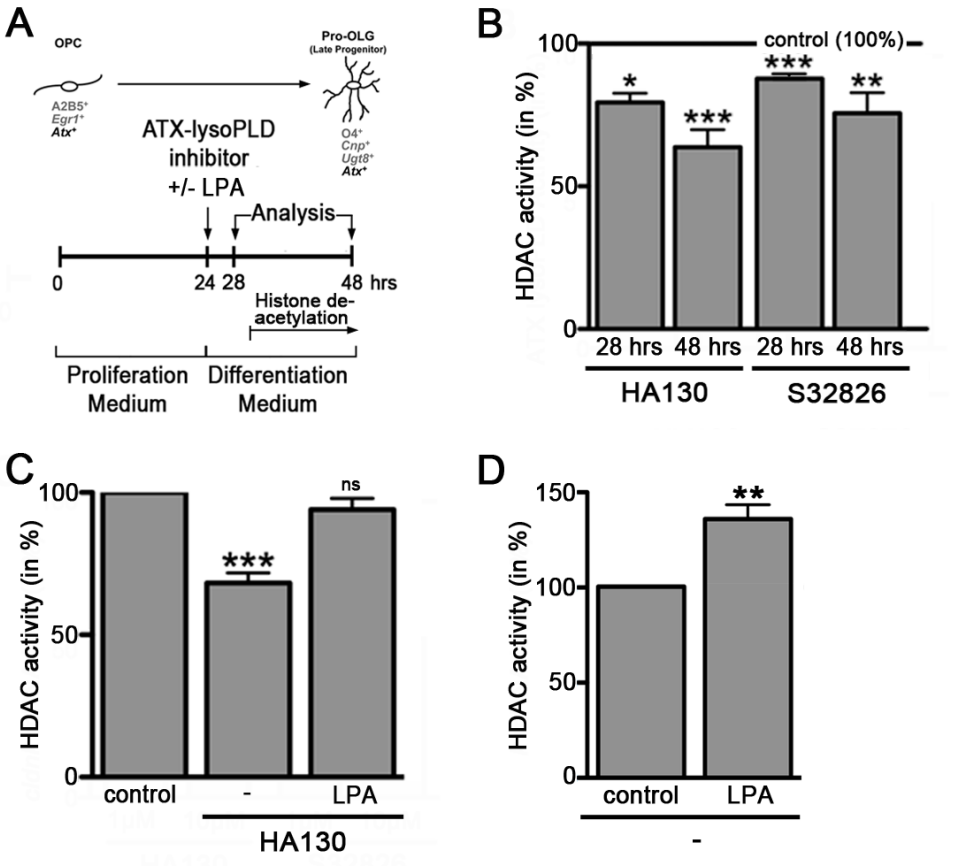
A
OPC
A2B5+
Egr1+
Atx+
Pro-OLG
(Late Progenitor)
O4+
Cnp+
Ugt8+
Atx+
ATX-lysoPLD
inhibitor
+/- LPA
Analysis
0
24 28
48 hrs
Histone de-
acetylation
Proliferation
Medium
Differentiation
Medium
B
control (100%)
HDAC activity (in %)
100
50
0
*
***
***
**
28 hrs 48 hrs 28 hrs 48 hrs
HA130
S32826
C
HDAC activity (in %)
100
50
0
***
ns
control
-
LPA
HA130
D
HDAC activity (in %)
150
100
50
0
**
control
LPA
-

**Figure 2.6.** In rodent OLG cultures, inhibition of ATX's lysoPLD activity leads a reduction in HDAC activity. ***A,*** Experimental design. Timing of histone deacetylation is marked as described by Marin-Husstege et al. (2002). OPC: OLG progenitor. ***B-D,*** Bar graphs showing HDAC activity as determined by using the fluorogenic substrate Boc-Lys(Ac)-AMC. Control (vehicle-treated) values were set to 100% (see horizontal line in ***B*** and control bars in ***C,D***) and experimental values were calculated accordingly. Data represent means ± SEM. $^{ns}$not significant, *p≤0.05, **p≤0.01, ***p≤0.001.

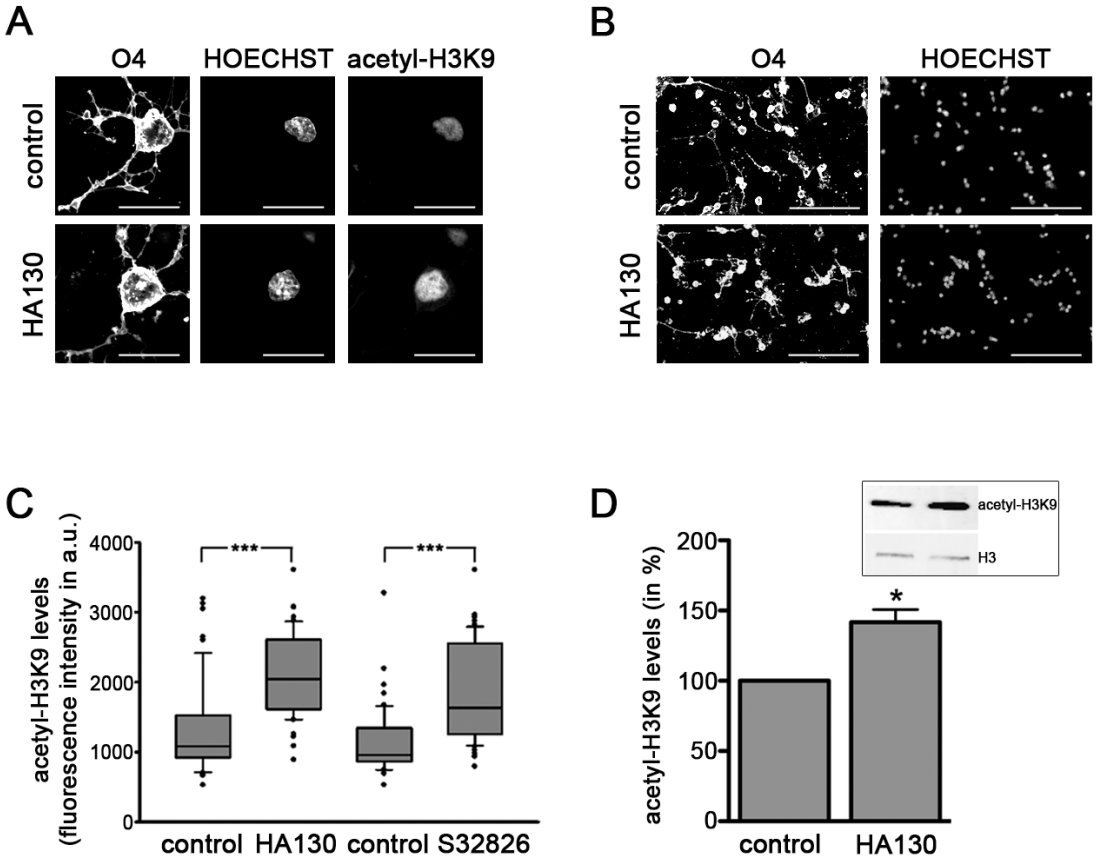
A
O4
HOECHST
acetyl-H3K9
control
HA130
B
O4
HOECHST
control
HA130
C
acetyl-H3K9 levels
(fluorescence intensity in a.u.)
4000
3000
2000
1000
0
***
***
control
HA130
control
S32826
D
acetyl-H3K9
H3
acetyl-H3K9 levels (in %)
200
150
100
50
0
*
control
HA130

**Figure 2.7.** In rodent OLG cultures, inhibition of ATX's lysoPLD activity leads to an increase in nuclear histone acetylation at lysine residue 9 of histone 3 (H3K9). ***A,B,*** Representative confocal images of differentiating OLGs treated with vehicle (control, upper panel) or HA130 (lower panel) and immuno-labeled using O4 hybridoma supernatants (***A,B***) and anti-acetyl-histone H3K9 antibodies (***A***). Nuclei are visualized via staining with Hoechst (***A,B***). Scale bars: 20 μm in ***A***, 100 μm in ***B. C,*** Box and whisker plot depicting nuclear acetyl-H3K9 levels as assessed by determining fluorescence intensities shown in arbitrary units (a.u.). The plot depicts medians and quartiles of three independent experiments. Whiskers represent the 10th and 90th percentile. ***p≤0.001. ***D,*** Bar graph illustrating acetyl-H3K9 levels as assessed by Western blot analysis. A representative Western blot image is shown in the inset (upper right). For the bar graph, control (vehicle-treated) values were set to 100% (see control bar) and experimental values were calculated accordingly. Data represent means ± SEM. *p≤0.05 (Student's *t*-test).

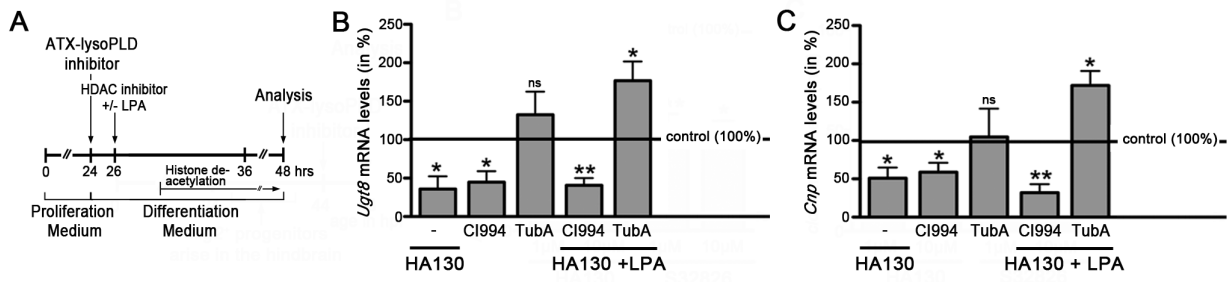
A
ATX-lysoPLD inhibitor
HDAC inhibitor +/- LPA
Analysis
0
24
26
Histone de-acetylation
36
48 hrs
Proliferation Medium
Differentiation Medium
B
Ugt8 mRNA levels (in %)
250
200
150
100
50
0
control (100%)
ns
*
**
-
CI994
TubA
CI994
TubA
HA130
HA130 +LPA
C
Cnp mRNA levels (in %)
250
200
150
100
50
0
control (100%)
ns
*
**
-
CI994
TubA
CI994
TubA
HA130
HA130 + LPA

**Figure 2.8.** In rodent OLG cultures, LPA rescue of ATX-lysoPLD activity inhibition requires the activity of class I HDAC members HDAC1 and HDAC2 but not the class II HDAC member HDAC6. ***A,*** Experimental design. Timing of histone deacetylation is marked as described by Marin-Husstege et al. (2002). OPC: OLG progenitor. ***B,C,*** Bar graphs depicting mRNA levels for the OLG differentiation genes *Ugt8* (***B***) and *Cnp* (***C***) as determined by real-time reverse transcription (RT)-qPCR analysis. Control (vehicle-treated) values were set to 100% (see horizontal line) and experimental values were calculated accordingly. Data represent means ± SEM. $^{ns}$not significant, *p≤0.05, **p≤0.01.

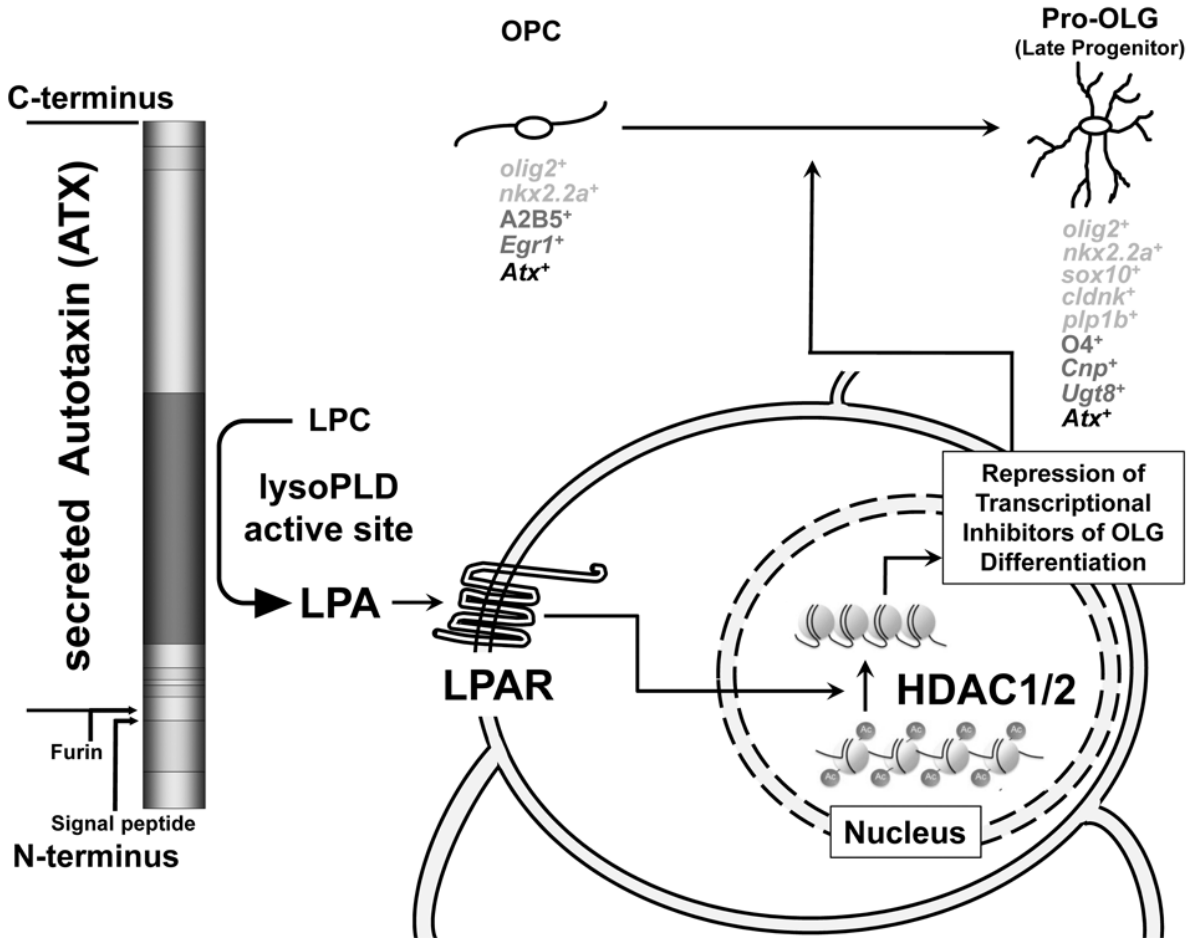
C-terminus
secreted Autotaxin (ATX)
Furin
Signal peptide
N-terminus
LPC
lysoPLD
active site
LPA
OPC
olig2+
nkx2.2a+
A2B5+
Egr1+
Atx+
Pro-OLG
(Late Progenitor)
olig2+
nkx2.2a+
sox10+
cldnk+
plp1b+
O4+
Cnp+
Ugt8+
Atx+
LPAR
Repression of
Transcriptional
Inhibitors of OLG
Differentiation
HDAC1/2
Nucleus

**Figure 2.9.** Proposed model for the role of the ATX-LPA axis in OLG differentiation. ATX, which has been found secreted by OLGs throughout the early stages of the lineage, generates the lipid signaling molecule lysophosphatidic acid (LPA) via its enzymatically active lysoPLD site. LPA, in turn, activates one (or more) of its cognate receptors (LPARs) on the surface of OLG progenitors, which leads to the downstream activation of histone deacetylase 1 and 2 (HDAC1/2) in the nucleus. Histone deacetylation mediates the repression of transcriptional inhibitors of OLG differentiation and thereby promotes gene expression changes associated with the differentiation from an OLG progenitor (OPC) to an early differentiating OLG (Pro-OLG). Expression markers identifying individual stages of the OLG lineage are listed below each OLG stage. Markers in black were used in both the zebrafish and rodent studies, while markers in light and dark grey are unique for the zebrafish and rodent studies, respectively.

# Chapter 3

## Introduction to Lysophosphatidic Acid (LPA) and their Receptors

### Lysophosphatidic acid (LPA)

Lysophospholipids are phospholipid derivatives originating from cell membranes and one of the best studied lysophospholipids is lysophosphatidic acid (LPA). First known as a biosynthetic metabolite of cell membrane phospholipids, LPA is now regarded as an important regulator for diverse biological functions. The molecular species of LPA encompass diverse ligands that can vary in length and degree of saturation of their fatty acid chain, which is esterified at the *sn*-1 or *sn*-2 position of the glycerol backbone. The most abundant plasma species of LPA, in humans, is the 16:0 form, which contains a palmityl chain (Choi et al., 2010a). The term LPA, however, commonly refers to the 18:1 species, which is also the most commonly used research reagent for LPA signaling studies (Yung et al., 2014). The 18:0 and 18:1 species are the most common species found in the spinal cord (Das and Hajra, 1989a; Santos-Nogueira et al., 2015). Remaining LPA moieties reported in serum and plasma are 18:2, 16:1 and 20:4. All known LPA species are synthesized via two major metabolic routes (Fig. 3.1), and exhibit different functional effects.

LPA species are generated by the conversion of membrane phospholipids to lysophospholipids, such as LPC, by the action of phospholipase A1 (PLA1), phospholipase A2 (PLA2), or PLA1 and lecithin-cholesterol acyltransferase (LCAT), depending on the location of synthesis. ATX's lysoPLD active site is needed to convert the lysophospholipids into LPA species (Aoki et al., 2008a; Moolenaar and Perrakis, 2011). Lysophosphatidyl choline (LPC), the main substrate of ATX's lysoPLD active

site, is by far the most abundant lysophospholipid, in plasma and serum, and is mainly found bound to albumin (Croset et al., 2000; Ojala et al., 2006; Tokumura et al., 1999). The amount of LPC sufficient for ATX to mediate the conversion to LPA, and subsequently activate LPA receptors, is limited to a few micromolars (Jongsma et al., 2011; Umezu-Goto et al., 2002). Although ATX is the primary LPA producing phospholipase in plasma, an alternative, but less common, route of LPA production requires the hydrolysis of phosphatidic acid (PA) by the membrane- associated phospholipase A1/A2 (PA-PLA1/2) (Aoki et al., 2002, 2008b; Inoue et al., 2011).

**LPA receptors**

The pluripotent, lipid signaling mediator, LPA, exerts its widespread functions through the binding and activation of six distinct G protein-coupled receptors (GPCRs), which are differentially expressed and show both overlapping and distinct signaling properties (Chun, 2013; Chun et al., 2010). In 1996, the first LPA receptor, $LPA_1$ was identified in the ventricular zone of the embryonic brain (Hechtet al., 1996; Chun et al., 2007). $LPA_{1-6}$ can be divided into two families and are named in the order in which they were discovered. The classical receptors, $LPA_1$/Edg-2/vzg-1, $LPA_2$/Edg-4 and $LPA_3$/Edg-7, belong to the endothelial differentiation gene (Edg) family, which also includes five GPCRs for the lipid mediator sphingosine 1-phosphate (S1P) (An et al., 1997; Bandoh et al., 1999; Chun, 2013; Hecht et al., 1996). Three additional LPA receptors $LPA_4$/ P2Y9/GPR23, $LPA_5$/GPR92 and $LPA_6$/P2Y5/GPR87 are more closely related to the purinergic receptor (P2Y) family of GPCRs (Kotarsky et al., 2006; Lee et al., 2009a, 2009b; Noguchi et al., 2003; Tabata et al., 2007; Yanagida et al., 2009b, 2013). These LPARs couple to all four $G_\alpha$ proteins ($G_{12/13}$, $G_{q/11}$, $G_{i/o}$, and $G_s$) and have

several converging signaling pathways.

Albeit with different potencies, all six LPA receptors can be stimulated by 1-acyl-LPA. $LPA_3$ and $LPA_6$ stand out as they prefer unsaturated 2-acyl-LPA as a ligand, while $LPA_5$ exhibits a strong preference for ether-linked 1-alkyl-LPA species (Jongsma et al., 2011; Williams et al., 2009). Additionally, LPA receptors are expressed in most cell types of the nervous system, including neural progenitors, primary neurons, astrocytes, microglia, OLGs and Schwann cells (Noguchi et al., 2009). Due to the complexity of the LPAR pathways, overall heterogeneity of subtypes and different expression patterns, the effects of LPA are diverse and extensive, regulating many biological functions including cell growth, differentiation, survival, motility, and cytoskeletal morphology (Choi et al., 2010b; Sano et al., 2002).

**LPA-mediated effects on cells of the CNS**

The initial finding outlining that the brain has the highest tissue concentration of LPA (Das and Hajra, 1989b), triggered investigative studies of LPA in the CNS. All six known LPA receptors are expressed at varying levels in the CNS during development and/or postnatal life (Choi et al., 2010a; Fukushima et al., 2001; Lin et al., 2012; Noguchi et al., 2009; Pasternack et al., 2009). LPA has been shown to influence myriad responses in neurons and glia cell types through its cognate receptors. These receptor–mediated activities have been identified as important factors in disease states, including fetal hypoxia and hydrocephalus (Herr et al., 2011; Yung et al., 2011), neuropathic pain (Inoue et al., 2004; Lin et al., 2012; Nagai et al., 2010), ischemic stroke (Li et al., 2008), neurotrama (Frugier et al., 2011), neuropsychiatric disorders (Mirendil et al., 2015), developmental disorders, Sandhoff disease and MS (Choi and Chun, 2013).

With regard to glia cells, astrocytes, microglia and OLGs all express LPA receptors. Of particular interest to my studies, $LPA_{1-6}$ receptors are all expressed on OLGs, though at different levels. Through them LPA can initiate a variety of signaling cascades in the cell. More specifically, LPA modulates calcium signaling and activates the ERK1/2 pathway in OLGs , and can increase MBP expression in differentiating OLGs (Nogaroli et al., 2009a). Additionally, LPA plays a role in the cytoskeletal maturation of OLGs, as its expression leads to the inhibition of process formation in OPCs and increased membrane formation of OLGs, revealing a time dependent role for LPA (Dawson et al., 2003; Nogaroli et al., 2009a; Stankoff et al., 2002). Furthermore, LPA has been shown to promote OLG cell survival, though these effects were only seen in an OLG cell line (Li et al., 2003; Matsushita et al., 2005; Stankoff et al., 2002; Weiner and Chun, 1999).

The LPAR expression profile in astrocytes is quite confusing as cultured astrocytes have been shown to express *Lpar1-5* (Shano et al., 2008; Sorensen et al., 2008), however, *in vivo*, astrocytes appear to express few LPA receptor subtypes aside from low levels of *Lpar1* (Cervera et al., 2002; Tabuchi et al., 2000). The expression of *Lpar6* in astrocytes has also yet to be confirmed. Interestingly, LPA has been found to stimulate astrocyte proliferation (Shano et al., 2008). Studies investigating LPARs in microglia, the resident immune cells of the CNS, found *Lpar1* and *Lpar3* expression in rodents (Möller et al., 2001; Tham et al., 2003), and *Lpar1-3* expression in human microglia cells lines (Bernhart et al., 2010; Möller et al., 2001).

LPAR expression can also be seen in neurons. Both *Lpar1* and *Lpar2* are expressed, with *Lpar2* more abundantly (Fukushima et al., 2002; Noguchi et al., 2009).

Additionally, the expression of *Lpar5* in sensory and motor neurons of the spinal cord has been linked to pain, whereby *Lpar5* null mice appear to have a reduced pain phenotype (Lin et al., 2012). Interestingly, LPA promotes cortical neuronal progenitor cells (NPCs) to commit to the neuronal lineage via $LPA_1$ signaling (Fukushima et al., 2007; Kingsbury et al., 2003). In regards to neuronal morphology, LPA can alter the actin cytoskeleton and promote microtubule rearrangement (Fukushima and Morita, 2006; Fukushima et al., 2002), as well as influence the morphology and motility of young postmitotic neurons (Fukushima et al., 2002). All in all, LPA, and its cognate receptor signaling pathways, plays an integral role in CNS circuitry and development, as well as disease pathology, and further investigative studies are needed to uncover the multitude of effects brought on by LPA.

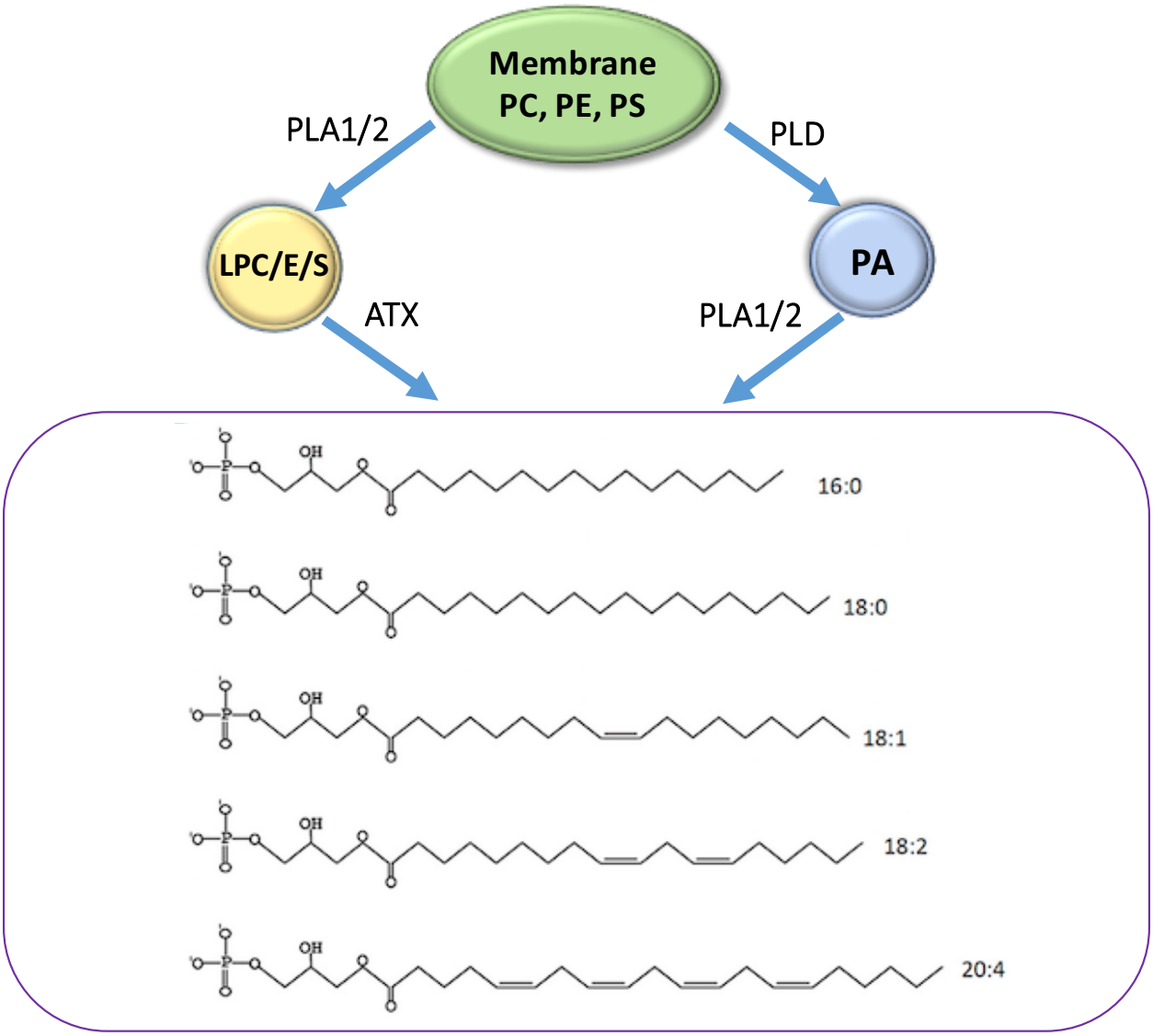
Membrane
PC, PE, PS
PLA1/2
PLD
LPC/E/S
PA
ATX
PLA1/2
16:0
18:0
18:1
18:2
20:4

**Figure 3.1. Biosynthesis of lysophosphatidic acid (LPA).** The membrane phospholipids phosphatidyl choline (PC), phosphatidyl ethanolamine (PE) or phosphatidyl serine (PS) get converted into their corresponding lyso-forms by the action of phospholipase A1 and A2 (PLA1/2). Autotaxin (ATX) then generates different LPA species using the lyso-forms of membrane lipids. Alternatively, PC, PE or PS are catalyzed into phosphatidic acid (PA) by phospholipase D (PLD). PLA1/2 then acts on phosphatidic acid (PA) and form LPA. The structures of some common human LPAs are shown.

# Chapter 4

## The role of $LPA_6$ in Oligodendrocyte Differentiation

*(This chapter is in preparation as a manuscript to be submitted to Glia. Samantha Spencer, Minh Nguyen and myself contributed to the work reported for this manuscript. Samantha Spencer performed the CRISPR/Cas9 injections and Minh Nguyen performed process network area and H3K9ac analysis)*

### Introduction

Previously, we have shown that the ATX-LPA signaling axis is necessary to promote differentiation of OLGs. Since the product of ATX's enzymatic lysoPLD active site, the lipid signaling molecule LPA, is well known to exert its function via the activation of one or more of its cognate signaling receptors, the LPA receptors, these data suggest a crucial role of LPA receptor signaling in the regulation of OLG differentiation and myelination. There are six known G protein-coupled, LPA receptors, all of which are expressed on OLGs ($LPA_{1-6}$). However, loss of function studies have so far come up short in providing information regarding their *in vivo* role in myelination, potentially due to the redundant functions among LPA receptors and/or compensation upon the genetic deletion of a single receptor (Contos et al., 2000; Contos et al., 2002). On the other hand, changes in the molecular mechanisms that govern OLG development have not been extensively analyzed in these animals, with the exception of *Lpar1* KO mice. Transgenic mice carrying a mutated *lpar1* gene ($maLPA_1$-null mice) exhibit decreased expression of myelin protein MBP, PLP/DM20 and CNPase (Garcia-Diaz et al., 2015), however, these studies suggest $LPA_1$ plays a role in the later stages of OLG development, and not during early OLG differentiation. Our studies, therefore, sought to further explore the role of LPARs in OLG differentiation.

In the studies presented here, we focused on an LPA receptor about which there

is still little known, namely, $LPA_6$. $LPA_6$ is the most recently characterized member of the LPA receptor family. First identified as an orphan GPCR (Kaplan et al., 1993), activation of $LPA_6$ by LPA has been shown to increase intracellular $Ca^{2+}$ and ERK1/2 phosphorylation (via $G_{i/o}$) and to activate Rho GTPase (via $G_{12/13}$) (Lee et al., 2009c; Pasternack et al., 2008, 2009; Yanagida et al., 2009a). Little is known about the role of $LPA_6$ in cellular physiology, except that it is required for human hair growth (Pasternack et al., 2008, 2009; Shimomura et al., 2008, 2009).

After initial investigative studies, we report that $LPA_6$ plays a novel role in OLG differentiation. $LPA_6$ is found in differentiating OLGs, both in primary rat cultures as well as in the developing zebrafish. $LPA_6$ expression is needed for proper OLG differentiation as siRNA mediated down-regulation or CRISPR(cas9) mediated mutation of $LPA_6$ reduces the expression of differentiation genes, *Cnp* and *Ugt8*, in primary OLGs and a myelin specific gene, *plp1b*, in the developing zebrafish, respectively. Additionally, down-regulation of *Lpar6* does not appear to affect overall OLG process network area. Therefore, the role of $LPA_6$ appears to mediate the gene regulatory, rather than the cytoskeletal maturation, portion of OLG development along the lineage. Interestingly, down-regulation of *Lpar6* did not alter specific epigenetic changes seen affected by the ATX-LPA axis and, therefore, may act in an alternative-signaling pathway.

**Materials and Methods**

*Cell culture.* Primary OLG progenitors were isolated from postnatal day 2 (P2) rat brains by A2B5 immunopanning and cultured as previously described (Barres et al., 1992; Lafrenaye and Fuss, 2010; Martinez-Lozada et al., 2014). Plated OLG

progenitors were cultured in serum-free proliferation medium (Dulbecco's modified Eagle's medium (DMEM) containing human PDGF and basic fibroblast growth factor (bFGF) (Gemini Bio-Products, Sacramento, CA) for 24hrs, after which cells were treated with siRNA reagents in antibiotic/FCS free DMEM containing PDGF/bFGF for 3hrs followed by removal of reagents and incubation in antibiotic/FCS free DMEM containing PDGF/bFGF for an additional 24hrs before allowed to differentiate in serum-free medium (DMEM containing 40 ng/mL tri-iodo-thyronine (T3; Sigma, St. Louis, MO) and N2 supplement (Life Technologies, Grand Island, NY); DMEM/T3/N2) over the time periods indicated. Typically, at least three independent experiments were performed, whereby an independent experiment refers to an experiment in which cells were isolated from a separate P2 rat litter at an independent time point (day) and treated separately from all other independent experiments.

*CRISPR/Cas9 genome editing.* CRISPR target sequences for *lpar6a and lpar6b* as depicted in Fig. 4.2, were identified as described by Wheeler et al., 2015. sgRNAs were generated using the cloning-free/short oligonucleotide approach described by Talbot and Amacher (2014). Briefly, short-guide oligonucleotides containing a T7 promoter and genomic target site were synthesized as described in Wheeler et al., 2015. 1 nanoliter of a mixture of Cas9 mRNA (100 ng/µl) and sgRNA (120 ng/µl for *lpar6a*; 95 ng/µl for *lpar6b*) was injected per one-cell stage zebrafish embryo. Zebrafish were analyzed at 48 hpf. Brightfield images of whole embryos were taken using an Olympus SZX12 zoom stereo microscope (Olympus America Inc., Melville, NY) equipped with an Olympus DP70 digital camera system.

*RNA isolation and real-time RT-qPCR Analysis.* For the isolation of RNA from whole zebrafish embryos or cultured rodent OLGs, samples were collected and analyzed as described in Wheeler et al., 2015. Gene-specific primers were designed and *in silico* tested for specificity using NCBI/Primer-BLAST (Ye et al., 2012). All primers were designed to amplify all known splice variants.

*atx/enpp2*: forward (5'-CAATGTATGCAGCATTCAAACGAGTG-3'), reverse (5'CACCATTTTTCTCACTAGCGTAACG-3')

*plp1b:* forward (5'TGCCATGCCAGGGGTTGTTTGTGGA-3), reverse (5'-GGCGACCATGTAAACGAACAGGGC-3)

*cldnk*: forward (5'-TGGCATTTCGGCTCAAGCTCTGGA-3'), reverse: (5'-GGTACAGACTGGGCAATGGACCTGA-3)

*lpar6a:* forward (5'-GCGGAGAGGATTGTAACTGCC-3'), reverse: (5'-TTCGGGCAGTGAGTGACGTT-3)

*lpar6b:* forward (5'-ACGGTGGGCTTCCTGATTCC-3'), reverse: (5'-GACTGATGGTCTCGGGGTGG-3)

*β-actin (actb2*)(Buckley et al., 2010) was used as reference gene; *eef1a1/1* has been assessed as additional reference gene for the analysis of RNA derived from the developing zebrafish and no pronounced differences were noted (Yuelling et al., 2010).

The following unmodified rat gene-specific primer pairs were used:

*Cnp*: forward (5'-ATGCCCAACAGGATGTGGTG-3'), reverse (5'-AGGGCTTGTCCAGGTCACTT-3')

*Ugt8*:forward (5'-AGGAGCTCTGGGGAGATTGC-3'), reverse (5'-TTTGAATGGCCAAGCAGGTCA-3')

*Egr1*:forward (5'-CCTGACCACAGAGTCCTTTTCT-3'), reverse (5'-AAAGTGTTGCCACTGTTGGG-3')

*Lpar6*: forward (5'-GTAAGCGCCAACGGCTCCA-3'),

reverse (5'-GTAAGCGCCAACGGCTCCCA -3')

*Pgk1* (as reference gene): forward (5'-ATGCAAAGACTGGCCAAGCTAC-3'), reverse (5'-AGCCACAGCCTCAGCATATTTC-3')

*Pgk1* was used as reference gene due to its previously established expression stability in rat OLGs (Nelissen et al., 2010). In addition, *Ppia* has been assessed as additional reference gene for the analysis of RNA derived from differentiating OLG cultures and no pronounced differences were noted.

RT-qPCR reactions with at least 2 technical replicates per sample were performed on a CFX96 real-time PCR detection system (BioRad, Hercules, CA) using the iQ SYBR Green Supermix (BioRad, Hercules, CA). PCR conditions were as follows: 95°C for 3 min followed by 40 cycles of 95°C for 15 s, 58°C for 30 s, and 95°C for 10 s. For all primer pairs, melting curves were used to ensure specificity. Relative expression levels were determined using the ΔΔCT method (Livak and Schmittgen, 2001).

*HDAC activity assay.* Rodent OLG progenitor cells were cultured and treated in fibronectin coated 96-well plates ($1x10^5$ cells/well) and then assayed as described by Wheeler et al., 2015.

*siRNA-mediate Gene Silencing*. OPCs were transfected with ON-TARGET*plus* siRNA SMARTpools directed against rat *Lpar6* (Thermo Fisher Scientific Inc., Pittsburg, PA) using Lipofectamine 2000 (Life Technologies Corp., Grand Island, NY). As control, an ON-TARGET*plus* non-targeting siRNA pool (Thermo Fisher Scientific Inc., Pittsburg,

PA) was used. Transfection medium containing siRNA-Lipofectamine complexes was replaced with serum-free medium (DMEM/PDGF/bFGF) after 3hrs, then the cells were cultured for 24hrs before replacing with differentiation medium (DMEM/N2/T3) as well as treatment (LPA, HA130 or vehicle) and was then cultured for an additional 24hrs. Knockdown of gene expression was assessed by qRT-PCR analysis.

*Immunocytochemistry*. For immunocytochemistry using O4 hybridoma supernatants, cells were fixed in 4% paraformaldehyde/PBS, nonspecific binding sites were blocked in 10% FCS/DMEM, and cells were incubated with the supernatant (1:1 diluted in 10% FCS/DMEM) overnight. Cells were fixed and in cases of dual staining, permeabilized using 0.5% Triton X-100/0.4 M sucrose/PBS and then incubated for 30 min in blocking solution (10% FCS/DMEM). Subsequently, cells were incubated overnight with anti-acetyl-histone H3 (Lys 9), anti- $LPA_6$, anti-Caspase 3 (active (cleaved) form) or anti-Ki67 antibodies overnight. Primary antibodies were detected using Alexa 488- or Alexa 568-conjugated secondary antibodies (Life Technologies, Grand Island, NY) and nuclei were counterstained using Hoechst 33342 (EMD Millipore, Billerica,MA). For the generation of representative images, confocal laser scanning microscopy was used (Zeiss LSM 700, Carl Zeiss Microscopy, LLC, Thornwood, NY). Images represent 2D maximum projections of stacks of 0.5 µm optical sections.

*Nuclear histone acetylation analysis.* Cells double-labeled for O4 and acetyl-histone H3 (Lys 9) were imaged using confocal laser scanning microscopy (LSM 700 Carl Zeiss Microscopy, LLC, Thornwood, NY) as described by Wheeler et al., 2015.

*Cell survival and proliferation analysis.* Cells were subjected to immunostaining using O4 hybridoma cell supernatants and antibodies specifically recognizing the active

(cleaved) form of caspase-3 or the Ki67 antigen. To determine the number of caspase-3 or Ki67 immunopositive cells, images of four fields per coverslip were taken with a 20x/0.8 n.a. plan-apochromat objective lens using a confocal laser scanning microscope (LSM 700 Carl Zeiss Microscopy, LLC, Thornwood, NY) as described by Wheeler et al., 2015.

*Isolation of OLG progenitors from zebrafish embryos using fluorescent activated cell-sorting (FACS).* OLG enriched populations extracted from *Tg(nkx2.2a:megfp;olig2:dsred2)* zebrafish embryos were collected as previously described by Wheeler et al., 2015.

*Statistical Analysis.* To determine significance, GraphPad Prism (GraphPad Software, La Jolla, CA) or SigmaPlot (Systat Software, Inc., San Jose, CA) software was used. Data composed of two groups were analyzed using the two-tailed Student's *t*-test or the Mann-Whitney *U*-test and presented in bar graphs depicting means ± SEM or box and whisker plots depicting medians and quartiles. Data compared to a set control value lacking variability were analyzed using the one-sample *t*-test (Dalgaard, 2008; Skokal and Rohlf, 1995) and presented in bar graphs.

## Results

### Down-regulation of *Lpar6* leads to a reduction in OLG differentiation genes and has no effect on OLG process network area

During the time of OLG differentiation, OLGs express $LPA_{1\text{-}6}$. To evaluate the role of $LPA_6$ individually, primary OPCs, extracted from P2 rats, were transfected with siRNA pools specifically silencing *Lpar6* expression. Knockdown of gene expression was confirmed by qRT-PCR, which revealed a reduction of roughly 50% (Fig. 4.1A).

Importantly, down-regulation of *Lpar6* was not associated with compensatory up or down-regulation of any other receptors ($LPA_{1-5}$) (Fig. 4.1A). In order to assess the role of $LPA_6$ on OLG differentiation, *Cnp* and *Ugt8* gene expression levels were assessed. Consequently, down-regulation of *Lpar6* led to a reduction in both *Cnp* and *Ugt8* mRNA levels (Fig. 4.1B). Interestingly, however, the subsequent down-regulation in OLG differentiation genes was not accompanied with an increase in the expression of an inhibitor of differentiation, namely *Egr1* (Fig. 4.1B). To assess the role of $LPA_6$ in morphological maturation of OLGs during differentiation, OLG process index was evaluated upon knockdown of *Lpar6.* Reduction of *Lpar6* did not significantly change overall OLG process index when compared to control (Fig. 4.1C). Additionally, when down-regulating *Lpar6*, LPA was unable to rescue OLG differentiation genes back to control levels, although a slight increase in *Ugt8* and *Lpar6* expression was noted (Fig. 4.1D). These effects were not found to be associated with changes in cell survival or proliferation as determined by immunostaining using antibodies specifically recognizing the active (cleaved) form of caspase-3 or the Ki67 antigen (data not shown). These data indicate that $LPA_6$ is needed for proper OLG differentiation and can not be excluded from the possible involvement in the ATX-LPA signaling axis.

**In the developing zebrafish, $LPA_6$ promotes myelin gene expression of *plp1b***

To further validate the role of $LPA_6$ in OLG differentiation, we assessed its function in the developing zebrafish, an emergent vertebrate model particularly suitable for *in vivo* and developmental research (Best and Alderton, 2008; Fleming et al., 2010). In order to examine the role of $LPA_6$, it was necessary to verify the expression of both *lpar6a* and *lpar6b*, two individual genes produced as a result of a genome duplication (Woods et

al., 2000), both in whole zebrafish and OLGs extracted from zebrafish, at 48hpf. To obtain an OLG enriched population from the developing zebrafish, we performed Fluorescent Activated Cell Sorting (FACS) as introduced in Fig. 2.4., using *Tg(nkx2.2a:megfp;olig2:dsred2)* fish. RNA extracted from FACS sorted OLG enriched populations and whole zebrafish, at 48hpf, was used to verify gene expression of *lpar6a* and *lpar6b* (Fig. 4.2A,B). To assess the role of *lpar6a* and *lpar6b* in OLG development, we performed the Clustered Regularly Interspaced Short Palindromic Repeats (CRISPR)/Cas9 genome editing technique. For these studies, we used the same codon-optimized Cas9 with nuclear localization signals system as described in Fig. 2.1. As shown in Fig. 4.2C-F, injection of guide RNAs against *lpar6a and lpar6b* genes and *in vitro* transcribed, capped, polyadenylated *nls-zCas9-nls* RNA into one-cell stage zebrafish embryos resulted in the generation of indel mutations over and upstream of the CRISPR targeting sequence. These mutations resulted in reduced levels of *lpar6a* and *lpar6b* mRNA (Fig. 4.2H), an effect that was not observed in uninjected zebrafish. Most importantly, the CRISPR/Cas9-mediated reduction in *lpar6a* and *lpar6b* expression was found associated with a decrease in the transcript levels for the later stage OLG differentiation marker *proteolipid protein* (*plp1b)* (Fig. 4.2H). As shown in Fig. 4.2G, injection of Cas9 mRNA with either of the guide RNAs was not found to be associated with changes in the gross morphology of the embryos. The above-described data, further support the role of $LPA_6$ in OLG differentiation, and verify its involvement *in vivo*.

**$LPA_6$ promoted progression along the lineage does not alter HDAC activity or histone acetylation**

As previously described, early stages of the OLG lineage are seen to be regulated by ATX's lysoPLD activity, in association with, epigenetic modifications that result in increased histone deacetylation (Marin-Husstege et al., 2002; Shen et al., 2005; He et al., 2007; Shen et al., 2008; Liu and Casaccia, 2010; Takada and Appel, 2010; Swiss et al., 2011). In order to assess if HDAC activity is affected by the down-regulation of *Lpar6*, siRNA mediated knockdown of *Lpar6* was performed on cells that were then subjected to a fluorogenic HDAC activity assay. The reduction of *Lpar6* did not significantly change overall HDAC activity (Fig. 4.3A). It has been previously shown that HDAC activity in differentiating OLGs is primarily directed to lysine residues of histone H3, including the lysine residue on the tail of histone H3 at position 9 (H3K9) (Swiss et al., 2011). To assess changes in acetylation at this site, cells treated, as depicted in Fig. 4.1, were analyzed by immunocytochemistry, assessing O4+ OLGs with H3K9ac nuclear staining, combined with confocal microscopy. Most importantly, siRNA mediated down-regulation of *Lpar6* did not significantly change the levels of H3K9ac (Fig. 4.3B). These findings differ from the epigenetic changes seen regulated by the ATX-LPA signaling axis and, thus, highlight $LPA_6$ as a regulator of alternative signaling pathways needed for OLG differentiation.

**Discussion**

Differentiation of OPCs into myelinating OLGs encompasses a complex sequence of events including cell cycle exit, RNA processing, branching, synthesis of myelin proteins and lipids and membranes wrapping around the axon (Raff, 2007; Simons and Trotter, 2007; Swiss et al., 2011). The mechanisms underlying many of these events are attributed to extracellular factors and specific signaling pathways. ATX, specifically

through its lysoPLD active site, is one extracellular factor that is needed for proper OLG differentiation through its capacity to epigenetically modify the OLG genome. LPA, the product of ATX's lysoPLD active site, is an essential ligand needed to bind its receptors on OLGs and activate such signaling cascades. The complexity of this regulation is apparent as LPA can bind six different receptors, with converging signaling pathways. Most importantly, little is known regarding the role of each receptor in OLG development. Such information is needed to therapeutically target these receptors and enhance OLG development pharmacologically. In an effort to understand the signaling events governing gene expression changes during OLG differentiation, we examined the role of $LPA_6$. The data obtained from these studies reveal that $LPA_6$ plays a novel role in OLG gene regulation during differentiation. These studies are the first of their kind and further enhance the importance of LPA signaling in OLG development.

We show for the first time that $LPA_6$ is needed for OLG differentiation. Down-regulation of *Lpar6,* and genetic mutation of *lpar6a* and *lpar6b*, leads to decreased expression of OLG differentiation genes, *Cnp* and *Ugt8*, and myelin gene, *plp1b*, respectively (Fig.4.1B; Fig4.2H). These results show a conserved role of $LPA_6$, for which OLG differentiation is dependent. Though reduction of *Lpar6* decreased the expression of OLG differentiation genes, it did not have an effect on the differentiation inhibitor, *Egr1* (Fig. 4.1B). The expression level of *Egr1* is known to decrease as OLG differentiation occurs and is followed by the up-regulation of genes involved in lipid metabolism and myelination (Swiss et al., 2011). Importantly, *Egr1* is a HDAC target gene (Swiss et al., 2011), specifically seen regulated by HDAC1/2 (Wheeler et al., 2015), and acetylation of lysine residues on the tail of histone H3 at position (H3K9ac) is

a critical residue that has been linked to the transcription of *Egr1* (Kubosaki et al., 2009; Tur et al., 2010; Wang et al., 2010). These results are the first to indicate that gene expression changes downstream of $LPA_6$ differ from those seen described by Wheeler et al., 2015. In this regard, the mechanisms associated with the activation of $LPA_6$ may be gene specific and work in conjunction with other signaling events to fine tune the genome wide changes needed for proper OLG differentiation.

Interestingly, LPA added to cells with reduced *Lpar6* expression were unable to rescue differentiation genes back to control levels, however a slight increase was noted in mRNA expression of *Ugt8* and *Lpar6* (Fig. 4.1D). These results show that $LPA_6$ is needed for proper OLG gene expression, although, another LPA receptor may also be involved in gene regulation at this time. It is of note that the addition of LPA did not affect gene expression levels of *Cnp*, thus, it is likely that the regulation of different OLG differentiation genes is governed by different signaling mechanisms. Nevertheless, these data suggest that OLG differentiation requires signaling via the activation of $LPA_6$ and, as such, highlight a novel role for $LPA_6$.

Moreover, the effects seen following siRNA mediated down-regulation of *Lpar6*, were primarily changes in gene expression and were independent of morphological aspects of OLG differentiation (Fig. 4.1C). Though LPA has been shown to increase membrane formation in later stages of OLG development (Nogaroli et al., 2009b), it is conceivable that these effects are a result of activation of a single, or a multitude of, remaining LPARs. Further analysis on the signaling pathways, led by the activation of different LPARs, will help delineate the specific roles they play in OLG development.

Our previous studies showed that the ATX-LPA signaling axis activates HDAC1/2 activity to regulate gene expression changes needed for proper OLG differentiation (Wheeler et al., 2015). In order to see if the signaling effects mediated downstream of $LPA_6$ were associated with the epigenetic changes previously described, HDAC activity was assessed after reduction of *Lpar6* expression. siRNA mediated *Lpar6* down-regulation did not alter overall HDAC activity (Fig. 4.3A). This finding outlines the notion that $LPA_6$ signaling does not involve HDAC regulation and differs from the ATX-LPA-HDAC1/2 signaling events. HDAC activity in differentiating OLGs is primarily directed to lysine residues of histones H4 and H3 including the lysine residue on the tail of histone H3 at position 9 (H3K9) (Swiss et al., 2011). When assessing the acetylation of lysine 9 on Histone 3 (H3K9ac) in siRNA treated cells when compared to control, no change was seen (Fig. 4.3B). H3K9ac is highly regulated by the activity of HDAC1/2, thus, without direct targeting of this protein complex, changes in acetylation of siRNA treated cells are likely to remain unchanged from control. These data validate the notion that signaling via $LPA_6$ does not activate HDAC1/2, and as such, effects the expression of differentiation and myelin genes by a pathway different from the one described in Chapter 2 (Wheeler et al., 2015).

Protein kinases have been identified as a bridge of communication between the extracellular and intracellular environments (Flores et al., 2008; Fyffe-Maricich et al., 2011; Guardiola-Diaz et al., 2012; Ishii et al., 2012; Narayanan et al., 2009; Tyler et al., 2009). With regard to OLGs, mTOR was found to regulate OLG differentiation *in vitro* (Tyler et al., 2009). Acting through its two effector complexes, mTOR complex 1 (mTORC1) and mTOR complex 2 (mTORC2), mTOR has been linked to the

transcription and translation of genes (Laplante and Sabatini, 2013). Interestingly, mTOR1 was found to play a major role in OLG differentiation, active myelination, and proper myelin compaction on large caliber axons in the CNS (Bercury et al., 2014). As signaling pathways involved in OLG differentiation begin to be understood, crosstalk between such pathways will be further impacted. Interestingly, pharmacological inhibition of the mTOR pathway has the ability to feedback and up-regulate the MAPK (mitogen-activating protein kinase) pathway (Carracedo et al., 2008) linking the before mentioned PI3K/Akt/mTOR pathway with that of the Ras/Raf/MEK/Erk pathway. Importantly, and with regard to OLGs, both major signaling pathways, through Akt/mTOR and MEK/Erk1/2, are necessary for full differentiation of OPCs to mature OLGs *in vitro* (Dai et al., 2014). Moreover, $LPA_6$ signaling is known to act through G protein-coupled receptors $G_{12/13}$ and $G_{i/o}$ (Chun, 2013). $G_{i/o}$ stands out as it initiates protein kinase signaling events including the activation of the PI3K/Akt/mTOR pathway and Ras/Raf/MEK/Erk pathways. Taken together, it is plausible that the gene expression changes seen with down-regulation or genetic manipulation of $LPA_6$ acts through the crosstalk between such signaling pathways. Future studies are needed to dissect these signaling events, however, these studies show that it is conceivable that the changes in gene expression downstream of $LPA_6$ signaling act, at least in part, through protein kinase signaling.

Cumulatively, $LPA_6$ stands out to be a novel LPA receptor governing gene expression patterns during OLG development. The actions of $LPA_6$ appear to be conserved across species and display similar characteristics. Interestingly, *Xenopus* embryos were found to express *lpar6* and loss of function analysis showed disruption of

neural development. Additionally, loss of function of *Xenopus lpar6* showed similar defects to that of loss of *enpp2* (ATX) (Geach et al., 2014). Mutations found in the human *Lpar6* gene, however, do not show the same neural development phenotype (Pasternack et al., 2008; Shimomura et al., 2008, 2009), and $LPA_6$ KO mice remain viable (mousephenotype.org). Nevertheless, $LPA_6$ displays a unique role in OLG differentiation and future studies will uncover the mechanistic effects of this novel receptor.

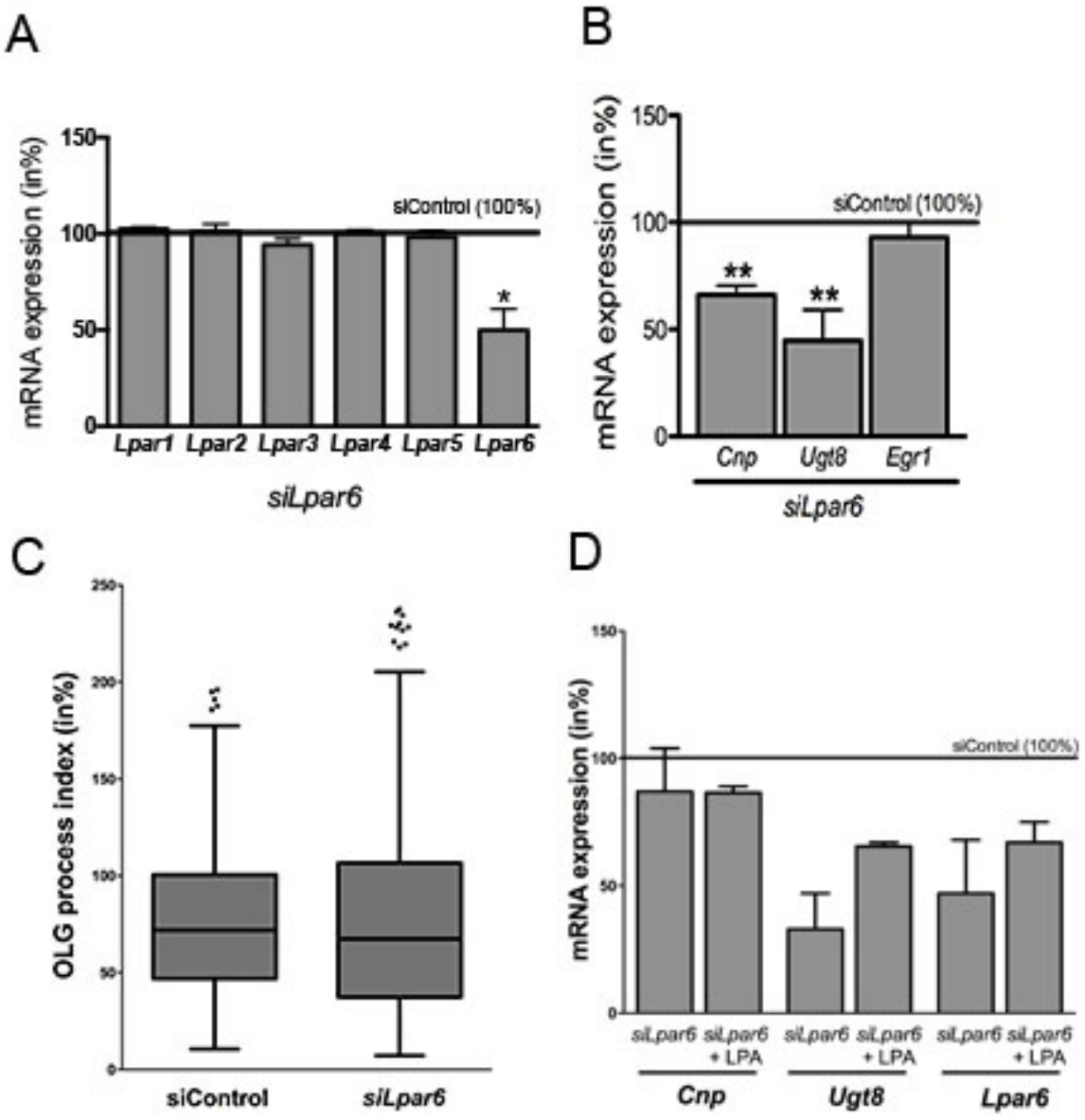
A
mRNA expression (in%)
150
100
50
0
siControl (100%)
*
Lpar1 Lpar2 Lpar3 Lpar4 Lpar5 Lpar6
siLpar6
B
mRNA expression (in%)
150
100
50
0
siControl (100%)
**
**
Cnp Ugt8 Egr1
siLpar6
C
OLG process index (in%)
250
200
150
100
50
0
siControl
siLpar6
D
mRNA expression (in%)
150
100
50
0
siControl (100%)
siLpar6 siLpar6 + LPA siLpar6 siLpar6 + LPA siLpar6 siLpar6 + LPA
Cnp
Ugt8
Lpar6

**Figure 4.1. In rodent OLG cultures, siRNA mediated down-regulation of *Lpar6* leads to a reduction in the levels of mRNAs encoding OLG differentiation genes, but does not change the level of mRNA encoding the transcriptional OLG differentiation inhibitor *Egr1*, or OLG process index. *A,*** Bar graph depicting mRNA levels for *Lpar1-6* as determined by real-time reverse transcription (RT)-qPCR analysis. Control (vehicle-treated) values were set to 100% (see horizontal line) and experimental values were calculated accordingly ***B,*** Bar graph depicting mRNA levels for the OLG differentiation genes *Cnp* and *Ugt8* and the transcriptional inhibitor *Egr1* as determined by real-time RT-qPCR analysis. Control (vehicle-treated) values were set to 100% (see horizontal line) and experimental values were calculated accordingly. ***C,*** Box and whisker graph depicting process index levels for control and siRNA treated cells as determined by immunostaining and morphology analysis. The plot depicts medians and quartiles of three independent experiments. Whiskers represent the 10th and 90th percentile. ***D,*** Bar graph depicting mRNA levels for the OLG differentiation genes *Cnp, Ugt8* and *Lpar6* in siRNA treated cells +/- the addition of LPA, as determined by real-time RT-qPCR analysis (n=2). Control (vehicle-treated) values were set to 100% (see horizontal line) and experimental values were calculated accordingly. Data shown in all graphs represent means ± SEM. $^{ns}$not significant, *p≤0.05, **p≤0.0.

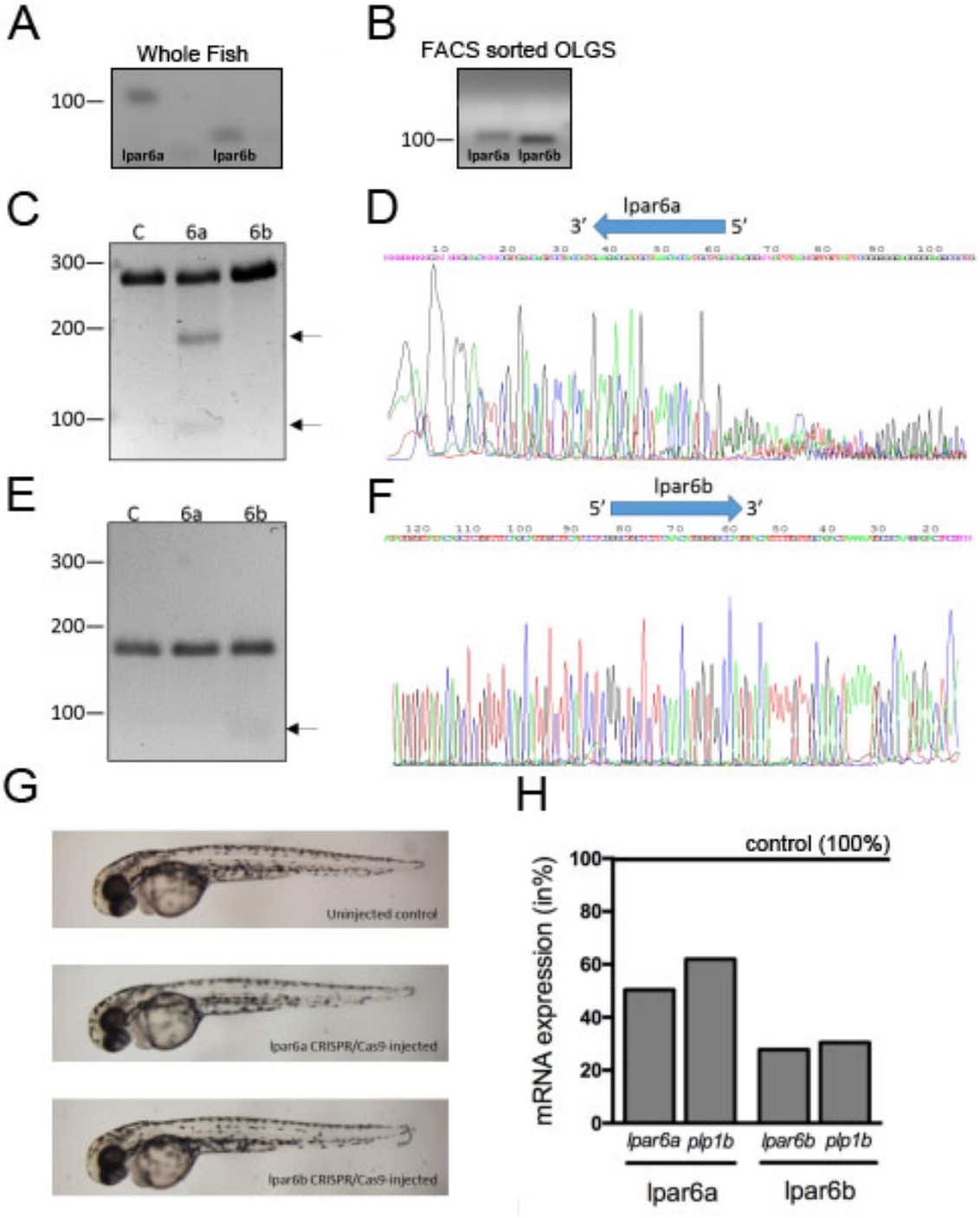
A
Whole Fish
100
lpar6a
lpar6b
B
FACS sorted OLGS
100
lpar6a lpar6b
C
C 6a 6b
300
200
100
D
lpar6a
3′
5′
E
C 6a 6b
300
200
100
F
lpar6b
5′
3′
G
Uninjected control
lpar6a CRISPR/Cas9-injected
lpar6b CRISPR/Cas9-injected
H
control (100%)
mRNA expression (in%)
100
80
60
40
20
0
lpar6a plp1b lpar6b plp1b
lpar6a
lpar6b

**Figure 4.2. In the developing zebrafish, CRISPR-Cas9-mediated mutagenesis of *lpar6a* and *lpar6b* leads to a reduction in the mRNA levels for OLG marker gene, *plp1b*. *A,B,*** Representative images of agarose gels showing RNA expression of *lpar6a* and *lpar6b* in whole fish (**A**) and FAC sorted OLGs (**B**). ***C,E,*** Representative images of agarose gels showing DNA fragments upon Surveyor nuclease treatment of control homoduplexes (c) and control/*lpar6a* (**C**) or control/*lpar6b* (**E**) homo/heteroduplexes. Numbers on the left indicate DNA sizes in bp. Arrowheads indicate cleaved PCR amplicon fragments at the expected sizes indicative of indel mutations generated by genome editing. ***D,F,*** Representative images of sequencing traces obtained from genomic DNA-derived PCR amplicons from control and Cas9 mRNA/sgRNA injected zebrafish embryos. Arrows at the top of each trace indicate the location of the target sequence, over and upstream of which a composite sequence trace indicates the presence of indel mutations generated by genome editing. ***G,*** Representative brightfield images of control (uninjected) and Cas9 mRNA/sgRNA injected embryos at 48 hpf. ***H,*** Bar graphs illustrating mRNA levels for *lpar6a, lpar6b* and the OLG marker gene *plp1b* in whole embryos as determined by real-time reverse transcription (RT)-qPCR analysis. Control (uninjected embryos) values were set to 100% (see horizontal line) and experimental values were calculated accordingly. Data shown represent means ± SEM.

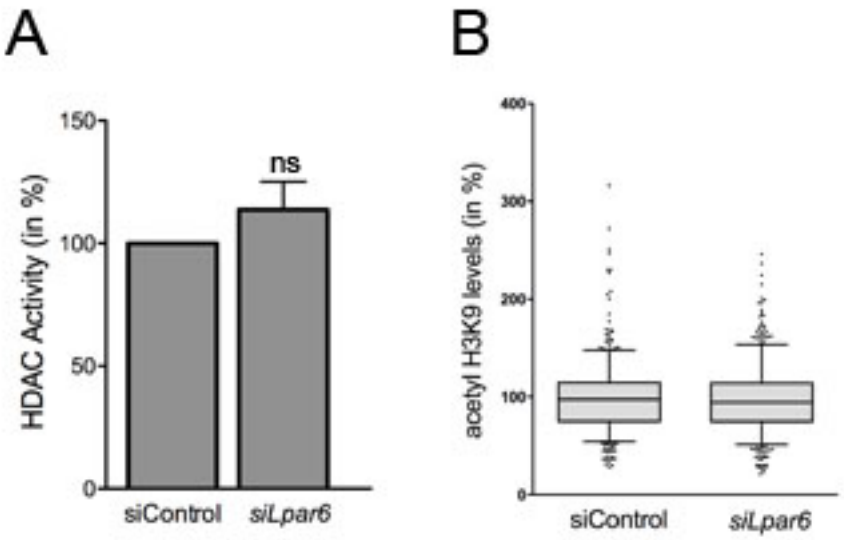
A
B
150
100
50
0
HDAC Activity (in %)
ns
siControl
siLpar6
400
300
200
100
0
acetyl H3K9 levels (in %)
siControl
siLpar6

**Fig. 4.3. In rodent OLG cultures, down-regulation of *Lpar6* does not effect HDAC activity or nuclear histone acetylation at lysine residue 9 of Histone 3 (H3K9). *A,*** Bar graphs showing HDAC activity as determined by using the fluorogenic substrate Boc-Lys(Ac)-AMC. Control (vehicle-treated) values were set to 100% and experimental values were calculated accordingly. Data represent means ± SEM. $^{ns}$not significant. ***B,*** Box and whisker plot depicting nuclear acetyl-H3K9 levels as assessed by determining fluorescence intensities shown in arbitrary units (a.u.). The plot depicts medians and quartiles of three independent experiments. Whiskers represent the 10th and 90th percentile. $^{ns}$not significant

# Chapter 5

# Introduction to HIV Neuropathology in the CNS

## Introduction to HIV

HIV, a member of the lentivirus family, comes in two forms, HIV-1 and HIV-2. HIV-2 is mainly found in Western Africa, with some cases arising in Europe and India (de Silva et al., 2008), and rarely progresses to AIDS or HAND (HIV Associated Neurological Disorders) (Rowland-Jones and Whittle, 2007). Thus, HIV infection through HIV-1 predominates as the most common form found worldwide. If HIV infection is left untreated, it can take roughly 10-12 years for AIDS to develop, a time period in which HIV can cause serious harm to both the immune and nervous system. Over 33 million individuals are currently infected by HIV (Power et al., 2012) and the CDC estimates 50,000 Americans will become infected with HIV each year.

The single-stranded RNA genome of HIV-1 encodes nine proteins comprising of envelope (Env), cor (Gag), polymerase (Pol) and six accessory proteins including Tat and Nef. HIV infection is initiated by the binding of the viral envelope protein, gp120 to CD4 receptors located on the surface of host cell (Sattentau et al., 1986). This interaction triggers a conformational change, which grants the entry of the virus genome and proteins. Once the host cell is infected, HIV makes viral DNA using its RNA genome template. Newly synthesized viral DNA can then integrate into the host genome to form the provirus. Infected cells can either be latent, or actively transcribed to produce the virus and viral proteins such as Tat.

cART (combination antiretroviral therapy), an HIV therapy created in 1996, has advanced the longevity of patients suffering from the virus and has had some progress

in aiding neurological pathogenesis, but falls short when treating HAND. Roughly 60% of the HIV infected population suffers from HAND (Williams et al., 2009). Moreover, AIDS remains the most common cause of dementia in non-aged individuals in the US. Thus, it is critical that further examination of CNS neuropathology, such as HIV-associated dementia and moderate cognitive and motor diseases, should be addressed so that proper therapies can be given.

**CNS Neuropathology and HIV infected cells**

As the survival rate and life expectancies for HIV+ patients have increased, so has the incidence of HIV neuropathology. HIV can enter the CNS at early stages of infection (Kramer-Hämmerle et al., 2005), through penetration of the Blood Brain Barrier (BBB) (Bagasra et al., 1996), or by HIV-1 infected macrophages that infiltrate the CNS and release the provirus (Merrill and Chen, 1991). Inflammation of the CNS induced by HIV-1 infection further disrupts the integrity of the BBB, leading to supplementary HIV-1 entry and infection (Eugenin et al., 2011). The effect of HIV-1 on neuropathology has gained increasing importance as it was reported that up to 70% of AIDS patients develop neurological disorders (Jellinger et al., 2000; Maschke et al., 2000). Additionally, children exposed to HIV infection were shown to display white matter (WM), an area of the brain consisting mostly of glial cells and myelinated axons, atrophy (Roy et al., 1992), and adult HIV+ patients demonstrated preferential damage to cerebral WM and subcortical brain structures (Jernigan et al., 1993).

In occurrence with the abnormal appearance of WM and brain inflammation seen in HIV infected patients, there is an increase in both microgliosis and astrogliosis (Esiri et al., 1991). Infected microglia have been shown to secrete pro-inflammatory cytokines

and chemokines in addition to HIV viral proteins, such as Tat, that exhibit toxicity to both myelin and OLGs (Herbein et al., 2010; Sui et al., 2004; Tyor et al., 1992). Viral proteins, such as Tat and gp120, can induce the production of toxic factors, including ROS, (Chauhan et al., 2003; Hurley et al., 2003; King et al., 2006; Lipton, 1998; Nath and Geiger, 1998) from infected glial cells in addition to further stimulating viral replication and production.

OLGs, the myelin producing cells of the CNS, are very vulnerable to HIV infection. Though lacking the expression of CD4, it has been reported that galactosylceramide (previously introduced, UGT8, is the enzyme responsible for its synthesis), expressed on the surface of OLGs can serve as an alternative receptor mediating HIV infections (Albright et al., 1996; Harouse et al., 1991; Yahi et al., 1992). It has not been concluded, however, that OLGs are in fact directly infected by HIV. Nevertheless, it is apparent that OLGs can be injured by HIV infection as hyperplasia of OLGs has been found in AIDS patients (Gyorkey et al., 1987) and, interestingly, HIV induces activation of the death pathways, p53 and BAX in OLGs (Jayadev et al., 2007). Accordingly, the effects of HIV on the CNS are quite significant with infection resulting in progressive atrophy to WM areas alongside glial cell reactivity and infection, and toxic factor release. A better understanding of the mechanisms that lead to injury in the CNS will help predict future therapies that, when used in conjunction with cART, will prolong survival, mental cognition and motor capabilities for patients.

**HIV-1 Tat**

Tat is an HIV viral protein that is essential for efficient viral transcription and replication. It is synthesized at both early and late stages of viral replication and has a

strong tendency to adhere to the surface of nearby cells. Tat is known to express a CCF motif which can mimic the CC-chemokines that attract CCR2, CCR3, and CXCR4 expressing glial cells (Cardona et al., 2006). The mRNA of the Tat protein consists of two coding exons, the first encoding amino acids 1-72, and the second encoding amino acids 73-101. In most research laboratories working with Tat, such as the laboratories in which we conducted Tat related studies, a recombinant truncated version of amino acids 1-86 is used.

The cellular responses induced by Tat expression appear to be robust as it can bind to many different receptors and cell surface markers. Tat can bind to chemokine receptors, reportedly leading to increased intracellular calcium levels, as well initiate iGluRs activation of the PLC, protein kinase C (PKC) and $G_{i/o}$ pathway, leading to IP3-dependent calcium release (Albini et al., 1998; Power et al., 1998; Song et al., 2003). In machrophages, Tat-induced calcium signaling results in the production of pro-inflammatory cytokines and chemokines (Puri and Aggarwal, 1992), further promoting inflammation. Microglia are also strongly affected by Tat as they appear to display a decrease in cAMP levels needed to induce expression of neuroprotective substances as well as an increase in their production of free radicals (Aloisi et al., 1999).

Other glial cells that fall victim to Tats influence are astrocytes. Tat activates astrocyte production of pro-inflammatory cytokines and chemokines, further promoting astroglial inflammatory responses (El-Hage et al., 2008; Zou et al., 2011). Additionally, Tat has been reported to cause an increase in free radical and ROS production in OLGs leading to process retraction and apoptosis (Fernández-Gamba et al., 2012; Rathnasamy et al., 2011). Though there is limited research on the effects of Tat on OLG

development and myelination, patients exhibiting symptoms associated with HAND display both motor and cognitive impairments that can be linked to WM injury in the CNS. It is imperative that we fully understand the dimensions in which HIV-1 and its viral proteins, such as Tat, inflict on the CNS to cause such impairments. It is of upmost importance to investigate the role of Tat on the development of the myelinating cells of the CNS, OLGs, in an effort to repair its function and WM injuries seen in HIV infected patients.

# Chapter 6

## HIV-1 Tat Modulates ATX lysoPLD Activity and Oligodendrocyte Differentiation

*(This chapter was submitted as a paper in ASN Neuro in April of 2016. Dr. Patrick Zou and myself equally contributed to the work reported for this manuscript)*

### Introduction

Neurocognitive complications are frequently reported in $HIV^+$ patients. Although combined anti-retroviral therapy (cART) effectively blocks HIV replication in the central nervous system (CNS) and profoundly decreases the incidence of severe neurocognitive impairments, such as HIV-associated dementia, ~50% of the HIV-infected population still develop various forms of milder neurocognitive deficits, collectively called HIV-associated neurocognitive disorders (HAND) (Ellis et al., 2007; McArthur et al., 2010). White matter injuries in HIV-infected patients are commonly observed, and have been shown to correlate to HAND pathogenesis (Filippi et al., 2001; Archibald et al., 2004; Pfefferbaum et al., 2007). Although cART can reduce the viral load in the cerebrospinal fluid (CSF) to below detectable levels, its effect is limited with regard to white matter damage and HAND (Yilmaz et al., 2006). This implies that toxic factors released by previously infected CNS cells may inflict more damage than the virus itself.

One candidate factor for HIV-induced white matter injury is the HIV-1 viral protein transactivator of transcription (Tat), which was originally discovered as a key component for efficient transcription of the HIV genome. Tat has been shown to be continuously expressed and secreted by infected CNS cells, and can be detected in the CSF (Wang et al., 2014) of HIV patients, even with cART (Johnson et al., 2013). Previously, we have reported that Tat significantly decreases immature OLG viability (Zou et al., 2015).

Importantly, Tat exposure also reduced the extensive networks formed by fine, branching processes that are typical for OLGs at this stage, suggesting Tat may also inhibit immature OLG differentiation.

OLG development has been extensively studied and well characterized both *in vivo* and *in vitro*. Newly formed oligodendrocyte progenitor cells (OPCs) migrate to their targeted destination to differentiate into pre-myelinating OLGs that will ultimately evolve into mature OLGs and myelinate axons. It is also well established that OLG differentiation is controlled by the fine-tuning of both intrinsic factors, such as transcriptional control and epigenetic regulation, and extracellular signals, including growth factors and mitogens (Zuchero and Barres, 2013; Mitew et al., 2014). One extracellular protein that has been shown to play a significant role in OLG development is Autotaxin (ATX), also known as ENPP2, phosphodiesterase-1α/ATX, or lysophospholipase D (lysoPLD), which is predominantly expressed and secreted by OLG lineage cells (Zhang et al., 2014), and has been shown to play an important role in OLG development. Previous studies in our lab have shown that ATX, via two functional domains, promotes OLG differentiation along the lineage. The first domain, the modulator of OLG remodeling and focal adhesion organization (MORFO) domain, was found to promote the morphological maturation of OLGs (Dennis et al., 2005). The second domain is an enzymatic lysoPLD-active site that generates the lipid signaling molecule lysophosphatidic acid (LPA) (Tokumura et al., 2002; Umezu-Goto et al., 2002; Nakanaga et al., 2010); it has been shown to promote OLG differentiation and myelination by epigenetically regulating the expression of OLG differentiation genes (Wheeler et al., 2015).

Since both Tat and ATX affect immature OLGs, we hypothesized that Tat inhibits OLG differentiation by interfering with the ATX-LPA signaling pathway. Our studies shown here demonstrated that 18 hr Tat treatment led to a reduction in the process network and OLG differentiation genes, *Ugt8* and *Cnp,* expression. Although LPA by itself did not affect OLG morphology, it protected OLGs from Tat-induced process retraction, and rescued gene expression down-regulated by Tat. Tat treatment also decreased ATX lysoPLD activity *in vitro*. Co-immunoprecipitation, using biotin-conjugated Tat and V5-tagged ATX, revealed a potential physical interaction between Tat and ATX, which may account for the reduced ATX lysoPLD activity in the presence of Tat. Together, these results strongly suggest that, in addition to its effects on OLG processes, Tat may physically bind to ATX, inhibiting ATX lysoPLD activity, and down-regulate LPA signaling. Thus, Tat-ATX interactions have the potential to interfere with OLG differentiation and also to block the protective effects of LPA on OLG process morphology. Disrupting interactions between ATX and Tat may be a potential therapeutic strategy for protecting HIV patients from white matter injury.

**Materials and Methods**

All animal procedures were performed strictly in compliance with protocols reviewed and approved by the Virginia Commonwealth University Institutional Animal Care and Use Committee (IACUC).

*Pharmacological compounds.* Lysophosphatidic acid (LPA; 18:1; Sigma, St. Louis, MO) was dissolved in DMEM containing 0.1% fatty acid-free bovine serum albumin. Recombinant $Tat_{1-86}$ and biotin-conjugated Tat (ImmunoDx, LLC Woburn, MA) were

dissolved in distilled water. In the experiments involving pharmacological compounds, vehicle control refers to the solvent that is used to dissolve the compounds.

*ATX-lysoPLD activity assay.* ATX-lysoPLD activity was determined using the fluorogenic assay previously described (Ferguson et al., 2006; Wheeler et al., 2015). Concentrated (40x) conditioned medium, obtained via centrifugal filters (EMD Millipore, Billerica, MA), from primary OLG cultures treated with vehicle control or Tat for 18hrs and grown in phenol-red-free DMEM were incubated with 2.5 μM FS-3 substrate (Echelon Biosciences Inc., Salt Lake City, UT) for 4 hr at 37°C. Alternatively, concentrated (40x) conditioned medium from untreated primary OLG cultures grown in phenol-red-free DMEM were incubated with vehicle control or Tat (100nM) and 2.5 μM FS-3 substrate (Echelon Biosciences Inc., Salt Lake City, UT) for 4 hr at 37°C. Increase in fluorescence with time was measured at an excitation wavelength of 485 nm and an emission wavelength of 520 nm using a PHERAstar multimode microplate reader (BMG LABTECH Inc. Cary, NC.).

*RNA isolation and real-time RT-qPCR analysis.* Isolation of RNA from control and treated OLGs were performed as previously published (Wheeler et al., 2015).

The following unmodified mouse gene-specific primer pairs were used:

*Cnp*:

forward (5'-ATGCCCAACAGGATGTGGTG-3'),

reverse (5'-AGGGCTTGTCCAGGTCACTT-3')

*Ugt8*:

forward (5'-AGGAGCTCTGGGGAGATTGC-3'),

reverse (5'-TTTGAATGGCCAAGCAGGTCA-3')

*Atx*:

forward (5’- GACCCTAAAACCATTATTGCTAA-3’),

reverse (5’-GGGAAGGTGCTGTTTCATGT -3’)

*Lpar1*:

forward (5’- GCCACCTGGCTGCTGCAGA -3’),

reverse (5’-GTGTCGATGAGGCCCTGCCG -3’)

*Lpar2*:

forward (5’- CTGTTCAGCCGCTCCTACCTGG -3’),

reverse (5’-GGCAGCTGACGTGCTCTCTGCCATAG -3’)

*Lpar3*:

forward (5’- ACGAGCTTCGTCCCCGTCCA -3’),

reverse (5’-ACGAGCTTCGTCCCCGTCCA -3’)

*Lpar4*:

forward (5’-GCCTTGGTACGTTCCCAAGCCATT-3’),

reverse (5’-AGTTGCAAGGCACAAGGTAATCGGG -3’)

*Lpar5*:

forward (5’-GGGACTAGAGGGGAGCTCACCGAA-3’),

reverse (5’- TAGCCTCTGGCTGGTGGCATCCTAG-3’)

*Lpar6*:

forward (5’-GTAAGCGCCAACGGCTCCA-3’),

reverse (5’-GTAAGCGCCAACGGCTCCCA -3’)

*Pgk1*: (as reference gene):

forward (5’- ATGCAAAGACTGGCCAAGCTAC-3’),

reverse (5’-AGCCACAGCCTCAGCATATTC -3’)

RT-qPCR reactions with at least 2 technical replicates per sample were performed on a CFX96 real-time PCR detection system (BioRad, Hercules, CA) using the iQ SYBR Green Supermix (BioRad, Hercules, CA). PCR conditions were as follows: 95°C for 3 min followed by 40 cycles of 95°C for 15 s, 58°C for 30 s, and 95°C for 10 s. For all primer pairs, melting curves were used to ensure specificity. Relative expression levels were determined using the ΔΔCT method (Livak and Schmittgen, 2001).

*Western Blot.* Concentration of proteins extracted from cultured OLGs or brain tissues were determined using a BCA protein assay kit (ThermoFisher Scientific, Waltham, MA). Equal amounts of protein samples were loaded on a Criterion precast 4-20% gradient SDS gel (Bio-Rad, Hercules, CA), electrophoretically separated, and probed with antibodies specific to 2',3'-cyclic-nucleotide 3'-phosphodiesterase (CNPase) (Abcam, Cambridge, MA). Bound primary antibodies were detected with appropriate IRDye secondary antibodies (1:3000, Li-COR, Lincoln, NE), and imaged using an Odyssey Imager (Li-COR). Protein bands were quantified using Li-COR image studio software.

*Cell culture.* Immature murine OLGs were cultured as previously described (Zou et al., 2015). In brief, primary mixed glial cells isolated from brains of postnatal day 0 - 2 mouse pups irrespective of sex (CD-1, Charles River Laboratory, Wilmington, MA) were plated in Dulbecco’s Modified Eagle’s Medium (DMEM) (Life Technologies, Carlsbad, CA) supplied with fetal bovine serum (10%, Thermo Scientific Hyclone, Logan, UT), glucose (6 g/L, Sigma, St. Louis, MO), Sodium Bicarbonate (0.13%, Life Technologies), Penicillin/Streptomycin (1x, Life Technologies). Culture medium was refreshed every

other day. At day 8, O2A/glial progenitor cells were collected from the mixed cultures and re-plated on poly-L-lysine coated 12-well plates or cover slips, at a density of 250,000 cells/well or 15,000 cells/cover slip, and incubated in DMEM supplied with CNTF (10 ng/ml, Peprotech, Rocky Hill, NJ), NAC (5 µg/ml, Sigma) and triiodothyronine (15 nM, Sigma) for 2 days before further experiments.

*Repeated measure paradigm.* Repeated measurements of the morphology of individual OLGs were performed as previously published (Zou et al., 2011). In brief, OLGs were cultured in 12-well plates for 2 days before treatment with vehicle or 100 nM Tat. Culture plates were then transferred to the environmental chamber (37°C, 5% $CO_2$) of a Zeiss Axio Observer Z1 system (Carl Zeiss Microscopy, LLC, Thornwood, NY). Individual OLGs were randomly selected, and imaged hourly for 18 hrs. Images were analyzed using the Zeiss Axiovision 4.8 software.

*Immunostaining.* O4 immunostaining was performed on live, unfixed cells. All other immunostaining was performed after cells were fixed with 4% paraformaldehyde. O4 monoclonal antibodies [1:20, grown from hybridoma cells in our lab (Knapp and Hauser, 1996)] was applied at room temperature for 15 min. Goat anti-mouse IgM-Cy3 (1:1000, Millipore, Billerica, MA) was used to probe bound O4 antibodies. All LPA receptor antibodies [Anti- LPAR1 (Abcam), LPAR2 and LPAR3 (Santa Cruz, Dallas, TX), LPAR4 (Alomone labs, Hadassah Ein Kerem, Israel), and LPAR6 (Acris, San Diego, CA)] were applied at 1:1000 at room temperature for 1 hr, and corresponding secondary antibodies were conjugated to Alexa 488 (1:2000, Life Technologies) were used as secondary antibodies. The cell nucleus was stained with the Hoechst 33342

dye (1:2000, Life Technologies). Images were taken on a confocal microscope (Zeiss LSM 700, Carl Zeiss, Thornwood, NY) and processed using Zeiss Zen 2010 software.

*Co-immunoprecipitation.* Dynabeads Protein G (1.5 mg/50 µl, Life Technologies) was first mixed with primary antibodies (5 µg): non-specific mouse IgG, mouse anti-V5, and rabbit anti-biotin, respectively (all from Abcam), and washed three times with PBS at room temperature. Concentrated supernatant from a COS-7 cell line (500 µl) was mixed with 5 µg biotin-conjugated Tat, and added to the Dynabeads-bound primary antibodies and gently rocked overnight at 4°C. The next day, Dynabeads (with bound proteins) were washed three times at room temperature with PBS before being collection and then resuspended in loading buffer (2x Laemmli buffer, Bio-Rad), heat denatured (95°C, 5 min) and loaded (40 µl/sample) to a 4 – 20% SDS-PAGE precast gel (Bio-Rad) for Western blotting.

## Results

### Tat-induced decrease in immature OLG process networks, is reversed by LPA

An earlier study reported that immature OLGs exposed to HIV-1 Tat show significantly decreased viability *in vitro* (Zou et al., 2015). In addition, surviving cells exhibit abnormal morphology, indicating that the differentiation of these cells is disrupted. To investigate the effect of Tat on the morphology of differentiating OLGs in more detail, immature OLGs at 2 days *in vitro* were treated with vehicle or Tat for 18 hrs before morphological analysis was performed. Compared to vehicle-treated OLGs, Tat treatment led to a loss of fine, branched processes in as little as early as 4 hrs and this continued throughout the 18 hr experimental period (Fig. 6.1). Statistical analysis from 4

independent experiments (≥ 30 cells/treatment group) showed a significant decrease in process network in Tat treated OLGs (Fig. 6.2).

Since LPA signaling has been shown to promote expression of genes involved in OLG differentiation (Wheeler et al., 2015), we examined whether LPA could reverse Tat induced reduction of the OLG process network. As shown in Fig. 6.2, the addition of 1 or 10 μM LPA does not affect the process network of OLGs. However, when added concurrently with Tat, LPA completely blocked Tat-induced process retraction, thus revealing a protective role of LPA against Tat-mediated effects on OLG process network.

**The effect of Tat to down-regulate *Cnp* and *Ugt8* expression is reversed by LPA**

The lysoPLD activity of ATX has been reported to regulate OLG gene expression (Wheeler et al., 2015). Thus, we investigated whether gene expression in immature OLGs was also affected. As seen in Fig. 6.3A, 18 hr Tat-treatment significantly decreased the expression of the OLG differentiation genes *Cnp* and *Ugt8*. Interestingly, Tat treatment did not alter *Atx* gene expression. Since the main function of ATX lysoPLD activity is to produce the lipid signaling molecule LPA, we next examined whether LPA could rescue the expression of genes down-regulated by Tat. The addition of LPA completely rescued the expression of *Cnp* and *Ugt8*, but did not have any significant effect on *Atx* expression (Fig. 6.3B). In addition, protein expression data from Western blot analysis verified that Tat treatment decreased CNP expression, which was reversed by the addition of LPA (Fig. 6.3C).

**Expression of LPA receptors is not affected by Tat treatment**

Since the effects of Tat on immature OLG morphology and differentiation gene expression can be rescued by LPA, we hypothesized that Tat interferes with the LPA signaling pathway. To assess the LPA receptors (LPARs) expression profile in our system, we performed immunostaining with antibodies specific to different LPARs in our 2 days *in vitro* immature OLGs. Results revealed the presence of $LPA_{1-4}$ and $LPA_6$ on $O4^+$ OLGs (Fig. 6.4A). To assess whether Tat alters LPAR expression, qRT-PCR was performed on 18 hr Tat- or vehicle- treated OLGs. Our results showed that Tat treatment had no effect on $LPA_{1-6}$ gene expression on immature OLGs (Fig. 6.4B).

**Tat decreases ATX lysoPLD activity**

Since Tat did not affect the expression of LPARs in immature OLGs, we next examined whether Tat disrupts LPA production. Extracellular LPA is predominantly produced by the lysoPLD activity of ATX, which converts lysophosphatidylcholine (LPC) to LPA by removing its choline group (Aoki et al., 2008). Thus, we assessed whether Tat treatment alters ATX lysoPLD enzymatic activity in OLGs. Immature OLGs were treated with vehicle or Tat for 18 hr before supernatant was collected for the ATX lysoPLD activity assay. OLGs treated with Tat showed significantly lower ATX lysoPLD activity in the supernatant during the 4 hr assay (Fig. 6.5A). The reduction of lysoPLD activity was seen as a steady inhibition that led to a ~10% overall decrease across all assay time points (Fig. 6.5B).

**Physical interaction between Tat and ATX decreases ATX lysoPLD activity**

Since Tat treatment did not alter *Atx* expression in OLGs, we next assessed whether the reduced Atx lysoPLD activity was mediated by an interaction between Tat and ATX. Vehicle or Tat was added to the supernatant collected from untreated primary

OLG cultures immediately before ATX lysoPLD activity was assessed. In this experimental paradigm, which bypassed any potential effect on cells, Tat directly and significantly decreased ATX lysoPLD activity (Fig. 6.6A). We next hypothesized that decreased ATX lysoPLD activity might be the result of a physical interaction between Tat and ATX. To test this hypothesis, we performed co-immunoprecipitation using biotin-conjugated Tat and V5-tagged ATX collected and concentrated from the supernatant of a stably transfected COS-7 cell line (Dennis et al., 2012). As seen in Fig. 6B, V5-tagged ATX was detected in anti-biotin precipitates and vice versa, suggesting a physical interaction between ATX and Tat. As a control for non-specific binding, neither V5-tagged ATX nor biotin-conjugated Tat was detected in precipitates collected using a mouse IgG1 monoclonal isotype control (Fig 6.6B, bottom panel). It has been previously reported that cell-associated ATX, compared to secreted ATX, migrates slower during SDS-PAGE due to differences in glycosylation (Jansen et al., 2005). Since we used high density cultures of adherent cells to obtain cell culture supernatants of high ATX concentration, the higher molecular weight ATX band (MW ~ 125 kDa) seen in Fig. 6.6B likely represents cell-associated ATX derived from floating and/or damaged cells.

**Discussion**

White matter injury is frequently reported in HIV+ patients at all stages (Gongvatana et al., 2009; Zhu et al., 2013; Ragin et al., 2015). The mammalian adult CNS has been known to maintain a population of OLG precursor cells, which migrate to the lesion site upon injury and differentiate into myelinating OLGs to replace the injured OLGs and regenerate lost, damaged myelin (Polito and Reynolds, 2005; Kang et al., 2010; Zuchero and Barres, 2013). Hence, it is interesting that white matter injury

persists when HIV RNA is undetectable in the cerebrospinal fluid (Yilmaz et al., 2006; Ragin et al., 2015). Our studies here showed that HIV-1 Tat, which is continuously secreted by infected CNS cells, even in the absence of viral replication, inhibits the lysoPLD activity of ATX, possibly via a potential physical interaction. The interaction between Tat and ATX not only attenuates OLG differentiation, but also disrupts the protective effects of LPA on OLG process morphology. Thus, targeting the interaction between Tat and ATX may be a therapeutic strategy to promote recovery of white matter injury in HIV patients.

OLG lineage cells are targets of HIV-1 Tat. Proliferation and migration of OLG precursor cells, viability of immature OLGs, morphology, and myelin-like membrane production of mature OLGs have all been reported to be disrupted by Tat both *in vivo* and *in vitro* (Hahn et al., 2012; Zou et al., 2015). Our initial experiments found that immature OLGs that survived 18 hr Tat treatment exhibit a decrease in process network (Fig. 6.1). Although LPA by itself does not promote process outgrowth, it protects OLG process network from Tat-induced damage (Fig. 6.2). Previously, we have reported that early OLG differentiation is regulated by epigenetic mechanisms downstream of the LPA signaling pathway (Wheeler et al., 2015). Consistently, gene expression studies and Western blot analysis showed that OLG differentiation genes, *Utg8* and *Cnp,* were down regulated by Tat (Fig. 6.3). This Tat-induced down regulation of OLG differentiation genes were also rescued with the addition of LPA (Fig. 6.3), strongly supporting our hypothesis that Tat affects OLG differentiation by interrupting the LPA signaling pathway. Additionally, *Atx* gene expression in OLGs treated with Tat and/or

LPA was not significantly different from control (Fig. 6.3), suggesting the LPA rescue of *Cnp* and *Ugt8* gene expression was not attributed to an increase in *Atx* expression.

There are six *bona fide* LPARs, all of which are found on OLGs, with LPAR1 being the most abundantly expressed (Zhang et al., 2014). Our experiments showed that 18 hr Tat exposure did not affect the expression of any LPAR gene in OLGs. Thus, the finding that LPA rescues both Tat-induced down regulation of OLG differentiation genes *Ugt8* and *Cnp* (Fig. 5)*,* and the decrease of OLG process networks (Fig. 6.2), strongly indicates that Tat might alter LPA production rather than LPAR expression.

In the CNS, LPA is predominantly produced by the lysoPLD activity of ATX. Although Tat did not affect *Atx* gene expression, supernatant collected from Tat-treated OLGs showed significantly decreased ATX lysoPLD activity. Since physical interactions between proteins may lead to an altered conformation and function, we hypothesized that Tat interacts with ATX, thus inhibiting its lysoPLD activity and production of LPA. Our experiments showed that ATX lysoPLD activity was significantly decreased when Tat was added directly to the supernatant collected from untreated OLGs. Further, when biotin-conjugated Tat was added to the supernatant collected from a COS-7 cell line, that stably expresses V5-tagged ATX, the two proteins were precipitated together. These results strongly implicate that Tat, by binding to ATX, inhibits ATX lysoPLD activity and LPA production. The crystal structures of Tat and ATX reveal that both proteins contain cysteine-rich domains, indicating the possibility of forming intermolecular disulfide bonds (Tahirov et al., 2010; Nishimasu et al., 2011; Gu et al., 2014). It is worth mentioning that the V5-tagged ATX used in the co-immunoprecipitation was collected from the supernatant of a stably transfected cell line.

Thus, the concentration of ATX cannot be effectively determined, and may exceed the physiological concentration of ATX *in vivo*. Additionally, both Tat and ATX have been reported to physically interact with integrin receptors (Hausmann et al., 2011; Urbinati et al., 2012), introducing the possibility that the binding between Tat and ATX may require participation of other components. Further studies are required to better characterize the affinity and stoichiometry of the ATX-Tat interaction, as well as whether this interaction requires additional adaptor proteins. Alternatively, it is reported that $Tat_{1-72}$ and $Tat_{1-86}$ can efficiently enter certain cells via endocytosis (Mann and Frankel, 1991). It is also thus conceivable that Tat enters the cell and interferes with the secretion of ATX, leading to decreased ATX lysoPLD activity in Tat-treated OLGs. In brief, the study reported here can be summated by our proposed working model (Fig. 6.7). The viral protein Tat, via its proposed interaction with ATX's lysoPLD active site, reduces the expression of OLG differentiation genes and interrupts the protective role of LPA on OLG morphology.

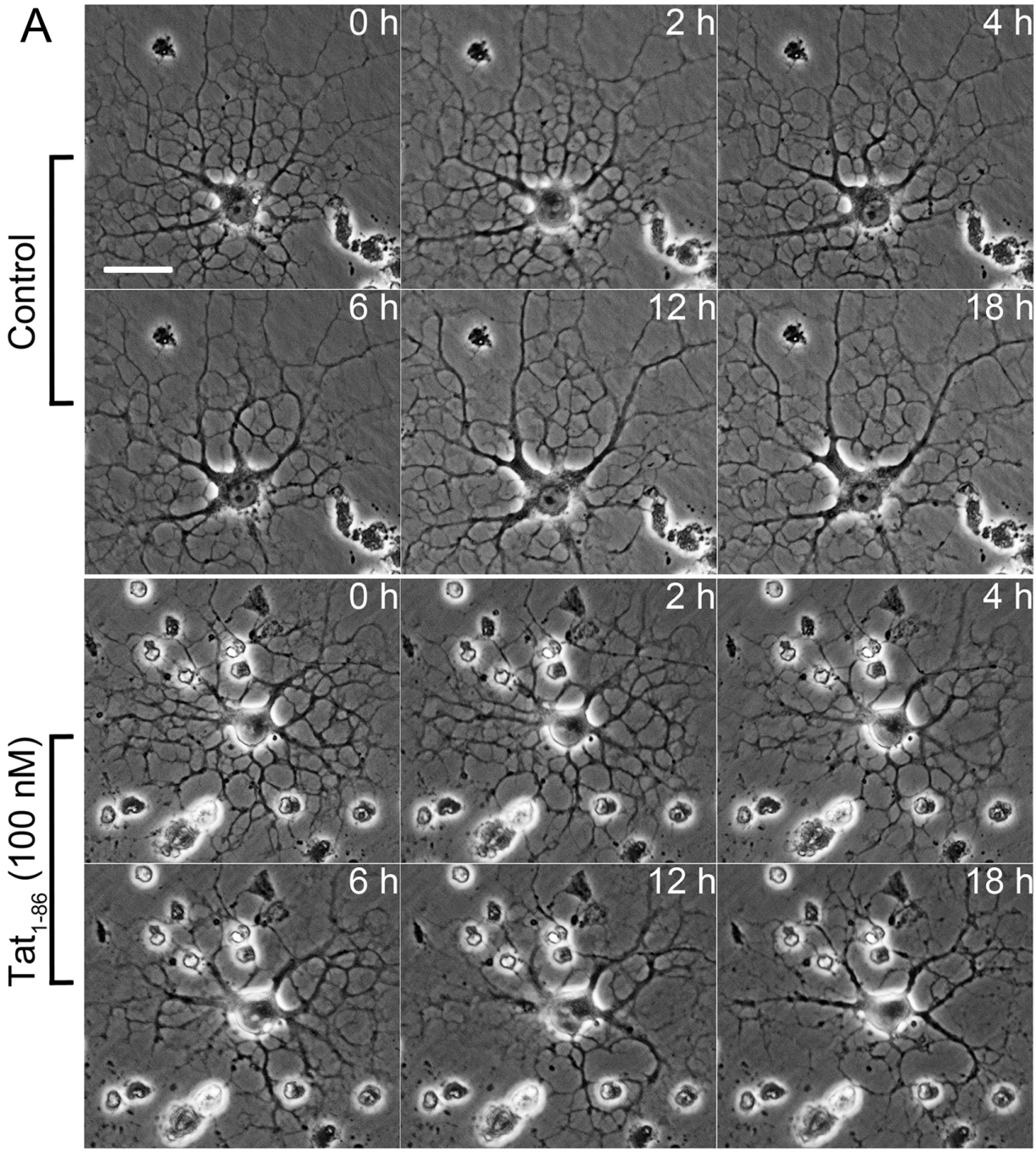
A
0 h
2 h
4 h
Control
6 h
12 h
18 h
0 h
2 h
4 h
Tat1-86 (100 nM)
6 h
12 h
18 h

**Figure 6.1: HIV-1 Tat decreases immature OLG process networks.** Sample phase contrast images of immature OLGs treated with vehicle- or 100 nM Tat at 0, 2, 4, 6, 12 and 18 hr. While normal growth was observed in vehicle-treated OLGs, Tat treatments leads to decreased process network, especially after 4 hr.

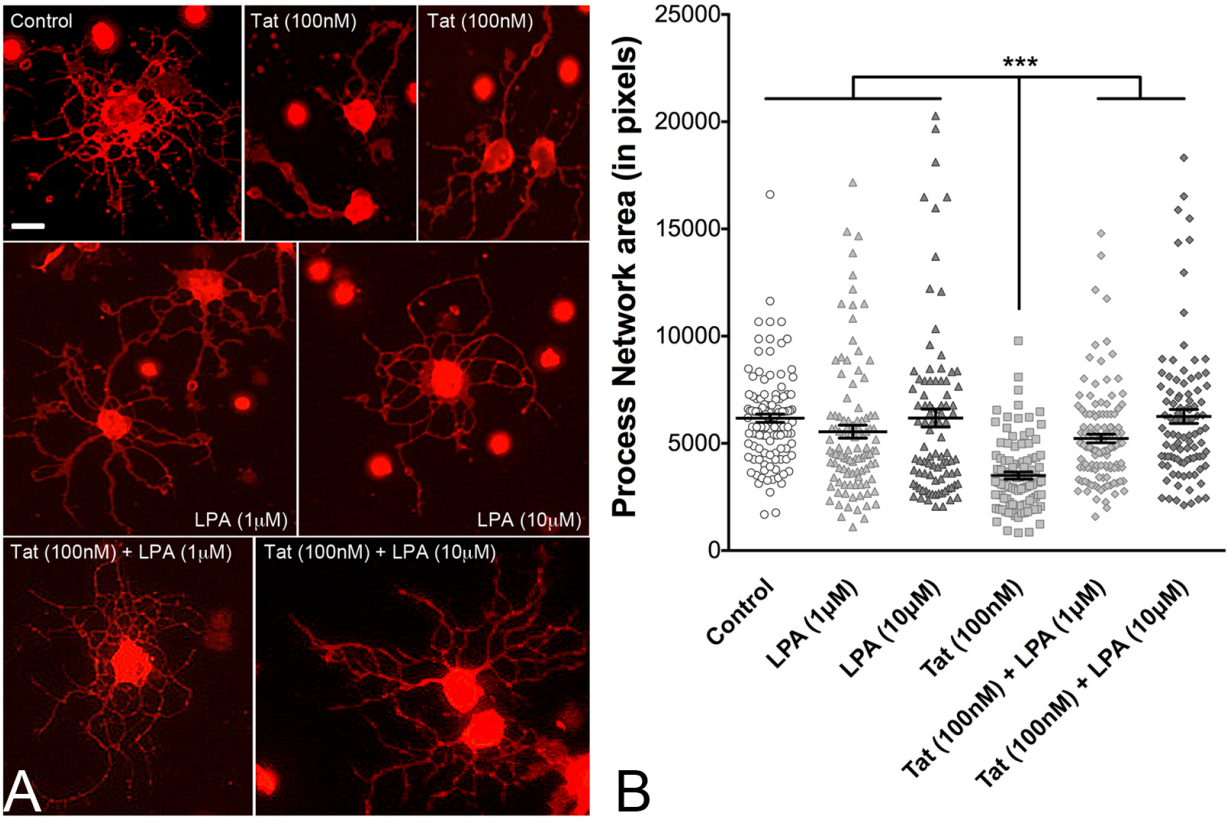
Control
Tat (100nM)
Tat (100nM)
LPA (1μM)
LPA (10μM)
Tat (100nM) + LPA (1μM)
Tat (100nM) + LPA (10μM)
A
Process Network area (in pixels)
25000
20000
15000
10000
5000
0
***
Control
LPA (1μM)
LPA (10μM)
Tat (100nM)
Tat (100nM) + LPA (1μM)
Tat (100nM) + LPA (10μM)
B

**Figure 6.2: LPA protects OLGs from Tat-induced process retraction.** (**A**) Representative images of Vehicle-, Tat-, LPA- and Tat + LPA- treated OLGs shown by O4+ immunostaining (Scale bar = 10 μm). (**B**) OLGs treated with 100 nM Tat showed significantly decreased process network at 18 hr. LPA at 1 or 10 μM rescued the decreased OLG process network induced by 100 nM Tat. LPA by itself at both concentrations has no effect on OLG process network. (*** $p<0.001$ vs. 100 nM Tat; One-Way ANOVA followed by post-hoc Bonferroni's test, N=4 individual experiments, ≥ 30 cells were counted for each N).

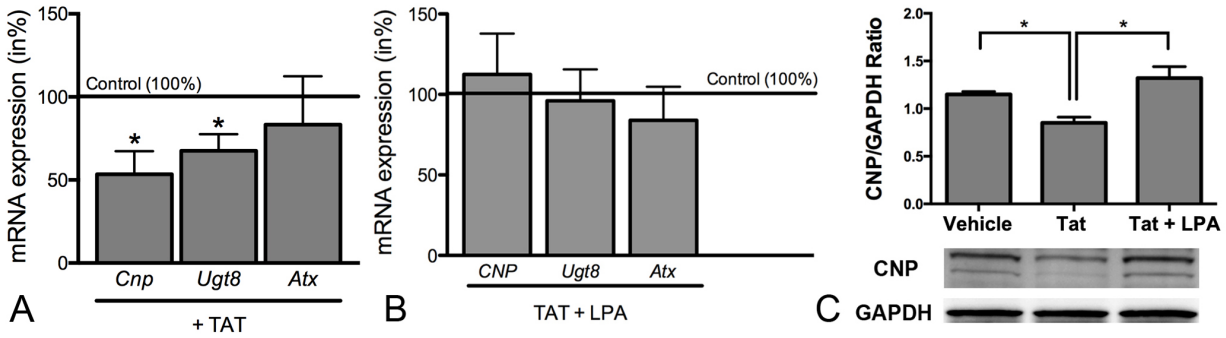
mRNA expression (in%)
150
100
50
0
Control (100%)
*
*
Cnp
Ugt8
Atx
+ TAT
A
mRNA expression (in%)
150
100
50
0
Control (100%)
CNP
Ugt8
Atx
TAT + LPA
B
CNP/GAPDH Ratio
2.0
1.5
1.0
0.5
0.0
*
*
Vehicle
Tat
Tat + LPA
CNP
GAPDH
C

**Figure 6.3: OLG differentiation genes are down-regulated with Tat treatment.** (**A-B**) Quantitative RT-PCR gene expression analysis of vehicle, Tat and LPA treated immature OLGs. (**A**) Immature OLGs treated with Tat for 18 hr showed decreased expression of *Ugt8* and *Cnp*. Tat treatment has no effect on expression of *Atx*. (**B**) Tat-induced decrease of *Ugt8* and *Cnp* expression can be rescued by adding LPA to culturing medium. Current addition of Tat and LPA also has no effect on *Atx* expression. (**C**) Western blot showed that 18 hr Tat treatment decreases protein expression of Cnp in immature OLGs, which can also be reversed by LPA (*: $p<0.05$ vs. Control. For Fig. 3A & 3B: student's t-test, N=5; For Fig 3C. One-Way ANOVA followed by post hoc Bonferroni's test, N=4 individual experiments).

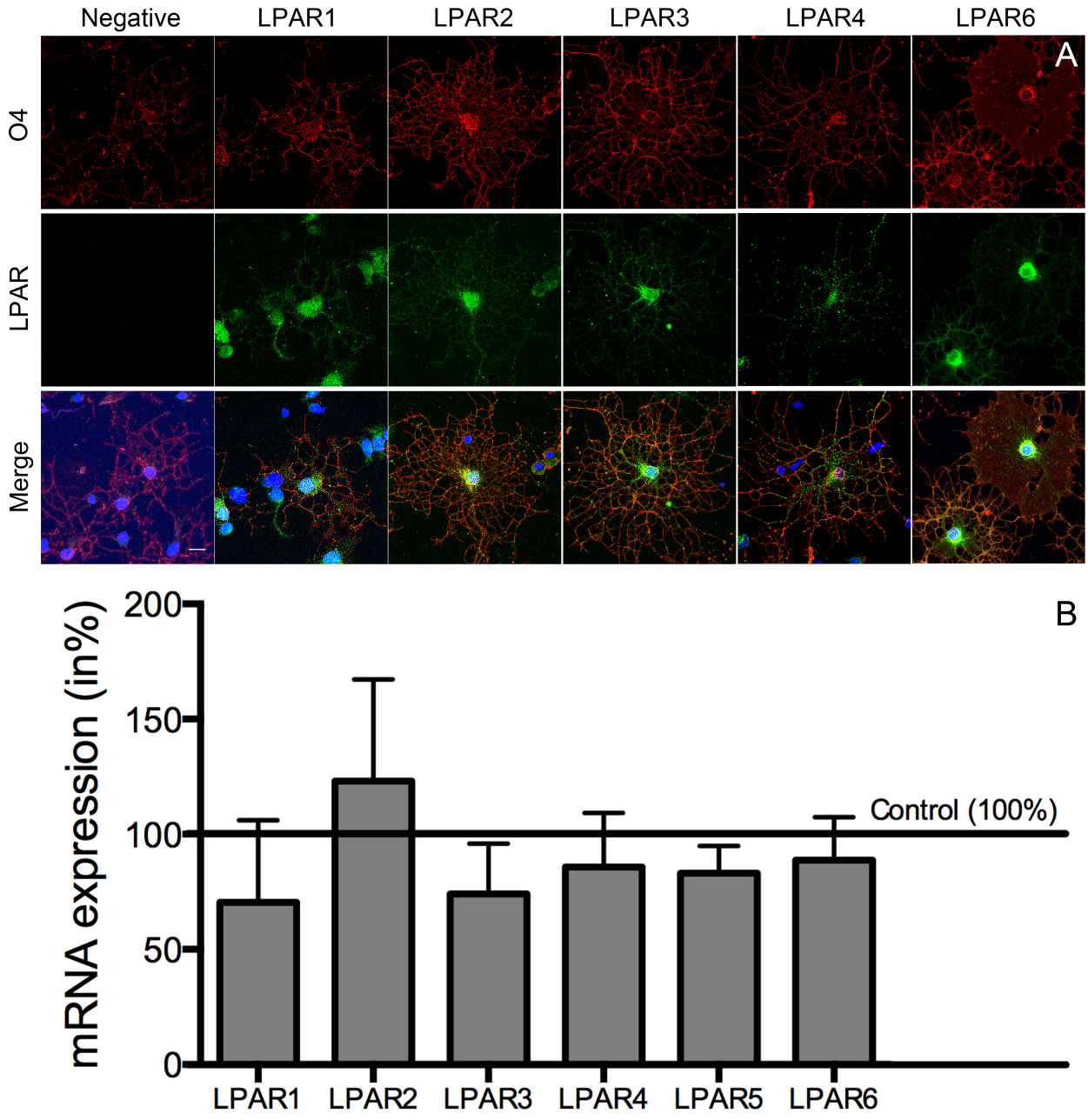
Negative
LPAR1
LPAR2
LPAR3
LPAR4
LPAR6
A
O4
LPAR
Merge
B
mRNA expression (in%)
200
150
100
50
0
Control (100%)
LPAR1
LPAR2
LPAR3
LPAR4
LPAR5
LPAR6

**Figure 6.4: Expression of LPA receptors are not affected by Tat treatment.** (**A**) Immunostaining showing $LPA_{1-4}$ and $LPA_6$ are found on $O4^+$ immature OLGs at 2 div (days *in vitro*) (Scale bar = 10 μm). (**B**) qRT-PCR gene expression data showing $LPA_{1-6}$ expression in OLGs is not altered by Tat treatment. The mean value for vehicle-treated OLGs was set to 100% (horizontal line) and values for Tat-treated cells were calculated accordingly. (student's t-test; N=4 individual experiments).

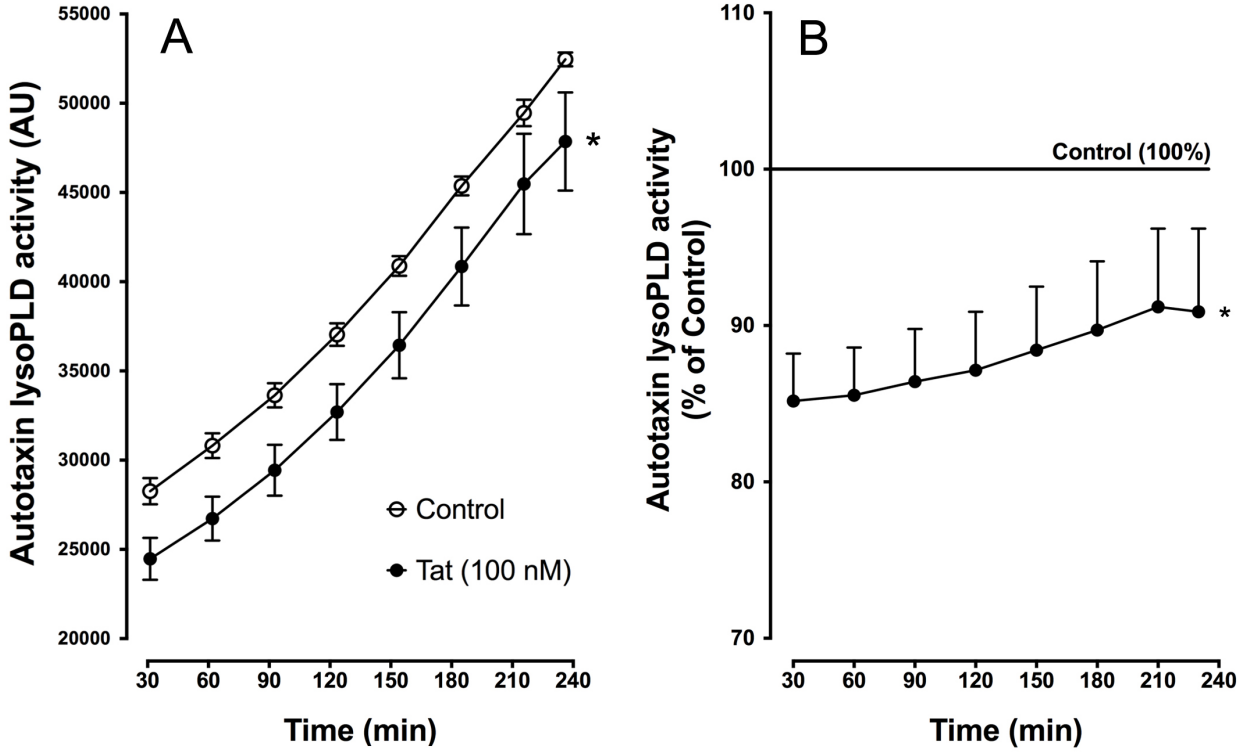
A
Autotaxin lysoPLD activity (AU)
55000
50000
45000
40000
35000
30000
25000
20000
30
60
90
120
150
180
210
240
Time (min)
Control
Tat (100 nM)
*
B
Autotaxin lysoPLD activity
(% of Control)
110
100
90
80
70
Control (100%)
*
Time (min)

**Figure 6.5: Tat decreases ATX lysoPLD activity.** ATX lysoPLD activity assay was performed using supernatant collected from 18 hr Tat- or vehicle-treated primary immature OLGs. (**A**) Tat-treatment significantly decreases overall lysoPLD activity. (**B**) The mean value of the lysoPLD activity of supernatant from vehicle-treated OLGs was set to 100% (horizontal line). Treat cells with Tat leads to ~10-15% drop of lysoPLD activity at all time points examined [*: $p<0.05$ vs. control; Two-way ANOVA (Tat, Time) followed by post-hoc bonferroni's test, N=5 individual experiments].

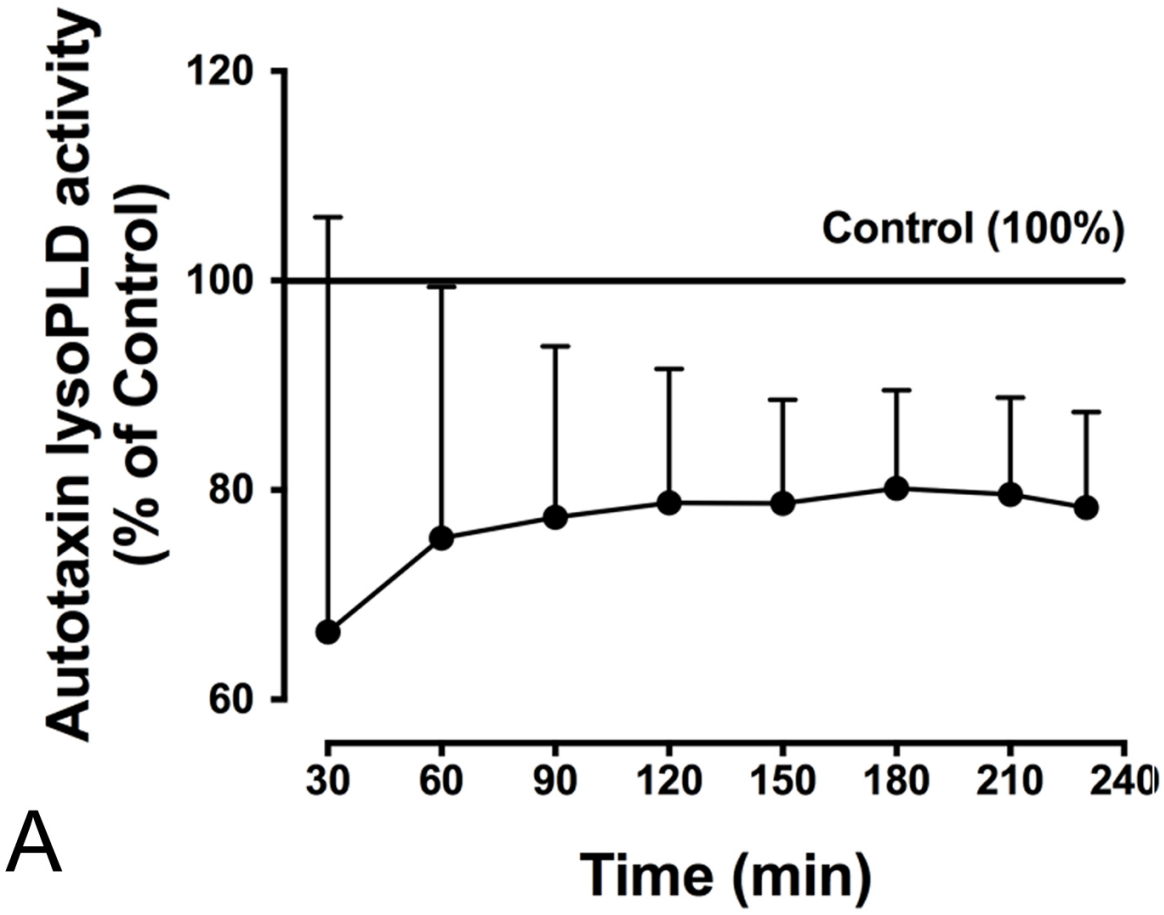
Autotaxin lysoPLD activity
(% of Control)
120
100
80
60
Control (100%)
30
60
90
120
150
180
210
240
Time (min)
A

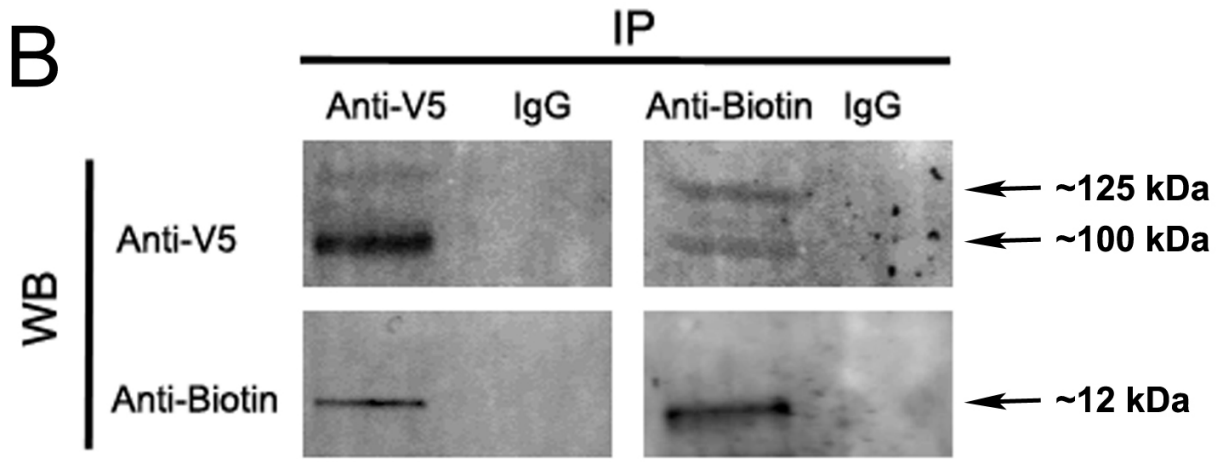
B
IP
Anti-V5
IgG
Anti-Biotin
IgG
WB
Anti-V5
Anti-Biotin
~125 kDa
~100 kDa
~12 kDa

**Figure 6.6: Physical interaction of TAT and ATX alters ATX activity.** (**A**) Adding Tat to the supernatant collected from untreated primary OLG cultures significantly decreased the ATX lysoPLD activity when compared with control [* $p<0.05$, vs. Control; Two-way ANOVA (Tat, Time) followed by post hoc Bonferroni's test, N=4 individual experiments]. (**B**) Concentrated supernatant collected from a stably transfected Cos7 cell line that secrets V5-tagged ATX was mixed with biotin-conjugated Tat, and immunoprecipitated (IP) with antibodies specific to V5 (left panels) or biotin (right panels) and processed for Western blot (WB) for biotin (bottom panels) or V5 (top panels), respectively. Mouse IgG has no known specificity was used as negative control. While nothing was detected from msIgG precipitates, V5-tagged ATX was detected in anti-Biotin precipitates, and vice versa.

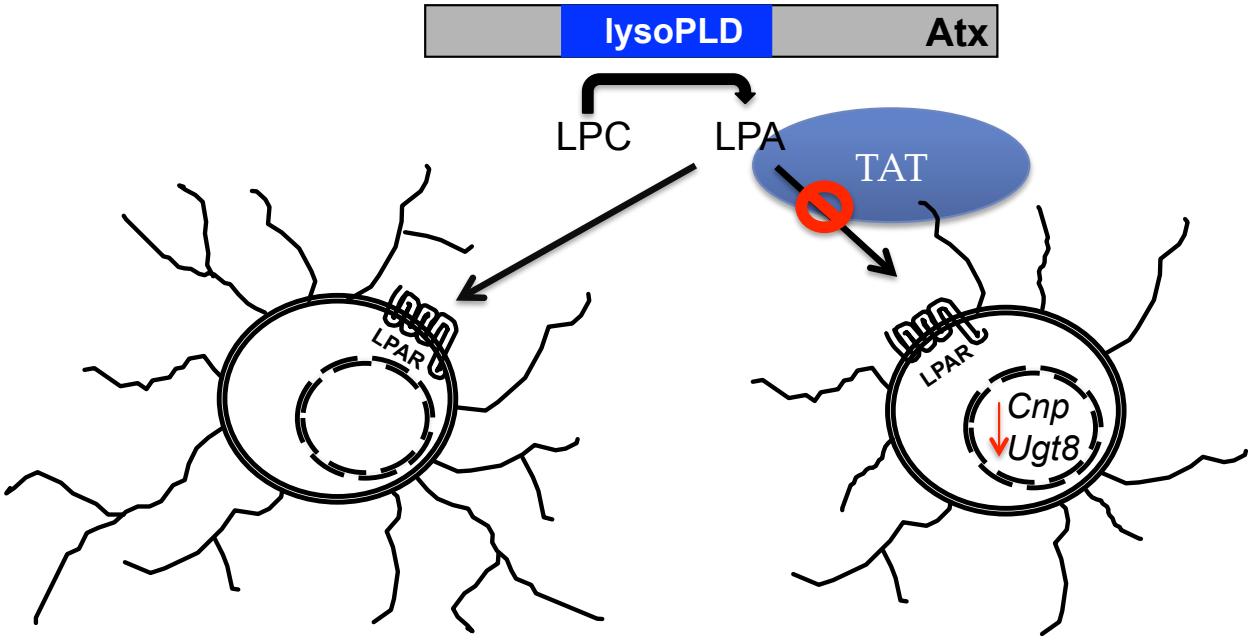


Immature Oligodendrocyte

**Figure 6.7: Proposed model for effects of Tat on immature OLG differentiation.** Tat interacts with ATX, decreasing its lysoPLD activity and subsequent LPA production. Changes in LPA prevent the protective ability of LPA towards Tat-induced retraction of OLG process network area and the differentiation promoting ability to regulated OLG genes, *Ugt8* and *Cnp*.

# Chapter 7

## Final Conclusions

In the CNS, OLGs repeatedly wrap their membranes around axons to form a highly compacted multilayered myelin sheath to ensure proper signaling in the CNS. The importance of the myelin sheath becomes apparent in diseases where it is injured or its function is impaired such as in MS and WM associated injuries found in HIV+ patients. In such cases, a better understanding of OLG differentiation is necessary to further recognize how to stimulate repair under pathological conditions. Focal areas of demyelination characterize MS in the CNS and cells with the potential to myelinate have been found present within MS lesions, however, remyelination remains inefficient, likely due to a block in OLG differentiation within the context of the lesioned CNS environment (Chang et al., 2002b; Kuhlmann et al., 2008c; Wolswijk, 2002). Additionally, there is WM atrophy and OLG impairment in the brains of HIV+ infected individuals (Sarma et al., 2014; Sclafani et al., 1997). In general, OLG differentiation requires changes in gene expression. Current knowledge underlying these molecular mechanisms is limited and represents a major hurdle in identifying therapeutic targets suitable for stimulating OLG differentiation and myelination under conditions as they are found in MS and HIV+ infection. Thus, the focus of the experiments outlined in this dissertation was to characterize a novel molecular mechanism governing changes in gene expression as they occur during OLG differentiation, i.e. mechanisms mediated by the extracellular protein ATX. In investigating this novel mechanism, additional roles of ATX were also revealed. The data obtained bring new knowledge to the field and will aid in the full understanding of how to stimulate repair of the myelin sheath after injury.

In the context of the demyelinating disease, MS, ATX mRNA and protein levels have been found reduced (Comabella and Martin, 2007), thus suggesting that promoting OLG differentiation under such pathological conditions may require the activation of the molecular mechanisms mediated by ATX. In this regard, ATX plays an important role in initiating the signaling pathways regulating gene expression changes during OLG differentiation. Specifically, these changes are mediated through the activity of its functionally active domain, the lysoPLD active site. More mechanistically, ATX's lysoPLD activity regulates HDAC1/2 activity and gene expression. Such a differentiation-promoting role of ATX via its lysoPLD active site and via activation of HDAC1/2 is supported by data in which the inhibition of ATX's lysoPLD activity by HA130 and S32826 both decreased overall HDAC activity, seen *in vivo* and *in vitro* (Figs. 2.4,6), and increased histone acetylation of lysine 9 on Histone 3 (H3K9ac) (Fig. 2.7). Conversely, OLGs treated with LPA, the enzymatic product of ATX's lysoPLD activity, showed an increase in HDAC activity (Fig. 2.6D). Furthermore, inhibition of the lysoPLD active site kept expression levels of *Ugt8* and *Cnp* down-regulated and maintained elevated *Egr1* expression, thus inhibiting progenitor cells from differentiating (Fig. 2.5D). In the zebrafish, genetic manipulation of *atx,* as well as specific inhibition of the lysoPLD active site, led to a reduction in both *cldnk* and *plp1b* expression (Figs. 2.1,2,3). In support of the hypothesis that HDAC1/2 activation is downstream of the ATX-LPA signaling cascade, inhibiting HDAC1/2, but not HDAC6, kept OLG differentiation genes, *Ugt8* and *Cnp* down-regulated and in a progenitor state; an effect that could not be rescued by the addition of LPA (Fig. 2.8B,C). Thus, LPA, formed via the lysoPLD active site of ATX, is essential in OLG differentiation as it enhances

HDAC1/2 activity and ultimately regulates the gene expression changes needed for proper OLG development (Fig. 2.9).

Although several extracellular signaling molecules, ATX included, are known to be essential for OLG differentiation (Mitew et al., 2014), the intracellular regulators are poorly understood. With regard to the data outlined in Chapter 2, the mechanism(s) by which the ATX- LPA axis activates HDAC1/2 activity, needed for OLG differentiation, has yet to be discovered**.** Previously, it has been reported that LPA induction of HDAC activity is blocked by inhibiting receptor activation with pertussis toxin (Ishdorj et al., 2008). The A-protomer of pertussis toxin ADP-ribosylates the $\alpha$ subunits of heterotrimeric $G_{i/o}$ proteins, resulting in the receptors uncoupling from the $G_{i/o}$ proteins. The uncoupling of GPCR from the $G_{i/o}$ proteins disrupts the communication between the receptor and the effector signaling cascades (Mangmool and Kurose, 2011). All current LPA receptors couple to $G_{i/o}$ (Chun, 2013). Thus, the inability of LPA to activate HDAC activity through $G_{i/o}$, reveals the possible involvement of signaling pathways initiated by $G_{i/o}$ in OLG differentiation**.** Although $LPA_6$ signals through $G_{i/o}$, data outlined in Chapter 4 reveal the unlikelihood that this receptor activates HDAC1/2 signaling during OLG differentiation. It is possible, however, that the signaling pathways, downstream of $LPA_6$ and the ATX-LPA signaling axis, converge and together mediate gene expression changes. Interestingly, LPA also failed to induce HDAC activity when $LPA_1$ expression was reduced by siRNA (Ishdorj et al., 2008). These findings, together with the ma$LPA_1$-null mice studies, in which $LPA_1$ plays a role in the later stages of OLG development, and not during early OPC differentiation (Garcia-Diaz et al., 2015), proves it unlikely that activation via $LPA_1$ stimulates HDAC1/2 activity during OPC differentiation.

Nonetheless, these experiments provide insight to possible signaling pathways linking the ATX-LPA axis to HDAC1/2 regulation of gene expression changes needed for OLG differentiation. Key players seen in the converging signaling cascades downstream of LPA receptors are protein kinases.

Signaling via protein kinases acts to connect the extracellular environment to the intracellular environment. As diverse protein signaling cascades are initiated via the activation of LPARs/$G_{i/o}$, it is possible that activation of HDAC1/2 is a result of protein kinase activity. Interestingly, hyperphosphorylation of HDAC1 and HDAC2 leads to a slight, but significant, increase in deacetylase activity (de Ruijter et al., 2003). HDAC1 has been reported to be phosphorylated by casein kinase 2 (CK2), cAMP-dependent protein kinase, and protein kinase G(Cai et al., 2001). HDAC2, however, is phosphorylated uniquely by protein kinase CK2 *in vitro* (Tsai and Seto, 2002). Thus, CK2 presents itself as an interesting protein kinase involved in the regulation of both HDAC1 and 2. Though initially considered to be a "constitutively active" protein, it is now understood that activated Akt can phosphorylate CK2 (Nguyen and Mitchell, 2013). Additionally, CK2 has been recorded to physically associate with Akt (Guerra, 2006), phosphorylate Akt on Ser129 (Di Maira et al., 2005), contribute to Akt activation (Di Maira et al., 2009), and interact with Akt within Wnt/β-catenin signaling (Ponce et al., 2011). In association with Akt, activation of the PI3K/Akt/mTOR pathway has recently been shown to trigger phosphorylation of HDAC1 in breast cancer cells (Citro et al., 2015). Interestingly, the PI3K/Akt/mTOR pathway is one of the signaling pathways initiated by $G_{i/o}$ activation. As such, activation and interaction of the PI3K/Akt/mTOR pathway with CK2 may contribute to the regulation of HDAC1/2. This hypothesis,

however, will need further examination to pinpoint the exact mechanisms leading the to epigenetic changes initiated via the ATX-LPA axis observed during OLG differentiation.

Targeting individual LPA receptors, and the signaling pathways by which they alter gene expression, is a conceivable approach to trigger differentiation of OLGs. Thus, a better understanding of the functions of individual LPA receptors involved in OLG differentiation are needed. In researching the effect of the under-investigated $LPA_6$ in OLG differentiation, it was found that $LPA_6$ is critically involved in the regulation of OLG differentiation genes, *Cnp* and *Ugt8*, *in vitro* (Fig 4.1) and myelin gene, *plp1b*, *in vivo* (Fig. 4.2). Though initially seen to parallel results seen when inhibiting the lysoPLD domain of ATX, and revealing a potential receptor downstream of the ATX-LPA axis, it was later revealed that gene expression changes induced by down-regulation of *Lpar6* somewhat differed from those that are epigenetically modulated.

Taking a closer look, the signaling events of the ATX-LPA-HDAC1/2 axis and those downstream of $LPA_6$ appear to have different effects on OLG gene regulation. Reduction of *Lpar6* expression by roughly 50%, maintained the down-regulated expression of OLG differentiation genes, *Ugt8* and *Cnp* (Fig. 4.1B), however, the expression of *Cnp* did not reach the same level of down-regulation as seen when inhibiting the lysoPLD active site (Fig. 2.5D). Most intriguingly, down-regulation of *Lpar6* did not have an effect on the expression of OLG differentiation inhibitor, *Egr1* (Fig. 4.1B), whereby, inhibition of the lysoPLD active site caused *Egr1* expression to remain elevated (Fig. 2.5D). Of utmost importance is the data revealing that the down-regulation of *Lpar6* does not effect HDAC activity (Fig. 4.3). In line with these findings, no change was found in the acetylation of lysine 9 on Histone 3 (H3K9ac) in siRNA

treated cells compared to control (Fig. 4.3). The data further exemplify the differences in signaling through the ATX-LPA-HDAC1/2 axis and through $LPA_6$.

One factor that remained consistent was the finding that following the inhibition of ATX's lysoPLD active site and by the siRNA mediated down-regulation of *Lpar6*, primary changes were found in gene expression and were independent of morphological aspects of OLG differentiation. Neither treatment had a significant effect on the process morphology of OLGs (Supp. Fig. 8.1;Fig.4.1C). As OLGs develop along the lineage, alterations in both gene expression and cytoskeletal maturation are seen. The studies outlined in this dissertation reveal that both the ATX-LPA-HDAC1/2 and $LPA_6$ signaling pathways influence immediate gene expression changes in OLG differentiation rather than directly mediating cytoskeletal changes. It is plausible, however, that changes in morphology could result as a consequence of the changes in gene expression.

The discrepancies seen between targeting the lysoPLD active site and $LPA_6$ were initially hypothesized to be the result of experimental timing differences. In this context, experimentation using siRNA prolongs the time in which OLGs are exposed to mitogens (in order to ensure proper knockdown of the gene) and though the time frame from mitogen removal remains consistent, it is plausible that subsets of these OPCs are differentiated. It is understood that there is a short time window in which HDAC1/2 play a crucial role in the differentiation phase of OLG development. Data outlined in this dissertation further confirms this role and links it to the extracellular signaling of LPA, by way of ATX's lysoPLD active site. It is conceivable, however, that if siRNA experiments targeted a subset of OPCs that were past the differentiation stage, differences would be

seen in gene expression and could underlie the variances seen in *Cnp* and *Egr1* expression levels. To address this idea, *Egr1* expression was analyzed following the same experimental timeline seen in siRNA experiments, whereby OLGs were subjected to mitogens for an additional 24hrs before treatment with HA130 (ATX lysoPLD active site inhibitor). *Egr1* expression remained up-regulated (Supp. Fig. 8.2), as was seen previously in Chapter 2, thereby dispensing the experimental timeline as a confounding factor contributing to the changes seen between the ATX-LPA-HDAC1/2 and $LPA_6$ pathways.

An alternative, and more plausible, hypothesis elucidating divergent gene expression patterns, is notion that signaling events downstream of $LPA_6$ differ from the ATX-LPA-HDAC1/2 pathway, in that they do not activate epigenetic players. $LPA_6$ exerts its effects through the activation of $G_{\alpha 12/13}$ and $G_{\alpha i/o}$ (Chun, 2013). Though many signaling pathways are found downstream of $G_{\alpha 12/13}$ and $G_{\alpha i/o}$, recently the PI3K/Akt/mTOR pathway has been shown to play a role in OLG development and myelination (Flores et al., 2008; Narayanan et al., 2009; Sherman et al., 2012). Specifically, mTOR, a serine threonine protein kinase, regulates OLG differentiation *in vitro* (Tyler et al., 2009). mTOR exists in two functionally distinct complexes, mTORC1 and mTORC2, which are more classically known to be associated with the regulation of translation, but have recently been found to play a role in the regulation of gene transcription (Bercury et al., 2014; Cunningham et al., 2007; Laplante and Sabatini, 2013). While there is a tight balance between the activity of mTORC1 and mTORC2 in OLG differentiation, it has recently been found that signaling through mTORC1 is critical for the regulation of OLG differentiation and myelination (Bercury et al., 2014).

Interestingly, ablation of Raptor, a protein component of mTORC1, reduced both protein and gene expression levels of CNP and PLP in the corpus callosum and spinal cord (Bercury et al., 2014). Though UGT8 was not analyzed in these studies, reduction of CNP and PLP, seen with the loss of mTORC1, parallels the reduction in *Cnp* and *plp1b* found by down-regulation or genetic manipulation of $LPA_6$. Additionally, Raptor has been shown to physically bind to and regulate how YY1 binds to gene promoters (Cunningham et al., 2007). This finding is particularly interesting with regard to OLGs, because YY1 has been shown to be essential for OLG progenitor differentiation (He et al., 2007).

Furthermore, multiple signaling pathways are often coordinately regulated by extensive crosstalk and the pharmacological inhibition of the mTOR pathway can feedback to up-regulate the MAPK (mitogen-activating protein kinase) pathway (Carracedo et al., 2008)**.** These studies link the PI3K/Akt/mTOR pathway with that of the Ras/Raf/MEK/Erk pathway. In evaluating the crosstalk between these two pathways (both found downstream of $G_{\alpha i/o}$), Dai et al., 2014 found that both major signaling pathways, through Akt/mTOR and MEK/Erk1/2, are necessary for full differentiation of OPCs to mature OLGs *in vitro*. Though these studies primarily focused on the expression of MBP, it does not exclude the possibility that these signaling events are initiated by the activation of $LPA_6$. As previously discussed, the PI3K/Akt/mTOR pathway plays a role in the phosphorylation of HDAC1 (Citro et al., 2015), and there is reason to hypothesize that protein kinases play a role in the epigenetic changes regulated by the ATX-LPA axis. Though $LPA_6$ does not appear to activate HDAC activity, as seen regulated by the ATX-LPA axis, it is plausible that there is crosstalk

between the two signaling pathways that regulate overall gene expression changes needed for proper OLG differentiation. Taken together, there are many implications that protein kinase signaling, downstream of $G_{i/o}$, play a role in OLG differentiation and further studies revealing a possible association with $LPA_6$ and the ATX-LPA axis will further elucidate the importance of LPA signaling in OLG development.

In brief, it is unlikely that the ATX-LPA-HDAC1/2 axis acts through $LPA_6$ to activate the epigenetic changes needed for proper OLG differentiation. It is plausible, however, that $LPA_{6,}$ works in conjunction with the ATX-LPA-HDAC1/2 signaling cascades to fine tune gene expression changes needed for proper development. It is also conceivable that the activation of $LPA_6$, by LPA, is a result of an alternative, LPA-producing source. ATX has been shown to be dispensable for hair follicle morphogenesis (Grisanti et al., 2013) and $LPA_6$ is essential for the maintenance of human hair growth (Pasternack et al., 2008, 2009). The ligand, LPA, needed to stimulate $LPA_6$ for hair growth, however, it not a product of ATX, but rather by PA-$PLA_1$ (Inoue et al., 2011). Thereby, we cannot rule out the possibility that other sources of LPA may stimulate $LPA_6$ in OLG differentiation.

ATX is involved in a wide range of physiological mechanisms including, but not limited to, lymphocyte homing (Knowlden and Georas, 2014), hyperoxic lung injury (Nowak-Machen et al., 2015), cancer motility (Jankowski, 2011) and the formation of the vasculature by vasculognesis and angiogenesis (Kleger et al., 2011). The role of ATX is becoming more evident as further research is conducted, however, a great deal of information is yet to be uncovered regarding this extracellular protein. Studies present in this dissertation display one of the newest discoveries regarding ATX, its subsequent

interaction with HIV-1 viral protein Tat. As seen in chapter 6, Tat has a negative effect on the differentiation of OLGs, both by down-regulating OLG differentiation genes and causing process retraction (Fig.6.1,2,3). As Tat is considered a “sticky” protein that binds many receptors, it was initially suspected that Tat binds LPA receptors and alters their expression. To our surprise, Tat had no effect on the expression of $LPA_{1\text{-}6}$ (Fig. 6.4). Looking further, the addition of LPA, formed via ATX’s lysoPLD domain, was able to rescue the effects of Tat on OLG mRNA expression and protected OLGs against Tat induced process retraction (Fig. 6.2,3). Thus, implying that Tat interferes with LPA signaling, which as outlined in this dissertation, is now known to play a large role in OLG differentiation. Rather than binding to LPA receptors on OLG, the negative effects of Tat are a result of a protein-protein interaction with ATX that results in the reduction of ATX’s lysoPLD activity (Fig.6.5,6). Hence, Tat released in HIV-1 individuals limits the protective properties of ATX lysoPLD active site on OLG differentiation and could attribute to the WM injuries seen in infected patients. These data provide another novel role of ATX in pathological conditions found in the injured CNS and exemplifies the importance of this protein in OLG differentiation.

To conclude, the data outlined in this dissertation, reveal novel molecular mechanisms, that are mediated by ATX and $LPA_6$, and are critically involved in the regulation of OLG differentiation; providing insight into innovative therapeutic targets suitable for stimulating remyelination under pathologic conditions such as those found in MS as well as HIV+ patients (Fig. 7.1). These studies are the first of their kind revealing the importance of the understudied $LPA_6$ in OLG differentiation, a finding that could lead to the creation of novel therapeutic drugs. Additionally, ATX was found to interact with

the viral protein, Tat, a unique discovery that may lead to future breakthroughs pinpointing the increasingly important role of ATX in glial biology. Further investigation into the epigenetic pathways that regulate OLG gene expression, LPAR expression and signaling, as well as ATX-Tat interactions may reveal important information regarding development that can be used when developing and testing future therapeutic approaches.

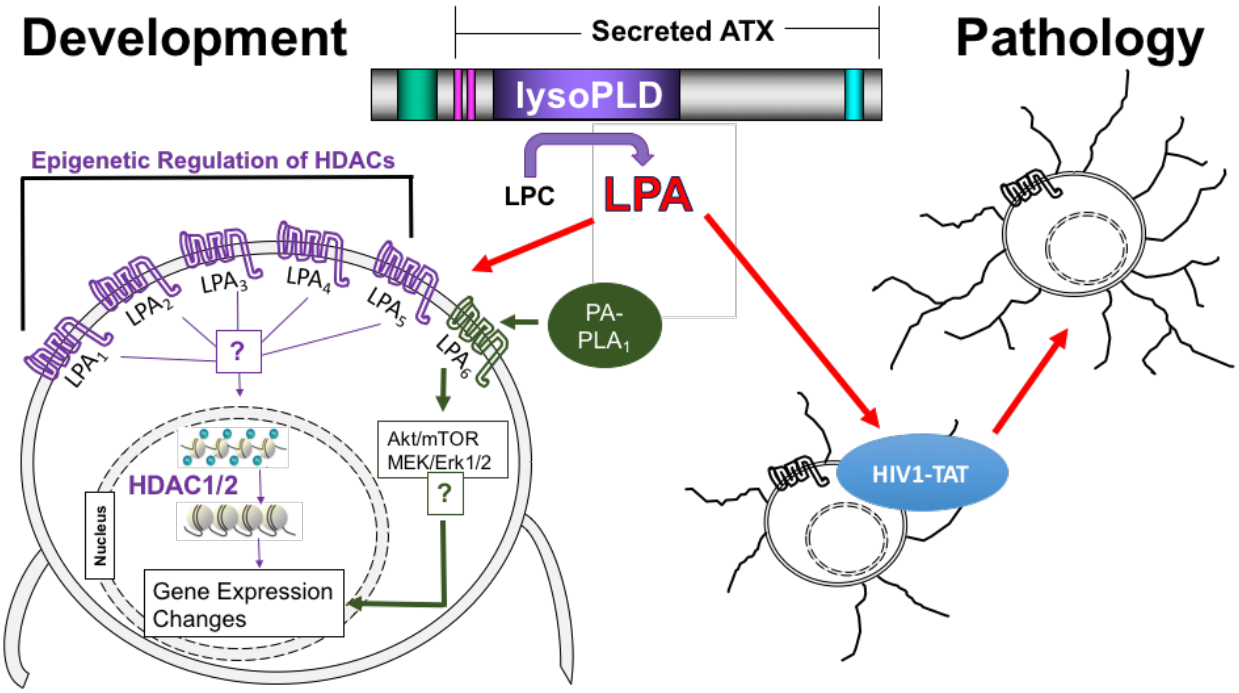
Development
Secreted ATX
Pathology
lysoPLD
Epigenetic Regulation of HDACs
LPC
LPA
LPA1
LPA2
LPA3
LPA4
LPA5
LPA6
?
PA-PLA1
Akt/mTOR
MEK/Erk1/2
?
HDAC1/2
Nucleus
Gene Expression Changes
HIV1-TAT

**Figure 7.1. Schematic cartoon representing effects of ATX's lysoPLD active site in development and pathology. Development:** LPA, formed via the lysoPLD active site of ATX binds to one or more of the LPA receptors, $LPA_{1\text{-}5}$, on OLGs, to activate HDAC1/2 and regulate gene expression changes needed for OLG differentiation. LPA signaling through $LPA_6$ likely acts through a different signaling pathway(s) (possibly through Akt/mTOR and/or MEK/Erk1/2) to regulate gene expression changes. LPA formed via PA-$PLA_1$ may be the ligand for $LPA_6$ signaling. **Pathology:** LPA acts as a protectant against HIV-Tat induced decreases in process network area of OLGs. LPA can also rescue the effect of HIV-Tat on OLG differentiation genes. At the same time, HIV-Tat can block the generation of LPA by negatively affecting ATX's lysoPLD activity.

## Chapter 8

## Supplemental Figures, Data and Protocols

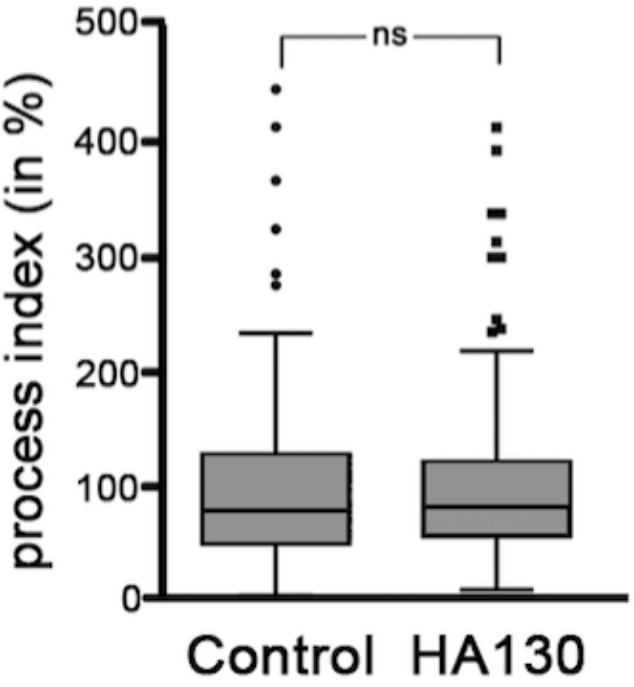

**Supplemental Figure 8.1: Inhibition of ATX's lysoPLD active site does not change overall process network area of OLGs.** Box and whisker plot depicting process network area of OLGs for HA130 treated cells as determined by immunostaining and morphology analysis. The plot depicts medians and quartiles of three independent experiments. Whiskers represent the 10th and 90th percentile.

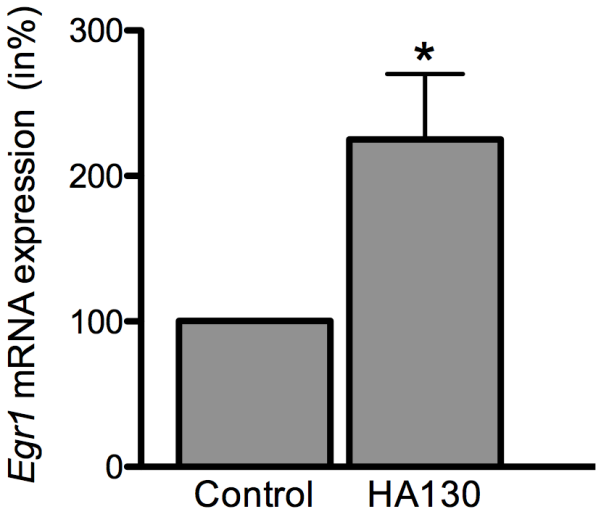
Egr1 mRNA expression (in%)
300
200
100
0
*
Control
HA130

**Supplemental Figure 8.2. *Egr1* remains up-regulated with HA130 treatment after 72hr.** Bar graph depicting mRNA levels for transcriptional inhibitor *Egr1* as determined by real-time reverse transcription (RT)-qPCR analysis. OLGs were treated with mitogens for 48hr before the addition of HA130 or DMSO control for an additional 24hr. Control (DMSO-treated) values were set to 100% and experimental values were calculated accordingly. Data shown represent means ± SEM. *p≤0.05.

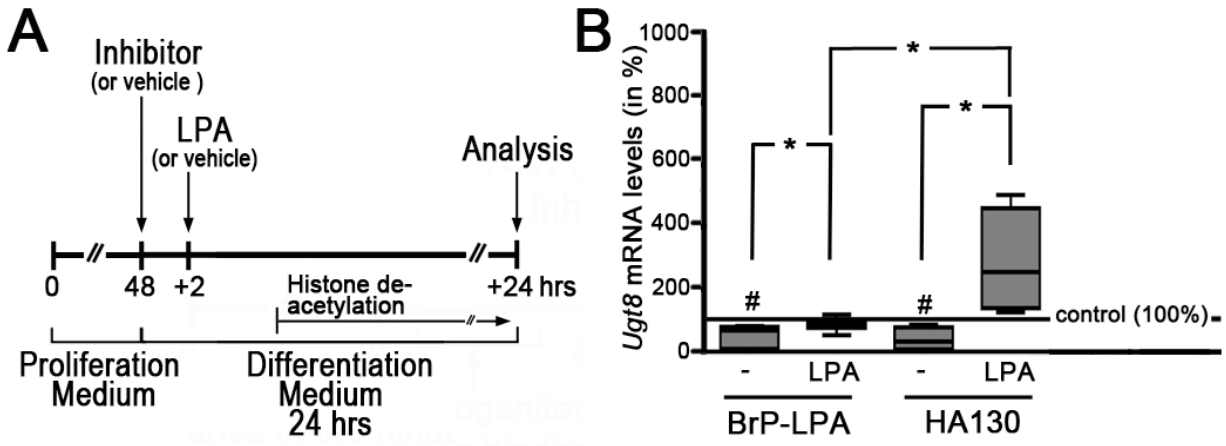
A
Inhibitor
(or vehicle )
LPA
(or vehicle)
Analysis
0
48
+2
Histone de-
acetylation
+24 hrs
Proliferation
Medium
Differentiation
Medium
24 hrs
B
Ugt8 mRNA levels (in %)
1000
800
600
400
200
0
*
*
*
#
#
control (100%)
-
LPA
-
LPA
BrP-LPA
HA130

**Supplemental Figure 8.3. $LPA_{1-4}$ inhibitor can be rescued by LPA, but not at the same magnitude as seen with rescue of the ATX lysoPLD active site alone. A.** Timeline depicting when cells were removed from mitogens and treated. **B.** Box and whisker plot depicting *Ugt8 mRNA* gene expression of OLGs treated with BrP-LPA (Inhibitor of $LPA_{1-4}$) or HA130 (ATX lysoPLD Inhibitor) +/- the addition of LPA as determined by qRT-PCR analysis. The plot depicts medians and quartiles of three independent experiments. Whiskers represent the 10th and 90th percentile. Control (DMSO-treated) values were set to 100% and experimental values were calculated accordingly. Data shown represent means ± SEM. #p≤0.05, *p≤0.05.

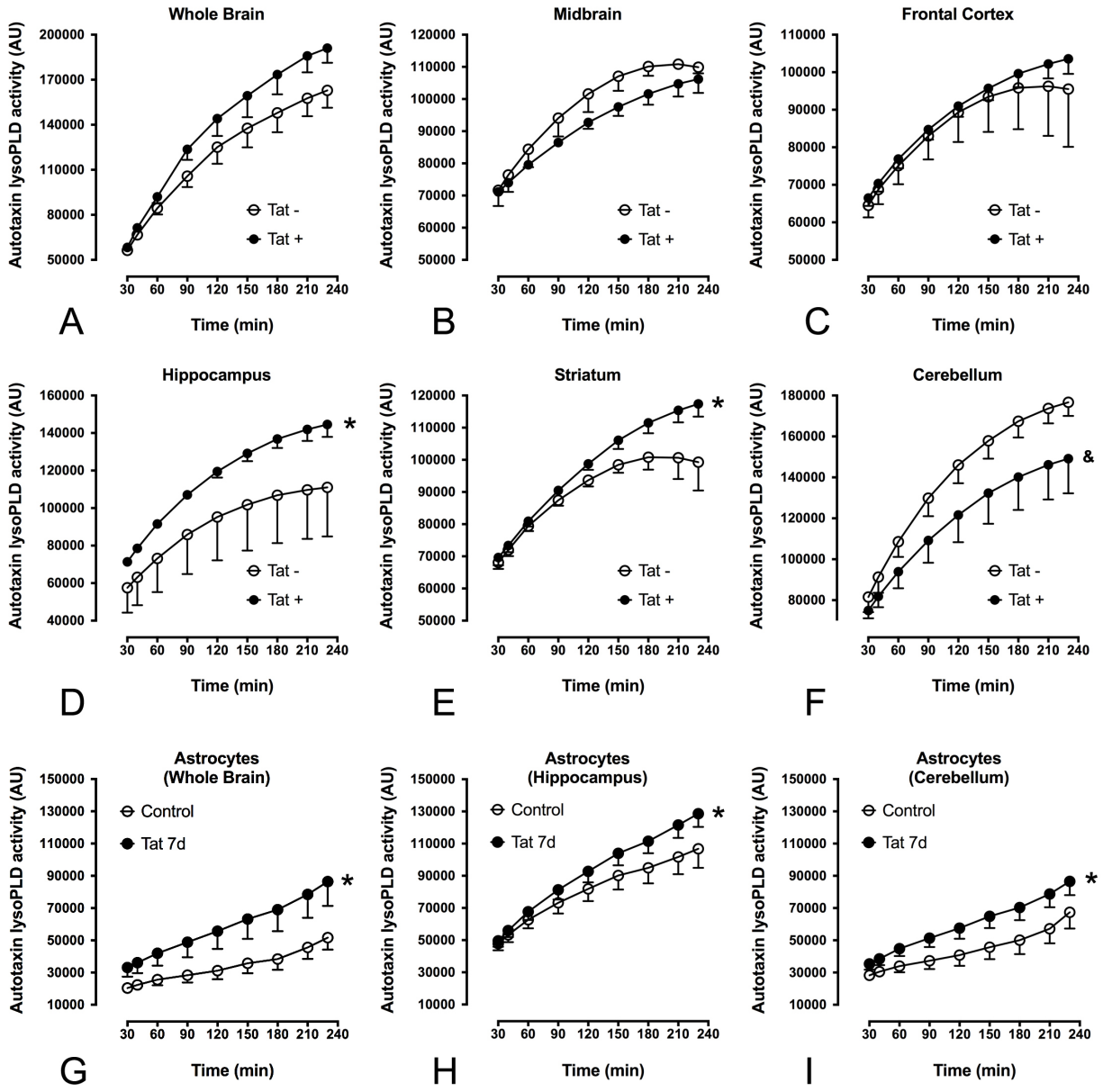
Whole Brain
Midbrain
Frontal Cortex
Hippocampus
Striatum
Cerebellum
Astrocytes (Whole Brain)
Astrocytes (Hippocampus)
Astrocytes (Cerebellum)
Autotaxin lysoPLD activity (AU)
Time (min)
Tat -
Tat +
Control
Tat 7d
*
&
A
B
C
D
E
F
G
H
I

**Figure 8.4: The effect of TAT on ATX lysoPLD activity has regional differences.** (**A-F**) Tat expression was induced for 10 days before animals were sacrificed and different regions of the mouse brain were dissected. (**A-C**) ATX lysoPLD activity in proteins extracted from whole brain, midbrain or frontal cortex were not affected by 10-day Tat expression. (**D-E**) In hippocampus or striatum, expression of Tat for 10 days significantly increases ATX lysoPLD activity. (**F**) ATX lysoPLD activity was significantly decreased by 10-day Tat expression in cerebellum. (**G-I**) Astrocytes from whole brain, hippocampus and cerebellum were cultured and treated with 100 nM Tat. ATX lysoPLD activity from astrocytes of all three areas was increased with Tat exposure. [**A-F**: $^{*,\&}$: $p<0.05$ vs. Tat-; **G-I**: * $p<0.05$ vs. Control; Two-way ANOVA (Tat, Time) followed by post-hoc Bonferroni's test, N=3].

## A2B5 Immunopanning for Oligodendrocytes

**Preparation of A2B5 plates**: (10 pups/150mm plate)

- Obtain 3 Falcon 150 x 15mm (non tissue culture) plates and put a line on the side of the plate with a sharpie (will help to ensure all areas of plate are washed)
- Prepare IgM (-20° freezer in purple box reading IgM) in 50mM Tris/HCL (pH 9.5). Add 12.5ml IgM to dish followed by 25ml Tris HCL (1x). Make sure the liquid covers the entire bottom of the dish.
- Put in 4°C T.C. Fridge O/N– keep sterile!! If a shorter time is needed, incubate in 37°C for 2-3hrs
- Remove (do not wash) IgM and replace with A2B5 supernatant media (-80° freezer on bottom left, place in water bath to defrost and centrifuge 1.5 X 1,000 for 3 min).
- Add A2B5 with 30ml pipette, 10ml for each plate. Then add 10ml of DMEM/Ab/FCS to each plate.
- Incubate O/N at 4°C

**Set Up**

- Remove plates from 4°C and wash 2x with PBS (sterile) and incubate 37°C/CO2 until required
- Obtain sterilization pouch filled with scissors and scalpel and filter paper pouch from the bottom drawer of the bench (with the microscope on top).
  - *Big Scissor*- cut the heads from the body
  - *Middle Scissor*- remove brain from skull
  - *Small Scissor*- remove meninges and mince in HANKS solution
- Obtain filter (blue- 40 micron) from the top drawer of the bench with the microscope on top
- Put 5 50ml tubes in hood (one for digestion, two for washing and two to hold mixed glia that will be given to Dr. Cabral's lab)
- Put DNase on ice and put trypsin in the water bath
- *If using coverslips*: put coverslips in ethanol and then sterile water and let them dry in the hood on white filter paper (middle drawer of bench in the middle of T.C.)
- UV everything in hood for about 10 min while getting the pups ($5^{th}$ floor rat room)

**Procedure**:

- Go to fifth floor to get pups, make sure to bring a box down to the animal room.
- Weigh pups on the T.C. scale and record weight
- Remove heads from pups using big scissor and put bodies in a plastic bag. Put heads on a petri dish on ice.
- Extract brains (whole) from P2-P4 pups Cut from the brain stem up to the nose, open skull and extract the whole brain. Place the brain on filter paper, remove the cerebellum, and carefully drag the brain along the paper to remove excess blood. Once clean place and mince in 60mm petri dish containing 5ml HANKS (T.C. fridge). Use a razor blade to further mince the brains. Wash plate with HANKS – final

volume + 10ml.

- Add minced brains to a 50ml tube- using the extra HANKS to obtain every cell.
- Add enzymes (2.5mL trypsin and 100ml DNAse I) incubate for 15 min at 37°C (swirl around every 5 minutes), stirring every 5min.
- Add fibronectin (human) to coverslips or wells. 1:10 dilution. Place in incubator for at least 30 minutes.
- Discard of paper towel and carcases in the freezer in T.C.
- Wash scissors with water and then D.I. water and lay on paper towel.
- **Inactivate enzymes**: add equal volume DMEM/10% FCS to cells taken from water bath
- Centrifuge cells at 1.2 x 1000 rpm for 3 min. Pour off supernatent, unless giving the astrocytes to another lab.
- Re-suspend pellet in 10ml DMEM/FCS. Aspirate with 16g, big (x5) and 22g, small (x3) needles to achieve single cell suspension. Needles are found on the bottom drawer of T.C. bench with microscope on top. Syringes are above the weigh station- 10ml volume.
- Increase volume of cell suspension. If you have three plates, add to final volume of 30ml, then add 30ml again for 10ml on each plate. Plate out evenly among panning plates (Mix 1 cell:1 media with DMEM/FCS per plate)
- Incubate 30 min at 37°C/$CO_2$
- Then, remove/discard media (mostly containing unwanted astrocytes and glial cells)
- Wash plates 2x with 1X PBS (discard washes)
- Wash cells off plates (x2) with 10mL DMEM/FCS. Check on microscope to ensure majority of cells are removed from plate. About 10 washes/quarter, physically force the cells off the dish and into the media.
- **Collected cells**: pass through FALCON 40mm cell strainer (top drawer of bench with microscope on top- blue), centrifuge and re-suspend in 10mL
- **Differential adhesion**: 10 min at 37°C/$CO_2$ on **non-TC** (not cell star, 1 on ice and 1 in hood) 100mm dish.
- **Fibronectin Removal**- during the 10 minute incubation, remove fibronectin from the plates and add 50ul of PBS for a total of 2 washes. Leave in PBS until add media.
- **Make Media**- Make sure to use FCS free media and add T3,N2, PDGF or bFGF.
- Collect media and count cells- vacuum out media and add 1ml FCS free media.
- Get a microcentrifuge tube and put 18ul of trypan blue in the tube. This dye will go into cells that are dead. Then add 2ul of the resuspended pellet in 1ml of your desired media. Take about 10ul of the dye and cells and put into cell counter. Count all squares at the top left, right, lower left and right.
- Plate out cells: (1-5x$10^4$ /well/100ml) in 24 well cluster plate
- Incubate for 30 min (*minimum*) at 37°C/$CO_2$ in DMEM/FCS
- Add 400ml media/well and incubate overnight (O/N)

Medium- T3, N2- TC working aliquots box
bFGF and PDGF in -20°- things that make oligos proliferate box
T.C.- DNase- bottom right rack (-20°)
Trypsin- bottom left rack (-20°, 15ml tube)

## Preparation of zebrafish embryos for FACS

*Need a negative control (non-fluorescent embryos) for setting the FACS machine
*Do not use more than ~150 embryos per tube (50-60 is best)
*Works for 48hpf, 72hpf and 4dpf zebrafish

1. Dechorionate embryos and place in 1.5mL eppendorf tubes
2. Anesthetize with MESAB (Tricaine)
3. De-yolk embryos in 100uL calcium-free Ringer's solution; pipette up and down with 200uL pipette (x20-50 depending on how many embryos in tube)
4. Let sit on ice for 2min
5. Spin down (quick spin), remove liquid and wash with 1X PBS (x2)
6. Prepare 1mL (per number of tubes needed) of trypsin-EDTA 0.25% + 5mg/mL collagenase + 100uL DNase. Will need separate tubes for different samples or if have a very large number of embryos. (Have also used 500uL volume and seems to work fine)
7. Add 200uL of trypsin/collagenase/DNase mix to each tube of embryos and aspirate with 20-gauge needle in a 1mL syringe (x10); add the remaining 800uL of solution and aspirate again with 20-gauge needle (x5)
8. Incubate in 30C water bath for 15min. At end of 15min aspirate again with 26-gauge needle (x5-10). Aspirate more if needed.
9. Spin at 3000rpm for 2min in +4 centrifuge, remove liquid and wash with 1mL ice-cold 5%GS/PBS then spin again. Note when removing liquid from tube: If pellet is very snotty and begins to suck up immediately, collect snotty pellet and put in a new tube then empty the rest of liquid and put pellet back into original tube and wash. This part can be tricky so be careful to not discard pellet.
10. At end, re-suspend pellet in 500uL ice-cold 5%GS/PBS and aspirate with 26-gauge needle (x5-10). If using multiple tubes, divide the 500uL 5%GS/PBS volume between tubes, aspirate, then combine into one tube at end with a final volume of 500uL). If first time doing protocol, verify that method has worked by running through a 40um cell strainer.
11. Collect cells from sorter in 500uL Trizol for RNA extraction or lysis buffer for protein extraction.
12.

Collagenase type 2 (Worthington 4174): Fisher # NC9870009
Trypsin-EDTA 0.25% (1x) (Gibco) Invitrogen # 25200-056
DNase I, type II Sigma D4527
Calcium-free Ringer's solution (recipe from the zebrafish book)

## Acetyl-Histone 3-Lysine 9 (H3K9ac) Staining of OLGs

**04+**

1. Fix with 4% Para for 10min (40µl)
2. Wash with PBS 3X5min (80µl)
3. Block with Media >30min
4. Primary Ab- 04 (make sure to spin down before add to cells) (60µl), leave overnight at 4°C
5. Wash with PBS 3X5min (80µl)
6. Add secondary Ab at a dilution of 1:250 for 1hr RT (IgM 488)
7. Wash with PBS 3X5min (80µl)

**Acetyl Histone 3 Lysine 9**

1. Optional fix with 4% Para for 10min
2. Wash with PBS 3X5min (80µl)
3. Permeabilize with 1%/0.4M Sucrose/1XPBS for 10 min (important step to make sure Ab can penetrate cell)
4. Wash with PBS 3X5min (80µl)
5. Block with media > 30min (50-60ul)
6. Add H3K9ac Ab at 1:400 O/N at 4°C
7. Wash with PBS 3X5min (80µl)
8. Add secondary Ab at a dilution of 1:250 for 1hr RT (Alexa Fluor Anti Rb)
9. Wash with PBS 3X5min (80µl)

**Hoechst**

1. Add Hoechst Stain for 10 min (50µl)
2. Wash with PBS 3X5min (80µl)

*Add vectoshield to slides and place coverslip on top. Use clear nail polish to seal the edges.

## Protein Assay

1. Add 100ul Total Cell Extract Buffer + 2AB- Protease + Phosphatase Inhibitor Cocktail (1:100) (per $1X10^6$ cells) to each well

**Total Cell Extract Buffer**

| Reagent | Volume (250ml) | Volume (100ml) |
|---|---|---|
| 20mM Hepes pH 7.0 | 5mL (1M) | 2mL (1M) |
| 150mM NaCl | 4.38g (2.19) | 1.75g (0.86) |
| 10mM KCL | 2.5mL (1M) | 74mg (1mL-1M) |
| 1mMMgCl2 | 250ul (1M) | 20mL |
| 20%Glycerol | 50ml (1M) | 1mL |
| 1% Triton X-100 | 2.5ml | |

2. Plate on ice and rock for 2 min
3. Use scraper to remove cells from plate
4. Spin down
5. Diluting Samples-
    a. 10x→ 2.5µl sample + 22.5µl of PBS
    b. 5x → 5.0µl sample + 20µl of PBS
6. ABS Reagents

| Tube | Vol. BSA | Vol. 1X BSA | Final |
|---|---|---|---|
| Stock | 300ul (stock) | - | 2000 |
| A | 375 (stock) | 125µl (1:4) | 1500 |
| B | 325 (stock) | 325µl (1:2) | 1000 |
| C | 175 (A) | 175µl (1:2) | 750 |
| D | 325 (B) | 325µl (1:2) | 500 |
| E | 325 (D) | 325µl (1:2) | 250 |
| F | 325 (E) | 325µl (1:2) | 125 |
| G | 100ul (F) | 400µl (1:5) | 25 |
| Blank | - | 25 | - |

    a. Amount= Samples (ex. 6) X 2= 12
    b. BSA= 9 X 3 = 27
    c. Total= 39, add another to make 40
    d. 200ul of ABC reagents/well= 200µl X 40= 8000µl
    e. A= 25 (.25 x 8000 = 2.0 X 2= **4.0ml**)
    f. B =24 (.24 x 8000 =1.920 X 2 = **3.840ml**)
    g. C=1 (.1 x 8000 = 80 x 2 = **.160ml**)
    h. Total of 50 parts or 8mls in a 15ml tube, vortex and wait to react.
    i. Add 200µl to BSA first and samples last.
7. Make plate
    a. BSA samples- start from left to right: Stock, A,B,C,D,E,F,G,Blank. Add to first three wells. Add 25µl of BSA

b. Diluted samples- start from left to right and in 4th and 5th rows. Add 25ul of sample

8. Incubate at 37°C in dark room for 1hr
9. Leave at RT for 15 min
10. Measure concentration on Pherastar under protein assay protocol

## IP Lab Data Analysis for Acetyl Histone 3 Lysine 9 Stain

`

Image Analysis 1
Username: Fuss lab
Password: 0825

Image Analysis 2
Username: Babette
Password: oligo

1. Obtain picture from the Q drive convert pictures to tif from Zen software. Open—File---Export—Save to Natalie Preetha folder
2. Convert the picture to .tif by opening ZEN and export the picture in .tif 12 bit and then save
3. Note units of measurements-pixel dimensions under scaling x
4. Under IP Lab open .tif file
5. **Analyze-** define XY units. Set 1 pixel=0.106 micrometers-add name or scroll down to find AcetylH3.
6. **Analyze**-set acetyl H3 –uncheck calibration bar
7. **Analyze-**segmentation-Blue
8. **segment color**-magenta set min- ~840covers nucleus w/o holes and max-4094 (threshold applied to each image in the same way)
9. **Math-**split color channels-RGB – can use this to determine min/max
10. **Enhance** – edit color table-monochrome may be easier to view
11. Red-min-264
12. **Analyze- Segmentation- Component**-
    a. blue min-840 AND Red min-264
    b. For NOT- select AND reverse
    c. Must have blue and red checked- should now give a magenta color over nucleus.
13. **Analyze**-Measure Segments-magenta segment-gives average intensity and area of RBG
14. To remove oligos that you do no want to be analyzed use the eraser tool
15. **Set measurements**-sum, min, max, mean, shape for area, limit-to filter out
16. **Measurement options**-erase failing criteria
    a. include interior holes
    b. include a side and vertical margin (left+top)
    c. outline-number
17. Max number-can have a limit
18. **Analyze** –*measure segments ROI*- gives table which gives individual
19. Sort by Area under set neasurements-3
20. **Qualify segments**-Magenta segments-table summarizes -gives average
21. Open multiple images
22. **Edit**-transfer attributes of original image-length units transfer to all or specific image

23. **Analyze-**segmentation-done
24. **Analyze**-quantify segments-summary will be added to same table
25. If need to erase non oligodendrocytes: Use erase tool-double click to choose pixels and then quantify
26. Click on X to export table to excel

## ATX lysoPLD Activity Assay

1. For fish studies using protein extracted from **whole zebrafish**:
   Prepare samples**:**
   - Dechorionate zebrafish and anesthetize with MESAB (at least 100µL/mL)
   - Quick wash embryos with 1x PBS (ensure they are anesthetized! – may take a couple of minutes)
   - Remove yolk sacs:
   - Suspend fish in ice-cold Ringer's solution (116mM NaCl; 2.9mM KCl; 1.8mM $CaCl_2$; 5mM HEPES, pH 7.2) + 1mM EDTA + protease inhibitors
   - Pipette up and down with 200µl pipette ~10x-30x; liquid will become cloudy
   - Quick spin to collect fish at bottom of tube
   - Wash with ice-cold Ringer's solution, quick spin, remove then add more Ringer's solution (x3) until solution is clear and can see fish (they should look thin and stringy due to removal of yolk sac-can check under microscope to see if most of yolk has been removed)
   - Quick spin and remove solution
   - Quick wash with 1X PBS then add 1X PBS at ~1µl/embryo + protease inhibitor
   - Homogenize with electronic pestle (~3sec/10µL) and spin 10,000rpm for 3min at +4°C
   - Transfer supernatant to fresh 1.5mL tube (keep homogenate on ice at all times!!)
   - Measure concentration with nanodrop "Protein A280"; Aliquot, label tubes and store at -80C
2. For all OLG samples, you must obtain OLG supernatant in PHENOL-FREE media. Spin down the supernatant to concentrate protein levels. Make sure you start the activity assay with the same amount in all conditions. Do not dilute samples from tissue culture- there is already a small amount of ATX being secreted
3. **Make master mixes for each sample (triplicates) in separate eppendorf tubes (all reagents multiply by 3.3)**
   - Dilute samples in 1xPBS to a final volume of 115.5µL (35µL x 3.3): 100µg/100µL x 3.3 = 330µg total
   - Do not forget to include a blank: 1X PBS only (no sample)
   - Dilute FS-3 substrate from stock solution of 1 mM (in 1XPBS) to 50 µM in reaction buffer (stock for assay) (Echelon L-2000)
   - Working FS-3 concentration can vary from 0.5 to 5 µM.
   - We currently use 2.5µM final in a volume of 5µL per reaction x 3.3 = 16.5µL per sample master mix
   - (New FS-3 should be reconstituted to a stock concentration of 1mM in 1X PBS, not dH2O!)
4. In a black 96 well plate (Corning #3991), pipette the following reagents per well (done in triplicates). Be sure to add FS-3 last!

| Volume | Volume (x3.3) | Reagent | [Stock] | [Final] |
|---|---|---|---|---|
| 35µL | 115.5µL | Sample + 1X PBS | | |
| 10µL | 33µL | FAF-BSA | 10 mg/mL | 1 mg/mL |
| 50µL | 165µL | Rxn Buffer | | |
| 5µL | 16.5µL | FS-3 substrate | 50 µM | 2.5 µM |

5. Read samples in the PHERAstar - Set to 37°C (turn on incubator in PHERAstar several minutes before reading to allow to warm up). Incubation time can vary depending on enzyme activity and concentration.
   **Settings:**
   - Protocol name: ATX Activity Assay – Fluorescence (Do not change settings so can compare different runs)
   - Excitation = 494nm / Emission = 520nm
   - Cycle time: 600sec (10 min); Number of flashes per well: 10
   - Focal height and gain have already been set on this machine for this type of plate and samples, do not change!
   - Focal height: 5.0mm; Gain: 110 (set to 20% maximum so signal will not saturate)
6. Incubator will not shut off on its own. After the run is over, take the plate out and shut off incubator because if plate left in overnight, all wells will evaporate into machine!

## RNA extraction from whole zebrafish

1. Dechorionate zebrafish embryos and transfer to a 1.5mL tube

2. Anthesthetize with MESAB (42uL/mL system water) and wait ~5-10min – check that fish are no longer swimming around by inverting tube a few times **All steps involving Trizol should be performed in fume hood!** (Trizol is located in 4C refridgerator)

3. Remove system water and add ~200uL Trizol and homogenize with electronic pestle for a few seconds until embryos are in solution (be careful with homogenizer and make sure Trizol does not spill out of tube) (Note: can store homogenized embyros in Trizol at -80C if cannot finish protocol)

4. Add 300uL more of Trizol and vortex to completely mix – total volume = 500uL. Incubate samples at RT for 5min

5. Add 100uL of chloroform. Cap tubes securely and shake vigorously by hand for 15sec and incubate at RT for 2-3min

6. Centrifuge at 12,000xg for 15 min at 4C. Mixture will separate into a lower red (phenol/chloroform phase), a white interphase and a clear aqueous phase. RNA is located in this top aqueous phase (volume is ~60% of total volume)

7. Transfer aqueous phase only to a new tube and precipitate RNA by adding 250uL isopropanol. Incubate at RT for 10min and spin at 12,000xg for 10min at 4C (The RNA will form a gel-like pellet on side of tube)

8. Remove supernatant and wash pellet with 500uL 75% ethanol. Mix sample by vortexing

9. Centrifuge at 7500xg for 5min at 4C

10. Remove as much supernatant as possible without disturbing RNA pellet and let air dry for 5-10min (leave caps open)

11. Elute in RNase-free dH2O (~20-100uL dH2O)

12. Measure concentration on nanodrop label tubes and store at -80C

## Image Analysis

Username: Fusslab
Password: 0825
Software: IP lab
Q drive for pictures
Dennis_VCU script for analysis- don't save anything to the script

1. Get image (TIF) of interest from Q drive. Make sure to take only one cell with one nucleus. Always take pictures that were taken with 40X magnification.
2. Free hand the region of interest using the dotted tool. Trace around the cell, leaving out anything not connected to the cell.
3. Go to the MATH tab and split color channels. Keep under RGB, and get rid of blue.
4. Click RUN- segmentation.
5. Create own threshold, mask to select the processes, and move min slider back and forth.
6. Receive measurement results: sum of the threshold value, mean/area
7. The *top* number is the ***network area*** and the *bottom* is the ***process index***
8. * If you have a big gap- it may count as 2 cells and give 4 numbers. If you know that it is part of the same cell, you can add the numbers.
9. Go back to the free hand tool and draw around the cell body, make sure the nucleus is covered.
10. With receive 2 numbers- make sure they are the same! Subtract the cell body from the whole cell measurement.
11. * If the cell body is below 50- the program will not be able to measure it.
12. Go to **FILE- EXPORT-EXCELL**
13. Put Measurement Results in sheet 1 of excel.

Jameel EZ- enable macros

1. Set cursor to A1-column 1 (blank)
2. Tools- MACRO-MACROS-RUN
3. Take 4 numbers and put horizontally
4. Highlight all horizontal numbers
5. Use the filter cone, drop down menu and get rid of the blanks
6. Copy 1$^{st}$ three columns
7. Clear contents and paste into H2
8. NA/PI/Cell Body
9. Copy formula from old experiment
10. NA PI complexity- take average from each column and paste values in column O.
11. Normalize to control cells
12. The average of the normalized cells should all equal 100.
13. Highlight three column: net area/ proc are/ complexity and the avg/ NA norm/PI norm/NC
14. Go back to treated cells and copy

15. Take the average and this number is compared to 100 (control)
16. Never want number to be 0.
17. Take figures and go to sigmaplot and measure standard error, etc.
18. Use about 30-35 cells per experiment and have an N of at least 3, may need 4 or 5.

## References


Abramoff, M.D., Magalhães, P.J., and Ram, S.J. (2004). Image processing with ImageJ. Biophotonics Int. *11*, 36–42.

Aixiao Liu, Y.R.H. (2007). The Glial or Neuronal Fate Choice of Oligodendrocyte Progenitors Is Modulated by Their Ability to Acquire an Epigenetic Memory. J. Neurosci. Off. J. Soc. Neurosci. *27*, 7339–7343.

Albers, H.M.H.G., Dong, A., van Meeteren, L.A., Egan, D.A., Sunkara, M., van Tilburg, E.W., Schuurman, K., van Tellingen, O., Morris, A.J., Smyth, S.S., et al. (2010). Boronic acid-based inhibitor of autotaxin reveals rapid turnover of LPA in the circulation. Proc. Natl. Acad. Sci. U. S. A. *107*, 7257–7262.

Albini, A., Ferrini, S., Benelli, R., Sforzini, S., Giunciuglio, D., Aluigi, M.G., Proudfoot, A.E., Alouani, S., Wells, T.N., Mariani, G., et al. (1998). HIV-1 Tat protein mimicry of chemokines. Proc. Natl. Acad. Sci. U. S. A. *95*, 13153–13158.

Albright, A.V., Strizki, J., Harouse, J.M., Lavi, E., O'Connor, M., and González-Scarano, F. (1996). HIV-1 infection of cultured human adult oligodendrocytes. Virology *217*, 211–219.

Aloisi, F., De Simone, R., Columba-Cabezas, S., and Levi, G. (1999). Opposite effects of interferon-gamma and prostaglandin E2 on tumor necrosis factor and interleukin-10 production in microglia: a regulatory loop controlling microglia pro- and anti-inflammatory activities. J. Neurosci. Res. *56*, 571–580.

An, S., Bleu, T., Huang, W., Hallmark, O.G., Coughlin, S.R., and Goetzl, E.J. (1997). Identification of cDNAs encoding two G protein-coupled receptors for lysosphingolipids. FEBS Lett. *417*, 279–282.

Aoki, J., Taira, A., Takanezawa, Y., Kishi, Y., Hama, K., Kishimoto, T., Mizuno, K., Saku, K., Taguchi, R., and Arai, H. (2002). Serum lysophosphatidic acid is produced through diverse phospholipase pathways. J. Biol. Chem. *277*, 48737–48744.

Aoki, J., Inoue, A., and Okudaira, S. (2008a). Two pathways for lysophosphatidic acid production. Biochim. Biophys. Acta *1781*, 513–518.

Aoki, J., Inoue, A., and Okudaira, S. (2008b). Two pathways for lysophosphatidic acid production. Biochim. Biophys. Acta *1781*, 513–518.

Asklund, T., Appelskog, I.B., Ammerpohl, O., Ekström, T.J., and Almqvist, P.M. (2004). Histone deacetylase inhibitor 4-phenylbutyrate modulates glial fibrillary acidic protein and connexin 43 expression, and enhances gap-junction communication, in human glioblastoma cells. Eur. J. Cancer Oxf. Engl. 1990 *40*, 1073–1081.

Bagasra, O., Lavi, E., Bobroski, L., Khalili, K., Pestaner, J.P., Tawadros, R., and Pomerantz, R.J. (1996). Cellular reservoirs of HIV-1 in the central nervous system of

infected individuals: identification by the combination of in situ polymerase chain reaction and immunohistochemistry. AIDS Lond. Engl. *10*, 573–585.

Bai, Z., Cai, L., Umemoto, E., Takeda, A., Tohya, K., Komai, Y., Veeraveedu, P.T., Hata, E., Sugiura, Y., Kubo, A., et al. (2013). Constitutive lymphocyte transmigration across the basal lamina of high endothelial venules is regulated by the autotaxin/lysophosphatidic acid axis. J. Immunol. Baltim. Md 1950 *190*, 2036–2048.

Bandoh, K., Aoki, J., Hosono, H., Kobayashi, S., Kobayashi, T., Murakami-Murofushi, K., Tsujimoto, M., Arai, H., and Inoue, K. (1999). Molecular cloning and characterization of a novel human G-protein-coupled receptor, EDG7, for lysophosphatidic acid. J. Biol. Chem. *274*, 27776–27785.

Bansal, R., Warrington, A.E., Gard, A.L., Ranscht, B., and Pfeiffer, S.E. (1989). Multiple and novel specificities of monoclonal antibodies O1, O4, and R-mAb used in the analysis of oligodendrocyte development. J. Neurosci. Res. *24*, 548–557.

Bansal, R., Stefansson, K., and Pfeiffer, S.E. (1992). Proligodendroblast antigen (POA), a developmental antigen expressed by A007/O4-positive oligodendrocyte progenitors prior to the appearance of sulfatide and galactocerebroside. J. Neurochem. *58*, 2221–2229.

Baracskay, K.L., Kidd, G.J., Miller, R.H., and Trapp, B.D. (2007). NG2-positive cells generate A2B5-positive oligodendrocyte precursor cells. Glia *55*, 1001–1010.

Barres, B.A., Hart, I.K., Coles, H.S., Burne, J.F., Voyvodic, J.T., Richardson, W.D., and Raff, M.C. (1992). Cell death and control of cell survival in the oligodendrocyte lineage. Cell *70*, 31–46.

Barres, B.A., Lazar, M.A., and Raff, M.C. (1994). A novel role for thyroid hormone, glucocorticoids and retinoic acid in timing oligodendrocyte development. Dev. Camb. Engl. *120*, 1097–1108.

Bauer, N.G., Richter-Landsberg, C., and Ffrench-Constant, C. (2009). Role of the oligodendroglial cytoskeleton in differentiation and myelination. Glia *57*, 1691–1705.

Baumann, N., and Pham-Dinh, D. (2001). Biology of oligodendrocyte and myelin in the mammalian central nervous system. Physiol. Rev. *81*, 871–927.

Beckers, T., Burkhardt, C., Wieland, H., Gimmnich, P., Ciossek, T., Maier, T., and Sanders, K. (2007). Distinct pharmacological properties of second generation HDAC inhibitors with the benzamide or hydroxamate head group. Int. J. Cancer J. Int. Cancer *121*, 1138–1148.

Ben-Hur, T., Einstein, O., Mizrachi-Kol, R., Ben-Menachem, O., Reinhartz, E., Karussis, D., and Abramsky, O. (2003). Transplanted multipotential neural precursor cells migrate into the inflamed white matter in response to experimental autoimmune encephalomyelitis. Glia *41*, 73–80.

Bercury, K.K., Dai, J., Sachs, H.H., Ahrendsen, J.T., Wood, T.L., and Macklin, W.B. (2014). Conditional ablation of raptor or rictor has differential impact on oligodendrocyte differentiation and CNS myelination. J. Neurosci. Off. J. Soc. Neurosci. *34*, 4466–4480.

Berger, S.L. (2007). The complex language of chromatin regulation during transcription. Nature *447*, 407–412.

Bernardos, R.L., and Raymond, P.A. (2006). GFAP transgenic zebrafish. Gene Expr. Patterns GEP *6*, 1007–1013.

Bernhart, E., Kollroser, M., Rechberger, G., Reicher, H., Heinemann, A., Schratl, P., Hallström, S., Wintersperger, A., Nusshold, C., DeVaney, T., et al. (2010). Lysophosphatidic acid receptor activation affects the C13NJ microglia cell line proteome leading to alterations in glycolysis, motility, and cytoskeletal architecture. Proteomics *10*, 141–158.

Best, J.D., and Alderton, W.K. (2008). Zebrafish: An in vivo model for the study of neurological diseases. Neuropsychiatr. Dis. Treat. *4*, 567–576.

Bischof, M., Weider, M., Küspert, M., Nave, K.-A., and Wegner, M. (2015). Brg1-dependent chromatin remodelling is not essentially required during oligodendroglial differentiation. J. Neurosci. Off. J. Soc. Neurosci. *35*, 21–35.

Bollen, M., Gijsbers, R., Ceulemans, H., Stalmans, W., and Stefan, C. (2000). Nucleotide pyrophosphatases/phosphodiesterases on the move. Crit. Rev. Biochem. Mol. Biol. *35*, 393–432.

Bosio, A., Binczek, E., and Stoffel, W. (1996). Functional breakdown of the lipid bilayer of the myelin membrane in central and peripheral nervous system by disrupted galactocerebroside synthesis. Proc. Natl. Acad. Sci. U. S. A. *93*, 13280–13285.

Boucher, J., Quilliot, D., Pradères, J.P., Simon, M.F., Grès, S., Guigné, C., Prévot, D., Ferry, G., Boutin, J.A., Carpéné, C., et al. (2005). Potential involvement of adipocyte insulin resistance in obesity-associated up-regulation of adipocyte lysophospholipase D/autotaxin expression. Diabetologia *48*, 569–577.

Bradl, M., and Lassmann, H. (2010). Oligodendrocytes: biology and pathology. Acta Neuropathol. (Berl.) *119*, 37–53.

Brazel, C.Y., Romanko, M.J., Rothstein, R.P., and Levison, S.W. (2003). Roles of the mammalian subventricular zone in brain development. Prog. Neurobiol. *69*, 49–69.

Brösamle, C., and Halpern, M.E. (2002). Characterization of myelination in the developing zebrafish. Glia *39*, 47–57.

Buckley, C.E., Goldsmith, P., and Franklin, R.J.M. (2008). Zebrafish myelination: a transparent model for remyelination? Dis. Model. Mech. *1*, 221–228.

Buckley, C.E., Marguerie, A., Alderton, W.K., and Franklin, R.J.M. (2010). Temporal dynamics of myelination in the zebrafish spinal cord. Glia *58*, 802–812.

Buckley, M.F., Loveland, K.A., McKinstry, W.J., Garson, O.M., and Goding, J.W. (1990). Plasma cell membrane glycoprotein PC-1. cDNA cloning of the human molecule, amino acid sequence, and chromosomal location. J. Biol. Chem. *265*, 17506–17511.

Burrell, A.M., Handel, A.E., Ramagopalan, S.V., Ebers, G.C., and Morahan, J.M. (2011). Epigenetic mechanisms in multiple sclerosis and the major histocompatibility complex (MHC). Discov. Med. *11*, 187–196.

Butler, K.V., Kalin, J., Brochier, C., Vistoli, G., Langley, B., and Kozikowski, A.P. (2010). Rational design and simple chemistry yield a superior, neuroprotective HDAC6 inhibitor, tubastatin A. J. Am. Chem. Soc. *132*, 10842–10846.

Buttery, P.C., and ffrench-Constant, C. (1999). Laminin-2/integrin interactions enhance myelin membrane formation by oligodendrocytes. Mol. Cell. Neurosci. *14*, 199–212.

Cai, J., Qi, Y., Hu, X., Tan, M., Liu, Z., Zhang, J., Li, Q., Sander, M., and Qiu, M. (2005a). Generation of oligodendrocyte precursor cells from mouse dorsal spinal cord independent of Nkx6 regulation and Shh signaling. Neuron *45*, 41–53.

Cai, J., Qi, Y., Hu, X., Tan, M., Liu, Z., Zhang, J., Li, Q., Sander, M., and Qiu, M. (2005b). Generation of oligodendrocyte precursor cells from mouse dorsal spinal cord independent of Nkx6 regulation and Shh signaling. Neuron *45*, 41–53.

Cai, R., Kwon, P., Yan-Neale, Y., Sambuccetti, L., Fischer, D., and Cohen, D. (2001). Mammalian histone deacetylase 1 protein is posttranslationally modified by phosphorylation. Biochem. Biophys. Res. Commun. *283*, 445–453.

Campagnoni, A.T. (1988). Molecular biology of myelin proteins from the central nervous system. J. Neurochem. *51*, 1–14.

Cardona, A.E., Pioro, E.P., Sasse, M.E., Kostenko, V., Cardona, S.M., Dijkstra, I.M., Huang, D., Kidd, G., Dombrowski, S., Dutta, R., et al. (2006). Control of microglial neurotoxicity by the fractalkine receptor. Nat. Neurosci. *9*, 917–924.

Carracedo, A., Ma, L., Teruya-Feldstein, J., Rojo, F., Salmena, L., Alimonti, A., Egia, A., Sasaki, A.T., Thomas, G., Kozma, S.C., et al. (2008). Inhibition of mTORC1 leads to MAPK pathway activation through a PI3K-dependent feedback loop in human cancer. J. Clin. Invest. *118*, 3065–3074.

de Castro, F., and Bribián, A. (2005). The molecular orchestra of the migration of oligodendrocyte precursors during development. Brain Res. Brain Res. Rev. *49*, 227–241.

Cervera, P., Tirard, M., Barron, S., Allard, J., Trottier, S., Lacombe, J., Daumas-Duport, C., and Sokoloff, P. (2002). Immunohistological localization of the myelinating cell-specific receptor LP(A1). Glia *38*, 126–136.

Chang, A., Tourtellotte, W.W., Rudick, R., and Trapp, B.D. (2002a). Premyelinating oligodendrocytes in chronic lesions of multiple sclerosis. N. Engl. J. Med. *346*, 165–173.

Chang, A., Tourtellotte, W.W., Rudick, R., and Trapp, B.D. (2002b). Premyelinating oligodendrocytes in chronic lesions of multiple sclerosis. N. Engl. J. Med. *346*, 165–173.

Chauhan, A., Turchan, J., Pocernich, C., Bruce-Keller, A., Roth, S., Butterfield, D.A., Major, E.O., and Nath, A. (2003). Intracellular human immunodeficiency virus Tat expression in astrocytes promotes astrocyte survival but induces potent neurotoxicity at distant sites via axonal transport. J. Biol. Chem. *278*, 13512–13519.

Choi, J.W., and Chun, J. (2013). Lysophospholipids and their receptors in the central nervous system. Biochim. Biophys. Acta *1831*, 20–32.

Choi, J.W., Herr, D.R., Noguchi, K., Yung, Y.C., Lee, C.-W., Mutoh, T., Lin, M.-E., Teo, S.T., Park, K.E., Mosley, A.N., et al. (2010a). LPA Receptors: Subtypes and Biological Actions. Annu. Rev. Pharmacol. Toxicol. *50*, 157–186.

Choi, J.W., Herr, D.R., Noguchi, K., Yung, Y.C., Lee, C.-W., Mutoh, T., Lin, M.-E., Teo, S.T., Park, K.E., Mosley, A.N., et al. (2010b). LPA receptors: subtypes and biological actions. Annu. Rev. Pharmacol. Toxicol. *50*, 157–186.

Chomczynski, P., and Sacchi, N. (1987). Single-step method of RNA isolation by acid guanidinium thiocyanate-phenol-chloroform extraction. Anal. Biochem. *162*, 156–159.

Chun, J. (2013). Lysophospholipid Receptors: Signaling and Biochemistry (John Wiley & Sons).

Chun, J., Hla, T., Lynch, K.R., Spiegel, S., and Moolenaar, W.H. (2010). International Union of Basic and Clinical Pharmacology. LXXVIII. Lysophospholipid receptor nomenclature. Pharmacol. Rev. *62*, 579–587.

Chung, A.-Y., Kim, S., Kim, H., Bae, Y.-K., and Park, H.-C. (2011). Microarray Screening for Genes Involved in Oligodendrocyte Differentiation in the Zebrafish CNS. Exp. Neurobiol. *20*, 85–91.

Cimpean, A., Stefan, C., Gijsbers, R., Stalmans, W., and Bollen, M. (2004). Substrate-specifying determinants of the nucleotide pyrophosphatases/phosphodiesterases NPP1 and NPP2. Biochem. J. *381*, 71–77.

Citro, S., Miccolo, C., Meloni, L., and Chiocca, S. (2015). PI3K/mTOR mediate mitogen-dependent HDAC1 phosphorylation in breast cancer: a novel regulation of estrogen receptor expression. J. Mol. Cell Biol. *7*, 132–142.

Clair, T., Lee, H.Y., Liotta, L.A., and Stracke, M.L. (1997). Autotaxin is an exoenzyme possessing 5'-nucleotide phosphodiesterase/ATP pyrophosphatase and ATPase activities. J. Biol. Chem. *272*, 996–1001.

Coetzee, T., Fujita, N., Dupree, J., Shi, R., Blight, A., Suzuki, K., Suzuki, K., and Popko, B. (1996). Myelination in the absence of galactocerebroside and sulfatide: normal structure with abnormal function and regional instability. Cell *86*, 209–219.

Comabella, M., and Martin, R. (2007). Genomics in multiple sclerosis--current state and future directions. J. Neuroimmunol. *187*, 1–8.

Contos, J.J., Ishii, I., and Chun, J. (2000). Lysophosphatidic acid receptors. Mol. Pharmacol. *58*, 1188–1196.

Contos, J.J.A., Ishii, I., Fukushima, N., Kingsbury, M.A., Ye, X., Kawamura, S., Brown, J.H., and Chun, J. (2002). Characterization of lpa(2) (Edg4) and lpa(1)/lpa(2) (Edg2/Edg4) lysophosphatidic acid receptor knockout mice: signaling deficits without obvious phenotypic abnormality attributable to lpa(2). Mol. Cell. Biol. *22*, 6921–6929.

Conway, G.D., O'Bara, M.A., Vedia, B.H., Pol, S.U., and Sim, F.J. (2012). Histone deacetylase activity is required for human oligodendrocyte progenitor differentiation. Glia *60*, 1944–1953.

Copray, S., Huynh, J.L., Sher, F., Casaccia-Bonnefil, P., and Boddeke, E. (2009). Epigenetic mechanisms facilitating oligodendrocyte development, maturation, and aging. Glia *57*, 1579–1587.

Croset, M., Brossard, N., Polette, A., and Lagarde, M. (2000). Characterization of plasma unsaturated lysophosphatidylcholines in human and rat. Biochem. J. *345 Pt 1*, 61–67.

Culp, J.S., and Butler, L.G. (1985). Alkaline phosphatase and 5'-nucleotide phosphodiesterase from bovine intestine are cross-reactive. Biochemistry (Mosc.) *24*, 6825–6829.

Cunliffe, V.T., and Casaccia-Bonnefil, P. (2006). Histone deacetylase 1 is essential for oligodendrocyte specification in the zebrafish CNS. Mech. Dev. *123*, 24–30.

Cunningham, J.T., Rodgers, J.T., Arlow, D.H., Vazquez, F., Mootha, V.K., and Puigserver, P. (2007). mTOR controls mitochondrial oxidative function through a YY1-PGC-1alpha transcriptional complex. Nature *450*, 736–740.

Czopka, T. (2016). Insights into mechanisms of central nervous system myelination using zebrafish. Glia *64*, 333–349.

Dai, J., Bercury, K.K., and Macklin, W.B. (2014). Interaction of mTOR and Erk1/2 signaling to regulate oligodendrocyte differentiation. Glia *62*, 2096–2109.

Dalgaard, P. (2008). Introductory Statistics with R (New York, NY: Springer New York).

Das, A.K., and Hajra, A.K. (1989a). Quantification, characterization and fatty acid composition of lysophosphatidic acid in different rat tissues. Lipids *24*, 329–333.

Das, A.K., and Hajra, A.K. (1989b). Quantification, characterization and fatty acid composition of lysophosphatidic acid in different rat tissues. Lipids *24*, 329–333.

Dawson, J., Hotchin, N., Lax, S., and Rumsby, M. (2003). Lysophosphatidic acid induces process retraction in CG-4 line oligodendrocytes and oligodendrocyte precursor cells but not in differentiated oligodendrocytes. J. Neurochem. *87*, 947–957.

Dennis, J., Nogaroli, L., and Fuss, B. (2005). Phosphodiesterase-Ialpha/autotaxin (PD-Ialpha/ATX): a multifunctional protein involved in central nervous system development and disease. J. Neurosci. Res. *82*, 737–742.

Dennis, J., White, M.A., Forrest, A.D., Yuelling, L.M., Nogaroli, L., Afshari, F.S., Fox, M.A., and Fuss, B. (2008). Phosphodiesterase-Ialpha/autotaxin's MORFO domain regulates oligodendroglial process network formation and focal adhesion organization. Mol. Cell. Neurosci. *37*, 412–424.

Dennis, J., Morgan, M.K., Graf, M.R., and Fuss, B. (2012). P2Y12 receptor expression is a critical determinant of functional responsiveness to ATX's MORFO domain. Purinergic Signal. *8*, 181–190.

Dewald, L.E., Rodriguez, J.P., and Levine, J.M. (2011). The RE1 binding protein REST regulates oligodendrocyte differentiation. J. Neurosci. Off. J. Soc. Neurosci. *31*, 3470–3483.

Dodd, J., Jessell, T.M., and Placzek, M. (1998). The when and where of floor plate induction. Science *282*, 1654–1657.

Doodnath, R., Dervan, A., Wride, M.A., and Puri, P. (2010). Zebrafish: an exciting model for investigating the spatio-temporal pattern of enteric nervous system development. Pediatr. Surg. Int. *26*, 1217–1221.

van Driel, I.R., and Goding, J.W. (1987). Plasma cell membrane glycoprotein PC-1. Primary structure deduced from cDNA clones. J. Biol. Chem. *262*, 4882–4887.

Dugas, J.C., Tai, Y.C., Speed, T.P., Ngai, J., and Barres, B.A. (2006). Functional Genomic Analysis of Oligodendrocyte Differentiation. J. Neurosci. *26*, 10967–10983.

Duncan, I.D., Hammang, J.P., Goda, S., and Quarles, R.H. (1989). Myelination in the jimpy mouse in the absence of proteolipid protein. Glia *2*, 148–154.

Dupree, J.L., Girault, J.A., and Popko, B. (1999). Axo-glial interactions regulate the localization of axonal paranodal proteins. J. Cell Biol. *147*, 1145–1152.

Dyson, M.H., Thomson, S., and Mahadevan, L.C. (2005). Heat shock, histone H3 phosphorylation and the cell cycle. Cell Cycle Georget. Tex *4*, 13–17.

Edgar, J.M., McLaughlin, M., Yool, D., Zhang, S.-C., Fowler, J.H., Montague, P., Barrie, J.A., McCulloch, M.C., Duncan, I.D., Garbern, J., et al. (2004). Oligodendroglial modulation of fast axonal transport in a mouse model of hereditary spastic paraplegia. J. Cell Biol. *166*, 121–131.

Edgar, J.M., McLaughlin, M., Werner, H.B., McCulloch, M.C., Barrie, J.A., Brown, A., Faichney, A.B., Snaidero, N., Nave, K.-A., and Griffiths, I.R. (2009). Early ultrastructural defects of axons and axon-glia junctions in mice lacking expression of Cnp1. Glia *57*, 1815–1824.

Emery, B. (2010). Regulation of oligodendrocyte differentiation and myelination. Science *330*, 779–782.

Emery, B., Agalliu, D., Cahoy, J.D., Watkins, T.A., Dugas, J.C., Mulinyawe, S.B., Ibrahim, A., Ligon, K.L., Rowitch, D.H., and Barres, B.A. (2009). Myelin gene regulatory factor is a critical transcriptional regulator required for CNS myelination. Cell *138*, 172–185.

Esiri, M.M., Morris, C.S., and Millard, P.R. (1991). Fate of oligodendrocytes in HIV-1 infection. AIDS Lond. Engl. *5*, 1081–1088.

Estivill-Torrús, G., Llebrez-Zayas, P., Matas-Rico, E., Santín, L., Pedraza, C., De Diego, I., Del Arco, I., Fernández-Llebrez, P., Chun, J., and De Fonseca, F.R. (2008). Absence of LPA1 signaling results in defective cortical development. Cereb. Cortex N. Y. N 1991 *18*, 938–950.

Eugenin, E.A., Clements, J.E., Zink, M.C., and Berman, J.W. (2011). Human immunodeficiency virus infection of human astrocytes disrupts blood-brain barrier integrity by a gap junction-dependent mechanism. J. Neurosci. Off. J. Soc. Neurosci. *31*, 9456–9465.

Fernández-Gamba, A., Leal, M.C., Maarouf, C.L., Richter-Landsberg, C., Wu, T., Morelli, L., Roher, A.E., and Castaño, E.M. (2012). Collapsin response mediator protein-2 phosphorylation promotes the reversible retraction of oligodendrocyte processes in response to non-lethal oxidative stress. J. Neurochem. *121*, 985–995.

Ferreirinha, F., Quattrini, A., Pirozzi, M., Valsecchi, V., Dina, G., Broccoli, V., Auricchio, A., Piemonte, F., Tozzi, G., Gaeta, L., et al. (2004). Axonal degeneration in paraplegin-deficient mice is associated with abnormal mitochondria and impairment of axonal transport. J. Clin. Invest. *113*, 231–242.

Ferry, G., Tellier, E., Try, A., Grés, S., Naime, I., Simon, M.F., Rodriguez, M., Boucher, J., Tack, I., Gesta, S., et al. (2003). Autotaxin is released from adipocytes, catalyzes lysophosphatidic acid synthesis, and activates preadipocyte proliferation. Up-regulated expression with adipocyte differentiation and obesity. J. Biol. Chem. *278*, 18162–18169.

Ferry, G., Giganti, A., Cogé, F., Bertaux, F., Thiam, K., and Boutin, J.A. (2007). Functional invalidation of the autotaxin gene by a single amino acid mutation in mouse is lethal. FEBS Lett. *581*, 3572–3578.

Ferry, G., Moulharat, N., Pradère, J.-P., Desos, P., Try, A., Genton, A., Giganti, A., Beucher-Gaudin, M., Lonchampt, M., Bertrand, M., et al. (2008). S32826, a nanomolar inhibitor of autotaxin: discovery, synthesis and applications as a pharmacological tool. J. Pharmacol. Exp. Ther. *327*, 809–819.

Fleming, A., Jankowski, J., and Goldsmith, P. (2010). In vivo analysis of gut function and disease changes in a zebrafish larvae model of inflammatory bowel disease: a feasibility study. Inflamm. Bowel Dis. *16*, 1162–1172.

Flores, A.I., Narayanan, S.P., Morse, E.N., Shick, H.E., Yin, X., Kidd, G., Avila, R.L., Kirschner, D.A., and Macklin, W.B. (2008). Constitutively-active Akt induces enhanced myelination in the central nervous system. J. Neurosci. Off. J. Soc. Neurosci. *28*, 7174–7183.

Fogarty, M., Richardson, W.D., and Kessaris, N. (2005). A subset of oligodendrocytes generated from radial glia in the dorsal spinal cord. Dev. Camb. Engl. *132*, 1951–1959.

Fok-Seang, J., and Miller, R.H. (1994). Distribution and differentiation of A2B5+ glial precursors in the developing rat spinal cord. J. Neurosci. Res. *37*, 219–235.

Fox, M.A., Colello, R.J., Macklin, W.B., and Fuss, B. (2003). Phosphodiesterase-Ialpha/autotaxin: a counteradhesive protein expressed by oligodendrocytes during onset of myelination. Mol. Cell. Neurosci. *23*, 507–519.

Fox, R.J., Bethoux, F., Goldman, M.D., and Cohen, J.A. (2006). Multiple sclerosis: advances in understanding, diagnosing, and treating the underlying disease. Cleve. Clin. J. Med. *73*, 91–102.

Franco, P.G., Silvestroff, L., Soto, E.F., and Pasquini, J.M. (2008). Thyroid hormones promote differentiation of oligodendrocyte progenitor cells and improve remyelination after cuprizone-induced demyelination. Exp. Neurol. *212*, 458–467.

Freedman, D.M., Dosemeci, M., and Alavanja, M.C. (2000). Mortality from multiple sclerosis and exposure to residential and occupational solar radiation: a case-control study based on death certificates. Occup. Environ. Med. *57*, 418–421.

Frugier, T., Crombie, D., Conquest, A., Tjhong, F., Taylor, C., Kulkarni, T., McLean, C., and Pébay, A. (2011). Modulation of LPA receptor expression in the human brain following neurotrauma. Cell. Mol. Neurobiol. *31*, 569–577.

Fukushima, N., and Morita, Y. (2006). Actomyosin-dependent microtubule rearrangement in lysophosphatidic acid-induced neurite remodeling of young cortical neurons. Brain Res. *1094*, 65–75.

Fukushima, N., Ishii, I., Contos, J.J., Weiner, J.A., and Chun, J. (2001). Lysophospholipid receptors. Annu. Rev. Pharmacol. Toxicol. *41*, 507–534.

Fukushima, N., Weiner, J.A., Kaushal, D., Contos, J.J.A., Rehen, S.K., Kingsbury, M.A., Kim, K.Y., and Chun, J. (2002). Lysophosphatidic acid influences the morphology and motility of young, postmitotic cortical neurons. Mol. Cell. Neurosci. *20*, 271–282.

Fukushima, N., Shano, S., Moriyama, R., and Chun, J. (2007). Lysophosphatidic acid stimulates neuronal differentiation of cortical neuroblasts through the LPA1-G(i/o) pathway. Neurochem. Int. *50*, 302–307.

Fuss, B., Baba, H., Phan, T., Tuohy, V.K., and Macklin, W.B. (1997). Phosphodiesterase I, a novel adhesion molecule and/or cytokine involved in oligodendrocyte function. J. Neurosci. Off. J. Soc. Neurosci. *17*, 9095–9103.

Fyffe-Maricich, S.L., Karlo, J.C., Landreth, G.E., and Miller, R.H. (2011). The ERK2 mitogen-activated protein kinase regulates the timing of oligodendrocyte differentiation. J. Neurosci. Off. J. Soc. Neurosci. *31*, 843–850.

García-Díaz, B., Riquelme, R., Varela-Nieto, I., Jiménez, A.J., de Diego, I., Gómez-Conde, A.L., Matas-Rico, E., Aguirre, J.Á., Chun, J., Pedraza, C., et al. (2015). Loss of lysophosphatidic acid receptor LPA1 alters oligodendrocyte differentiation and myelination in the mouse cerebral cortex. Brain Struct. Funct. *220*, 3701–3720.

Gard, A.L., and Pfeiffer, S.E. (1993). Glial cell mitogens bFGF and PDGF differentially regulate development of O4+GalC- oligodendrocyte progenitors. Dev. Biol. *159*, 618–630.

Gardell, S.E., Dubin, A.E., and Chun, J. (2006). Emerging medicinal roles for lysophospholipid signaling. Trends Mol. Med. *12*, 65–75.

Geach, T.J., Faas, L., Devader, C., Gonzalez-Cordero, A., Tabler, J.M., Brunsdon, H., Isaacs, H.V., and Dale, L. (2014). An essential role for LPA signalling in telencephalon development. Development *141*, 940–949.

Giganti, A., Rodriguez, M., Fould, B., Moulharat, N., Cogé, F., Chomarat, P., Galizzi, J.-P., Valet, P., Saulnier-Blache, J.-S., Boutin, J.A., et al. (2008). Murine and human autotaxin alpha, beta, and gamma isoforms: gene organization, tissue distribution, and biochemical characterization. J. Biol. Chem. *283*, 7776–7789.

Gijsbers, R., Ceulemans, H., Stalmans, W., and Bollen, M. (2001). Structural and catalytic similarities between nucleotide pyrophosphatases/phosphodiesterases and alkaline phosphatases. J. Biol. Chem. *276*, 1361–1368.

Gijsbers, R., Aoki, J., Arai, H., and Bollen, M. (2003). The hydrolysis of lysophospholipids and nucleotides by autotaxin (NPP2) involves a single catalytic site. FEBS Lett. *538*, 60–64.

Goding, J.W., Grobben, B., and Slegers, H. (2003). Physiological and pathophysiological functions of the ecto-nucleotide pyrophosphatase/phosphodiesterase family. Biochim. Biophys. Acta *1638*, 1–19.

Goldberg, A.D., Allis, C.D., and Bernstein, E. (2007). Epigenetics: a landscape takes shape. Cell *128*, 635–638.

Goldschmidt, T., Antel, J., König, F.B., Brück, W., and Kuhlmann, T. (2009). Remyelination capacity of the MS brain decreases with disease chronicity. Neurology *72*, 1914–1921.

Griffiths, I., Klugmann, M., Anderson, T., Yool, D., Thomson, C., Schwab, M.H., Schneider, A., Zimmermann, F., McCulloch, M., Nadon, N., et al. (1998a). Axonal swellings and degeneration in mice lacking the major proteolipid of myelin. Science *280*, 1610–1613.

Griffiths, I., Klugmann, M., Anderson, T., Thomson, C., Vouyiouklis, D., and Nave, K.A. (1998b). Current concepts of PLP and its role in the nervous system. Microsc. Res. Tech. *41*, 344–358.

Grisanti, L., Rezza, A., Clavel, C., Sennett, R., and Rendl, M. (2013). Enpp2/Autotaxin in dermal papilla precursors is dispensable for hair follicle morphogenesis. J. Invest. Dermatol. *133*, 2332–2339.

Grunstein, M. (1997). Histone acetylation in chromatin structure and transcription. Nature *389*, 349–352.

Grupp, L., Wolburg, H., and Mack, A.F. (2010). Astroglial structures in the zebrafish brain. J. Comp. Neurol. *518*, 4277–4287.

Guardiola-Diaz, H.M., Ishii, A., and Bansal, R. (2012). Erk1/2 MAPK and mTOR signaling sequentially regulates progression through distinct stages of oligodendrocyte differentiation. Glia *60*, 476–486.

Guerra, B. (2006). Protein kinase CK2 subunits are positive regulators of AKT kinase. Int. J. Oncol. *28*, 685–693.

Gupte, R., Patil, R., Liu, J., Wang, Y., Lee, S.C., Fujiwara, Y., Fells, J., Bolen, A.L., Emmons-Thompson, K., Yates, C.R., et al. (2011). Benzyl and naphthalene methylphosphonic acid inhibitors of autotaxin with anti-invasive and anti-metastatic activity. ChemMedChem *6*, 922–935.

Gutierrez-Arcelus, M., Rich, S.S., and Raychaudhuri, S. (2016). Autoimmune diseases - connecting risk alleles with molecular traits of the immune system. Nat. Rev. Genet. *17*, 160–174.

Gyorkey, F., Melnick, J.L., and Gyorkey, P. (1987). Human immunodeficiency virus in brain biopsies of patients with AIDS and progressive encephalopathy. J. Infect. Dis. *155*, 870–876.

El-Hage, N., Bruce-Keller, A.J., Yakovleva, T., Bazov, I., Bakalkin, G., Knapp, P.E., and Hauser, K.F. (2008). Morphine exacerbates HIV-1 Tat-induced cytokine production in astrocytes through convergent effects on [Ca(2+)](i), NF-kappaB trafficking and transcription. PloS One *3*, e4093.

Hagström, C., and Olsson, C. (2010). Glial cells revealed by GFAP immunoreactivity in fish gut. Cell Tissue Res. *341*, 73–81.

Hama, K., Aoki, J., Fukaya, M., Kishi, Y., Sakai, T., Suzuki, R., Ohta, H., Yamori, T., Watanabe, M., Chun, J., et al. (2004). Lysophosphatidic acid and autotaxin stimulate cell motility of neoplastic and non-neoplastic cells through LPA1. J. Biol. Chem. *279*, 17634–17639.

Hammack, B.N., Fung, K.Y.C., Hunsucker, S.W., Duncan, M.W., Burgoon, M.P., Owens, G.P., and Gilden, D.H. (2004). Proteomic analysis of multiple sclerosis cerebrospinal fluid. Mult. Scler. Houndmills Basingstoke Engl. *10*, 245–260.

Harouse, J.M., Bhat, S., Spitalnik, S.L., Laughlin, M., Stefano, K., Silberberg, D.H., and Gonzalez-Scarano, F. (1991). Inhibition of entry of HIV-1 in neural cell lines by antibodies against galactosyl ceramide. Science *253*, 320–323.

Hart, I.K., Richardson, W.D., Bolsover, S.R., and Raff, M.C. (1989a). PDGF and intracellular signaling in the timing of oligodendrocyte differentiation. J. Cell Biol. *109*, 3411–3417.

Hart, I.K., Richardson, W.D., Heldin, C.H., Westermark, B., and Raff, M.C. (1989b). PDGF receptors on cells of the oligodendrocyte-type-2 astrocyte (O-2A) cell lineage. Dev. Camb. Engl. *105*, 595–603.

Hartline, D.K., and Colman, D.R. (2007). Rapid conduction and the evolution of giant axons and myelinated fibers. Curr. Biol. CB *17*, R29–R35.

Hauser, S.L., and Oksenberg, J.R. (2006). The neurobiology of multiple sclerosis: genes, inflammation, and neurodegeneration. Neuron *52*, 61–76.

He, Y., Sandoval, J., and Casaccia-Bonnefil, P. (2007a). Events at the transition between cell cycle exit and oligodendrocyte progenitor differentiation: the role of HDAC and YY1. Neuron Glia Biol. *3*, 221–231.

He, Y., Dupree, J., Wang, J., Sandoval, J., Li, J., Liu, H., Shi, Y., Nave, K.A., and Casaccia-Bonnefil, P. (2007b). The transcription factor Yin Yang1 is essential for oligodendrocyte progenitor differentiation. Neuron *55*, 217–230.

Hecht, J.H., Weiner, J.A., Post, S.R., and Chun, J. (1996). Ventricular zone gene-1 (vzg-1) encodes a lysophosphatidic acid receptor expressed in neurogenic regions of the developing cerebral cortex. J. Cell Biol. *135*, 1071–1083.

Herbein, G., Gras, G., Khan, K.A., and Abbas, W. (2010). Macrophage signaling in HIV-1 infection. Retrovirology *7*, 34.

Herr, K.J., Herr, D.R., Lee, C.-W., Noguchi, K., and Chun, J. (2011). Stereotyped fetal brain disorganization is induced by hypoxia and requires lysophosphatidic acid receptor 1 (LPA1) signaling. Proc. Natl. Acad. Sci. U. S. A. *108*, 15444–15449.

Hoppenbrouwers, I.A., and Hintzen, R.Q. (2011). Genetics of multiple sclerosis. Biochim. Biophys. Acta *1812*, 194–201.

Hsieh, J., Nakashima, K., Kuwabara, T., Mejia, E., and Gage, F.H. (2004). Histone deacetylase inhibition-mediated neuronal differentiation of multipotent adult neural progenitor cells. Proc. Natl. Acad. Sci. U. S. A. *101*, 16659–16664.

Hurley, R.A., Ernst, T., Khalili, K., Del Valle, L., Simone, I.L., and Taber, K.H. (2003). Identification of HIV-associated progressive multifocal leukoencephalopathy: magnetic resonance imaging and spectroscopy. J. Neuropsychiatry Clin. Neurosci. *15*, 1–6.

Iglesias-Rozas, J.R., and Garrosa, M. (2012). The discovery of oligodendroglia cells by Rio-Hortega: his original articles. 1921. Clin. Neuropathol. *31*, 437–439.

Iñiguez-Lluhí, J.A. (2006). For a healthy histone code, a little SUMO in the tail keeps the acetyl away. ACS Chem. Biol. *1*, 204–206.

Inoue, A., Arima, N., Ishiguro, J., Prestwich, G.D., Arai, H., and Aoki, J. (2011). LPA-producing enzyme PA-PLA$_1$α regulates hair follicle development by modulating EGFR signalling. EMBO J. *30*, 4248–4260.

Inoue, M., Rashid, M.H., Fujita, R., Contos, J.J.A., Chun, J., and Ueda, H. (2004). Initiation of neuropathic pain requires lysophosphatidic acid receptor signaling. Nat. Med. *10*, 712–718.

Inoue, M., Ma, L., Aoki, J., Chun, J., and Ueda, H. (2008a). Autotaxin, a synthetic enzyme of lysophosphatidic acid (LPA), mediates the induction of nerve-injured neuropathic pain. Mol. Pain *4*, 6.

Inoue, M., Xie, W., Matsushita, Y., Chun, J., Aoki, J., and Ueda, H. (2008b). Lysophosphatidylcholine induces neuropathic pain through an action of autotaxin to generate lysophosphatidic acid. Neuroscience *152*, 296–298.

Ishdorj, G., Graham, B.A., Hu, X., Chen, J., Johnston, J.B., Fang, X., and Gibson, S.B. (2008). Lysophosphatidic acid protects cancer cells from histone deacetylase (HDAC) inhibitor-induced apoptosis through activation of HDAC. J. Biol. Chem. *283*, 16818–16829.

Ishii, A., Fyffe-Maricich, S.L., Furusho, M., Miller, R.H., and Bansal, R. (2012). ERK1/ERK2 MAPK signaling is required to increase myelin thickness independent of oligodendrocyte differentiation and initiation of myelination. J. Neurosci. Off. J. Soc. Neurosci. *32*, 8855–8864.

Iyer, P., Lalane, R., Morris, C., Challa, P., Vann, R., and Rao, P.V. (2012). Autotaxin-lysophosphatidic acid axis is a novel molecular target for lowering intraocular pressure. PloS One *7*, e42627.

Jacob, C., Lebrun-Julien, F., and Suter, U. (2011). How histone deacetylases control myelination. Mol. Neurobiol. *44*, 303–312.

Jankowski, M. (2011). Autotaxin: Its Role in Biology of Melanoma Cells and as a Pharmacological Target. Enzyme Res. *2011*.

Jansen, S., Stefan, C., Creemers, J.W.M., Waelkens, E., Van Eynde, A., Stalmans, W., and Bollen, M. (2005). Proteolytic maturation and activation of autotaxin (NPP2), a secreted metastasis-enhancing lysophospholipase D. J. Cell Sci. *118*, 3081–3089.

Jansen, S., Andries, M., Vekemans, K., Vanbilloen, H., Verbruggen, A., and Bollen, M. (2009). Rapid clearance of the circulating metastatic factor autotaxin by the scavenger receptors of liver sinusoidal endothelial cells. Cancer Lett. *284*, 216–221.

Jao, L.-E., Wente, S.R., and Chen, W. (2013). Efficient multiplex biallelic zebrafish genome editing using a CRISPR nuclease system. Proc. Natl. Acad. Sci. U. S. A. *110*, 13904–13909.

Jayadev, S., Yun, B., Nguyen, H., Yokoo, H., Morrison, R.S., and Garden, G.A. (2007). The glial response to CNS HIV infection includes p53 activation and increased expression of p53 target genes. J. Neuroimmune Pharmacol. Off. J. Soc. NeuroImmune Pharmacol. *2*, 359–370.

Jellinger, K.A., Setinek, U., Drlicek, M., Böhm, G., Steurer, A., and Lintner, F. (2000). Neuropathology and general autopsy findings in AIDS during the last 15 years. Acta Neuropathol. (Berl.) *100*, 213–220.

Jernigan, T.L., Archibald, S., Hesselink, J.R., Atkinson, J.H., Velin, R.A., McCutchan, J.A., Chandler, J., and Grant, I. (1993). Magnetic resonance imaging morphometric analysis of cerebral volume loss in human immunodeficiency virus infection. The HNRC Group. Arch. Neurol. *50*, 250–255.

Ji, S., Doucette, J.R., and Nazarali, A.J. (2011). Sirt2 is a novel in vivo downstream target of Nkx2.2 and enhances oligodendroglial cell differentiation. J. Mol. Cell Biol. *3*, 351–359.

Jongsma, M., Matas-Rico, E., Rzadkowski, A., Jalink, K., and Moolenaar, W.H. (2011). LPA is a chemorepellent for B16 melanoma cells: action through the cAMP-elevating LPA5 receptor. PloS One *6*, e29260.

Kanda, H., Newton, R., Klein, R., Morita, Y., Gunn, M.D., and Rosen, S.D. (2008). Autotaxin, an ectoenzyme that produces lysophosphatidic acid, promotes the entry of lymphocytes into secondary lymphoid organs. Nat. Immunol. *9*, 415–423.

Kapitonov, D., and Yu, R.K. (1997). Cloning, characterization, and expression of human ceramide galactosyltransferase cDNA. Biochem. Biophys. Res. Commun. *232*, 449–453.

Kaplan, M.H., Smith, D.I., and Sundick, R.S. (1993). Identification of a G protein coupled receptor induced in activated T cells. J. Immunol. *151*, 628–636.

Kazantsev, A.G., and Thompson, L.M. (2008). Therapeutic application of histone deacetylase inhibitors for central nervous system disorders. Nat. Rev. Drug Discov. *7*, 854–868.

Kessaris, N., Fogarty, M., Iannarelli, P., Grist, M., Wegner, M., and Richardson, W.D. (2006). Competing waves of oligodendrocytes in the forebrain and postnatal elimination of an embryonic lineage. Nat. Neurosci. *9*, 173–179.

Kettenmann, H., and Ransom, B.R. (2013). Neuroglia (OUP USA).

Kihara, Y., Maceyka, M., Spiegel, S., and Chun, J. (2014). Lysophospholipid receptor nomenclature review: IUPHAR Review 8. Br. J. Pharmacol. *171*, 3575–3594.

Kimmel, C.B., Ballard, W.W., Kimmel, S.R., Ullmann, B., and Schilling, T.F. (1995). Stages of embryonic development of the zebrafish. Dev. Dyn. Off. Publ. Am. Assoc. Anat. *203*, 253–310.

King, J.E., Eugenin, E.A., Buckner, C.M., and Berman, J.W. (2006). HIV tat and neurotoxicity. Microbes Infect. Inst. Pasteur *8*, 1347–1357.

Kingsbury, M.A., Rehen, S.K., Contos, J.J.A., Higgins, C.M., and Chun, J. (2003). Non-proliferative effects of lysophosphatidic acid enhance cortical growth and folding. Nat. Neurosci. *6*, 1292–1299.

Kirby, B.B., Takada, N., Latimer, A.J., Shin, J., Carney, T.J., Kelsh, R.N., and Appel, B. (2006). In vivo time-lapse imaging shows dynamic oligodendrocyte progenitor behavior during zebrafish development. Nat. Neurosci. *9*, 1506–1511.

Kleger, A., Liebau, S., Lin, Q., von Wichert, G., and Seufferlein, T. (2011). The Impact of Bioactive Lipids on Cardiovascular Development. Stem Cells Int. *2011*.

Knapp, P.E., Skoff, R.P., and Redstone, D.W. (1986). Oligodendroglial cell death in jimpy mice: an explanation for the myelin deficit. J. Neurosci. Off. J. Soc. Neurosci. *6*, 2813–2822.

Knowlden, S., and Georas, S.N. (2014). The autotaxin-LPA axis emerges as a novel regulator of lymphocyte homing and inflammation. J. Immunol. Baltim. Md 1950 *192*, 851–857.

Koh, E., Clair, T., Woodhouse, E.C., Schiffmann, E., Liotta, L., and Stracke, M. (2003). Site-directed mutations in the tumor-associated cytokine, autotaxin, eliminate nucleotide phosphodiesterase, lysophospholipase D, and motogenic activities. Cancer Res. *63*, 2042–2045.

Koike, S., Keino-Masu, K., Ohto, T., and Masu, M. (2006). The N-terminal hydrophobic sequence of autotaxin (ENPP2) functions as a signal peptide. Genes Cells Devoted Mol. Cell. Mech. *11*, 133–142.

Koike, S., Keino-Masu, K., and Masu, M. (2010). Deficiency of autotaxin/lysophospholipase D results in head cavity formation in mouse embryos through the LPA receptor-Rho-ROCK pathway. Biochem. Biophys. Res. Commun. *400*, 66–71.

Kok, F.O., Shin, M., Ni, C.-W., Gupta, A., Grosse, A.S., van Impel, A., Kirchmaier, B.C., Peterson-Maduro, J., Kourkoulis, G., Male, I., et al. (2015). Reverse genetic screening reveals poor correlation between morpholino-induced and mutant phenotypes in zebrafish. Dev. Cell *32*, 97–108.

Kondo, T., and Raff, M. (2000a). Basic helix-loop-helix proteins and the timing of oligodendrocyte differentiation. Dev. Camb. Engl. *127*, 2989–2998.

Kondo, T., and Raff, M. (2000b). The Id4 HLH protein and the timing of oligodendrocyte differentiation. EMBO J. *19*, 1998–2007.

Kondo, T., and Raff, M. (2004). Chromatin remodeling and histone modification in the conversion of oligodendrocyte precursors to neural stem cells. Genes Dev. *18*, 2963–2972.

Kotarsky, K., Boketoft, A., Bristulf, J., Nilsson, N.E., Norberg, A., Hansson, S., Owman, C., Sillard, R., Leeb-Lundberg, L.M.F., and Olde, B. (2006). Lysophosphatidic acid binds to and activates GPR92, a G protein-coupled receptor highly expressed in gastrointestinal lymphocytes. J. Pharmacol. Exp. Ther. *318*, 619–628.

Kouzarides, T. (2007). Chromatin modifications and their function. Cell *128*, 693–705.

Kraker, A.J., Mizzen, C.A., Hartl, B.G., Miin, J., Allis, C.D., and Merriman, R.L. (2003). Modulation of histone acetylation by [4-(acetylamino)-N-(2-amino-phenyl) benzamide] in HCT-8 colon carcinoma. Mol. Cancer Ther. *2*, 401–408.

Kramer-Hämmerle, S., Rothenaigner, I., Wolff, H., Bell, J.E., and Brack-Werner, R. (2005). Cells of the central nervous system as targets and reservoirs of the human immunodeficiency virus. Virus Res. *111*, 194–213.

Kremer, A.E., Martens, J.J.W.W., Kulik, W., Ruëff, F., Kuiper, E.M.M., van Buuren, H.R., van Erpecum, K.J., Kondrackiene, J., Prieto, J., Rust, C., et al. (2010). Lysophosphatidic acid is a potential mediator of cholestatic pruritus. Gastroenterology *139*, 1008–1018, 1018.e1.

Kubosaki, A., Tomaru, Y., Tagami, M., Arner, E., Miura, H., Suzuki, T., Suzuki, M., Suzuki, H., and Hayashizaki, Y. (2009). Genome-wide investigation of in vivo EGR-1 binding sites in monocytic differentiation. Genome Biol. *10*, R41.

Kucenas, S., Snell, H., and Appel, B. (2008). nkx2.2a promotes specification and differentiation of a myelinating subset of oligodendrocyte lineage cells in zebrafish. Neuron Glia Biol. *4*, 71–81.

Kuhlmann, T., Miron, V., Cui, Q., Cuo, Q., Wegner, C., Antel, J., and Brück, W. (2008a). Differentiation block of oligodendroglial progenitor cells as a cause for remyelination failure in chronic multiple sclerosis. Brain J. Neurol. *131*, 1749–1758.

Kuhlmann, T., Miron, V., Cui, Q., Cuo, Q., Wegner, C., Antel, J., and Brück, W. (2008b). Differentiation block of oligodendroglial progenitor cells as a cause for remyelination failure in chronic multiple sclerosis. Brain J. Neurol. *131*, 1749–1758.

Kuhlmann, T., Lassmann, H., and Brück, W. (2008c). Diagnosis of inflammatory demyelination in biopsy specimens: a practical approach. Acta Neuropathol. (Berl.) *115*, 275–287.

Lafrenaye, A.D., and Fuss, B. (2010). Focal adhesion kinase can play unique and opposing roles in regulating the morphology of differentiating oligodendrocytes. J. Neurochem. *115*, 269–282.

Lai, S.-L., Yao, W.-L., Tsao, K.-C., Houben, A.J.S., Albers, H.M.H.G., Ovaa, H., Moolenaar, W.H., and Lee, S.-J. (2012). Autotaxin/Lpar3 signaling regulates Kupffer's vesicle formation and left-right asymmetry in zebrafish. Dev. Camb. Engl. *139*, 4439–4448.

Lam, C.S., März, M., and Strähle, U. (2009). gfap and nestin reporter lines reveal characteristics of neural progenitors in the adult zebrafish brain. Dev. Dyn. Off. Publ. Am. Assoc. Anat. *238*, 475–486.

Langley, B., Gensert, J.M., Beal, M.F., and Ratan, R.R. (2005). Remodeling chromatin and stress resistance in the central nervous system: histone deacetylase inhibitors as novel and broadly effective neuroprotective agents. Curr. Drug Targets CNS Neurol. Disord. *4*, 41–50.

Laplante, M., and Sabatini, D.M. (2013). Regulation of mTORC1 and its impact on gene expression at a glance. J. Cell Sci. *126*, 1713–1719.

Lappe-Siefke, C., Goebbels, S., Gravel, M., Nicksch, E., Lee, J., Braun, P.E., Griffiths, I.R., and Nave, K.-A. (2003). Disruption of Cnp1 uncouples oligodendroglial functions in axonal support and myelination. Nat. Genet. *33*, 366–374.

Leake, D., Asch, W.S., Canger, A.K., and Schechter, N. (1999). Gefiltin in zebrafish embryos: sequential gene expression of two neurofilament proteins in retinal ganglion cells. Differ. Res. Biol. Divers. *65*, 181–189.

Lee, C.-W., Rivera, R., Gardell, S., Dubin, A.E., and Chun, J. (2006). GPR92 as a new G12/13- and Gq-coupled lysophosphatidic acid receptor that increases cAMP, LPA5. J. Biol. Chem. *281*, 23589–23597.

Lee, H.Y., Clair, T., Mulvaney, P.T., Woodhouse, E.C., Aznavoorian, S., Liotta, L.A., and Stracke, M.L. (1996). Stimulation of tumor cell motility linked to phosphodiesterase catalytic site of autotaxin. J. Biol. Chem. *271*, 24408–24412.

Lee, J., Gravel, M., Zhang, R., Thibault, P., and Braun, P.E. (2005). Process outgrowth in oligodendrocytes is mediated by CNP, a novel microtubule assembly myelin protein. J. Cell Biol. *170*, 661–673.

Lee, M., Choi, S., Halldén, G., Yo, S.J., Schichnes, D., and Aponte, G.W. (2009a). P2Y5 is a G(alpha)i, G(alpha)12/13 G protein-coupled receptor activated by lysophosphatidic acid that reduces intestinal cell adhesion. Am. J. Physiol. Gastrointest. Liver Physiol. *297*, G641–G654.

Lee, M., Choi, S., Halldén, G., Yo, S.J., Schichnes, D., and Aponte, G.W. (2009b). P2Y5 is a Gαi, Gα12/13 G protein-coupled receptor activated by lysophosphatidic acid that reduces intestinal cell adhesion. Am. J. Physiol. - Gastrointest. Liver Physiol. *297*, G641–G654.

Lee, M., Choi, S., Halldén, G., Yo, S.J., Schichnes, D., and Aponte, G.W. (2009c). P2Y5 is a G(alpha)i, G(alpha)12/13 G protein-coupled receptor activated by lysophosphatidic acid that reduces intestinal cell adhesion. Am. J. Physiol. Gastrointest. Liver Physiol. *297*, G641–G654.

Levison, S.W., Chuang, C., Abramson, B.J., and Goldman, J.E. (1993). The migrational patterns and developmental fates of glial precursors in the rat subventricular zone are temporally regulated. Dev. Camb. Engl. *119*, 611–622.

Leyk, J., Goldbaum, O., Noack, M., and Richter-Landsberg, C. (2015). Inhibition of HDAC6 modifies tau inclusion body formation and impairs autophagic clearance. J. Mol. Neurosci. MN *55*, 1031–1046.

Li, H., Lu, Y., Smith, H.K., and Richardson, W.D. (2007). Olig1 and Sox10 interact synergistically to drive myelin basic protein transcription in oligodendrocytes. J. Neurosci. Off. J. Soc. Neurosci. *27*, 14375–14382.

Li, Y., Gonzalez, M.I., Meinkoth, J.L., Field, J., Kazanietz, M.G., and Tennekoon, G.I. (2003). Lysophosphatidic acid promotes survival and differentiation of rat Schwann cells. J. Biol. Chem. *278*, 9585–9591.

Li, Z.-G., Yu, Z.-C., Wang, D.-Z., Ju, W.-P., Zhan, X., Wu, Q.-Z., Wu, X.-J., Cong, H.-M., and Man, H.-H. (2008). Influence of acetylsalicylate on plasma lysophosphatidic acid level in patients with ischemic cerebral vascular diseases. Neurol. Res. *30*, 366–369.

Lin, M.-E., Rivera, R.R., and Chun, J. (2012). Targeted Deletion of LPA5 Identifies Novel Roles for Lysophosphatidic Acid Signaling in Development of Neuropathic Pain. J. Biol. Chem. *287*, 17608–17617.

Lipton, S.A. (1998). Neuronal injury associated with HIV-1: approaches to treatment. Annu. Rev. Pharmacol. Toxicol. *38*, 159–177.

Liu, J., and Casaccia, P. (2010). Epigenetic regulation of oligodendrocyte identity. Trends Neurosci. *33*, 193–201.

Liu, A., Li, J., Marin-Husstege, M., Kageyama, R., Fan, Y., Gelinas, C., and Casaccia-Bonnefil, P. (2006). A molecular insight of Hes5-dependent inhibition of myelin gene expression: old partners and new players. EMBO J. *25*, 4833–4842.

Liu, H., Hu, Q., Kaufman, A., D'Ercole, A.J., and Ye, P. (2008). Developmental expression of histone deacetylase 11 in the murine brain. J. Neurosci. Res. *86*, 537–543.

Liu, H., Hu, Q., D'ercole, A.J., and Ye, P. (2009). Histone deacetylase 11 regulates oligodendrocyte-specific gene expression and cell development in OL-1 oligodendroglia cells. Glia *57*, 1–12.

Liu, J., Magri, L., Zhang, F., Marsh, N.O., Albrecht, S., Huynh, J.L., Kaur, J., Kuhlmann, T., Zhang, W., Slesinger, P.A., et al. (2015). Chromatin landscape defined by repressive histone methylation during oligodendrocyte differentiation. J. Neurosci. Off. J. Soc. Neurosci. *35*, 352–365.

Liu, Y.-B., Kharode, Y., Bodine, P.V.N., Yaworsky, P.J., Robinson, J.A., and Billiard, J. (2010). LPA induces osteoblast differentiation through interplay of two receptors: LPA1 and LPA4. J. Cell. Biochem. *109*, 794–800.

Liu, Z., Hu, X., Cai, J., Liu, B., Peng, X., Wegner, M., and Qiu, M. (2007). Induction of oligodendrocyte differentiation by Olig2 and Sox10: evidence for reciprocal interactions and dosage-dependent mechanisms. Dev. Biol. *302*, 683–693.

Livak, K.J., and Schmittgen, T.D. (2001). Analysis of relative gene expression data using real-time quantitative PCR and the 2(-Delta Delta C(T)) Method. Methods San Diego Calif *25*, 402–408.

Lyssiotis, C.A., Walker, J., Wu, C., Kondo, T., Schultz, P.G., and Wu, X. (2007a). Inhibition of histone deacetylase activity induces developmental plasticity in oligodendrocyte precursor cells. Proc. Natl. Acad. Sci. U. S. A. *104*, 14982–14987.

Lyssiotis, C.A., Walker, J., Wu, C., Kondo, T., Schultz, P.G., and Wu, X. (2007b). Inhibition of histone deacetylase activity induces developmental plasticity in oligodendrocyte precursor cells. Proc. Natl. Acad. Sci. *104*, 14982–14987.

Maes, J., Verlooy, L., Buenafe, O.E., de Witte, P.A.M., Esguerra, C.V., and Crawford, A.D. (2012). Evaluation of 14 organic solvents and carriers for screening applications in zebrafish embryos and larvae. PloS One *7*, e43850.

Di Maira, G., Salvi, M., Arrigoni, G., Marin, O., Sarno, S., Brustolon, F., Pinna, L.A., and Ruzzene, M. (2005). Protein kinase CK2 phosphorylates and upregulates Akt/PKB. Cell Death Differ. *12*, 668–677.

Di Maira, G., Brustolon, F., Pinna, L.A., and Ruzzene, M. (2009). Dephosphorylation and inactivation of Akt/PKB is counteracted by protein kinase CK2 in HEK 293T cells. Cell. Mol. Life Sci. CMLS *66*, 3363–3373.

Mangmool, S., and Kurose, H. (2011). G(i/o) protein-dependent and -independent actions of Pertussis Toxin (PTX). Toxins *3*, 884–899.

Marcus, J., and Popko, B. (2002). Galactolipids are molecular determinants of myelin development and axo-glial organization. Biochim. Biophys. Acta *1573*, 406–413.

Marin-Husstege, M., Muggironi, M., Liu, A., and Casaccia-Bonnefil, P. (2002). Histone deacetylase activity is necessary for oligodendrocyte lineage progression. J. Neurosci. Off. J. Soc. Neurosci. *22*, 10333–10345.

Marshall, C.A.G., Suzuki, S.O., and Goldman, J.E. (2003). Gliogenic and neurogenic progenitors of the subventricular zone: who are they, where did they come from, and where are they going? Glia *43*, 52–61.

Martinez-Lozada, Z., Waggener, C.T., Kim, K., Zou, S., Knapp, P.E., Hayashi, Y., Ortega, A., and Fuss, B. (2014). Activation of sodium-dependent glutamate transporters regulates the morphological aspects of oligodendrocyte maturation via signaling through calcium/calmodulin-dependent kinase IIβ's actin-binding/-stabilizing domain. Glia *62*, 1543–1558.

Maschke, M., Kastrup, O., Esser, S., Ross, B., Hengge, U., and Hufnagel, A. (2000). Incidence and prevalence of neurological disorders associated with HIV since the introduction of highly active antiretroviral therapy (HAART). J. Neurol. Neurosurg. Psychiatry *69*, 376–380.

Mastronardi, F.G., Wood, D.D., Mei, J., Raijmakers, R., Tseveleki, V., Dosch, H.-M., Probert, L., Casaccia-Bonnefil, P., and Moscarello, M.A. (2006). Increased citrullination of histone H3 in multiple sclerosis brain and animal models of demyelination: a role for

tumor necrosis factor-induced peptidylarginine deiminase 4 translocation. J. Neurosci. Off. J. Soc. Neurosci. *26*, 11387–11396.

Matsushita, T., Amagai, Y., Soga, T., Terai, K., Obinata, M., and Hashimoto, S. (2005). A novel oligodendrocyte cell line OLP6 shows the successive stages of oligodendrocyte development: late progenitor, immature and mature stages. Neuroscience *136*, 115–121.

van Meeteren, L.A., and Moolenaar, W.H. (2007). Regulation and biological activities of the autotaxin-LPA axis. Prog. Lipid Res. *46*, 145–160.

van Meeteren, L.A., Ruurs, P., Stortelers, C., Bouwman, P., van Rooijen, M.A., Pradère, J.P., Pettit, T.R., Wakelam, M.J.O., Saulnier-Blache, J.S., Mummery, C.L., et al. (2006). Autotaxin, a secreted lysophospholipase D, is essential for blood vessel formation during development. Mol. Cell. Biol. *26*, 5015–5022.

Merrill, J.E., and Chen, I.S. (1991). HIV-1, macrophages, glial cells, and cytokines in AIDS nervous system disease. FASEB J. Off. Publ. Fed. Am. Soc. Exp. Biol. *5*, 2391–2397.

Michan, S., and Sinclair, D. (2007). Sirtuins in mammals: insights into their biological function. Biochem. J. *404*, 1–13.

Miller, R.H. (1996). Oligodendrocyte origins. Trends Neurosci. *19*, 92–96.

Miller, R.H. (2002). Regulation of oligodendrocyte development in the vertebrate CNS. Prog. Neurobiol. *67*, 451–467.

Mirendil, H., Thomas, E.A., De Loera, C., Okada, K., Inomata, Y., and Chun, J. (2015). LPA signaling initiates schizophrenia-like brain and behavioral changes in a mouse model of prenatal brain hemorrhage. Transl. Psychiatry *5*, e541.

Mitew, S., Hay, C.M., Peckham, H., Xiao, J., Koenning, M., and Emery, B. (2014). Mechanisms regulating the development of oligodendrocytes and central nervous system myelin. Neuroscience *276*, 29–47.

Möller, T., Contos, J.J., Musante, D.B., Chun, J., and Ransom, B.R. (2001). Expression and function of lysophosphatidic acid receptors in cultured rodent microglial cells. J. Biol. Chem. *276*, 25946–25952.

Moolenaar, W.H., and Perrakis, A. (2011). Insights into autotaxin: how to produce and present a lipid mediator. Nat. Rev. Mol. Cell Biol. *12*, 674–679.

Mori, S., and Leblond, C.P. (1970). Electron microscopic identification of three classes of oligodendrocytes and a preliminary study of their proliferative activity in the corpus callosum of young rats. J. Comp. Neurol. *139*, 1–28.

Münzel, E.J., Schaefer, K., Obirei, B., Kremmer, E., Burton, E.A., Kuscha, V., Becker, C.G., Brösamle, C., Williams, A., and Becker, T. (2012). Claudin k is specifically expressed in cells that form myelin during development of the nervous system and regeneration of the optic nerve in adult zebrafish. Glia *60*, 253–270.

Murata, J., Lee, H.Y., Clair, T., Krutzsch, H.C., Arestad, A.A., Sobel, M.E., Liotta, L.A., and Stracke, M.L. (1994). cDNA cloning of the human tumor motility-stimulating protein, autotaxin, reveals a homology with phosphodiesterases. J. Biol. Chem. *269*, 30479–30484.

Nagai, J., Uchida, H., Matsushita, Y., Yano, R., Ueda, M., Niwa, M., Aoki, J., Chun, J., and Ueda, H. (2010). Autotaxin and lysophosphatidic acid1 receptor-mediated demyelination of dorsal root fibers by sciatic nerve injury and intrathecal lysophosphatidylcholine. Mol. Pain *6*, 78.

Nakamura, K., Ohkawa, R., Okubo, S., Yokota, H., Ikeda, H., Yatomi, Y., Igarashi, K., Ide, K., Kishimoto, T., Masuda, A., et al. (2009). Autotaxin enzyme immunoassay in human cerebrospinal fluid samples. Clin. Chim. Acta Int. J. Clin. Chem. *405*, 160–162.

Nakanaga, K., Hama, K., and Aoki, J. (2010). Autotaxin--an LPA producing enzyme with diverse functions. J. Biochem. (Tokyo) *148*, 13–24.

Nakasaki, T., Tanaka, T., Okudaira, S., Hirosawa, M., Umemoto, E., Otani, K., Jin, S., Bai, Z., Hayasaka, H., Fukui, Y., et al. (2008). Involvement of the lysophosphatidic acid-generating enzyme autotaxin in lymphocyte-endothelial cell interactions. Am. J. Pathol. *173*, 1566–1576.

Narayanan, S.P., Flores, A.I., Wang, F., and Macklin, W.B. (2009). Akt signals through the mammalian target of rapamycin, mTOR, pathway to regulate central nervous system myelination. J. Neurosci. Off. J. Soc. Neurosci. *29*, 6860–6870.

Nath, A., and Geiger, J. (1998). Neurobiological aspects of human immunodeficiency virus infection: neurotoxic mechanisms. Prog. Neurobiol. *54*, 19–33.

Nave, K.-A., and Trapp, B.D. (2008). Axon-glial signaling and the glial support of axon function. Annu. Rev. Neurosci. *31*, 535–561.

Nelissen, K., Smeets, K., Mulder, M., Hendriks, J.J.A., and Ameloot, M. (2010). Selection of reference genes for gene expression studies in rat oligodendrocytes using quantitative real time PCR. J. Neurosci. Methods *187*, 78–83.

Nguyen, L.X.T., and Mitchell, B.S. (2013). Akt activation enhances ribosomal RNA synthesis through casein kinase II and TIF-IA. Proc. Natl. Acad. Sci. U. S. A. *110*, 20681–20686.

Noack, M., Leyk, J., and Richter-Landsberg, C. (2014). HDAC6 inhibition results in tau acetylation and modulates tau phosphorylation and degradation in oligodendrocytes. Glia *62*, 535–547.

Nogaroli, L., Yuelling, L.M., Dennis, J., Gorse, K., Payne, S.G., and Fuss, B. (2009a). Lysophosphatidic acid can support the formation of membranous structures and an increase in MBP mRNA levels in differentiating oligodendrocytes. Neurochem. Res. *34*, 182–193.

Nogaroli, L., Yuelling, L.M., Dennis, J., Gorse, K., Payne, S.G., and Fuss, B. (2009b). Lysophosphatidic acid can support the formation of membranous structures and an increase in MBP mRNA levels in differentiating oligodendrocytes. Neurochem. Res. *34*, 182–193.

Noguchi, K., Ishii, S., and Shimizu, T. (2003). Identification of p2y9/GPR23 as a novel G protein-coupled receptor for lysophosphatidic acid, structurally distant from the Edg family. J. Biol. Chem. *278*, 25600–25606.

Noguchi, K., Herr, D., Mutoh, T., and Chun, J. (2009). Lysophosphatidic acid (LPA) and its receptors. Curr. Opin. Pharmacol. *9*, 15–23.

Noll, E., and Miller, R.H. (1993). Oligodendrocyte precursors originate at the ventral ventricular zone dorsal to the ventral midline region in the embryonic rat spinal cord. Dev. Camb. Engl. *118*, 563–573.

Nowak-Machen, M., Lange, M., Exley, M., Wu, S., Usheva, A., and Robson, S.C. (2015). Lysophosphatidic acid generation by pulmonary NKT cell ENPP-2/autotaxin exacerbates hyperoxic lung injury. Purinergic Signal. *11*, 455–461.

Oda, S.K., Strauch, P., Fujiwara, Y., Al-Shami, A., Oravecz, T., Tigyi, G., Pelanda, R., and Torres, R.M. (2013). Lysophosphatidic acid inhibits CD8 T cell activation and control of tumor progression. Cancer Immunol. Res. *1*, 245–255.

Oikonomou, N., Mouratis, M.-A., Tzouvelekis, A., Kaffe, E., Valavanis, C., Vilaras, G., Karameris, A., Prestwich, G.D., Bouros, D., and Aidinis, V. (2012). Pulmonary autotaxin expression contributes to the pathogenesis of pulmonary fibrosis. Am. J. Respir. Cell Mol. Biol. *47*, 566–574.

Ojala, P.J., Hermansson, M., Tolvanen, M., Polvinen, K., Hirvonen, T., Impola, U., Jauhiainen, M., Somerharju, P., and Parkkinen, J. (2006). Identification of alpha-1 acid glycoprotein as a lysophospholipid binding protein: a complementary role to albumin in the scavenging of lysophosphatidylcholine. Biochemistry (Mosc.) *45*, 14021–14031.

Okudaira, S., Yukiura, H., and Aoki, J. (2010). Biological roles of lysophosphatidic acid signaling through its production by autotaxin. Biochimie *92*, 698–706.

Olivier, C., Cobos, I., Perez Villegas, E.M., Spassky, N., Zalc, B., Martinez, S., and Thomas, J.L. (2001). Monofocal origin of telencephalic oligodendrocytes in the anterior entopeduncular area of the chick embryo. Dev. Camb. Engl. *128*, 1757–1769.

Osterhout, D.J., Wolven, A., Wolf, R.M., Resh, M.D., and Chao, M.V. (1999). Morphological differentiation of oligodendrocytes requires activation of Fyn tyrosine kinase. J. Cell Biol. *145*, 1209–1218.

Parab, S., Shetty, O., Gaonkar, R., Balasinor, N., Khole, V., and Parte, P. (2015). HDAC6 deacetylates alpha tubulin in sperm and modulates sperm motility in Holtzman rat. Cell Tissue Res. *359*, 665–678.

Park, H.-C., Mehta, A., Richardson, J.S., and Appel, B. (2002). olig2 is required for zebrafish primary motor neuron and oligodendrocyte development. Dev. Biol. *248*, 356–368.

Park, H.-C., Shin, J., and Appel, B. (2004). Spatial and temporal regulation of ventral spinal cord precursor specification by Hedgehog signaling. Dev. Camb. Engl. *131*, 5959–5969.

Pasternack, S.M., von Kügelgen, I., Aboud, K. Al, Lee, Y.-A., Rüschendorf, F., Voss, K., Hillmer, A.M., Molderings, G.J., Franz, T., Ramirez, A., et al. (2008). G protein-coupled receptor P2Y5 and its ligand LPA are involved in maintenance of human hair growth. Nat. Genet. *40*, 329–334.

Pasternack, S.M., von Kügelgen, I., Müller, M., Oji, V., Traupe, H., Sprecher, E., Nöthen, M.M., Janecke, A.R., and Betz, R.C. (2009). In vitro analysis of LIPH mutations causing hypotrichosis simplex: evidence confirming the role of lipase H and lysophosphatidic acid in hair growth. J. Invest. Dermatol. *129*, 2772–2776.

Pedre, X., Mastronardi, F., Bruck, W., López-Rodas, G., Kuhlmann, T., and Casaccia, P. (2011). Changed histone acetylation patterns in normal-appearing white matter and early multiple sclerosis lesions. J. Neurosci. Off. J. Soc. Neurosci. *31*, 3435–3445.

Peserico, A., and Simone, C. (2011). Physical and functional HAT/HDAC interplay regulates protein acetylation balance. J. Biomed. Biotechnol. *2011*, 371832.

Pfeiffer, S.E., Warrington, A.E., and Bansal, R. (1993). The oligodendrocyte and its many cellular processes. Trends Cell Biol. *3*, 191–197.

Philpott, N.J., Turner, A.J., Scopes, J., Westby, M., Marsh, J.C., Gordon-Smith, E.C., Dalgleish, A.G., and Gibson, F.M. (1996). The use of 7-amino actinomycin D in identifying apoptosis: simplicity of use and broad spectrum of application compared with other techniques. Blood *87*, 2244–2251.

Placzek, M., and Briscoe, J. (2005). The floor plate: multiple cells, multiple signals. Nat. Rev. Neurosci. *6*, 230–240.

Ponce, D.P., Yefi, R., Cabello, P., Maturana, J.L., Niechi, I., Silva, E., Galindo, M., Antonelli, M., Marcelain, K., Armisen, R., et al. (2011). CK2 functionally interacts with AKT/PKB to promote the β-catenin-dependent expression of survivin and enhance cell survival. Mol. Cell. Biochem. *356*, 127–132.

Popot, J.L., Pham Dinh, D., and Dautigny, A. (1991). Major myelin proteolipid: the 4-alpha-helix topology. J. Membr. Biol. *123*, 278.

Power, C., McArthur, J.C., Nath, A., Wehrly, K., Mayne, M., Nishio, J., Langelier, T., Johnson, R.T., and Chesebro, B. (1998). Neuronal death induced by brain-derived human immunodeficiency virus type 1 envelope genes differs between demented and nondemented AIDS patients. J. Virol. *72*, 9045–9053.

Power, C., Hui, E., Vivithanaporn, P., Acharjee, S., and Polyak, M. (2012). Delineating HIV-associated neurocognitive disorders using transgenic models: the neuropathogenic actions of Vpr. J. Neuroimmune Pharmacol. Off. J. Soc. NeuroImmune Pharmacol. *7*, 319–331.

Preston, M.A., and Macklin, W.B. (2015). Zebrafish as a model to investigate CNS myelination. Glia *63*, 177–193.

Pringle, N.P., and Richardson, W.D. (1993). A singularity of PDGF alpha-receptor expression in the dorsoventral axis of the neural tube may define the origin of the oligodendrocyte lineage. Dev. Camb. Engl. *117*, 525–533.

Pringle, N.P., Yu, W.P., Guthrie, S., Roelink, H., Lumsden, A., Peterson, A.C., and Richardson, W.D. (1996). Determination of neuroepithelial cell fate: induction of the oligodendrocyte lineage by ventral midline cells and sonic hedgehog. Dev. Biol. *177*, 30–42.

Privat, A., and Leblond, C.P. (1972). The subependymal layer and neighboring region in the brain of the young rat. J. Comp. Neurol. *146*, 277–302.

Puri, R.K., and Aggarwal, B.B. (1992). Human immunodeficiency virus type 1 tat gene up-regulates interleukin 4 receptors on a human B-lymphoblastoid cell line. Cancer Res. *52*, 3787–3790.

Raddatz, B.B.R., Hansmann, F., Spitzbarth, I., Kalkuhl, A., Deschl, U., Baumgärtner, W., and Ulrich, R. (2014). Transcriptomic meta-analysis of multiple sclerosis and its experimental models. PloS One *9*, e86643.

Raff, M. (2007). Intracellular developmental timers. Cold Spring Harb. Symp. Quant. Biol. *72*, 431–435.

Raff, M.C., Miller, R.H., and Noble, M. (1983). A glial progenitor cell that develops in vitro into an astrocyte or an oligodendrocyte depending on culture medium. Nature *303*, 390–396.

Raff, M.C., Williams, B.P., and Miller, R.H. (1984). The in vitro differentiation of a bipotential glial progenitor cell. EMBO J. *3*, 1857–1864.

Raghuwanshi, A., Joshi, S.S., and Christakos, S. (2008). Vitamin D and Multiple Sclerosis. J. Cell. Biochem. *105*, 338–343.

Rathnasamy, G., Ling, E.-A., and Kaur, C. (2011). Iron and iron regulatory proteins in amoeboid microglial cells are linked to oligodendrocyte death in hypoxic neonatal rat periventricular white matter through production of proinflammatory cytokines and reactive oxygen/nitrogen species. J. Neurosci. Off. J. Soc. Neurosci. *31*, 17982–17995.

Readhead, C., and Hood, L. (1990). The dysmyelinating mouse mutations shiverer (shi) and myelin deficient (shiml d). Behav. Genet. *20*, 213–234.

Readhead, C., Takasashi, N., Shine, H.D., Saavedra, R., Sidman, R., and Hood, L. (1990). Role of myelin basic protein in the formation of central nervous system myelin. Ann. N. Y. Acad. Sci. *605*, 280–285.

Richardson, W.D., Pringle, N., Mosley, M.J., Westermark, B., and Dubois-Dalcq, M. (1988). A role for platelet-derived growth factor in normal gliogenesis in the central nervous system. Cell *53*, 309–319.

Richardson, W.D., Kessaris, N., and Pringle, N. (2006). Oligodendrocyte wars. Nat. Rev. Neurosci. *7*, 11–18.

Robert R. Sokal, F.J.R. (2013). Biometry : the principles and practice of statistics in biological research / Robert R. Sokal and F. James Rohlf. SERBIULA Sist. Libr. 20.

Romm, E., Nielsen, J.A., Kim, J.G., and Hudson, L.D. (2005). Myt1 family recruits histone deacetylase to regulate neural transcription. J. Neurochem. *93*, 1444–1453.

Rowland-Jones, S.L., and Whittle, H.C. (2007). Out of Africa: what can we learn from HIV-2 about protective immunity to HIV-1? Nat. Immunol. *8*, 329–331.

Roy, S., Geoffroy, G., Lapointe, N., and Michaud, J. (1992). Neurological findings in HIV-infected children: a review of 49 cases. Can. J. Neurol. Sci. J. Can. Sci. Neurol. *19*, 453–457.

de Ruijter, A.J.M., van Gennip, A.H., Caron, H.N., Kemp, S., and van Kuilenburg, A.B.P. (2003). Histone deacetylases (HDACs): characterization of the classical HDAC family. Biochem. J. *370*, 737–749.

Saab, A.S., Tzvetanova, I.D., and Nave, K.-A. (2013). The role of myelin and oligodendrocytes in axonal energy metabolism. Curr. Opin. Neurobiol. *23*, 1065–1072.

Saha, R.N., and Pahan, K. (2006). HATs and HDACs in neurodegeneration: a tale of disconcerted acetylation homeostasis. Cell Death Differ. *13*, 539–550.

Samanta, J., and Kessler, J.A. (2004). Interactions between ID and OLIG proteins mediate the inhibitory effects of BMP4 on oligodendroglial differentiation. Dev. Camb. Engl. *131*, 4131–4142.

Sano, T., Baker, D., Virag, T., Wada, A., Yatomi, Y., Kobayashi, T., Igarashi, Y., and Tigyi, G. (2002). Multiple mechanisms linked to platelet activation result in

lysophosphatidic acid and sphingosine 1-phosphate generation in blood. J. Biol. Chem. *277*, 21197–21206.

Santos, A.N., Riemann, D., Santos, A.N., Kehlen, A., Thiele, K., and Langner, J. (1996). Treatment of fibroblast-like synoviocytes with IFN-gamma results in the down-regulation of autotaxin mRNA. Biochem. Biophys. Res. Commun. *229*, 419–424.

Santos-Nogueira, E., López-Serrano, C., Hernández, J., Lago, N., Astudillo, A.M., Balsinde, J., Estivill-Torrús, G., de Fonseca, F.R., Chun, J., and López-Vales, R. (2015). Activation of Lysophosphatidic Acid Receptor Type 1 Contributes to Pathophysiology of Spinal Cord Injury. J. Neurosci. Off. J. Soc. Neurosci. *35*, 10224–10235.

Sarma, M.K., Nagarajan, R., Keller, M.A., Kumar, R., Nielsen-Saines, K., Michalik, D.E., Deville, J., Church, J.A., and Thomas, M.A. (2014). Regional brain gray and white matter changes in perinatally HIV-infected adolescents. NeuroImage Clin. *4*, 29–34.

Sasaki, D.T., Dumas, S.E., and Engleman, E.G. (1987). Discrimination of viable and non-viable cells using propidium iodide in two color immunofluorescence. Cytometry *8*, 413–420.

Sattentau, Q.J., Dalgleish, A.G., Weiss, R.A., and Beverley, P.C. (1986). Epitopes of the CD4 antigen and HIV infection. Science *234*, 1120–1123.

Sauvageot, C.M., and Stiles, C.D. (2002). Molecular mechanisms controlling cortical gliogenesis. Curr. Opin. Neurobiol. *12*, 244–249.

Savaskan, N.E., Rocha, L., Kotter, M.R., Baer, A., Lubec, G., van Meeteren, L.A., Kishi, Y., Aoki, J., Moolenaar, W.H., Nitsch, R., et al. (2007). Autotaxin (NPP-2) in the brain: cell type-specific expression and regulation during development and after neurotrauma. Cell. Mol. Life Sci. CMLS *64*, 230–243.

Schulte, S., and Stoffel, W. (1993). Ceramide UDPgalactosyltransferase from myelinating rat brain: purification, cloning, and expression. Proc. Natl. Acad. Sci. U. S. A. *90*, 10265–10269.

SCLAFANI, V.D., MACKAY, R.D.S., MEYERHOFF, D.J., NORMAN, D., WEINER, M.W., and FEIN, G. (1997). Brain atrophy in HIV infection is more strongly associated with CDC clinical stage than with cognitive impairment. J. Int. Neuropsychol. Soc. JINS *3*, 276–287.

Sengupta, N., and Seto, E. (2004). Regulation of histone deacetylase activities. J. Cell. Biochem. *93*, 57–67.

Shano, S., Moriyama, R., Chun, J., and Fukushima, N. (2008). Lysophosphatidic acid stimulates astrocyte proliferation through LPA1. Neurochem. Int. *52*, 216–220.

Shen, S., and Casaccia-Bonnefil, P. (2008). Post-Translational Modifications of Nucleosomal Histones in Oligodendrocyte Lineage Cells in Development and Disease. J. Mol. Neurosci. MN *35*, 13–22.

Shen, S., Li, J., and Casaccia-Bonnefil, P. (2005). Histone modifications affect timing of oligodendrocyte progenitor differentiation in the developing rat brain. J. Cell Biol. *169*, 577–589.

Shen, S., Sandoval, J., Swiss, V.A., Li, J., Dupree, J., Franklin, R.J.M., and Casaccia-Bonnefil, P. (2008). Age-dependent epigenetic control of differentiation inhibitors is critical for remyelination efficiency. Nat. Neurosci. *11*, 1024–1034.

Sher, F., Boddeke, E., Olah, M., and Copray, S. (2012). Dynamic changes in Ezh2 gene occupancy underlie its involvement in neural stem cell self-renewal and differentiation towards oligodendrocytes. PloS One *7*, e40399.

Sherman, D.L., Krols, M., Wu, L.-M.N., Grove, M., Nave, K.-A., Gangloff, Y.-G., and Brophy, P.J. (2012). Arrest of myelination and reduced axon growth when Schwann cells lack mTOR. J. Neurosci. Off. J. Soc. Neurosci. *32*, 1817–1825.

Shilatifard, A. (2006). Chromatin modifications by methylation and ubiquitination: implications in the regulation of gene expression. Annu. Rev. Biochem. *75*, 243–269.

Shimomura, Y., Wajid, M., Ishii, Y., Shapiro, L., Petukhova, L., Gordon, D., and Christiano, A.M. (2008). Disruption of P2RY5, an orphan G protein–coupled receptor, underlies autosomal recessive woolly hair. Nat. Genet. *40*, 335–339.

Shimomura, Y., Garzon, M.C., Kristal, L., Shapiro, L., and Christiano, A.M. (2009). Autosomal recessive woolly hair with hypotrichosis caused by a novel homozygous mutation in the P2RY5 gene. Exp. Dermatol. *18*, 218–221.

Shine, H.D., Readhead, C., Popko, B., Hood, L., and Sidman, R.L. (1990). Myelin basic protein and myelinogenesis: morphometric analysis of normal, mutant and transgenic central nervous system. Prog. Clin. Biol. Res. *336*, 81–92.

Sidik, H., and Talbot, W.S. (2015). A zinc finger protein that regulates oligodendrocyte specification, migration and myelination in zebrafish. Dev. Camb. Engl. *142*, 4119–4128.

Siebzehnrubl, F.A., Buslei, R., Eyupoglu, I.Y., Seufert, S., Hahnen, E., and Blumcke, I. (2007). Histone deacetylase inhibitors increase neuronal differentiation in adult forebrain precursor cells. Exp. Brain Res. *176*, 672–678.

de Silva, T.I., Cotten, M., and Rowland-Jones, S.L. (2008). HIV-2: the forgotten AIDS virus. Trends Microbiol. *16*, 588–595.

Sim, F.J., McClain, C.R., Schanz, S.J., Protack, T.L., Windrem, M.S., and Goldman, S.A. (2011). CD140a identifies a population of highly myelinogenic, migration-

competent and efficiently engrafting human oligodendrocyte progenitor cells. Nat. Biotechnol. *29*, 934–941.

Simons, M., and Trotter, J. (2007). Wrapping it up: the cell biology of myelination. Curr. Opin. Neurobiol. *17*, 533–540.

Sloane, J.A., and Vartanian, T.K. (2007). Myosin Va controls oligodendrocyte morphogenesis and myelination. J. Neurosci. Off. J. Soc. Neurosci. *27*, 11366–11375.

Smyth, S.S., Mueller, P., Yang, F., Brandon, J.A., and Morris, A.J. (2014). Arguing the case for the autotaxin-lysophosphatidic acid-lipid phosphate phosphatase 3-signaling nexus in the development and complications of atherosclerosis. Arterioscler. Thromb. Vasc. Biol. *34*, 479–486.

Song, M.-R., and Ghosh, A. (2004). FGF2-induced chromatin remodeling regulates CNTF-mediated gene expression and astrocyte differentiation. Nat. Neurosci. *7*, 229–235.

Song, L., Nath, A., Geiger, J.D., Moore, A., and Hochman, S. (2003). Human immunodeficiency virus type 1 Tat protein directly activates neuronal N-methyl-D-aspartate receptors at an allosteric zinc-sensitive site. J. Neurovirol. *9*, 399–403.

Sorensen, A., Moffat, K., Thomson, C., and Barnett, S.C. (2008). Astrocytes, but not olfactory ensheathing cells or Schwann cells, promote myelination of CNS axons in vitro. Glia *56*, 750–763.

Spassky, N., Goujet-Zalc, C., Parmantier, E., Olivier, C., Martinez, S., Ivanova, A., Ikenaka, K., Macklin, W., Cerruti, I., Zalc, B., et al. (1998). Multiple restricted origin of oligodendrocytes. J. Neurosci. Off. J. Soc. Neurosci. *18*, 8331–8343.

Spassky, N., Olivier, C., Perez-Villegas, E., Goujet-Zalc, C., Martinez, S., Thomas, J. l, and Zalc, B. (2000). Single or multiple oligodendroglial lineages: a controversy. Glia *29*, 143–148.

Spassky, N., Heydon, K., Mangatal, A., Jankovski, A., Olivier, C., Queraud-Lesaux, F., Goujet-Zalc, C., Thomas, J.L., and Zalc, B. (2001). Sonic hedgehog-dependent emergence of oligodendrocytes in the telencephalon: evidence for a source of oligodendrocytes in the olfactory bulb that is independent of PDGFRalpha signaling. Dev. Camb. Engl. *128*, 4993–5004.

Sprong, H., Kruithof, B., Leijendekker, R., Slot, J.W., van Meer, G., and van der Sluijs, P. (1998). UDP-galactose:ceramide galactosyltransferase is a class I integral membrane protein of the endoplasmic reticulum. J. Biol. Chem. *273*, 25880–25888.

Stankoff, B., Barron, S., Allard, J., Barbin, G., Noël, F., Aigrot, M.S., Premont, J., Sokoloff, P., Zalc, B., and Lubetzki, C. (2002). Oligodendroglial expression of Edg-2 receptor: developmental analysis and pharmacological responses to lysophosphatidic acid. Mol. Cell. Neurosci. *20*, 415–428.

Stefan, C., Jansen, S., and Bollen, M. (2005). NPP-type ectophosphodiesterases: unity in diversity. Trends Biochem. Sci. *30*, 542–550.

Stemple, D.L. (2005). Structure and function of the notochord: an essential organ for chordate development. Dev. Camb. Engl. *132*, 2503–2512.

Stolt, C.C., Rehberg, S., Ader, M., Lommes, P., Riethmacher, D., Schachner, M., Bartsch, U., and Wegner, M. (2002). Terminal differentiation of myelin-forming oligodendrocytes depends on the transcription factor Sox10. Genes Dev. *16*, 165–170.

Stolt, C.C., Lommes, P., Sock, E., Chaboissier, M.-C., Schedl, A., and Wegner, M. (2003). The Sox9 transcription factor determines glial fate choice in the developing spinal cord. Genes Dev. *17*, 1677–1689.

van Straaten, H.W., and Hekking, J.W. (1991). Development of floor plate, neurons and axonal outgrowth pattern in the early spinal cord of the notochord-deficient chick embryo. Anat. Embryol. (Berl.) *184*, 55–63.

van Straaten, H.W., Hekking, J.W., Beursgens, J.P., Terwindt-Rouwenhorst, E., and Drukker, J. (1989). Effect of the notochord on proliferation and differentiation in the neural tube of the chick embryo. Dev. Camb. Engl. *107*, 793–803.

Stracke, M.L., Krutzsch, H.C., Unsworth, E.J., Arestad, A., Cioce, V., Schiffmann, E., and Liotta, L.A. (1992). Identification, purification, and partial sequence analysis of autotaxin, a novel motility-stimulating protein. J. Biol. Chem. *267*, 2524–2529.

Sui, Y., Potula, R., Dhillon, N., Pinson, D., Li, S., Nath, A., Anderson, C., Turchan, J., Kolson, D., Narayan, O., et al. (2004). Neuronal apoptosis is mediated by CXCL10 overexpression in simian human immunodeficiency virus encephalitis. Am. J. Pathol. *164*, 1557–1566.

Swiss, V.A., Nguyen, T., Dugas, J., Ibrahim, A., Barres, B., Androulakis, I.P., and Casaccia, P. (2011). Identification of a gene regulatory network necessary for the initiation of oligodendrocyte differentiation. PloS One *6*, e18088.

Tabata, K., Baba, K., Shiraishi, A., Ito, M., and Fujita, N. (2007). The orphan GPCR GPR87 was deorphanized and shown to be a lysophosphatidic acid receptor. Biochem. Biophys. Res. Commun. *363*, 861–866.

Tabuchi, S., Kume, K., Aihara, M., and Shimizu, T. (2000). Expression of lysophosphatidic acid receptor in rat astrocytes: mitogenic effect and expression of neurotrophic genes. Neurochem. Res. *25*, 573–582.

Tager, A.M., LaCamera, P., Shea, B.S., Campanella, G.S., Selman, M., Zhao, Z., Polosukhin, V., Wain, J., Karimi-Shah, B.A., Kim, N.D., et al. (2008). The lysophosphatidic acid receptor LPA1 links pulmonary fibrosis to lung injury by mediating fibroblast recruitment and vascular leak. Nat. Med. *14*, 45–54.

Takada, N., and Appel, B. (2010). Identification of genes expressed by zebrafish oligodendrocytes using a differential microarray screen. Dev. Dyn. Off. Publ. Am. Assoc. Anat. *239*, 2041–2047.

Takebayashi, H., Nabeshima, Y., Yoshida, S., Chisaka, O., Ikenaka, K., and Nabeshima, Y. (2002). The basic helix-loop-helix factor olig2 is essential for the development of motoneuron and oligodendrocyte lineages. Curr. Biol. CB *12*, 1157–1163.

Tanaka, M., Okudaira, S., Kishi, Y., Ohkawa, R., Iseki, S., Ota, M., Noji, S., Yatomi, Y., Aoki, J., and Arai, H. (2006). Autotaxin stabilizes blood vessels and is required for embryonic vasculature by producing lysophosphatidic acid. J. Biol. Chem. *281*, 25822–25830.

Tarrade, A., Fassier, C., Courageot, S., Charvin, D., Vitte, J., Peris, L., Thorel, A., Mouisel, E., Fonknechten, N., Roblot, N., et al. (2006). A mutation of spastin is responsible for swellings and impairment of transport in a region of axon characterized by changes in microtubule composition. Hum. Mol. Genet. *15*, 3544–3558.

Tekki-Kessaris, N., Woodruff, R., Hall, A.C., Gaffield, W., Kimura, S., Stiles, C.D., Rowitch, D.H., and Richardson, W.D. (2001). Hedgehog-dependent oligodendrocyte lineage specification in the telencephalon. Dev. Camb. Engl. *128*, 2545–2554.

Temple, S., and Raff, M.C. (1985). Differentiation of a bipotential glial progenitor cell in a single cell microculture. Nature *313*, 223–225.

Tham, C.-S., Lin, F.-F., Rao, T.S., Yu, N., and Webb, M. (2003). Microglial activation state and lysophospholipid acid receptor expression. Int. J. Dev. Neurosci. Off. J. Int. Soc. Dev. Neurosci. *21*, 431–443.

Thisse, B., and Thisse, C. (2014). In situ hybridization on whole-mount zebrafish embryos and young larvae. Methods Mol. Biol. Clifton NJ *1211*, 53–67.

Thisse, C., and Thisse, B. (2008). High-resolution in situ hybridization to whole-mount zebrafish embryos. Nat. Protoc. *3*, 59–69.

Timsit, S., Martinez, S., Allinquant, B., Peyron, F., Puelles, L., and Zalc, B. (1995). Oligodendrocytes originate in a restricted zone of the embryonic ventral neural tube defined by DM-20 mRNA expression. J. Neurosci. Off. J. Soc. Neurosci. *15*, 1012–1024.

Tokumura, A., Tsutsumi, T., and Tsukatani, H. (1992). Transbilayer movement and metabolic fate of ether-linked phosphatidic acid (1-O-Octadecyl-2-acetyl-sn-glycerol 3-phosphate) in guinea pig peritoneal polymorphonuclear leukocytes. J. Biol. Chem. *267*, 7275–7283.

Tokumura, A., Majima, E., Kariya, Y., Tominaga, K., Kogure, K., Yasuda, K., and Fukuzawa, K. (2002). Identification of human plasma lysophospholipase D, a

lysophosphatidic acid-producing enzyme, as autotaxin, a multifunctional phosphodiesterase. J. Biol. Chem. *277*, 39436–39442.

Tripathi, R.B., Rivers, L.E., Young, K.M., Jamen, F., and Richardson, W.D. (2010). NG2 glia generate new oligodendrocytes but few astrocytes in a murine experimental autoimmune encephalomyelitis model of demyelinating disease. J. Neurosci. Off. J. Soc. Neurosci. *30*, 16383–16390.

Tsai, S.-C., and Seto, E. (2002). Regulation of histone deacetylase 2 by protein kinase CK2. J. Biol. Chem. *277*, 31826–31833.

Tur, G., Georgieva, E.I., Gagete, A., López-Rodas, G., Rodríguez, J.L., and Franco, L. (2010). Factor binding and chromatin modification in the promoter of murine Egr1 gene upon induction. Cell. Mol. Life Sci. CMLS *67*, 4065–4077.

Tyler, W.A., Gangoli, N., Gokina, P., Kim, H.A., Covey, M., Levison, S.W., and Wood, T.L. (2009). Activation of the mammalian target of rapamycin (mTOR) is essential for oligodendrocyte differentiation. J. Neurosci. Off. J. Soc. Neurosci. *29*, 6367–6378.

Tyor, W.R., Glass, J.D., Griffin, J.W., Becker, P.S., McArthur, J.C., Bezman, L., and Griffin, D.E. (1992). Cytokine expression in the brain during the acquired immunodeficiency syndrome. Ann. Neurol. *31*, 349–360.

Umezu-Goto, M., Kishi, Y., Taira, A., Hama, K., Dohmae, N., Takio, K., Yamori, T., Mills, G.B., Inoue, K., Aoki, J., et al. (2002). Autotaxin has lysophospholipase D activity leading to tumor cell growth and motility by lysophosphatidic acid production. J. Cell Biol. *158*, 227–233.

Vallstedt, A., Klos, J.M., and Ericson, J. (2005). Multiple dorsoventral origins of oligodendrocyte generation in the spinal cord and hindbrain. Neuron *45*, 55–67.

Wang, B., Chen, J., Santiago, F.S., Janes, M., Kavurma, M.M., Chong, B.H., Pimanda, J.E., and Khachigian, L.M. (2010). Phosphorylation and acetylation of histone H3 and autoregulation by early growth response 1 mediate interleukin 1beta induction of early growth response 1 transcription. Arterioscler. Thromb. Vasc. Biol. *30*, 536–545.

Warf, B.C., Fok-Seang, J., and Miller, R.H. (1991). Evidence for the ventral origin of oligodendrocyte precursors in the rat spinal cord. J. Neurosci. Off. J. Soc. Neurosci. *11*, 2477–2488.

Watanabe, N., Ikeda, H., Nakamura, K., Ohkawa, R., Kume, Y., Tomiya, T., Tejima, K., Nishikawa, T., Arai, M., Yanase, M., et al. (2007a). Plasma lysophosphatidic acid level and serum autotaxin activity are increased in liver injury in rats in relation to its severity. Life Sci. *81*, 1009–1015.

Watanabe, N., Ikeda, H., Nakamura, K., Ohkawa, R., Kume, Y., Aoki, J., Hama, K., Okudaira, S., Tanaka, M., Tomiya, T., et al. (2007b). Both plasma lysophosphatidic acid

and serum autotaxin levels are increased in chronic hepatitis C. J. Clin. Gastroenterol. *41*, 616–623.

Weake, V.M., and Workman, J.L. (2008). Histone ubiquitination: triggering gene activity. Mol. Cell *29*, 653–663.

Wegner, M. (2008). A matter of identity: transcriptional control in oligodendrocytes. J. Mol. Neurosci. MN *35*, 3–12.

Wei, Q., Miskimins, W.K., and Miskimins, R. (2005). Stage-specific expression of myelin basic protein in oligodendrocytes involves Nkx2.2-mediated repression that is relieved by the Sp1 transcription factor. J. Biol. Chem. *280*, 16284–16294.

Weiner, J.A., and Chun, J. (1999). Schwann cell survival mediated by the signaling phospholipid lysophosphatidic acid. Proc. Natl. Acad. Sci. U. S. A. *96*, 5233–5238.

Weiner, J.A., Hecht, J.H., and Chun, J. (1998). Lysophosphatidic acid receptor gene vzg-1/lpA1/edg-2 is expressed by mature oligodendrocytes during myelination in the postnatal murine brain. J. Comp. Neurol. *398*, 587–598.

Wells, M.R., and Sprinkle, T.J. (1981). Purification of rat 2',3'-cyclic nucleotide 3'-phosphodiesterase. J. Neurochem. *36*, 633–639.

Wheeler, N.A., Lister, J.A., and Fuss, B. (2015). The Autotaxin–Lysophosphatidic Acid Axis Modulates Histone Acetylation and Gene Expression during Oligodendrocyte Differentiation. J. Neurosci. *35*, 11399–11414.

Williams, J.R., Khandoga, A.L., Goyal, P., Fells, J.I., Perygin, D.H., Siess, W., Parrill, A.L., Tigyi, G., and Fujiwara, Y. (2009). Unique ligand selectivity of the GPR92/LPA5 lysophosphatidate receptor indicates role in human platelet activation. J. Biol. Chem. *284*, 17304–17319.

Wolswijk, G. (2002). Oligodendrocyte precursor cells in the demyelinated multiple sclerosis spinal cord. Brain J. Neurol. *125*, 338–349.

Woodruff, R.H., Tekki-Kessaris, N., Stiles, C.D., Rowitch, D.H., and Richardson, W.D. (2001). Oligodendrocyte development in the spinal cord and telencephalon: common themes and new perspectives. Int. J. Dev. Neurosci. Off. J. Int. Soc. Dev. Neurosci. *19*, 379–385.

Woods, I.G., Kelly, P.D., Chu, F., Ngo-Hazelett, P., Yan, Y.-L., Huang, H., Postlethwait, J.H., and Talbot, W.S. (2000). A Comparative Map of the Zebrafish Genome. Genome Res. *10*, 1903–1914.

Wu, M., Hernandez, M., Shen, S., Sabo, J.K., Kelkar, D., Wang, J., O'Leary, R., Phillips, G.R., Cate, H.S., and Casaccia, P. (2012). Differential modulation of the oligodendrocyte transcriptome by sonic hedgehog and bone morphogenetic protein 4

via opposing effects on histone acetylation. J. Neurosci. Off. J. Soc. Neurosci. *32*, 6651–6664.

Xie, Y., and Meier, K.E. (2004). Lysophospholipase D and its role in LPA production. Cell. Signal. *16*, 975–981.

Xin, M., Yue, T., Ma, Z., Wu, F., Gow, A., and Lu, Q.R. (2005). Myelinogenesis and axonal recognition by oligodendrocytes in brain are uncoupled in Olig1-null mice. J. Neurosci. Off. J. Soc. Neurosci. *25*, 1354–1365.

Yahi, N., Baghdiguian, S., Moreau, H., and Fantini, J. (1992). Galactosyl ceramide (or a closely related molecule) is the receptor for human immunodeficiency virus type 1 on human colon epithelial HT29 cells. J. Virol. *66*, 4848–4854.

Yanagida, K., Masago, K., Nakanishi, H., Kihara, Y., Hamano, F., Tajima, Y., Taguchi, R., Shimizu, T., and Ishii, S. (2009a). Identification and characterization of a novel lysophosphatidic acid receptor, p2y5/LPA6. J. Biol. Chem. *284*, 17731–17741.

Yanagida, K., Masago, K., Nakanishi, H., Kihara, Y., Hamano, F., Tajima, Y., Taguchi, R., Shimizu, T., and Ishii, S. (2009b). Identification and characterization of a novel lysophosphatidic acid receptor, p2y5/LPA6. J. Biol. Chem. *284*, 17731–17741.

Yanagida, K., Kurikawa, Y., Shimizu, T., and Ishii, S. (2013). Current progress in non-Edg family LPA receptor research. Biochim. Biophys. Acta *1831*, 33–41.

Ye, F., Chen, Y., Hoang, T., Montgomery, R.L., Zhao, X., Bu, H., Hu, T., Taketo, M.M., van Es, J.H., Clevers, H., et al. (2009). HDAC1 and HDAC2 regulate oligodendrocyte differentiation by disrupting the beta-catenin-TCF interaction. Nat. Neurosci. *12*, 829–838.

Ye, J., Coulouris, G., Zaretskaya, I., Cutcutache, I., Rozen, S., and Madden, T.L. (2012). Primer-BLAST: a tool to design target-specific primers for polymerase chain reaction. BMC Bioinformatics *13*, 134.

Ye, X., Hama, K., Contos, J.J.A., Anliker, B., Inoue, A., Skinner, M.K., Suzuki, H., Amano, T., Kennedy, G., Arai, H., et al. (2005). LPA3-mediated lysophosphatidic acid signalling in embryo implantation and spacing. Nature *435*, 104–108.

Ye, X., Skinner, M.K., Kennedy, G., and Chun, J. (2008). Age-dependent loss of sperm production in mice via impaired lysophosphatidic acid signaling. Biol. Reprod. *79*, 328–336.

Younes-Rapozo, V., Felgueiras, L.O.R., Viana, N.L., Fierro, I.M., Barja-Fidalgo, C., Manhães, A.C., and Barradas, P.C. (2009). A role for the MAPK/ERK pathway in oligodendroglial differentiation in vitro: stage specific effects on cell branching. Int. J. Dev. Neurosci. Off. J. Int. Soc. Dev. Neurosci. *27*, 757–768.

Yu, W.P., Collarini, E.J., Pringle, N.P., and Richardson, W.D. (1994). Embryonic expression of myelin genes: evidence for a focal source of oligodendrocyte precursors in the ventricular zone of the neural tube. Neuron *12*, 1353–1362.

Yu, Y., Chen, Y., Kim, B., Wang, H., Zhao, C., He, X., Liu, L., Liu, W., Wu, L.M.N., Mao, M., et al. (2013). Olig2 targets chromatin remodelers to enhancers to initiate oligodendrocyte differentiation. Cell *152*, 248–261.

Yuelling, L.M., and Fuss, B. (2008). Autotaxin (ATX): a multi-functional and multi-modular protein possessing enzymatic lysoPLD activity and matricellular properties. Biochim. Biophys. Acta *1781*, 525–530.

Yuelling, L.W., Waggener, C.T., Afshari, F.S., Lister, J.A., and Fuss, B. (2012). Autotaxin/ENPP2 regulates oligodendrocyte differentiation in vivo in the developing zebrafish hindbrain. Glia *60*, 1605–1618.

Yukiura, H., Hama, K., Nakanaga, K., Tanaka, M., Asaoka, Y., Okudaira, S., Arima, N., Inoue, A., Hashimoto, T., Arai, H., et al. (2011). Autotaxin regulates vascular development via multiple lysophosphatidic acid (LPA) receptors in zebrafish. J. Biol. Chem. *286*, 43972–43983.

Yung, Y.C., Mutoh, T., Lin, M.-E., Noguchi, K., Rivera, R.R., Choi, J.W., Kingsbury, M.A., and Chun, J. (2011). Lysophosphatidic acid signaling may initiate fetal hydrocephalus. Sci. Transl. Med. *3*, 99ra87.

Yung, Y.C., Stoddard, N.C., and Chun, J. (2014). LPA receptor signaling: pharmacology, physiology, and pathophysiology. J. Lipid Res. *55*, 1192–1214.

Zannino, D.A., and Appel, B. (2009). Olig2+ precursors produce abducens motor neurons and oligodendrocytes in the zebrafish hindbrain. J. Neurosci. Off. J. Soc. Neurosci. *29*, 2322–2333.

Zhang, Y., Chen, Y.-C.M., Krummel, M.F., and Rosen, S.D. (2012). Autotaxin through lysophosphatidic acid stimulates polarization, motility, and transendothelial migration of naive T cells. J. Immunol. Baltim. Md 1950 *189*, 3914–3924.

Zhang, Y., Chen, K., Sloan, S.A., Bennett, M.L., Scholze, A.R., O'Keeffe, S., Phatnani, H.P., Guarnieri, P., Caneda, C., Ruderisch, N., et al. (2014). An RNA-sequencing transcriptome and splicing database of glia, neurons, and vascular cells of the cerebral cortex. J. Neurosci. Off. J. Soc. Neurosci. *34*, 11929–11947.

Zhao, C., Fernandes, M.J., Prestwich, G.D., Turgeon, M., Di Battista, J., Clair, T., Poubelle, P.E., and Bourgoin, S.G. (2008). Regulation of lysophosphatidic acid receptor expression and function in human synoviocytes: implications for rheumatoid arthritis? Mol. Pharmacol. *73*, 587–600.

Zhou, Q., and Anderson, D.J. (2002). The bHLH transcription factors OLIG2 and OLIG1 couple neuronal and glial subtype specification. Cell *109*, 61–73.

Zhou, Q., Choi, G., and Anderson, D.J. (2001). The bHLH transcription factor Olig2 promotes oligodendrocyte differentiation in collaboration with Nkx2.2. Neuron *31*, 791–807.

Zou, S., Fitting, S., Hahn, Y.-K., Welch, S.P., El-Hage, N., Hauser, K.F., and Knapp, P.E. (2011). Morphine potentiates neurodegenerative effects of HIV-1 Tat through actions at μ-opioid receptor-expressing glia. Brain J. Neurol. *134*, 3616–3631.

## Vita

Natalie Allen Wheeler was born in Long Valley, NJ on May 27th,1988. She graduated from West Morris Central High School in 2006. Natalie continued her education at Virginia Tech in Blacksburg, VA, where she received a Bachelor of Science in both Psychology and Biology. As an undergraduate, Natalie received an REU (Research Experiences for Undergraduates) from the NSF (National Science Foundation), which allowed her to work in the laboratory of Dr. Daniel Panaccione at West Virginia University, in Morgantown, WV. Her work focused on the role of ergot alkaloids in *Aspergillus fumigatus* and was published in *Curr Microbiol*, in which Natalie was the second author. During her final year at Virginia Tech, Natalie worked in the lab of Dr. John Phillips in the field of Ethology. After graduation from Virginia Tech, Natalie worked as a water chemist at the Walt Disney World Company in Lake Buena Vista, FL. In fall of 2011, Natalie entered the Neuroscience program at Virginia Commonwealth University and joined the laboratory of Dr. Babette Fuss in the department of Anatomy and Neurobiology in the summer of 2012. Throughout her research career, she was given many opportunities to present her research via oral and poster presentations at national meetings such as the American Society for Neurochemistry and the Great Lakes Glia Meeting. At VCU, Natalie participated in Central Virginia Chapter Society for Neuroscience poster session, Brain, Immunology and Glia poster session, as well as an oral presentation at the Forbes Day honors colloquium. Natalie was involved in many organizations as a graduate student, for which many of them she stood on the leadership committee. These positions include: Student Representative for the Central Virginia Chapter Society for Neuroscience, VP of Community Outreach for Women in Science, Host Committee Member and Community Outreach Chair for the ASCB local meeting Career Development Day: The Bench and Beyond, and the Scientific Meeting Organization Officer for the, second annual, Brain, Immunology and Glia meeting. Natalie also earned various awards such as travel awards from VCU Graduate School and Neuroscience Program, the YIEE award from the American Society for Neurochemistry, and poster awards from the Great Lakes Glia Meeting and the Brain, Immunology and Glia meeting.

Manuscripts resulting from Natalie's work at Virginia Commonwealth University:

**Wheeler NA**, Fuss B, Knapp PE and Zou S (**2016**) HIV-1 Tat Modulates ATX lysoPLD Activity and Oligodendrocyte Differentiation. Manuscript submitted to ASN Neuro.

**Wheeler NA** and Fuss B (**2016**) Extracellular cues influencing oligodendrocyte differentiation and (re)myelination. [epub ahead of print] Exp Neurol.

**Wheeler NA**, Spencer S, Lister JA and Fuss B **(2016)** The role of LPA receptor 6 in oligodendrocyte differentiation. Manuscript in preparation to J Neurosci.

Espirito-Santo S, Mendonça HR, **Wheeler NA,** Gomes F, Campello-Costa P, Jacobs K, Fuss B **(2016)** Cuprizone diet-induced inflammatory demyelination promotes increased glutamatergic excitation on dorsal lateral geniculate nucleus inhibitory interneurons and

retinogeniculate axonal sprouting. Manuscript in preparation to J Neurosci.

**Wheeler NA**, Lister JA and Fuss B (**2015**) The autotaxin-LPA axis modulates histone acetylation and gene expression during oligodendrocyte differentiation. J Neurosci. 35(32):11399-414